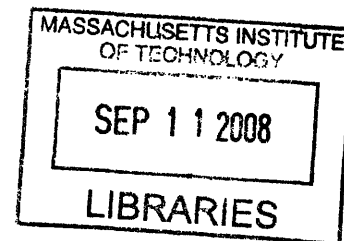


MECHANISM OF THE EFFICIENT QUENCHING OF TRYPTOPHAN  
FLUORESCENCE IN HUMAN GAMMA CRYSTALLIN

by

Jiejin Chen

B.S., Pharmaceutical Science (2000)  
Peking University Health Science Center  
M.S., Chemical Biology (2003)  
Peking University Health Science Center



Submitted to the Department of Chemistry  
in Partial Fulfillment of the Requirement for the Degree of

DOCTOR OF PHILOSOPHY

at the  
Massachusetts Institute of Technology

September 2008

© 2008 Massachusetts Institute of Technology  
All rights reserved

The author hereby grants MIT permission to reproduce and to distribute publicly paper  
and electronic copies of this thesis document in whole or in part.

Signature of Author \_\_\_\_\_

Handwritten signature of Jiejin Chen in black ink.

Department of Chemistry  
July 17<sup>th</sup>, 2008

Certified by \_\_\_\_\_

Handwritten signature of Jonathan King in black ink.

Jonathan King  
Thesis Supervisor

Accepted by \_\_\_\_\_

Robert W. Field  
Chairman, Departmental Committee on Graduate Students

This doctoral thesis has been examined by a committee of the Department of Chemistry as follows:

*1 1 2 1 1 1*

Professor Stuart S. Licht \_\_\_\_\_

Chair

Professor Daniel S. Kemp \_\_\_\_\_

*1 1 2 1 1 1*

Professor Jonathan King \_\_\_\_\_

Thesis Supervisor



# MECHANISM OF THE EFFICIENT QUENCHING OF TRYPTOPHAN FLUORESCENCE IN HUMAN GAMMA CRYSTALLIN

by

Jiejin Chen

Submitted to the department of Chemistry at the Massachusetts Institute of Technology in July 2008 in partial fulfillment of the requirements for the degree of Doctor of Philosophy in Chemistry

## ABSTRACT

Quenching of the fluorescence of buried tryptophans (Trps) is an important reporter of protein conformation. Human  $\gamma$ D-crystallin (H $\gamma$ D-Crys) and human  $\gamma$ S-crystallin (H $\gamma$ S-Crys) are both very stable eye lens protein that must remain soluble and folded throughout the human lifetime. Aggregation of non-native or covalently damaged H $\gamma$ D-Crys or H $\gamma$ S-Crys is associated with the prevalent eye disease mature-onset cataract. Both H $\gamma$ D-Crys and H $\gamma$ S-Crys have two homologous  $\beta$ -sheet domains, each containing a pair of highly conserved buried tryptophans (see Fig. 1). The overall fluorescence of the

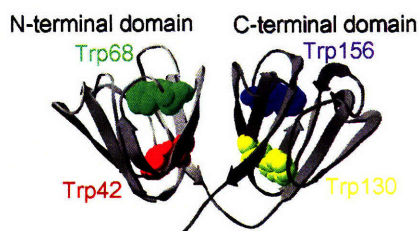


Figure 1: The crystal structure of wild-type H $\gamma$ D-Crys depicted in ribbon representation showing the four intrinsic tryptophans in spacefill, Trp42 and Trp68 in the N-terminal domain and Trp130 and Trp156 in the C-terminal domain (Protein Data Bank Code: 1HK0).

Trps is quenched in the native state of H $\gamma$ D-Crys and H $\gamma$ S-Crys. In crystallin proteins, these Trps will be absorbing UV radiation that reaches the lens. The dispersal of the excited state energy is likely to be physiological relevant for the lens crystallins.

Steady-state and time-resolved fluorescence measurements combined with hybrid quantum mechanical-molecular mechanical (QM-MM) simulations revealed the quenching mechanism of H $\gamma$ D-Crys. From fluorescence of triple Trp to Phe mutants, the homologous pair Trp68 and Trp156 are found to be extremely quenched, with quantum yields close to 0.01, and with very short lifetimes,  $\tau \sim 0.1$  ns. In contrast, the homologous pair Trp42 and Trp130 are moderately fluorescent, with quantum yields of 0.13 and 0.17, respectively, and with longer lifetimes,  $\tau \sim 3$  ns.

In an attempt to identify quenching and/or electrostatically perturbing residues, a set of 17 candidate amino acids around Trp68 and Trp156 were substituted with neutral or hydrophobic residues. None of these mutants showed significant changes in the fluorescence intensity compared to their own background.

Hybrid quantum mechanical-molecular mechanical (QM-MM) simulations were carried out by Prof. Patrik R. Callis at Montana State University. Computations with the four different excited Trps as electron donors strongly indicate that electron transfer rates to the amide backbone of Trp68 and Trp156 are extremely fast relative to those for Trp42 and Trp130. This is in agreement with the quantum yields I measured experimentally and consistent with the absence of a quenching sidechain. Efficient electron transfer to the

backbone is possible for Trp68 and Trp156 because of the net favorable location of several charged residues and the orientation of nearby waters, which collectively stabilize electron transfer electrostatically.

The fluorescence emission spectra of single and double Trp to Phe mutants provide strong evidence for energy transfer from Trp42 to Trp68 in the N-terminal domain and from Trp130 to Trp156 in the C-terminal domain. In the presence of the energy acceptor (Trp68 or Trp156), the lifetime of the energy donor (Trp42 or Trp130) decreased from ~3ns to ~1ns. The intradomain energy transfer efficiency is 56% in the N-terminal domain and is 71% in the C-terminal domain. The experimental values of energy transfer efficiency are in good agreement with those calculated theoretically. Time-resolved fluorescence anisotropy measurements with the single-Trp containing proteins, Trp42-only and Trp130-only, indicate that the protein rotates as a rigid body and no segmental motion is detected. The absence of a time-dependent red shift in the time-resolved emission spectra of Trp130 proves that its local environment is very rigid. A combination of energy transfer with electron transfer results in short excited-state lifetimes of all Trps, which, together with the high rigidity of the protein matrix around Trps, could protect HyD-Crys from excited-state reactions causing permanent covalent damage.

Similar experimental and computational studies indicate that the quenching of the Trp fluorescence in HyS-Crys is also caused by fast electron transfer and intradomain Förster resonance energy transfer. The electrostatically enabled excited state quenching by electron transfer to the backbone amide is highly conserved in other  $\beta$ -,  $\gamma$ -crystallins despite the absence of precise sequence homology. This striking conservation, together with the observation of Tallmadge and Borkman [Tallmadge and Borkman, 1990] that the conserved quenched Trps in bovine  $\gamma$ B-crystallin were protected from photolysis relative to the more fluorescent Trps, strongly suggests that the quenching is an evolved property of the protein fold that allows it to absorb ultraviolet light while suffering minimal photodamage.

Thesis Supervisor: Jonathan King, Professor of Biology

## ACKNOWLEDGEMENTS

It is very difficult to just use words to express my gratitude for all the people who have helped me in the past. I have been extremely lucky to meet some key person in graduate school. Without any of them, I could not imagine I can ever reach the point today.

Professor Jonathan King. I always think it has to be some kind of miracle to make me to meet you. Sometimes I am still in doubt about myself and do not think I deserve being here. You have always been extremely supportive, patient, and understanding. I had a difficult time at the beginning of the graduate school. As an international student with an introverted personality, at that point, I have nothing to prove that I can be a good student but you took me into the group with great amount of trust. Because you are so generous and nice, every time after I talked to you about either my experiments or my personal issues, I always feel that I owe you even more and get more motivation to work hard. You are so actively involved in education and various community services. It is probably difficult for me to follow your path but it certainly helps me to improve. You always treat every group member as part of your family and help them out as much as you can. You taught me how to ask important questions in science and how to put pieces of data into a big picture. You not only teach us science but also share the tips with us on how to survive in the competitive academics and how to build up good relationships with different collaborators, and so much more. You are truly a role model. I feel very lucky for being your student. Hopefully I can make some achievement in the future to make you feel proud of me.

Dr. Shannon L. Thol. You were my TA for protein folding lecture and were my first mentor in the Lab. I have always admired your attitude and commitment to the science; your deep love and caring to the nature and wild life; your courage to follow your true passion in career. You taught me how to live green, how to recycle and so many things in the life. We are very different person but you always give me great helps and advice. The “team crystallin” has been passed on because your great contributions.

Dr. Ishara Mills-Henry, you have taught me so much in the crystallin world. No matter how busy you are, you always make efforts to improve the minority education. Your hardworking, positive attitude to the life, and generosity always make me miss the past time we spent together.

Thank you for all the past and present members of “team crystallin”. Ligia Acosta-Sampson, the  $\alpha$ -crystallin master and protein purification expert in the lab. You brought me so much fun. Thank you for being supportive and sharing your knowledge and life with me. You have conquered many difficulties and achieved a lot in the past. Keep up the good work! Kate Drahos, it is always fun to have you around. You have broad interests in the life. It is very enjoyable to talk to you about science and life. Dr. Yongting Wang, all the best to you in Shanghai. Little by little I started to realize the difficulties in balancing between the work and family, but you have handled these so well. You also have helped many other people even though you had busy schedule. Dr. Kelly Knee, you bring us great expertise in spectroscopy. Happy chaperoning and happy aggregation. Dr.

Melissa Kosinski-Collins, I always admire your productivity and enthusiasm to the life. Fanrong Kong, the youngest generation of “team crystallin”, enjoy your journey of exploring the crystallins world. Be patient and you will find so much more wonderful things about them. Brian Sosa, good luck for your first year in graduate school, and do not forget to teach us some fabulous dancing movement. Jeannie Chew, you were a delight to have in the lab. Maybe I taught you something in the lab but you definitely brought me more fun in the life. Shea Jameel and Dan Goulet, good luck for your study and it is fun to have you in the lab. To all members of the King Lab, thank you for making the lab as me second home. Dr. Peter Weigele, thank you for your observing and caring. Cammie Haase-Pettingell, the mom of the lab. Without you the lab cannot function well. Cindy Woolley, thank you for all the thorough and elegant work. We have had so many great lab parties under your organizations. Thank you also to Jacqueline Piret, Greg Pintilie, Dessy Raytcheva, Erika Erickson, and Dr. Ryan Simkovsky. Thank you for my classmates and friends. Your friendships will forever stay in my heart.

Thank you to my thesis committee. Professors Stuart Licht, you have been very supportive in the past years. You helped me in many ways to go through the difficult situation and also give me good suggestions and encouragement throughout the years. Professor Daniel Kemp, you have deep knowledge on proteins and fluorescence. Thank you for being my committee member. I appreciate all the effort that you have made to help me through my graduate career.

Professor Patrik R. Callis. You have been such a wonderful collaborator. Even though we have not met each other in person before we published the paper together, you have always been very helpful for my projects. You always reply my E-mail promptly and send me very detailed information to answer all the questions I had for the experiments. I got very lucky to be able to collaborate with you. Without your helps, the quenching of tryptophan fluorescence in crystallins might still be a mystery. I am looking forward to doing more good work with you.

Professor Ludwig Brand. I have spent unforgettable time at Johns Hopkins University with you. You will ask me my career plan over and over again and introduce me to all the faculty members we run into. You are so passionate about science. You treat me not just like a visiting student, but more than your granddaughter. I hope I can see you again soon. Dr. Dmitri Topygin. Thank you for spending so much time with me for all the time-resolved fluorescence measurements and data analysis. You have taught me everything from scratch. Without you this work cannot be done. All the best for you and your family.

Thank you to my whole family. Even if I do not say it very often, you know how much I love you. To make you proud of me and not to worry about me has always encouraged myself to survive at MIT. I hope one day I can give it back to you and somewhat contribute to the family.

This research was supported by NIH grant GM17980 and NEI grant EY 015834 Health awarded to Jonathan King.

## TABLE OF CONTENTS

Title page .....	1
Signature page .....	2
Abstract .....	3
Acknowledgements .....	5
Table of Contents .....	7
List of Figures .....	11
List of Tables .....	13
<b>Chapter One: Introduction .....</b>	<b>14</b>
A. Vision and the optic system.....	15
B. Eye lens crystallin proteins .....	17
1. $\alpha$ -crystallin .....	17
2. $\beta$ - and $\gamma$ -crystallins .....	18
3. <i>Ciona</i> $\beta\gamma$ -crystallin .....	26
4. Taxon-specific crystallins .....	26
C. Tryptophan fluorescence .....	27
1. Protein photobleaching .....	27
2. Quenching of tryptophan fluorescence .....	28
a. Electron transfer .....	28
b. Proton transfer .....	29
c. Resonance energy transfer .....	29
d. Other mechanisms .....	30
3. Application of time-resolved fluorescence measurements to intrinsic Trp fluorescence .....	30
4. Tryptophan fluorescence studies on crystallins .....	31
D. Cataract .....	32
1. Mature-onset cataract is a protein aggregation disease .....	32
2. Human congenital cataracts .....	33
3. Diabetes and cataract formation .....	34
E. UV-B exposure and cataract .....	34
1. Distribution of solar radiation .....	34
2. Epidemiologic studies on the effects of UV radiation .....	36
a. Proposed chemical model of UV radiation induced cataract formation .....	38
b. UV damage to lens epithelium .....	38
3. UV radiation effects on the retina .....	39
F. Protective mechanism of eye lens from UV radiation .....	39
1. UV filters .....	39
2. Other protective mechanisms of the lens .....	40
G. Summary of thesis .....	40
Note on the organization of the thesis .....	41

<b>Chapter Two: Mechanism of the highly efficient quenching of tryptophan fluorescence in human <math>\gamma</math>D-crystallin</b> .....	42
A. Abstract .....	43
B. Introduction .....	44
C. Materials and Methods .....	48
1. Mutagenesis, expression and purification of recombinant HyD-Crys ....	48
2. Fluorescence spectroscopy .....	49
3. Quantum yield determinations .....	50
4. QM-MM simulations .....	51
D. Results .....	52
1. Fluorescence emission spectra and quantum yields .....	52
2. Resonance energy transfer between the two Trps within each domain ...	56
3. Investigation of nearby side chain contributions to Trp quenching .....	57
4. QM-MM estimates of relative fluorescence quantum yields .....	62
5. Investigation of the stabilization effect of charged and polar side chains on the charge transfer state .....	67
E. Discussion .....	74
1. Trp to Trp energy transfer .....	74
2. Charge transfer mechanism .....	75
3. The potential physiological role for lens UV absorption in protecting the retina .....	77
4. Does fluorescence quenching protect the crystallins from UV photodamage? .....	78
F. Conclusion .....	80

<b>Chapter Three: Mechanism of the efficient tryptophan fluorescence quenching in human <math>\gamma</math>D-crystallin studied by time-resolved fluorescence</b> .....	81
A. Abstract .....	82
B. Introduction .....	83
C. Materials and Methods .....	89
1. Mutagenesis, expression and purification of proteins .....	89
2. Time-resolved fluorescence intensity and anisotropy measurements .....	90
3. Steady-state fluorescence and absorption measurements .....	92
4. Analysis of time-resolved intensity data .....	92
5. Reversible Förster resonance energy transfer rates .....	93
6. Calculation of the Förster Resonance Energy Transfer Efficiencies .....	95
7. Determination of R and $\kappa^2$ from Protein Crystal Structure .....	97
D. Results .....	98
1. Global analysis of time-resolved intensity data .....	98
2. Lifetimes of Trp residues in single-Trp containing proteins and double-Trp containing proteins with both Trp residues in the same domain .....	106
3. Lifetimes for double-Trp containing proteins with the two Trps in the different domains .....	114
4. Reversible Förster resonance energy transfer rates .....	119
5. Förster resonance energy transfer efficiencies .....	120

6. Time-resolved emission spectra of Trp130-only HyD-Crys .....	124
7. Time-resolved fluorescence anisotropy .....	125
E. Discussion .....	130
1. Time constants $\tau_n$ of multiple Trp containing proteins .....	131
2. Multi-exponential fluorescence of Trps and charge transfer mechanism .....	132
3. Time-resolved fluorescence anisotropy .....	133
4. Ocular lens protects retina from near-UV radiation .....	135
5. Properties of Trp in $\gamma$ -crystallin may be important to protect themselves from UV-induced photo reactions .....	135
F. Conclusion .....	137
<b>Chapter Four: The <math>\gamma</math>-crystallin fold protects conserved tryptophan residues from UV radiation damage by fast electron transfer .....</b>	<b>138</b>
A. Abstract .....	139
B. Introduction .....	140
C. Materials and Methods .....	144
1. Mutagenesis, expression and purification of recombinant HyS-Crys ...	144
2. Fluorescence spectroscopy and quantum yield determinations .....	145
3. QM-MM simulations .....	145
D. Results .....	146
1. Fluorescence emission spectra and quantum yields .....	146
2. Förster resonance energy transfer .....	158
E. Discussion .....	161
1. Conservation of fluorescence quenching by charge transfer in $\beta$ -, $\gamma$ -crystallins .....	162
2. Have crystallin folds evolved to protect Trps from UV irradiation damage by photoinduced electron transfer? .....	168
F. Conclusion .....	170
<b>Chapter Five: Concluding Discussion .....</b>	<b>171</b>
A. Conservation of fluorescence quenching of tryptophans in vertebrate $\beta\gamma$ -crystallins .....	172
B. Crystallins and UV radiation .....	173
1. UV filters .....	174
2. Fluorescence Quenching of Trps in $\beta\gamma$ -crystallins may protect themselves from UV induced photodamage .....	174
3. Interaction with $\alpha$ -crystallin .....	175
C. Concluding remarks .....	175
<b>Chapter Six: References .....</b>	<b>176</b>

<b>Chapter Seven: Appendices</b> .....	190
A. Supporting information for Chapter Two .....	191
B. Supporting information for Chapter Three .....	205
C. Supporting information for Chapter Four .....	219
<b>Curriculum Vitae</b> .....	232



## LIST OF FIGURES

<b>Chapter One: Introduction</b> .....	14
1-1 Schematic diagram of the human eye and lens .....	16
1-2 Topology diagram and ribbon structure of human $\gamma$ D crystallin .....	19
1-3 Crystal structures of $\gamma$ - and $\beta$ -crystallins .....	22
1-4 Solar radiation spectrum .....	35
<b>Chapter Two: Mechanism of the highly efficient quenching of tryptophan fluorescence in human <math>\gamma</math>D-crystallin</b> .....	42
2-1 Structure of human $\gamma$ D-crystallin displaying four tryptophans .....	46
2-2 Fluorescence emission spectra of native and denatured W42-only, W68-only, W130F/W156F, W130-only, W156-only, W42F/W68F human $\gamma$ D-crystallin .....	53
2-3 Fluorescence emission spectra of native and denatured wild type, W68F, W156F, W42F, W130F human $\gamma$ D-crystallin .....	54
2-4 Structure of Cys and Tyr-His-Tyr “cage” surrounding Trp68 and Trp156 .....	58
2-5 The interaction between Trp68 (Trp156) and two nearby waters .....	66
2-6 Residues around Trp68 and Trp156 that were mutated .....	68
<b>Chapter Three: Mechanism of the efficient tryptophan fluorescence quenching in human <math>\gamma</math>D-crystallin studied by time-resolved fluorescence</b> .....	81
3-1 Structure of human $\gamma$ D-crystallin displaying four tryptophans .....	84
3-2 Pre-exponential amplitude spectra of Trp130-only human $\gamma$ D-crystallin .....	100
3-3 Instantaneous fluorescence emission spectra of Trp130-only human $\gamma$ D-crystallin .....	102
3-4 Pre-exponential amplitude spectra of Trp42/Trp68 human $\gamma$ D-crystallin .....	108
3-5 Pre-exponential amplitude spectra of Trp42-only human $\gamma$ D-crystallin .....	109
3-6 Deconvoluted fluorescence intensity as a function of time for Trps in the N-terminal domain of human $\gamma$ D-crystallin .....	112
3-7 Deconvoluted fluorescence intensity as a function of time for Trps in the C-terminal domain of human $\gamma$ D-crystallin .....	113
3-8 Deconvoluted fluorescence intensity as a function of time for Trp42-only, Trp156-only, and Trp42/Trp156 of human $\gamma$ D-crystallin .....	117
3-9 Deconvoluted fluorescence intensity as a function of time for Trp68-only, Trp130-only, and Trp68/Trp130 of human $\gamma$ D-crystallin .....	118
3-10 Charged residues around Trp130 .....	125
3-11 Time-resolved anisotropy of Trp130-only human $\gamma$ D-crystallin .....	127
3-12 Semi-log plots of time-resolved anisotropy for Trp42-only and Trp130-only human $\gamma$ D-crystallin .....	128
3-13 Time-resolved anisotropy of Trp42-only human $\gamma$ D-crystallin .....	129

<b>Chapter Four: The <math>\gamma</math>-crystallin fold protects conserved tryptophan residues from UV radiation damage by fast electron transfer .....</b>	<b>138</b>
4-1 Crystal structure of C-terminal domain of human $\gamma$ S-crystallin and NMR structure of murine $\gamma$ S-crystallin .....	142
4-2 Fluorescence emission spectra of native and denatured Trp46-only, Trp72-only, Trp46/Trp72, Trp136-only, Trp162-only, Trp136/Trp162 human $\gamma$ S-crystallin ...	148
4-3 Fluorescence emission spectra of native and denatured wild type, W46F, W72F, W136F, W162F human $\gamma$ S-crystallin .....	149
4-4 QM-MM trajectories showing transition energies for the fluorescing state and the CT state for Trps 42 and 68 of human $\gamma$ D-crystallin.....	151
4-5 Comparison of calculated and experimental quantum yields of Trps in human $\gamma$ D-crystallin .....	154
4-6 Comparison of calculated and experimental quantum yields of Trp136 and Trp162 in human $\gamma$ S-crystallin .....	154
4-7 Comparison of calculated and experimental quantum yields of Trps in murine $\gamma$ S-crystallin .....	155
4-8 Computed electrostatic stabilization of the charge transfer state due to protein and water for Trps in human $\gamma$ D-crystallin .....	156
4-9 Computed electrostatic stabilization of the charge transfer state due to protein for Trps in human $\gamma$ D-crystallin .....	156
4-10 Two closeby waters of Trp162 in the human $\gamma$ S-crystallin .....	158
4-11 Two surrounding waters of Trp68 in the human $\gamma$ D-crystallin .....	162
4-12 Sequence alignment of $\gamma$ - and $\beta$ -crystallins .....	167

## LIST OF DIAGRAM

<b>Chapter Three: Mechanism of the efficient tryptophan fluorescence quenching in human <math>\gamma</math>D-crystallin studied by time-resolved fluorescence .....</b>	<b>81</b>
3-1 Schematic diagram of time-resolved fluorescence spectrophotometer .....	91

## LIST OF TABLES

<b>Chapter One: Introduction</b> .....	14
1-1 Conservation of aromatic residues in vertebrate $\gamma$ -crystallins .....	25
1-2 The percent transmittance of light through ocular media .....	37
<b>Chapter Two: Mechanism of the highly efficient quenching of tryptophan fluorescence in human <math>\gamma</math>D-crystallin</b> .....	42
2-1 Quantum yields of wild-type and triple Trp mutants of human $\gamma$ D-crystallin .....	55
2-2 Quantum yields of the mutants of nearby side chains surrounding Trp68 and Trp156 in the triple Trp substitution background .....	59
2-3 Quantum yields of the mutants of nearby side chains surrounding Trp68 and Trp156 in the wild-type or double Trp substitution background .....	60
2-4 Computed energy differences, electron transfer rates and quantum yields .....	63
2-5 Contribution of protein and water to shifts of the CT- <sup>1</sup> L <sub>a</sub> energy gap of each Trp .....	65
2-6 Effects of mutations on fluorescence intensity by affecting charge transfer states (in the triple Trp substitution background) .....	69
2-7 Effects of mutations on fluorescence intensity by affecting charge transfer states (in the wild-type or double Trp substitution background) .....	70
2-8 Effects of mutations on fluorescence intensity by affecting charge transfer states (in the single Trp substitution background) .....	71
<b>Chapter Three: Mechanism of the efficient tryptophan fluorescence quenching in human <math>\gamma</math>D-crystallin studied by time-resolved fluorescence</b> .....	81
3-1 Lifetimes for the single- and double-Trp containing proteins with both Trp in the same domain of human $\gamma$ D-crystallin .....	105
3-2 Lifetimes for the double-Trp containing proteins with two Trp in the different domain of human $\gamma$ D-crystallin .....	115
3-3 Energy transfer efficiencies for the two Trps in the same domain of human $\gamma$ D-crystallin .....	122
3-4 Energy transfer efficiencies for the two Trps in the different domain of human $\gamma$ D-crystallin .....	123
3-5 Parameters for the time-resolved anisotropy of Trp42 and Trp130 in human $\gamma$ D-crystallin .....	126
<b>Chapter Four: The <math>\gamma</math>-crystallin fold protects conserved tryptophan residues from UV radiation damage by fast electron transfer</b> .....	138
4-1 Quantum yields of wild-type, double and triple Trp mutants of human $\gamma$ S-crystallin .....	150
4-2 Comparison of predicted and experimental quantum yields of human $\gamma$ S-crystallin .....	153
4-3 Conformation of Trps at homologous position (Trp 68 and 156) in $\beta$ -, $\gamma$ -crystallins .....	163

## **CHAPTER ONE:**

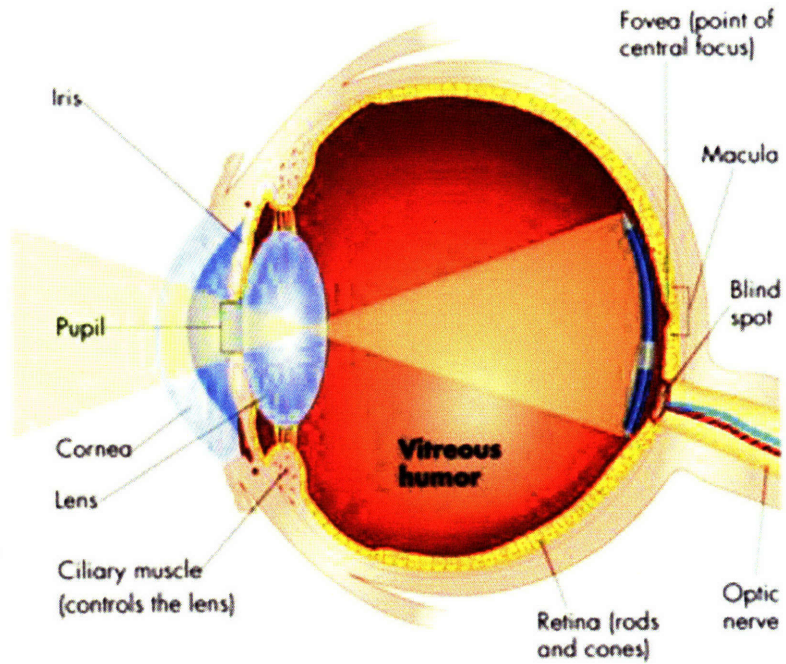
### **INTRODUCTION**

## **A. VISION AND THE OPTIC SYSTEM**

The human eye utilizes a refracting optic system (Fig. 1-1 A). The eye lens sits behind the cornea and functions to focus light onto the retina. The light induces chemical changes in the photosensitive cells of the retina and further triggers nerve impulses traveling to the brain (Oyster 1999). The lens must be transparent in the visible range of the spectrum, which places special demands on the cellular components of the lens.

The mature lens has an onion like structure and is packed with long ribbon-like fiber cells. The central portion of the lens is called the nucleus, which has the oldest cells. The outer layer is the cortex, with the younger cells. Three types of cells are present in the lens: nuclear cells in the center of the lens; cortical cells surrounding the nucleus; and a single layer of epithelial cells covering the anterior portion of the lens (Fig. 1-1B). The lens is formed during early embryonic development. The lens epithelial monocellular layer is formed from the anterior cells. The primary lens fiber cells are formed through elongation and differentiation of the posterior cells in the lens vesicle. At the last stage of differentiation, fiber cells go through a process similar to the early steps of apoptosis and lose their nuclei, mitochondria and ribosome.

**A**



**B**

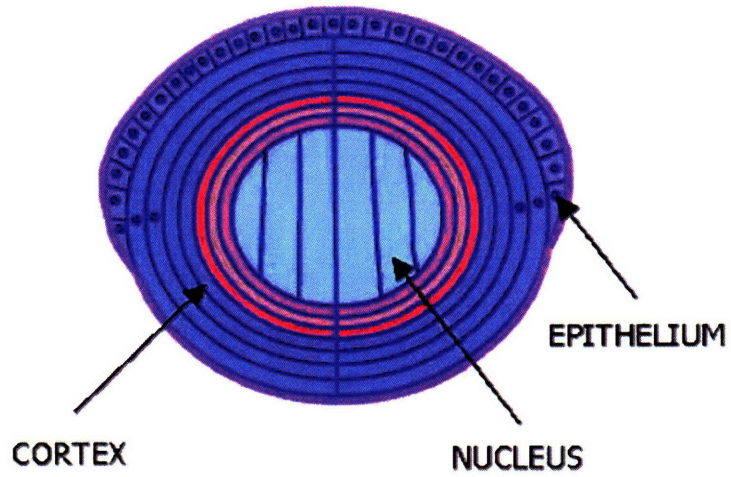


Figure 1-1. (A) A diagram of the eye. Different tissues of the eye are labeled. Courtesy of O'Connell ([www.astro.virginia.edu](http://www.astro.virginia.edu)). (B) Human eye lens in cross-section.

## B. EYE LENS CRYSTALLIN PROTEINS

The vertebrate eye lenses contain three classes of ubiquitous crystallins,  $\alpha$ -,  $\beta$ -, and  $\gamma$ -crystallins. These proteins are present in concentrations of 200-400 mg/mL. High protein concentrations are responsible for both lens refraction and transparency (Delaye M. et al., 1983). In addition to the three ubiquitous crystallins, there are several taxon-specific crystallins found in certain species, though not in primate (Oyster 1999). The mixture of different sized protein present inside the fibre cells is important to maintain the polydispersity and thus can prevent proteins from crystallization.

### 1. $\alpha$ -crystallin

$\alpha$ -crystallin is a structural protein and also functions as molecular chaperone. The molecular weight of each subunit of  $\alpha$ -crystallin is about 20kD. Two  $\alpha$ -crystallin,  $\alpha$ A and  $\alpha$ B, are present in the lens and they share about 60% sequence identity (Bloemendal and de Jong 1991). In the lens,  $\alpha$ A- and  $\alpha$ B-crystallin associate to form a polydisperse hetero-assembly with molecular weight ranged from 300 to 1200 kDa, corresponding to 15 to 55 subunits per complex. The expression of  $\alpha$ A-crystallin is limited to the lens. In contrast,  $\alpha$ B-crystallin is widely expressed and abundant in brain, heart and muscle. Both  $\alpha$ A- and  $\alpha$ B-crystallin continue to be synthesized in lens epithelial cells during lens development (Voorter et al. 1990).

The chaperone function of  $\alpha$ -crystallin is important for proper lens development. The  $\alpha$ A/ $\alpha$ B-crystallin double knock-out mouse showed severely disturbed fibre cell formation and much smaller lens compared to wild-type (Boyle et al. 2003). The  $\alpha$ B-crystallin null mouse has no lens phenotype (Brady et al. 2001) and  $\alpha$ A-crystallin null mouse has cataract formation (Brady et al. 1997).

For human, the ratio of  $\alpha$ A- to  $\alpha$ B-crystallin is about 2:1 in the younger lens and decreases to about 3:2 in the water soluble fraction of a lens in the adult (Ma et al. 1998). Due to the polydisperse property of  $\alpha$ -crystallin, the crystallization of lens  $\alpha$ -crystallin

has not been successful. The spectroscopic data suggested that the secondary structure of  $\alpha$ -crystallin subunit is primarily  $\beta$ -sheet and has less than 20%  $\alpha$ -helix. Cryo-electron microscopy indicated that  $\alpha$ -crystallin subunits associate to form a hollow sphere. The diameter of the shell of the complex is  $\sim 19$ nm and the one of the hollow internal cavity is  $\sim 8$ nm (Haley et al. 2000). The crystal structures of closely related small heat shock proteins have been solved and they contain a C-terminal “ $\alpha$ -crystallin domain” linked to different N-terminal regions (Kim et al. 1998). Unlike the tightly packed arrangement in the  $\beta\lambda$ -crystallin domain, the “ $\alpha$ -crystallin domain” fold is composed of two  $\beta$ -sheets arranged into a sandwich, surrounding by  $\alpha$ -helix and unstructured regions. For wheat heat shock protein 16.9, the monomers interact to form dimers by strand exchange. The six dimers associate to form the dodecamer (Van Montfort et al. 2001).

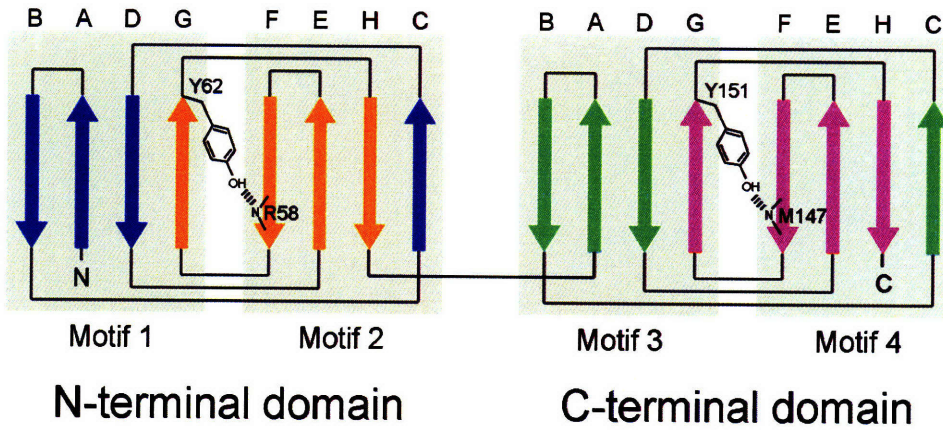
$\alpha$ -crystallins function not only as structural proteins but also as molecular chaperone by interacting with  $\beta$ -,  $\gamma$ -crystallins and other non-lens proteins (Horwitz 2000; MacRae 2000). Chaperone activity of  $\alpha$ -crystallins is important to prevent or delay cataract formation by binding and sequestering the partially unfolded or damaged crystallin proteins and therefore preventing them from aggregation.

## 2. $\beta$ - and $\gamma$ -crystallins

Different from  $\alpha$ -crystallin, the oligomeric  $\beta$ - and the monomeric  $\gamma$ -crystallins function solely as structural proteins. Both  $\beta$ - and  $\gamma$ -crystallin have two consecutive Greek key motifs consisting of eight  $\beta$ -strands in each domain (Figure 1-2). The Greek key motifs further interact to form a  $\beta$ -sandwich structure featured by  $\beta$ -strands wrapped around a central hydrophobic core.  $\beta$ - and  $\lambda$ -crystallin are characterized by high internal conformational symmetry and by a conserved folded hairpin structure in each motif.



A



B



Figure 1-2. (A) Topology diagram of the double Greek key motif fold in each domain characteristic in the  $\gamma$ - and  $\beta$ -crystallins. The strands are denoted by letters from A to H in each domain. Tyrosine corners in H $\gamma$ D-Crys, Tyr62 in the N-terminal domain and Tyr151 in the C-terminal domain, are labeled in the diagram. (B) Ribbon diagram of H $\gamma$ D-Crys. Two tyrosine corners are shown in stick representation.

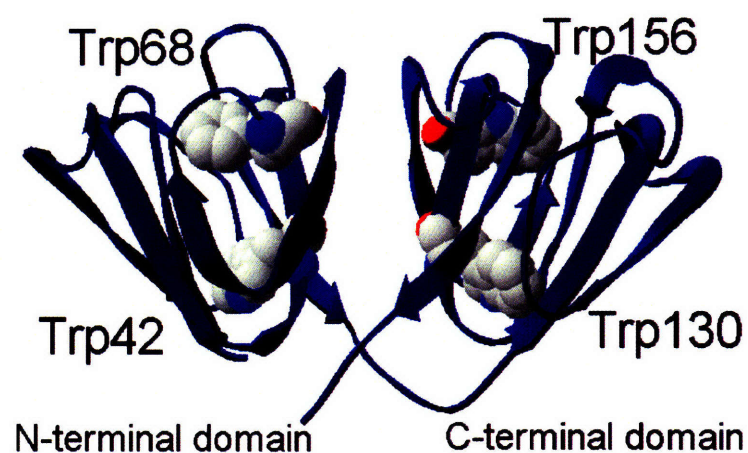
$\beta$ B1,  $\beta$ B2,  $\beta$ B3,  $\beta$ A1/A3,  $\beta$ A2, and  $\beta$ A4;  $\gamma$ A,  $\gamma$ B,  $\gamma$ C,  $\gamma$ D,  $\gamma$ E,  $\gamma$ F and  $\gamma$ S are the  $\beta\gamma$ -crystallins expressed in the mammalian lens (Bloemendal et al 2004). The  $\beta$ -crystallins are including a family of basic ( $\beta$ B1,  $\beta$ B2, and  $\beta$ B3) and acid ( $\beta$ A1/A3,  $\beta$ A2, and  $\beta$ A4) polypeptides. The main difference in sequences between  $\beta$ - and  $\lambda$ -crystallins is that  $\beta$ -crystallins have N-terminal extensions compared to  $\lambda$ -crystallins and the basic  $\beta$ -crystallins have additional C-terminal extensions.  $\beta$ B1- and  $\beta$ B3-crystallin genes are expressed early in lens development and their products are located in the lens nucleus. In contrast, the  $\beta$ B2- and acidic  $\beta$ -crystallins are expressed widely at all stages of lens development and their products are found both in the centre and the cortex of the lens (Lampi et al. 1998; Lampi et al. 2002; Ueda et al. 2002). Interestingly, in the human lens the  $\beta$ A2-crystallin is only present in trace amount.

The monomeric two-domain  $\gamma$ -crystallins are likely products of gene duplication of the Greek key motif sequence. Based on the x-ray structures of several  $\gamma$ A-F-crystallin, the N and C domain are always paired in a specific symmetrical manner around a hydrophobic interface. It is likely that the domain pairing mimics an ancestral single domain form that dimerized (Blundell et al. 1981). The  $\gamma$ D and  $\gamma$ C gene are expressed early in lens development and thus both  $\gamma$ D and  $\gamma$ C-crystallin are abundant in the lens nucleus.

The  $\gamma$ S gene is expressed post-natally and  $\gamma$ S-crystallin is localized in the lens cortex (Wistow et al. 2002). Only  $\gamma$ S-crystallin gene is common to all vertebrate of the seven mammalian  $\gamma$ -crystallin gene and it is also the only  $\gamma$ -crystallin gene found in birds. Unlike  $\gamma$ A-F-crystallins,  $\gamma$ S-crystallin is more divergent in sequence.  $\gamma$ S-crystallin has a short four amino acid long C-terminal arm, and lacks the two amino acid residue long C-terminal arm. Additionally, the linker region of the  $\gamma$ S-crystallin is one residue longer than that of the  $\gamma$ B-crystallin and two residues longer than that of the  $\gamma$ A-,  $\gamma$ C-,  $\gamma$ D-,  $\gamma$ E-, and  $\gamma$ F-crystallin. For human, the  $\gamma$ E and  $\gamma$ F gene are pseudogenes.  $\gamma$ A- and  $\gamma$ B-crystallin are expressed at a very low level in the human lens (Brakenhoff et al. 1990).

Even though  $\beta\gamma$ -crystallins have similar domain folds, there are structural differences between them. The  $\gamma$ -crystallins are solely monomeric by domain pairing intramolecularly (Figure 1-3). In contrast, the  $\beta$ -crystallins form higher order assemblies, from dimers to octamers (Wistow et al. 1983; Bax et al. 1990; Slingsby and Bateman 1990). As shown in Figure 1-3, N-terminal truncated human  $\beta$ B1-crystallin forms a dimer by domain swapping where the N-terminal domain of one monomer packs against the C-terminal domain of the other monomer (Van Montfort et al. 2003).

**A.** HyD-Crys



**B.** N-td truncated human  $\beta$ B1-crystallin

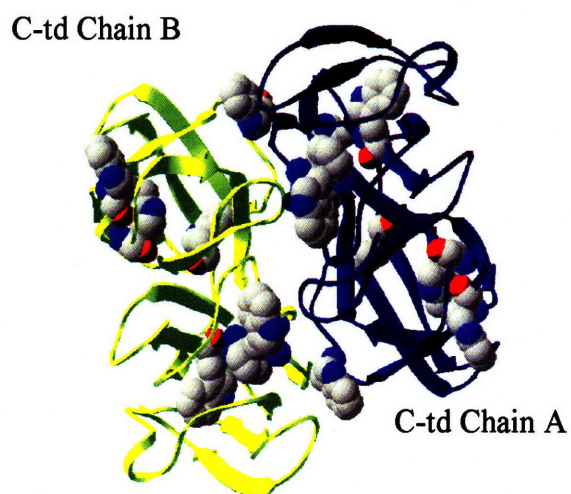


Figure 1-3. (A) Ribbon diagram showing the crystal structure of monomeric HyD-Crys (PDB code: 1HK0, Basak et al. 2003). Four buried Trps are shown in spacefill representation. (B) Ribbon structure of the dimeric N-terminal truncated human  $\beta$ B1-crystallin (PDB code: 1OKI, Van Montfort et al. 2003).

The  $\beta\gamma$  double Greek key fold is conserved in several other non-lens proteins, which belong to  $\beta\gamma$ -crystallin structural superfamily. They include human protein AIM1, EDSP from the amphibian *Cynops pyrrhogaster* (Wistow et al. 1995), microbial family members Spherulin 3a from *Physarum polycephalum* and Protein S from *Myxococcus xanthus*, yeast-killer toxin WmKT from *Williopsis mrakii* and a proteinase inhibitor SMPI from *Streptomyces nigrescens* (Bloemendal et al. 2004). These non-lens proteins share an evolutionary ancestor with the  $\beta$ - and  $\gamma$ -crystallins (Wistow 1990). It is very likely they played roles in the organism's stress response. It has been proposed that this ancestral protein was recruited to the lens in an early vertebrate. The gene encoding these proteins has been through several duplication events giving rise to the modern vertebrate  $\beta$ - and  $\gamma$ -crystallins (Shimeld et al. 2005; Wistow et al. 2005).

There is relative low sequence identity (~30%) between  $\beta$ - and  $\gamma$ -crystallins, while certain regions show high sequence conservations between the proteins. These regions presumably contribute to the important structural functions for  $\beta\gamma$ -crystallins. One example is conserved glycines located at the beginning of the B and F strands and conserved serines at the beginning of the D and H strands that hydrogen bond to peptides backbone of the A and E strands (Figure 1-1). It has been proposed that these residues stabilize the Greek key motif fold by packing the  $\beta$ -hairpin over the  $\beta$ -sheet (Blundell et al. 1981; MacDonald et al. 2005). These residues are also conserved in both Protein S and Spherulin 3a.

Both  $\beta$ - and  $\gamma$ -crystallins have high numbers of conserved aromatic residues throughout 35 vertebrate  $\gamma$ -crystallins (Table 1-1). These include four tryptophans buried inside the hydrophobic core (Figure 1-3) and a number of highly conserved tyrosines (14 Tyr in HyD-Crys). Wistow et al. (1983) proposed that interaction between the aromatic residues and neighboring cysteines or methionines may contribute to stability of the  $\gamma$ -crystallin structure. Burley and Petsko (1985) found that for globular protein, 80 percent of aromatic amino acids form networks of three or more interacting residues. The common "edge-to-face" interactions between aromatics in globular proteins, probably represents weak hydrogen bond formation and can stabilize packing of the aromatic residues (Levitt et al. 1988). The contribution of this interaction to protein stability is

relatively small (-0.6 to -1.3kcal/mol), but a network of such interactions in  $\beta$ - and  $\gamma$ -crystallins may play an important role in stability.

Among these conserved aromatic amino acids, tyrosine corner is a distinctive feature of Greek key  $\beta$ -sandwich proteins like the  $\beta$ - and  $\gamma$ -crystallins (Hemmingsen et al., 1994). This structure element is characterized by the hydroxyl group of a tyrosine on one  $\beta$ -strand forming an H-bond with backbone atoms of a  $\beta$ -strand from the opposite side of the sandwich. Contribution of the tyrosine corner to stability of four model  $\beta$ -sandwich proteins was determined by experimentally (Hamill S. et al., 2000). The tyrosine corners are conserved in Protein S but not in Spherulin 3a. Bagby et al. (1998) showed that tyrosine corner can stabilize the motif of Protein S, a two domain bacterial spore coat protein that resembles the  $\beta$ - and  $\gamma$ -crystallins. In HyD-Crys, Tyr62 in the N-terminal domain and Tyr151 in the C-terminal domain form the tyrosine corners (Fig. 1-2). These two tyrosines are largely buried and conserved throughout 35 vertebrate  $\gamma$ -crystallin sequences (Table 1-1).

Another example of an important aromatic residue is the tyrosine or phenylalanine found at position 50 in most  $\beta$ - and  $\gamma$ -crystallins, which is located in a  $\beta$ -hairpin. Human  $\beta$ B2-crystallin has a cysteine at position 50 instead of an aromatic. Macdonald et al. (2005) constructed the  $\beta$ B2-crystallin mutant C50F and observed an increase in stability compared to the wild type protein. This suggests that the aromatic residue at position 50 can stabilize the  $\beta$ -hairpin, potentially through aromatic interactions (Madonald et al., 2005).

Even though  $\beta\gamma$ -crystallins and their microbial relative proteins (such as Spherulin 3a and Protein S) share a lot of common structural features, there are some intriguing differences between them. The aromatic residues are only well conserved in  $\beta\gamma$ -crystallins but not in the non-lens proteins, Spherulin 3a and Protein S. For example, Protein S contains only six tyrosines and no tryptophan, and Spheruline 3a contains two tyrosines and only one tryptophan. The conservation of high percentages of aromatic residues may have been an evolved property in the lens proteins. Another possibility is that the aromatics were present in the ancestral protein and lost in the non-lens proteins. The high ratios of aromatic residues in  $\beta\gamma$ -crystallins may be an evolved feature to help the lens to absorb UV light and protect the retina from UV radiation.

Table 1-1. Conservation of aromatic residues among 35 vertebrate  $\gamma$ -crystallins.

<b>Residue in human <math>\gamma</math>D crystallin</b>	<b>% Identity</b>	<b>% Similarity</b>
Trp42	94	100
Trp68	80	80
Trp130	100	100
Trp156	83	89
Tyr6	89	100
Tyr16	100	100
Tyr28	94	97
Tyr45	100	100
Tyr50	54	100
Tyr55	89	97
Tyr62	100	100
Tyr92	89	97
Tyr97	34	80
Tyr133	100	100
Tyr138	100	100
Tyr143	83	97
Tyr150	100	100
Tyr153	54	86
Phe11	100	100
Phe56	80	100
Phe104	19	19
Phe115	86	100
Phe117	25	44
Phe172	25	28

### 3. *Ciona* $\beta\gamma$ -crystallin

The sea squirt *Ciona intestinalis*, belongs to invertebrate Urochordate groups. The genome of *Ciona intestinalis* has one gene coding for a single domain protein, which is homologous to vertebrate  $\beta\gamma$ -crystallin. The x-ray crystal structure of *Ciona*  $\beta\gamma$ -crystallin is very similar to that of vertebrate  $\beta\gamma$ -crystallin (Shimeld et al. 2005). *Ciona*  $\beta\gamma$ -crystallin has the typical features of Greek key motif, including a folded  $\beta$ -hairpin between the first two  $\beta$  strands, a tyrosine corner. It also has two Trps and one of them is buried inside the hydrophobic core. The similarities between the crystal structures indicate that both *Ciona*  $\beta\gamma$ -crystallin and the vertebrate  $\beta\gamma$ -crystallin have evolved from a single ancestral gene, encoding a  $\beta\gamma$ -crystallin domain, which is already expressed in the neuroecoderm of the prevertebrate ancestor.

### 4. taxon-specific crystallins

The taxon-specific crystallins are highly expressed in the lens in certain non-primate vertebrates, such as birds, reptiles, crocodiles, camel, Gecko, and etc (Piatigorsky and Wistow 1989; Wistow 1995; Van Rheede et al. 2003). The taxon-specific crystallins do not belong to the  $\alpha$ - or  $\beta\gamma$ -crystallin families. Some of them represent metabolic enzymes, including lactate dehydrogenase, aldehyde dehydrogenase, retinol-binding protein and etc. However, the taxon-specific enzyme crystallin were not recruited for metabolic or catalytic activity and instead they serve mainly as structural proteins due to their high intrinsic stability and possible “UV filter” function. It has been proposed that NAD(P)H cofactor can protect the lens against UV radiation induced oxidation (Wistow et al. 1987; van Boekel et al. 2001).



## C. TRYPTOPHAN FLUORESCENCE

Tryptophan (Trp) is the dominant intrinsic fluorophore in proteins. An important feature of intrinsic protein fluorescence is that Trp excited states are highly sensitive to their local environment. Trp has two lowest excited states,  $^1L_a$  and  $^1L_b$ .  $^1L_a$  has a large dipole compared to the ground state, and thus  $^1L_a$  is highly sensitive to environment. In most of cases,  $^1L_a$  is the emitting state in proteins (Chapter 16, Lakowics 1999).

The changes of emission spectra of Trp can be used to monitor protein conformational change, subunit assembly, substrate binding, and folding/unfolding process, all of which can change the local environment surrounding the indole ring. Additionally, Trp is also sensitive to collisional quenching, which is due to the tendency of excited state indole to donate its electrons.

Another common application of fluorescence is anisotropy measurements. Fluorescence anisotropy measurements are based on the principle of photoselective excitation of fluorophores by polarized light. If the molecules have such an orientation that their transition dipoles are parallel to the polarization direction of the light, then these molecules will be most often excited. Fluorescence anisotropy measurements can provide information on the size and shape of proteins and the rigidity of fluorophores environments (Lakowics 1999).

### 1. *Protein photobleaching*

Photobleaching is defined as the photochemical destruction of a fluorophore (Herman et al. 2006). Protein photobleaching can be attributed to the photodegradation reactions of tryptophan residues. By absorbing energy from photons, Trp residue can reach the excited singlet state and form cation radical via photoionization, and further undergoes other photo-oxidation reactions (Creed 1984). A short lived Trp cation radical

is involved in the reaction and it leads to the cleavage of the C(2-3) bond of the Trp indole ring. N-formylkynurenine is the final product of the covalent damage reaction of Trp residues (Bent and Hayon, 1975; Bryant et al., 1975).

## 2. *Quenching of tryptophan fluorescence*

One of the most intriguing phenomena related to the intrinsic fluorescence of Trp is the variation of the fluorescence quantum yields and lifetimes in different proteins. Without knowing the detailed mechanisms, this feature has been widely taken advantage to study protein conformation, protein-protein interaction, protein and substrate binding and folding/unfolding process. Several mechanisms can cause the variation of Trp quantum yields. In proteins, Trp fluorescence can be quenched by electron transfer, proton transfer, Förster resonance energy transfer and etc.

### a. *Electron transfer*

The origin of weak Trp fluorescence in some proteins has long been believed to be electron transfer from excited Trp indole ring to an amide carbonyl group (Cowgill et al. 1963; Chang et al. 1983; Colucci et al. 1990). The location of charged groups around the Trp ring and electron acceptor will strongly influence the rate of electron transfer (Callis and Vivian, 2003; Callis et al. 2007). For instance, Trp126 of the disulfide oxidoreductase DsbA has low quantum yield, only 0.012. By site directed mutagenesis and fluorescence measurements, all other candidates for electron transfer quencher residues were ruled out except for the local backbone amide groups (Hennecke et al. 1997; Sillen et al. 1999).

Other efficient electron transfer-based quenchers of Trp fluorescence are protonated His, Cys, disulfide, protonated Asp and Glu, and the amides of Asn and Gln (Chen and Barkley, 1998; Loewenthal et al. 1991; Weisenborn et al. 1996; Hennecke et al. 1997; Harris and Hudson 1990; Harris and Hudson 1991). For instance, Trp158 in T4 lysozyme has a low quantum yield of 0.013. It was suggested that its fluorescence is

quenched by a nearby Cys, an efficient quencher (Harris and Hudson, 1990; Harris and Hudson, 1991).

*b. Proton transfer*

In addition to electron transfer, hydronium ion, the side chain of Lys and protonated Tyr can quench Trp fluorescence by proton transfer mechanism (Chen and Barkley 1998; Vander 1969). Additionally, the side chains of Gln, Asn, and neutral His are relatively weak quenchers; the neutral Glu and Asp are moderate quenchers. The distance between the indole ring and these quenching side chains also affects the fluorescence intensity. Glu, Asp, and His residues usually have anomalous pKa values in proteins. It requires extra efforts to determine their ionization state, which directly affects their quenching ability (Chen and Barkley 1998).

*c. Resonance energy transfer*

Trp fluorescence can also be quenched by Förster resonance energy transfer to either Trp or cofactors. Bacteriophage T4 lysozyme has three native Trps. Trp138 (quantum yield = 0.044) and Trp158 (quantum yield = 0.013) displays low fluorescence intensity and Trp126 has higher quantum yield 0.060. Trp126 transfers its energy to both Trp138 and Trp158. The quantum yield of Trp126/Trp138 is 0.039 and that of Trp126/Trp158 is 0.030. These two values (quantum yields of Trp126/Trp138 and Trp126/Trp158) are lower than the average values of the corresponding single Trp containing proteins. Because of the resonance energy transfer (RET) from Trp126 to Trp138 and Trp158, the fluorescence intensity of Trp126 is quenched by RET (Harris and Hudson, 1990; Harris and Hudson, 1991). Trp can also transfer its energy to cofactors bound with proteins. For instance, Trp314 of horse liver alcohol dehydrogenase is quenched by coenzyme (NAD<sup>+</sup>) by resonance energy transfer (Ross et al. 1981). Similarly, Trp fluorescence of hemoglobin is quenched by heme due to the resonance energy transfer (Alpert and Lopez-Delgado 1976; Alpert et al. 1980).

#### d. *Other mechanisms*

If the Trp indole ring forms hydrogen bond with a proximate residue, its fluorescence can also be quenched. For instance, Trp138 in T4 lysozyme forms hydrogen bond with Gln105 through the indole N-H. This hydrogen bond contributes to hold Trp138 rigidly. Because Ala cannot form hydrogen bond with Trp, it was used to substitute Gln105. The substitution causes a three fold increase in fluorescence intensity (Harris and Hudson, 1991).

A weak NH $\cdots\pi$  hydrogen bond involving the indole nitrogen of the Trp and the benzene ring of a nearby Phe residue was also suggested to cause the Trp fluorescence quenching of FKBP59-1 (Rouviere et al. 1997; Craescu et al. 1996) and human interleukin-2 (Nanda et al. 2000). Nanda and Brand (2000) proposed that an NH $\cdots\pi$  hydrogen bond between Trp48 and Phe8 in a homeodomain is responsible for the quenching of Trp48. However, the F8A mutant (Subramaniam et al. 2001) still maintained low Trp fluorescence intensity, suggesting that the NH $\cdots\pi$  hydrogen bond was not responsible for Trp quenching in this homeodomain.

### 3. *Application of Time-resolved fluorescence measurements to intrinsic Trp fluorescence*

Time-resolved fluorescence measurements have been widely used to study bimolecular structure and dynamics with time scale range from a few picoseconds to hundreds of nanosecond. It has been applied to investigate the protein conformational changes, enzyme and substrate binding, DNA-protein binding, protein-protein interaction (Zheng 2005; Harley 2002; Wang 1998). Although the steady-state fluorescence measurement is more commonly used, it only reflects the intensity weighted average of the underlying decay process and is proportional to the decay components emits most of the light. Time-resolved measurement provides more molecular information that is lost during the time-average process of steady-state measurement. It is particular interesting to use time-resolved fluorescence to study the decay of tryptophan fluorescence, whose emission spectrum is very sensitive to its local environment. However, Trp fluorescence

decay is quite complex and even for the single Trp containing proteins, they normally display multi-exponential decay. It is not surprising to observe multiple components resolved from the fluorescence decay of protein containing more than one Trps (Beechem 1985). The origin of the multi-exponential decay of single Trp can be due to either the ground state heterogeneity or its excited state reactions. For some cases, heterogeneity can be attributed to the presence of different conformational isomers (rotamers) (Chen et al. 1991). There are several different circumstances accountable for the excited state reactions, including exciplex formation, solvent relaxation (Grinvald and Steinberg 1974; Toptygin et al. 2006; Toptygin et al. 2001), macromolecular conformational change, energy transfer from tryptophan to other chromophoric groups (such as heme in tuna myoglobin) (Hochstrasser and Negus 1984), etc.

Time-resolved fluorescence can also characterize segmental and overall motions of macromolecular by measuring their anisotropy decay. By using time-resolved fluorescence anisotropy measurement, we can get information about the shape of the macromolecular and its flexibility. This shape information is lost in the average process of steady-state anisotropy. Time-resolved fluorescence anisotropy has been used to investigate the protein dynamic, DNA-protein binding (Harley et al. 2002; Wang et al. 1998).

#### *4. Tryptophan fluorescence studies on crystallins*

A few fluorescence studies have been reported for crystallin proteins. For example, the fluorescence quantum yields ( $\Phi_F = 0.040 \pm 0.005$ ) and the fluorescence decay rate of bovine  $\gamma$ B crystallin were measured previously (Borkman et al. 1993; Mandal et al. 1985). However, these data only addressed the total contribution from all four tryptophans of the protein. Borkman et al. (1985) calculated the efficiency of energy transfer from tyrosine to tryptophan in bovine  $\gamma$ B-crystallin and the efficiency was found to be about 78% (Borkman et al. 1985). Some nanosecond time-resolved fluorescence studies have also been reported for crystallin proteins. Borkman described time-resolved

studies of  $\alpha$ -crystallin and bovine  $\gamma$ B-crystallin (Borkman et al. 1993; Borkman et al. 1993), which contain two and four Trp residues, respectively. In those studies the time-resolved fluorescence were fit by a biexponential function, with a long lifetime of 2-3 ns and a short lifetime of 0.3-0.5ns. However, the authors did not address the question what are the lifetimes of the individual Trp residue and whether they change in the presence of the other Trp residues or not.

## **D. CATARACT**

Cataract, the leading cause of blindness in the world, is an opacity developed in the crystalline lens of the eye or in its envelope. Currently, the only treatment for cataract is surgical removal of the affected lens. Cataract is still a major global health problem especially in the developing country. As the population ages, cataract surgery and vision loss from cataract will become an even more serious issue worldwide.

### *1. Mature-onset cataract is a protein aggregation disease*

Mature-onset cataract is a protein deposition disease. The protein inclusions recovered from cataract lenses contain all members of the  $\alpha$ -,  $\beta$ -, and  $\gamma$ -crystallins (Searle et al. 2005). The covalent damages of crystallins in the aged lens can be attributed to age and environmental and cellular stress (Hanson et al. 1998; Hanson et al. 2000; Searle et al. 2005). The prevalent damages in the insoluble crystallins of aged lenses are deamidation, disulfide bonds formation, methionine oxidation, and truncations (Hanson et al. 2000). Other common modifications of crystallins include glycation and carbamylation (Harding 2002). Additionally, a number of oxidized tryptophan residues are also identified in the cataract lenses (Searle et al. 2005; Hains and Truscott, 2007).

The conformation of crystallins in the insoluble inclusions and the molecular mechanisms of mature-onset cataract formation are still unknown. Solubilizing the protein components of the cataract requires strong denaturing conditions. The covalent damage might have induced protein partially unfolding and caused the protein aggregation and deposition in the inclusions associated with cataract. Alternatively, the covalent modification could be enhanced in the aggregated conformation trapped in the insoluble inclusions in the cataract lenses. *In vitro* studies have shown that the covalent damage of human  $\beta$ -crystallin can destabilize and partially unfold the protein (Kim et al. 2002; Lampi et al. 2006). Deamidation of the  $\alpha$ -crystallin chaperone altered the secondary and tertiary structure and decreased chaperone activity (Gupta and Srivastava 2004). The biochemical studies suggest that covalent damage on crystallins can be detrimental enough to induce protein partial unfolding. The partially unfolded intermediate is aggregation prone *in vitro* and may contribute to cataract formation *in vivo*.

## 2. Human congenital cataracts

Several cases of heritable congenital cataracts caused by mutations in the gene encoding  $\gamma$ -,  $\beta$ -, and  $\alpha$ -crystallins have been reported (Stephan et al. 1999; Kmoch et al. 2000; Mackay et al. 2002; Mackay et al. 2003). In H $\gamma$ D-Crys the mutations are R14C, P23T, R36S, R58H, E107A, and W156X (Stephan et al. 1999; Santhiya et al. 2002; Kmoch et al. 2000; Heon et al. 1999; Messina-Baas et al. 2006). *In vitro* biochemistry studies on the recombinant proteins containing these mutations have indicated that the R14C mutant caused cataract by intermolecular disulfide bonding (Pande et al. 2000), the P23T mutant by precipitation (Evans et al. 2004), and the R36S and R58H mutants by lowering the solubility and enhancing the crystal nucleation rate (Kmoch et al. 2000; Pande et al. 2001; Basak et al. 2003). In human  $\gamma$ C-crystallin, the congenital mutant T5P has an altered protein conformation, reduced solubility and stability (Fu and Liang 2002) and much less interaction with other crystallins (Liang 2004).

### *3. Diabetes and cataract formation*

Diabetes is one of the significant risk factors for cataract formation (Rowe et al. 2000). Glycation of lens proteins has been considered as one of the possible mechanisms responsible for diabetic cataract. Preferential glycation of  $\alpha$ -crystallin with decreased chaperone activity was observed in diabetic cataract human lens (Swamy et al. 1992). It suggested that  $\alpha$ -crystallin chaperone function is the primary target of glycation, which could results in the development of cataracts.

## **E. UV-B EXPOSURE AND CATARACT**

### *1. Distribution of solar radiation*

The sun is the natural source for most of the electromagnetic radiation in the atmosphere. We are constantly exposed to a portion of sunlight. The most important parts of the sunlight electromagnetic spectrum are including ultraviolet (UV), visible, and infrared (IR) regions. UV and IR are invisible to the eye and visible light allows us to see. The ozone, oxygen, water, and carbon dioxide molecules in the atmosphere filter out large portion of the solar radiation. As shown in Fig. 1-4, oxygen and the ozone layer protect us from the detrimental shorter wavelength (10 to 250nm) of the UV region (Forsyth 1969). Water and carbon dioxide decrease the levels of IR radiation. The highest intensity of the sun's radiation reaching the earth's surface is located in the visible portion (400 to 800nm). The maximum intensity of sunlight that we are exposed to (yellow region from 560 to 590nm) is corresponding to the spectral sensitivity range of the photoreceptor cells (cones) in the retina, which is responsible for daylight vision (Oyster 1999). This possibly results from an evolutionary adaptation of human eye to the sun's radiation.



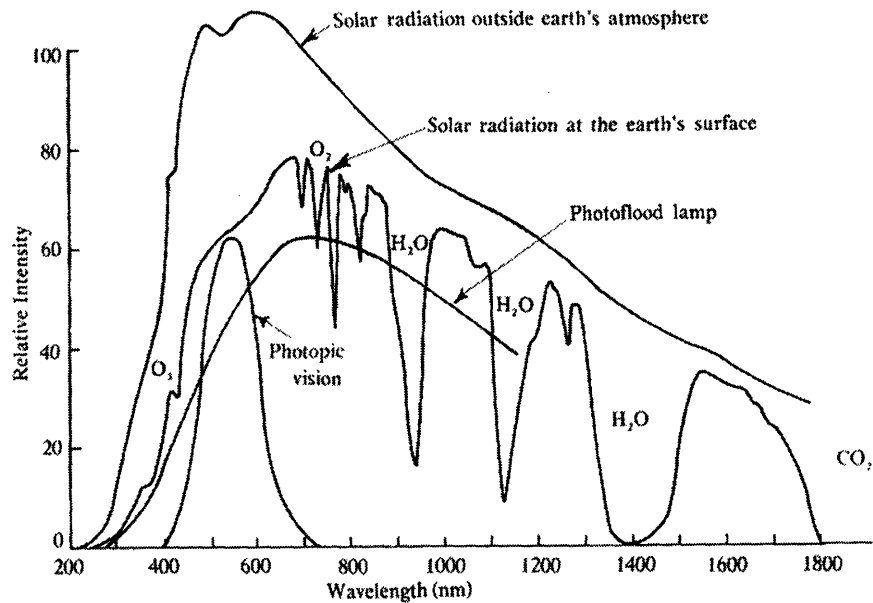


Figure 1-4. Solar radiation spectrum outside the earth's atmosphere and at sea level. The wavelength parameter for our daylight vision (photopic vision) is shown here for comparison. The detrimental ultraviolet radiation is absorbed by the ozone layer in our atmosphere. The H<sub>2</sub>O and CO<sub>2</sub> absorb significant percentages of the infrared radiation. Courtesy of "Smithsonian Physical Tables" by Forsyth W.E., in *Smithsonian Miscellaneous Collections*, 1969 Vol. 120, Washington D.C.: Smithsonian Institution Press, Tenth revised edition.

## *2. Epidemiologic studies on the effects of UV radiation*

Ultraviolet radiation is often classified into three bands based on their biological effects: UVA (400-320 nm), UVB (320-290 nm), and UVC (290-100 nm). There are some discrepancies among different epidemiologic studies on the effects of UV radiation. It is mainly due to the variations in individual behavior, which can account for up to an 18-fold difference in UV-B exposure, in the area with the same level of ambient sunlight (Robman and Taylor, 2005). Several epidemiologic studies have shown that lifetime exposure to ultraviolet radiation has a direct association with prevalence of cortical cataract (McCarty and Taylor, 2002). World Health Organization estimated that 20% of world blindness from cataract may be due to UV light exposure (WHO 2006). There are photo biological, biochemical, and experimental reasons to propose that exposure to sunlight, especially UV-B radiation, may be a cause of senile cataracts. Cataracts occur more frequently in tropical or sunny regions than in more temperate areas (Zigman et al. 1979).

Two arguments have been made to question the role of UV radiation in the cataract formation. One is the percentage of UV radiation in normal daylight is small, less than 8%. The second one is the absorption by the cornea and aqueous humor makes the amount of UV reaching the lens negligible. However, because of the very slow rate of repair, the lens is more vulnerable to repetitive irradiations. At 300nm, 14.3% of the incident light at the cornea reaches the lens (Table 1-2). Wavelengths up to 313nm may be effective in causing lens damage (Kinsey 1948; Sliney 1986). By using animal models, the induction of cataract by UV irradiation (300-400nm) has been observed (Zigman 1977). Bachem (Bachem 1956) reported that exposure to high dose of UV in the range of 295 to 315nm produces pig lens opacities while the rest of the near-UV spectrum did not. Under low dose UV radiation ( $8 \text{ kJ/m}^2$ ) at 300nm, the cortical regions of the rat lenses become cloudy only after 15min (Ayala et al. 2000). There are strong associations between the degree of ultraviolet B exposure and the risk of cortical cataracts (Taylor et al. 1988). The anterior cortical surface likely receives the most radiant energy, partially explaining the predominant findings of higher cortical cataract risk than the nuclear cataract risk induced by UV (West et al. 1998).

Table 1-2. The percent transmittance of light at different wavelength through various ocular media <sup>a</sup>

$\lambda$ (nm)	Cornea (%)	Aqueous humor (%)	Lens (%)	Vitreous humor (%)	Retina (%)
230	2.7	—	—	—	—
235	10.8	—	—	—	—
240	19.0	—	—	—	—
245	26.0	—	—	—	—
250	26.0	—	—	—	—
260	26.0	—	—	—	—
265	26.5	—	—	—	—
270	28.7	—	—	—	—
275	30.7	—	—	—	—
280	33.2	—	—	—	—
285	41.5	—	—	—	—
290	51.5	2.0	0.4	—	—
295	63.0	8.7	3.2	—	—
300	70.0	27.0	14.3	—	—
305	75.0	50.0	37.0	—	—
310	78.0	64.0	50.5	—	—
320	81.0	78.0	74.0	0.33	0.29
330	84.0	80.0	76.6	0.52	0.45
350	86.5	86.0	82.5	1.82	1.62
360	88.5	88.0	84.5	4.2	3.8
370	89.5	90.0	87.0	12.1	11.0
380	93.0	91.2	88.2	28.2	25.8
390	94.0	92.8	91.4	48.5	44.6
400	94.5	94.0	93.0	68.5	63.5
450	—	96.0	96.0	84.0	80.5
500	—	96.0	96.0	86.5	84.0

<sup>a</sup> From Kinsey 1948

*a. Proposed chemical model of UV radiation induced cataract formation*

At 295nm, 97% of the radiation absorbed by protein is by Trp residues, while Tyr absorbs only 2% and Cys absorbs 1% of the radiation (Sellers and Ghiron, 1973). Trp dominates the absorption of UV light in the lens and is probably the key species for long-term, low-level radiation damage to the lens. Trp can be elevated to an excited state, either by absorbing near UV radiation or by absorbing the energy transferred from other molecules. To return to the ground state the molecules must dissipate the energy in some way, such as by breaking chemical bonds or by reradiating photons at another frequency. These processes compete with each other. The excited state of Trp is responsible for photochemical damage. Covalent damage of Trp residues can lead to the indole ring cleavage, which might originate from the formation of a short lived Trp cation radical (Bent and Hayon 1975; Bryant et al. 1975). The final product in the Trp decomposition reaction involves the cleavage of the C(2-3) bond of the indole ring to form N-formylkynurenine (NFK) (Creed 1984). The covalent damage of Trp inside the hydrophobic core of crystallins may cause partial unfolding of the protein. The partially unfolded intermediate has been proposed to be the aggregation-prone precursor of cataract formation in the eye lens (Flaugh et al. 2005).

*b. UV damage to lens Epithelium*

The radiation can inhibit epithelial cell conversion to fiber cells (Zigman and Vaughan 1974). The lens membrane irradiated *in vivo* demonstrated a decreased ability of taking up <sup>14</sup>C-labeled amino acid (Zigman et al. 1973). Zigman et al. have proposed that the UV-induced alteration in membrane permeability caused a decrease in protein synthesis. The radiation absorbed by the membrane can further inhibit respiration and energy production, which are necessary for active amino acid transport across the membrane.

### *3. UV radiation effects on the retina*

For the normal individual, the lens filters out radiation from 293 to 400nm (Kamel and Parker 1973), which protects the retina from exposure to the radiation. Based on the data in Table 1-2, at  $\lambda = 350\text{nm}$ , only 1.6% of the radiation incident on the eye reaches the retina. The patients with lens removed are especially at risk of damage at wavelengths ranging from 293 to 400nm. For those patients, damage can become manifest at normal intensities of solar radiation exposure. Near-UV light can damage the retina photoreceptor in a lensless eye in the animal models (Li et al. 1990; Ham et al. 1982).

## **F. PROTECTIVE MECHANISM OF EYE LENS FROM UV RADIATION**

### *1. UV filters*

Many mammals have pigmented corneas, or colored oil droplets in the cones as well as colored lenses. The human eye is quite different and only its lens contains pigment (Kurznel et al. 1977). This pigment is present since birth. In 1973, Van Heyningen identified the pigment in the human lens, including O- $\beta$ -D-glucoside of 3-hydroxykynurenine, 3-hydroxykynurenine, kynurenine and others (Van Heyningen 1973). Van Heyningen proposed that these pigments are formed in the lens from precursors such as tryptophan and its metabolic products (Van Heyningen 1973).

Lens pigments serve a protective role in filtering out near-UV radiation from reaching the retina. The retina of the eye with the lens removed is 1000 times more sensitive to radiation of 365nm wavelength. The sensitivity of the rods and cones of the retina is extended to wavelength to wavelength down to 300nm (Wald 1952). Indirected evidence pointing to the protective role of the lens pigments has been shown by Van Heyningen (1973). She demonstrated a variation in the composition of the lens pigments with respect to age. The retina of the newborn is immature, thus it is reasonable to expect the effects of UV radiation to be especially harmful in the newborn. Even though the lens

pigments present in the child are the same as those present in the adult. The amount of o- $\beta$ -D glucoside of 3-hydroxykynurenine was increased for ages 0-7 years, and steadily decreased as the human lens ages.

## *2. Other protective mechanisms of the lens*

The eye lenses of diurnal geckos contain ~12%  $\iota$ -crystallin, which belongs to taxon-specific crystallin.  $\iota$ -crystallin is a cellular retinol-binding protein. 3,4-didehydroretinol, the cofactor bound with  $\iota$ -crystallin, gives the Gecko's lens a yellow color. It can absorb the UV light and thus protect the retina from the radiation with short wavelength (Werten et al. 2000).

Some NAD(P)H dependent metabolic enzymes were recruited into cornea or vertebrate lenses to function as structure proteins. NAD(P)H was proposed to protect other proteins against UV-induced damage by the competitive absorption of UVB (Estey et al. 2007). Similar protective function has also been proposed for other fluorophores in the eye system. Dillon et al. observed a very short fluorescence lifetime (<10ps) for 3-hydroxyl kynurenine in the lens and suggested that this fast fluorescence decay may provide a harmless deactivation path for the ambient UV radiation (Dillon and Atherton 1990; Dillon et al. 1990).

## **G. SUMMARY OF THESIS**

In this thesis I have used steady-state and time-resolved fluorescence measurement to study the mechanism of Trp fluorescence quenching in HyD-Crys (Chapters 2 and 3). Similar fluorescence quenching mechanism is also identified in human  $\gamma$ S-crystallin by experiments and computational studies (Chapter 4). The conservation of electrostatically enabled excited state quenching by electron transfer to the backbone amide indicated that the quenching may be an evolved property of the  $\beta\lambda$ -crystallins fold that allows them to absorb ultraviolet light while suffering minimal photodamage.

## NOTE ON THE ORGANIZATION OF THE THESIS:

1. The descriptions of the Materials and Methods are with each chapter.
2. To help the reader keep track of the special relationships among the four tryptophans in H $\gamma$ D-Crys and H $\gamma$ S-Crys, we will write the two concerved efficiently quenched Trps in italics, such as *Trp68* and *Trp156* in H $\gamma$ D-Crys and *Trp72* and *Trp162* in H $\gamma$ S-Crys. The other two moderately fluorescent will be in regular text, such as Trp42 and Trp130 in H $\gamma$ D-Crys and Trp46 and Trp136 in H $\gamma$ S-Crys.
3. All the site directed mutagenesis, protein expression and purification, and fluorescence measurements were carried out by the author. The QM-MM calculations were done by Prof. Callis P.R. However, since many of the experiments of the fluorescence measurements were designed to test or support the theoretical calculations, I have included the results of QM-MM calculations in the results and discussion sections directly.
4. For the time-resolved fluorescence measurements, I spent about three months at Johns Hopkins University making the measurement in Prof. Ludwig Brand's laboratory.

## CHAPTER TWO:

### MECHANISM OF THE HIGHLY EFFICIENT QUENCHING OF TRYPTOPHAN FLUORESCENCE IN HUMAN $\gamma$ D CRYSTALLIN<sup>1</sup>

---

<sup>1</sup> This work includes results of collaboration with Prof. Callis P.R. at Montana State University.

**Reprinted from:** Chen, J., Flaugh, S.L., Callis, P.R., and King, J. (2006) Mechanism of the highly efficient quenching of tryptophan fluorescence in human  $\gamma$ D-crystallin. *Biochemistry*. 45(38): 11552-63



## A. ABSTRACT

Quenching of the fluorescence of buried tryptophans (Trps) is an important reporter of protein conformation. Human  $\gamma$ D-crystallin (H $\gamma$ D-Crys) is a very stable eye lens protein that must remain soluble and folded throughout the human lifetime. Aggregation of covalently damaged H $\gamma$ D-Crys is associated with the prevalent eye disease mature-onset cataract. H $\gamma$ D-Crys has two homologous  $\beta$ -sheet domains, each containing a pair of highly conserved buried tryptophans. The overall fluorescence of the Trps is quenched in the native state despite the absence of the metal ligands or cofactors. We report the results of detailed quantitative measurements of the fluorescence emission spectra and the quantum yields of 51 site-directed mutants of H $\gamma$ D-Crys. From fluorescence of triple Trp to Phe mutants, *Trp68* and *Trp156* are found to be extremely quenched, with quantum yields close to 0.01. Trp42 and Trp130 are moderately fluorescent, with quantum yields of 0.13 and 0.17, respectively. In an attempt to identify quenching and/or electrostatically perturbing residues, a set of candidate amino acids around *Trp68* and *Trp156* were substituted with neutral or hydrophobic residues. None of these mutants showed significant changes in the fluorescence intensity compared to their own background. Hybrid quantum mechanical-molecular mechanical (QM-MM) simulations with the four different excited Trps as electron donors strongly indicate that electron transfer rates to the amide backbone of *Trp68* and *Trp156* are extremely fast relative to those for Trp42 and Trp130, in agreement with the quantum yields measured experimentally and consistent with the absence of a quenching sidechain. Efficient electron transfer to the backbone is possible for *Trp68* and *Trp156* because of the net favorable location of several charged residues and the orientation of nearby waters, which collectively stabilize electron transfer electrostatically. The fluorescence emission spectra of single and double Trp to Phe mutants provide strong evidence for energy transfer from Trp42 to *Trp68* in the N-terminal domain and from Trp130 to *Trp156* in the C-terminal domain. The backbone conformation of Trps in H $\gamma$ D-Crys may have evolved in part to enable the lens to become a very effective UV filter, while the efficient quenching provides an in situ mechanism to protect the Trps of the crystallins from photochemical degradation.

## B. INTRODUCTION

The ~30-fold variation of intrinsic Trp fluorescence intensity and lifetime in proteins is widely exploited to follow changes in protein structure such as folding/unfolding, substrate or ligand binding, and protein-protein interactions (Lakowicz 1999; Beechem et al. 1985; Eftink 1991; Smirnov et al. 1997; Prendergast 1991). The origin of weak Trp fluorescence in some proteins has long been believed to be electron transfer from excited Trp to an amide carbonyl group (Cowgill et al. 1963; Chang et al. 1983; Colucci et al. 1990, Chen et al. 1990). Recent experiments affirm that the local backbone amides can be efficient quenchers in peptides (Pan et al. 2006) and in proteins (Sillen et al. 1997). Other efficient amino acid electron transfer-based quenchers of Trp fluorescence are protonated His, Cys, disulfide, protonated Asp and Glu, and the amides of Asn and Gln (Chen and Barkley 1998; Loewenthal et al. 1991; Weisenborn et al. 1996; Hennecke et al. 1997; Harris and Hudson 1990; Harris and Hudson 1991). In addition, hydronium ion, Lys and Tyr can quench Trp fluorescence by proton transfer (Chen and Barkley 1998; Vander 1969). Met has also been implicated as a fluorescence quencher (Kuznetsova 1998; Yuan et al. 1998). An unusual NH... $\pi$  hydrogen bond involving the indole nitrogen of the Trp and the benzene ring of a nearby Phe residue was also suggested to cause the Trp fluorescence quenching of FKBP59-1 (Rouviere et al. 1997; Craescu et al. 1996) and human interleukin-2 (Nanda et al. 2000). Nanda and Brand (2000) proposed that an NH... $\pi$  hydrogen bond between Trp48 and Phe8 in a homeodomain is responsible for the quenching of Trp48. However, the F8A mutant (Subramaniam et al. 2001) still maintain low Trp fluorescence intensity, suggesting that the NH... $\pi$  hydrogen bond was not responsible for Trp quenching in this homeodomain.

Despite these considerable investigations, a reliable understanding of when a particular quenching process will be exceptionally efficient in a protein has been elusive. A reasonable basis for the large Trp quantum yield variation using quantum mechanics-molecular mechanics (QM-MM) simulations has recently been presented (Callis and Liu 2004; Callis and Vivian 2003; Kurz et al. 2005; Liu et al. 2005; Xu et al. 2006). The

method keys on the average energy and fluctuations of the lowest Trp ring-to-amide backbone charge transfer (CT) state relative to the fluorescing state. The latter can be assigned as the  $1L_a$  state in protein environments (Callis 1997). The energy difference (CT- $^1L_a$  gap) is monitored during dynamics trajectories. The energy, fluctuations, and relaxation of normally high lying CT states are extremely sensitive to protein environment (local electric field direction and strength). Charged or polar environmental residues (including water) can either stabilize or destabilize the charge transfer and thus affect quantum yields (Callis and Liu 2004; Callis and Vivian 2003; Vivian and Callis 2001). When the energy gap is large and fluctuations small, the probability that the fluorescing and CT states will have the same energy is low. Electron transfer (the quenching process) is only possible when the fluorescing and CT states have the same energy.

The  $\alpha$ -,  $\beta$ -, and  $\gamma$ -crystallins are the main protein components of the mammalian lens. The  $\beta$ -, and  $\gamma$ -crystallins are structural proteins, while  $\alpha$ -crystallin is molecular chaperone and a structural protein (Horwitz 1992; Singh et al. 1995). The oligomeric  $\beta$ - and the monomeric  $\gamma$ -crystallins have similar structures that contain four  $\beta$ -sheet Greek key motifs separated into two domains (Lapatto et al. 1991; Basak et al. 2003). High protein concentrations are responsible for both lens refraction and transparency (Delaye et al. 1983). Because there is no protein turnover in the lens, the crystallins have to remain soluble and stable throughout the life (Oyster C. 1999). Cataract, the leading cause of blindness worldwide (Hyman 1987; Rahmani et al. 1996), may be due to aggregation and deposition of partially unfolded crystallins (Bloemendal et al. 2004). Cataracts removed from the human lens are composed of different species of aggregated crystallins, including covalently damaged human  $\gamma$ D crystallin (H $\gamma$ D-Crys) (Hanson et al. 2000). The oxidation species of *Trp156* in H $\gamma$ D-Crys has been identified from aged cataractous human lens by mass spectrometry (Searle et al. 2005). Mutations in the gene encoding H $\gamma$ D-Crys have been found to cause juvenile-onset cataract, further supporting a role of H $\gamma$ D-Crys in cataractogenesis (Pande et al. 2000; Nandrot et al. 2003).

H $\gamma$ D-Crys is a two domain, 173 amino acid protein that is predominantly found in the lens nucleus (Oyster 1999). The structure of the protein has been solved at 1.25 Å resolution by Basak et al. (Basak et al. 2003). This monomeric protein is composed of antiparallel  $\beta$ -sheets arranged in four Greek key motifs. The two domains show high levels of structural and sequence homology. H $\gamma$ D-Crys has four intrinsic buried Trps at positions 42 and 68 in the N-terminal domain and 130 and 156 in the C-terminal domain (Fig. 2-1, Basak et al. 2003).

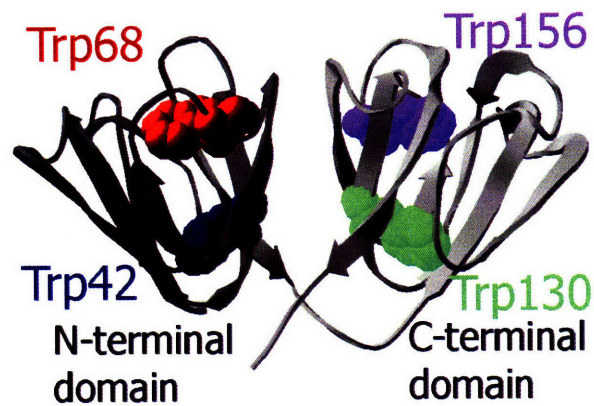


Figure 2-1. Ribbon structure of wild-type H $\gamma$ D-Crys showing Trp42 and *Trp*68 in the N-terminal domain, and Trp130 and *Trp*156 in the C-terminal domain (PDB 1HK0).

H $\gamma$ D-Crys is considerably more fluorescent in the denatured state than in the native state, despite the absence of metal ligands or cofactors (Kosinski-Collins and King 2003). Native state fluorescence quenching has also been observed for other  $\beta$ - and  $\gamma$ -crystallins (Kim et al. 2002; Wenk et al. 2000). To investigate which Trps are involved in the quenching phenomenon, Kosinski-Collins et al. (Kosinski-Collins et al. 2004) constructed triple Trp mutants, each with three of the four endogenous Trps substituted with Phe. Based on the fluorescence spectra of the triple Trp mutants, it was found that *Trp68* and *Trp156* displayed extremely low fluorescence intensity, whereas *Trp42* and *Trp130* showed much higher fluorescence intensity (Kosinski-Collins et al. 2004).

Ultraviolet radiation is considered one of the risk factors for cataract formation (Oliva et al. 2005). Although the cornea filters out almost all UV radiation of wavelengths shorter than 295nm, the crystallin proteins within the lens are continuously exposed to ambient UV radiation of wavelengths longer than 295nm throughout life (Colitz et al. 2005). Photochemical reactions of Trps in the lens crystallins correlate with cataract formation (Kurzel et al. 1973; Borkman et al. 1993). Trp, His, Met and Cys residues have been identified as photo-oxidization targets in bovine  $\gamma$ B crystallin that was UV irradiated in vitro (Hott et al. 1992). N-formylkynurenine was found to be the main photoproduct of Trp from UV irradiated protein (Spodheim-Maurizot M. et al. 1985), which may result from an electron ejection mechanism (Hibbard L.B. et al. 1985). The photolysis reaction of UV-irradiated Trp may originate from the excited singlet state, and may compete with fluorescence emission (Kurzel et al. 1973; Borkman et al. 1993). The quenching of Trp fluorescence in H $\gamma$ D-Crys shortens the lifetime of the excited state, and thus may minimize the chance of photoreaction, and protect Trp residues from UV damage.

The fluorescence quantum yield ( $\Phi_F= 0.040\pm 0.005$ ) and the fluorescence decay rate of bovine  $\gamma$ B crystallin have been previously measured (Borkman R. et al. 1993; Mandal K. et al. 1985). Their study measured the total quantum yield of all four Trps of the protein but it did not address their individual contributions. In this chapter, we report the detailed quantitative measurement of the individual fluorescence emission spectra and

the quantum yields of the four Trps in HyD-Crys. From characterization of single, double and triple Trp mutants, partial Förster resonance energy transfer from the strongly (Trp42 and Trp130) to the weakly (*Trp68* and *Trp156*) emitting Trp of the same domain was observed. A thorough search for a quenching residue through construction of mutants in different Trp backgrounds failed to identify plausible electron transfer to a neighboring residue. Similarly, substitution of charged and polar residues around *Trp68* and *Trp156* did not show a significant effect on the fluorescence intensities. The QM-MM simulations reported here decisively support highly efficient quenching by electron transfer from the excited Trp ring to its backbone amide as the reason for the weak fluorescence from *Trp68* and *Trp156*. This is enabled by the large collective stabilization of the CT state by several charged residues and nearby waters. The corresponding CT states of Trp42 and Trp130, in contrast, show less environmental stabilization, and are predicted to have much higher quantum yields that are nevertheless lower than the maximum possible.

## C. MATERIALS AND METHODS

### 1. *Mutagenesis, expression, and purification of recombinant HyD-Crys*

Primers encoding the substitutions described below (IDT-DNA) were used to amplify a pQE.1 plasmid encoding the HyD-Crys gene with an N-terminal 6-His tag (Kosinski-Collins et al. 2004). The single, double and triple Trp to Phe substitutions were constructed by Kosinski-Collins et al. (Kosinski-Collins et al. 2004). Forty-one site-directed mutants in the different Trp backgrounds were constructed at seventeen unique positions. These are summarized below in Figs. 4 and 6 and Tables 2, 3, 6, 7 and 8. The mutants C32S, N33A, Y55F, Y62F, Y55F/Y62F, D64S, H65Q, Q66A, Q67A, M69S, D73S and R79S were constructed in the W68-only background. The mutants H121Q, Y143F, Y150F, Y143F/Y150F, R152S, Y153Q, and D155S were constructed in the *W156-only* background. The mutants D64S, H65Q, M69S, D73S and R79S were

constructed in the W130F/W156F background. The mutants H121Q and Y153Q were constructed in the W42F/W68F background. The mutants D64S, H65Q, M69S, D73S and R79S were constructed in the W42F background. The mutant Y153Q was constructed in the W130F background. The mutants D64S, H65Q, M69S, D73S, R79S, H121Q, H65Q/H121Q, Y153Q, R79S/Y153Q were constructed in the wild-type background. All of the mutations were confirmed by DNA sequencing (Massachusetts General Hospital).

The wild-type and mutant HyD-Crys proteins were expressed by *E. coli* M15 [pREP4] cells. All of the mutants accumulated as native-like soluble proteins. The proteins were purified by affinity chromatography using a Ni-NTA resin (Qiagen) as previously described (Kosinski-Collins et al. 2004). The purities of the proteins were confirmed by SDS-PAGE.

## 2. *Fluorescence spectroscopy*

The emission spectra of native proteins were recorded in S buffer (10mM sodium phosphate, 5mM DTT, 1mM EDTA at pH 7.0). Buffer conditions for denatured proteins were S buffer plus 5.5M GuHCl. Proteins were incubated in the denaturing buffer at 37°C for six hours prior to measuring fluorescence spectra. Concentrations of the wild-type and mutant His-tagged proteins were determined by measuring absorbance at 280nm using extinction coefficients calculated with ProtParam (ExPASy). Fluorescence emission spectra were collected at 37°C using a Hitachi F-4500 fluorescence spectrophotometer equipped with a circulating water bath. Intrinsic Trp fluorescence emission spectra of all the proteins were measured in the range of 310 to 420nm using an excitation wavelength of 300nm. A protein concentration of 1.38µM was used for all experiments except for the quantum yield and energy transfer experiments. The protein concentrations used for experiments described in the results and discussion section, “*Resonance energy transfer between the Trps within each domain*”, were 2.75µM. The buffer signal was subtracted from all spectra.

To measure how much the fluorescence intensity increased or decreased due to mutations in the different Trp backgrounds, the fluorescence emission spectra of native and unfolded proteins were recorded from three sets of samples prepared in parallel. The average value of the integrated fluorescence intensity was calculated and signals of the native proteins were normalized for concentration by comparison with intensities of the unfolded protein spectra. The increase or decrease in quantum yields was calculated by comparing quantum yields of the mutants with those of their respective Trp backgrounds.

### 3. *Quantum Yield Determinations.*

Quantum yields were calculated according to equation (1) (Lakowicz 1999):

$$Q = Q_R \frac{I}{I_R} \frac{OD_R}{OD} \frac{n^2}{n_R^2} \quad (1)$$

where Q and QR are the quantum yield of the protein and reference (L-Trp in water), I and IR are the integrated fluorescence intensities of the protein and reference, OD and ODR are the optical densities of the protein and reference at the excitation wavelength, and n and nR are the refractive indices of the protein and reference solutions (Lakowicz, 1999; Chen, 1967). The absolute quantum yield of Trp in water was taken to be 0.14 (Chen, 1967). The buffer for protein and Trp was S buffer at 37°C. Quantum yields of the four Trps in HyD-Crys were measured using the proteins W42-only, W68-only, W130-only and W156-only. Because there are 14 tyrosines in HyD-Crys, which may cause uncertainty in quantum yield measurements, an excitation wavelength of 300 nm was used in order to minimize tyrosine fluorescence. The emission spectra of wild-type HyD-Crys and the triple Trp mutants have maximal emission wavelengths that are close to the blue area (Table 2-1). There were significant portions of the blue edge of the emission spectra that could not be observed using a 300 nm excitation wavelength. We estimated the unobservable areas of the protein spectra by matching the longer wavelength areas of protein spectra with spectra of 3-methyl indole (3MI) in different solvent systems. The solvent system used to match 3MI spectra with the spectra of wild-type HyD-Crys was Cyclohexane: Dioxane (70:30), and the spectra of 3MI in Cyclohexane: Dioxane (83:17) were used to match the spectra of W42-only and W130-only. The spectra of 3MI in



Methanol: Dioxane (25:75), were used to match the spectra of *W68-only*, and the spectra of 3MI in Methanol: Dioxane (10:90) were use to match the spectra of *W156-only*.

#### 4. *QM-MM simulations (carried out by Prof. Callis P.R. at Montana State University)*

The hybrid QM-MM method used in this work has been described in recent publications (Callis and Liu 2004; Callis and Vivian 2003; Kurz et al. 2005; Liu et al. 2005; Xu et al. 2006) for applications to Trp fluorescence quenching in proteins. The method grew from an earlier QM-MM procedure used to predict the fluorescence wavelengths of Trp in proteins (Vivian and Callis 2001). Briefly, the QM method is Zerner's INDO/S-CIS method, (Ridley and Zerner 1973), modified to include the local electric fields and potentials at the atoms. The MM part is Charmm (version 26b) (MacKerell et al. 1998). Hydrogens were added to the crystal structure (PDB code 1HK0) and the entire protein solvated within a 30 Å radius sphere of TIP3 explicit water. The waters were held within the 30 Å radius with a quartic potential. The quantum mechanical part includes the selected Trp and the amide of the preceding residue, capped with hydrogens, N-formyltryptophanamide. The electric potential due to all non-QM atoms in the protein and solvent is calculated with dielectric constant = 1 for each QM atom and added to the QM Hamiltonian.

## D. RESULTS

### 1. *Fluorescence emission spectra and quantum yields*

Fluorescence emission spectra of native and denatured wild-type HyD-Crys and the important Trp to Phe mutants are shown in Figs. 2-2 and 2-3. An excitation wavelength of 300 nm was used in order to minimize tyrosine fluorescence. Instrument settings were the same for all spectra such that the areas under the curves are proportional to quantum yields. Fig 2-2 A compares fluorescence spectra of native and denatured double and triple Trp mutants that give fluorescence only from Trps in the N-terminal domain (Trps 42 and/or 68). Fig. 2-2 B does the same for the C-terminal domain (Trps 130 and/or 156). Fig. 2-3 A compares native and denatured wild type and single mutants of the weakly emitting Trps (W68F and W156F). Fig. 2-3 B does the same for the strongly emitting Trps (W42F and W130F).

Figs 2-2 A and 2-2 B show that the fluorescence from *Trps 68* and *156* is extremely weak compared to that of Trps 42 and 130. The maximal emission wavelength for *Trps 68* and *156* is red shifted approximately 10 nm compared to Trp42 and Trp130, consistent with a somewhat more polar environment for the former (*Trps 68* and *156*).

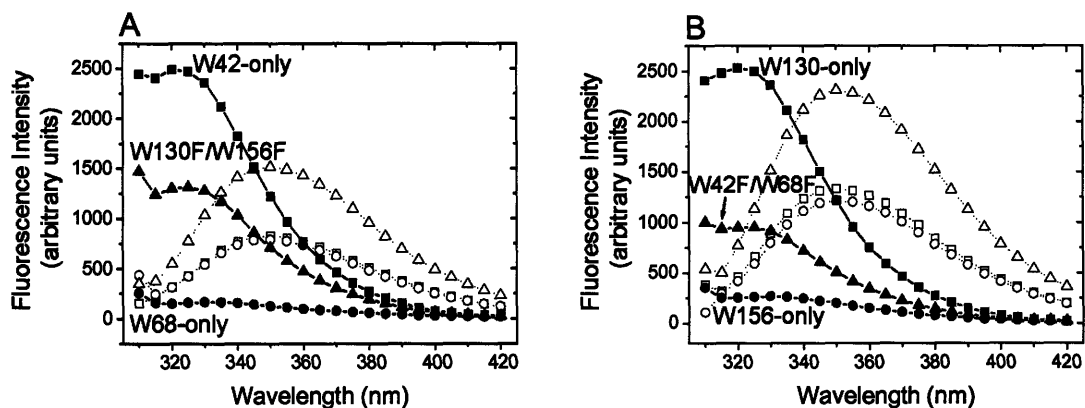


Figure 2-2. (A) Fluorescence emission spectra of native W42-only (■), W68-only (●) and W130F/W156F (▲) and denatured W42-only (□), W68-only (○) and W130F/W156F (Δ). (B) Fluorescence emission spectra of native W130-only (■), W156-only (●) and W42F/W68F (▲) and denatured W130-only (□), W156-only (○) and W42F/W68F (Δ).

The solid lines represent the emission spectra of native proteins and the dotted lines represent the unfolded proteins. An excitation wavelength of 300nm was used for samples of 2.75 $\mu$ M protein at 37°C. Native proteins were incubated in S buffer and unfolded proteins were incubated in S buffer plus 5.5M GuHCl for six hours at 37°C before the measurements. The buffer signal was subtracted from all spectra.

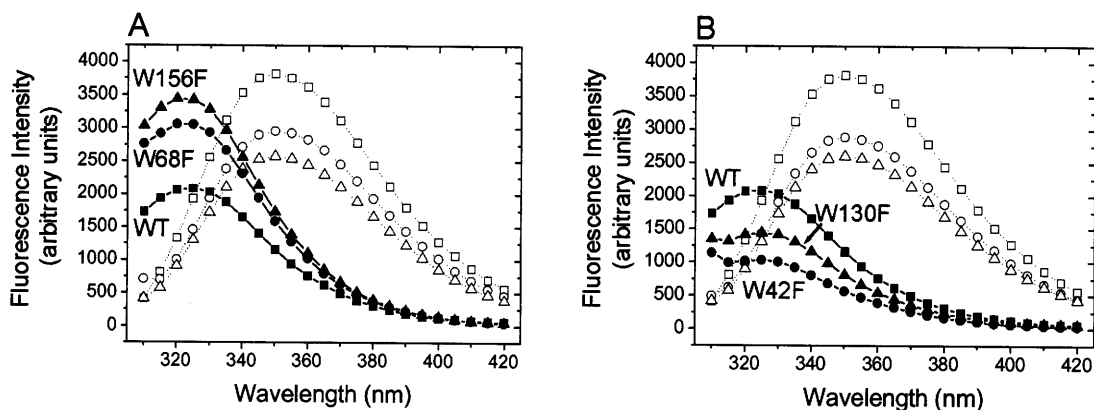


Figure 2-3. (A) Fluorescence emission spectra of native wild type (WT) (■), W68F (●) and W156F (▲) and denatured wild type (□), W68F (○) and W156F (△). (B) Fluorescence emission spectra of native wild type (■), W42F (●) and W130F (▲) and denatured wild type (□), W42F (○) and W130F (△). The solid lines represent the emission spectra of native proteins and the dotted lines represent the unfolded proteins. An excitation wavelength of 300nm was used for samples of 2.75 $\mu$ M protein at 37°C. Native proteins were incubated in S buffer and unfolded proteins were incubated in S buffer plus 5.5M GuHCl for six hours at 37°C before recording emission. The buffer signal was subtracted from all spectra.

Figs 2-2 A and 2-2 B show that the fluorescence from *Trps 68* and *156* is extremely weak compared to that of *Trps 42* and *130*. The maximal emission wavelength for *Trps 68* and *156* is red shifted approximately 10 nm compared to *Trp42* and *Trp130*, consistent with a somewhat more polar environment for the former (*Trps 68* and *156*).

Quantitative determinations of the quantum yields for wild type and the triple mutants are shown in Table 2-1. The quantum yields for *Trp42* and *Trp130* were found to be nearly 20 times higher than those of *Trp68* and *Trp156*. The average quantum yield for the triple mutants is 0.080, somewhat higher than that of the wild type, which is 0.058.

Table 2-1. The maximum fluorescence emission wavelengths and quantum yields of wild-type and triple Trp mutants

Protein	Maximum Em Wavelength (nm)	Quantum yield
Wild type	326	0.058 ± 0.006
W42-only	322	0.13 ± 0.01
W68-only	335	0.0076 ± 0.0008
W130-only	322	0.17 ± 0.02
W156-only	332	0.0099 ± 0.001

## 2. Resonance energy transfer between the two Trps within each domain

The fluorescence spectra in Figs 2-2 and 2-3 for single, double and triple Trp mutants provide convincing evidence for intradomain Förster resonance energy transfer (FRET), with the donor being the more fluorescent Trp in each domain (Trp42 in the N-terminal domain and Trp130 in the C-terminal domain). When *Trp68* or *Trp156* were individually substituted with Phe, the integrated fluorescence intensity of W68F was 38% higher than wild type and the integrated fluorescence intensity of W156F was 52% higher than wild type (Fig. 2-3 A). In contrast, the integrated fluorescence intensities of W42F and W130F decreased 50% and 29% compared to wild type, respectively (Fig. 2-3 B). These observations are consistent with Trp42 and Trp130 acting as energy donors. A considerable fraction of the excitation energy is not emitted because it is transferred to the weakly emitting partner. Because Trp42 and Trp130 make the major contributions to the overall fluorescence intensity of wild-type HyD-Crys, substituting them with Phe caused a decrease in fluorescence intensity (Fig. 2-3).

Fluorescence emission spectra of double Trp mutants were measured and the results further support FRET. Fluorescence intensity of the double mutant W130F/W156F revealed the interaction of Trp42 and *Trp68* in the N-terminal domain. Fluorescence intensity of this mutant did not equal the simple addition of W42-only and *W68-only* fluorescence, but was instead about 43% lower than the intensity of W42-only and 6 times higher than the intensity of *W68-only* (Fig. 2-2 A). A similar result was found for the mutant W42F/W68F, which revealed the interaction between Trp130 and *Trp156* in the C-terminal domain (Fig. 2-2 B). The intensity of W42F/W68F was 59% lower than the intensity of W130-only and 3 times higher than *W156-only*.

Comparison of the spectrum of the double Trp mutant W42F/W68F (containing Trps 130 and 156) in Fig 2-2 B with the single Trp mutant W42F (containing Trps 130, 156, and 68) in Fig 2-3 B shows that there is no significant energy transfer from the highly fluorescent Trp130 in the C-terminal domain to the weakly fluorescent *Trp68* in the N-terminal domain. If there is interdomain energy transfer from Trp130 to *Trp68*, the

fluorescence intensity of double Trp mutant W42F/W68F (containing Trps 130 and 156 but not potential energy acceptor *Trp68*) should be higher than the single Trp mutant W42F (containing Trps 130, 156 and 68). Because the fluorescence intensities of W42F/W68F and W42F are very similar, there is probably little or no interdomain energy transfer from Trp130 to Trp68. Similarly, the comparison of the double Trp mutant W130F/W156F (containing Trps 42 and 68) in Fig 2-2 A and single Trp mutation W130F (containing Trps 42, 68 and 156) in Fig 2-3 B shows that there is little or no energy transfer from Trp42 in the N-terminal domain to *Trp156* in the C-terminal domain.

### 3. Investigation of nearby side chain contributions to Trp quenching

Quenching of the buried *Trp68* and *Trp156* in H $\gamma$ D-Crys could be due to immediate interaction with the side chains of nearby amino acids (Chen and Barkley, 1998). In the original  $\gamma$ -crystallin structure paper, Wistow et al. (Wistow et al. 1983) proposed that interaction between the aromatic residues and neighboring cysteines or methionines may contribute to stability of the  $\gamma$ -crystallin structure. The contributions of charged or polar residues around *Trp68* and *Trp156* to fluorescence quenching were determined by substitution with neutral or hydrophobic residues. The residues mutated were a cysteine nearby *Trp68* and the Tyr-His-Tyr triads around both *Trp68* and *Trp156* (Fig. 2-4; Table 2-2 and 2-3).

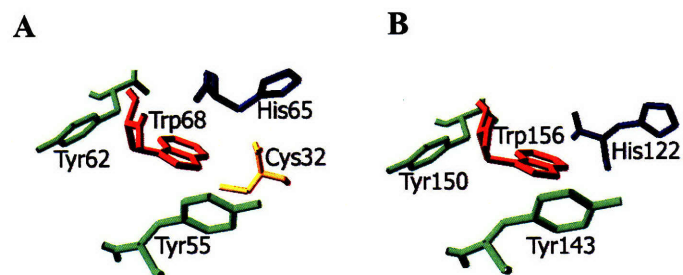


Figure 2-4. The crystal structure of Cys and Tyr-His-Tyr aromatic “cage” surrounding *Trp68* (A) and *Trp156* (B) (PDB code 1HK0).



Table 2-2. The quantum yields of the mutants of nearby side chains surrounding *Trp68* and *Trp156* in the triple Trp to Phe substitution background

<b>Protein</b>	<b>Quantum Yields (QY) <sup>a</sup></b>
<b><i>W68-only</i></b>	<b>QY 0.0076</b>
<i>C32S/W68-only</i>	- 0.0002 <sup>c</sup>
<i>H65Q/W68-only</i>	+ 0.0058 <sup>b</sup>
<i>Y55F/W68-only</i>	+ 0.0003
<i>Y62F/W68-only</i>	+ 0.0002
<i>Y55F/Y62F/W68-only</i>	+ 0.0002
<b><i>W156-only</i></b>	<b>QY 0.0099</b>
<i>H121Q/W156-only</i>	+ 0.0022
<i>Y143F/W156-only</i>	- 0.0002
<i>Y150F/W156-only</i>	- 0.0005
<i>Y143F/Y150F/ W156-only</i>	- 0.0008

<sup>a</sup> Standard deviation of quantum yields for all proteins were less than  $\pm 10\%$  of their absolute quantum yields values; <sup>b</sup> + represents an increase in quantum yields of the mutants compared to their background; <sup>c</sup> – represents a decrease in quantum yields of the mutants compared to their background

Table 2-3: The quantum yields of His to Gln mutants surrounding *Trp68* and *Trp156* in the wild-type or double Trp to Phe substitution background

<b>Protein</b>	<b>Quantum Yields (QY) <sup>a</sup></b>
<b>Wild type</b>	<b>QY 0.058</b>
H65Q	+ 0.001 <sup>b</sup>
H121Q	+ 0.001
H65Q/H121Q	+ 0.002
<b>W130F/W156F</b>	<b>QY 0.034</b>
H65Q/W130F/W156F	+ 0.0003
<b>W42F/W68F</b>	<b>QY 0.024</b>
H121Q/W42F/W68F	+ 0.0008

<sup>a</sup> Standard deviation of quantum yields for all proteins were less than  $\pm 10\%$  of their absolute quantum yields values; <sup>b</sup> + represents an increase in quantum yields of the mutants compared to their background

In aqueous solution, cysteine strongly quenches Trp fluorescence by excited-state electron transfer, apparently during collisions (Chen and Barkley, 1998). The distance between the SH group of Cys32 and the C6 of *Trp68* is 3.9Å, suggesting that Cys32 could be a potential quencher of *Trp68* (Borkman et al. 1993, Mandal et al. 1985). However, compared to the fluorescence intensity of *W68-only*, the mutant C32S/*W68-only* did not show a significant increase in fluorescence intensity (Table 2-2).

Previous inspection suggested that the Tyr-His-Tyr aromatic “cage” surrounding *Trp68* and *Trp156* may be the source of native-state quenching (Kosinski-Collins et al. 2004). To test whether the tyrosine residues quenched fluorescence by proton transfer (Chen and Barley 1998), the emission spectra of six tyrosine mutants have been characterized. None of the mutants displayed a significant increase or decrease in fluorescence intensity (variance < 10%) compared to the spectra of *W68-only* or *W156-only* (Fig. 2-4 and Table 2-2). On the basis of the triple Trp background, single tyrosine mutants (*Y55F/W68-only*, *Y62F/W68-only*, *Y143F/W156-only* and *Y150F/W156-only*) did not show effects on the fluorescence intensities compared to their background. Therefore, the double tyrosine mutants (*Y55F/Y62F/W68-only* and *Y143F/Y150F/W156-only*) were further constructed. It is possible that in the single tyrosine mutants, the other unchanged tyrosine in the aromatic “cage” may extensively quench Trp fluorescence and obscure the effect of the single tyrosine substitutions. The double tyrosine mutants did not display an increase in fluorescence, thus ruling out this possibility.

Histidine in its protonated form is another common fluorescence “quencher” via electron transfer (Willaert et al. 1992; Loewenthal et al. 1991; Harris and Hudson 1990; Harris and Hudson 1991). Fluorescence spectra of the mutants H65Q, *H65Q/W68-only*, *H65Q/W130F/W156F*, H121Q, *H121Q/W156-only*, *H121Q/W42F/W68F*, and *H65Q/H121Q* were recorded and compared to their respective Trp backgrounds (Table 2-2 and 2-3). The double mutant *H65Q/H121Q* was studied to investigate whether there is an additive quenching effect of these two histidines. Except for *H65Q/W68-only* and *H121Q/W156-only*, none of the mutants displayed an increase in native fluorescence intensity. However, the increases of *H65Q/W68-only* and *H121Q/W156-only* represent

insignificant variations in quantum yield magnitude (Table 2). Previous equilibrium unfolding and refolding experiments demonstrated that HyD-Crys was destabilized by the triple Trp substitutions (Kosinski-Collins et al. 2004). We have found that the mutant H65Q has a destabilized N-terminal domain and H121Q has a destabilized C-terminal domain (data not shown). Therefore, the fluorescence intensity increases of H65Q/*W68-only* and H121Q/*W156-only* are probably due to slight conformational changes or partial unfolding caused by the high number of mutation.

4. *QM-MM estimates of relative fluorescence quantum yields (QM-MM calculations were carried out by Prof. Callis P.R.)*

Using the same parameters and procedures as described previously (Callis and Liu, 2004), QM-MM simulations were carried out for HyD-Crys. The results are in accord with the experimental observations. Table 2-4 shows the average CT-<sup>1</sup>L<sub>a</sub> energy gap, the standard deviation of this gap, the computed electron transfer rate, and the predicted fluorescence quantum yield for each of the four Trps. The calculations predict *Trp68* and *Trp156* to be very weakly fluorescent and *Trp42* and *Trp130* to be moderately fluorescent. The detailed differences between experiment and theory are within the accuracy of the method.

Table 2-4: Computed Energy Differences, Electron Transfer Rates and Quantum Yields (Calculations were carried out by Prof. Callis P.R.)

Residue	CT- <sup>1</sup> L <sub>a</sub> gap kilo•cm <sup>-1</sup>	Std. Dev. kilo•cm <sup>-1</sup>	ET rate Constant 10 <sup>7</sup> s <sup>-1</sup>	Predicted Quantum yield
Trp42	5.2	1.7	86.3	0.040
<i>Trp68</i>	0.34	2.5	1180	0.003
Trp130	6.0	1.6	32.9	0.087
<i>Trp156</i>	1.0	2.6	1040	0.004
Trp42 (vacuum)	6.6	1.0	2.4	0.259
<i>Trp68</i> (vacuum)	8.4	0.5	0.0000	0.308
Trp130 (vacuum)	8.5	0.6	0.0000	0.308
<i>Trp156</i> (vacuum)	11.0	0.7	0.0000	0.308

The order of magnitude difference in the quantum yields between the two pairs of Trps arises primarily from the much larger energy gap and smaller fluctuation of the gap for Trp42 and Trp130. When the energy gap is large and fluctuations small, the probability that the fluorescing and CT states will have the same energy is low. Electron transfer (the quenching process) is only possible when the fluorescing and CT states have the same energy. For *Trp68* and *Trp156*, the CT state is much more stabilized by the local protein electrostatic environment, resulting in an electron transfer (ET) rate much faster than the natural deactivation rate, and therefore a much reduced quantum yield. For *Trp68* and *Trp156*, the lowest CT state has an electron transferred from the indole ring primarily to the  $\pi^*$  molecular orbital of the Trp backbone amide. Most of the transferred electron density is centered on the C, with minor amounts on the O and N. A net positive charge is distributed on several atoms of the indole ring. Therefore the CT state energy is quite sensitive to the strength and direction of the average electric field in the direction of electron transfer. Positive charges near the amide C and/or negative charges near the indole ring will lower the energy (stabilize), and the opposite case will raise the energy. Charged residues lying on a line perpendicular to the dipole of the CT state will have little effect. Hydrogen bonds donated to the amide carbonyl are a powerful source of CT state stabilization, and polar residues (including waters) near the indole ring will stabilize, destabilize, or have little effect on the CT state depending on the orientation of the dipole relative to ET direction.

Because of the reasonably long-range nature of Coulombic interaction energies involved (inverse distance squared for ion-dipole and inverse distance cubed for dipole-dipole), the net stabilization is a relatively small number derived from the sum of many large positive and negative terms. For example, Table 2-5 lists Coulombic contributions to the CT- $^1L_a$  energy gap from charged and uncharged protein residues, close waters, distant waters, and totals for *Trp68* and Trp42. The difference in each category is also listed.

Table 2-5: Shifts of the CT-<sup>1</sup>L<sub>a</sub> energy gap due to protein and water environment for Trp42 and *Trp68*. Energy contributions are in units of kilo•cm<sup>-1</sup><sup>a</sup>. Negative values mean stabilization of the CT state relative to <sup>1</sup>L<sub>a</sub>. (Calculations were carried out by Prof. Callis P.R.)

Source	<i>Trp68</i>	Trp42	difference	<i>Trp156</i>	Trp130	difference
Lys	0.99	2.66	-1.67	-0.13	-0.45	0.31
Arg	0.96	-4.77	5.72	4.02	8.51	-4.49
Asp	-6.75	-1.76	-4.98	-0.10	-0.92	0.81
Glu	-1.50	-1.17	-0.33	-6.58	-8.94	2.35
Gly1	0.63	-0.49	1.12	-0.15	-1.07	0.91
Ser173	-0.12	0.93	-1.05	-0.13	0.51	-0.64
charged	-5.79	-4.60	-1.19	-3.09	-2.35	-0.74
noncharged	0.74	1.09	-0.35	-2.84	0.91	-3.75
<b>all protein</b>	<b>-4.55</b>	<b>-3.07</b>	<b>-1.48</b>	<b>-6.21</b>	<b>-1.99</b>	<b>-4.22</b>
<b>all water</b>	<b>-3.82</b>	<b>2.08</b>	<b>-5.91</b>	<b>-4.07</b>	<b>0.55</b>	<b>-4.61</b>
wat< 9 Å	-6.64	-1.59	-5.06	-4.18	0.75	-4.93
wat> 9 Å	2.82	3.67	-0.85	0.11	-0.20	0.32
<b>protein + water</b>	<b>-8.37</b>	<b>-0.99</b>	<b>-7.38</b>	<b>-10.28</b>	<b>-1.44</b>	<b>-8.83</b>

<sup>a</sup> 1 kilo•cm<sup>-1</sup> = 0.125 eV = 2.9 kcal/mol

As shown in Table 2-5, the average contributions from charged groups are large and quite different for *Trp68* and *Trp42*, a reflection of positioning of the groups relative to the direction of electron transfer. The total average contribution from protein, is large and negative, with *Trp68* being stabilized overall by  $1480\text{ cm}^{-1}$  more than *Trp42*. A much larger effect comes from the water molecules, for which the CT state of *Trp68* is stabilized by  $3820\text{ cm}^{-1}$  while that of *Trp42* is destabilized by  $2080\text{ cm}^{-1}$ . Overall, the average CT state stabilization of *Trp68* is  $7380\text{ cm}^{-1}$  greater than for *Trp42*. The single most dominating reason for the much greater quenching rate of *Trp68* is the presence of ca. 10 waters on average within  $9\text{ \AA}$  that stabilize the CT state by  $6640\text{ cm}^{-1}$ . For *Trp42* there are only about 3 waters within  $9\text{ \AA}$ , and these only stabilize by about  $1600\text{ cm}^{-1}$  on average.

Two crystallographic waters present in the X-ray crystal structure (Basak et al. 2003) are close to the quenched Trps and appear to be highly stabilizing for electron transfer (Fig. 2-5). One water molecule donates an H-bond to the Trp backbone CO (the electron acceptor). The proximity of the positive charge of the H to the backbone CO group stabilizes the charge transfer complex. The other water molecule is an H-bond acceptor from the Trp indole NH. This H-bond places the negative charge of the O near the Trp ring (the electron donor) to further stabilize the charge transfer complex.

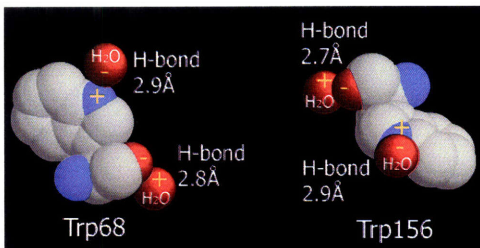


Figure 2-5: The interaction between *Trp68* (or *Trp156*) and the two nearby crystallographic waters, which will stabilize the electron transfer from indole ring to the amide backbone (PDB code 1HK0).



In addition to the external electrostatic perturbations from protein and water molecules, the internal electronic energy depends somewhat on the precise local conformation of the Trp and its associated amides. Of considerable importance is the distance between the electron acceptor and donor groups and the stabilization of these through proximity of the polar atoms of the amides within the QM unit. Table 2-4 also shows the CT-<sup>1</sup>L<sub>a</sub> average energy gap and standard deviation for the QM fragments in vacuum. The gap for *Trp68* is similar to that for many other proteins previously studied, but that for Trp42 is somewhat smaller. For this reason, the predicted quantum yield for Trp42 is not as high as normally expected when the environment stabilization is as small as found for this Trp.

Much the same summary picture is found for Trp130 and *Trp156*, although many details are different because the two domains are not identical. The stabilization difference between the *Trp156* and Trp130 CT states is somewhat greater than the difference between *Trp68* and Trp42. This is brought about by much more protein stabilization, moderated by less water stabilization for the *Trp156*-Trp130 pair than for the *Trp68*-Trp42 pair.

##### *5. Investigation of the stabilization effect of charged and polar side chains on the charge transfer state*

A subset of site directed mutants were constructed and analyzed to test the effect of charged or polar residues on the charge transfer state. These were chosen based on the QM-MM results described above.

In the X-ray crystal structure of HyD-Crys, the polar or charged residues Asn33, Asp64, His65, Gln66, Gln67, Met69, Asp73 are in proximity to *Trp68*. Arg152, Tyr153 and Asp155 are nearby *Trp156* (Fig. 2-6). QM-MM results predicted that Arg79 highly stabilizes and Tyr153 destabilizes charge transfer event of *Trp156* (See Appendix A). To experimentally investigate their contributions to electron transfer, neutral and polar

amino acid substitutions of these residues were constructed to test their role in stabilizing the charge transfer state (Table 2-6, 2-7 and 2-8). Based on the triple Trp mutant background, D64S, H65Q, D73S, R79S and Y153Q showed more than 30% increase in fluorescence intensity. Q67A, M69S and R152S showed about 20% increase in fluorescence intensity. Because of the extremely weak fluorescence from the triple mutants, *W68-only* or *W156-only*, these increases are very small on the scale of absolute quantum yield increase (Table 2-6).

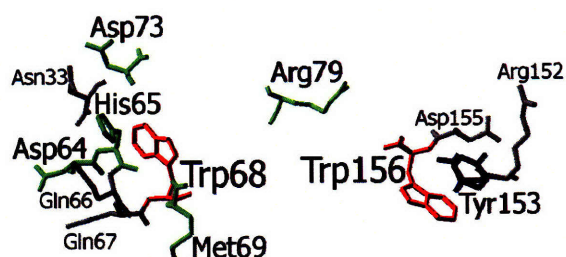


Figure 2-6: Residues around *Trp68* and *Trp156* that were mutated (PDB code 1HK0).

Table 2-6: The effect of mutations on fluorescence intensity by affecting charge transfer states (in the triple Trp to Phe substitution background)

<b>Protein</b>	<b>Quantum Yield (QY)<sup>a</sup></b>
<b><i>W68-only</i></b>	<b>QY 0.0076</b>
N33A/ <i>W68-only</i>	+ 0.0008 <sup>b</sup>
Q66A/ <i>W68-only</i>	+ 0.0009
Q67A/ <i>W68-only</i>	+ 0.0017
D64S/ <i>W68-only</i>	+ 0.0024
H65Q/ <i>W68-only</i>	+ 0.0058
M69S/ <i>W68-only</i>	+ 0.0019
D73S/ <i>W68-only</i>	+ 0.0047
R79S/ <i>W68-only</i>	+ 0.0038
<b><i>W156-only</i></b>	<b>QY 0.0099</b>
Y153Q/ <i>W156-only</i>	+ 0.0039
R152S/ <i>W156-only</i>	+ 0.0027
D155S/ <i>W156-only</i>	- 0.0001 <sup>c</sup>

<sup>a</sup> Standard deviation of quantum yields for all proteins were less than  $\pm 3\%$  of their absolute quantum yields values; <sup>b</sup> + represents an increase in quantum yields of the mutants compared to their background; <sup>c</sup> - represents a decrease in quantum yields of the mutants compared to their background

Table 2-7: The effect of mutations on fluorescence intensity by affecting charge transfer states (in the wild-type or double Trp to Phe substitution background)

<b>Protein</b>	<b>Quantum Yield (QY) <sup>a</sup></b>
<b>Wild type</b>	<b>QY 0.058</b>
D64S	- 0.0001 <sup>c</sup>
H65Q	+ 0.001
M69S	+ 0.0003
D73S	+ 0.0002
R79S	+ 0.0001
Y153Q	+ 0.010
<b>W130F/W156F</b>	<b>QY 0.034</b>
D64S/W130F/W156F	+ 0.0003 <sup>b</sup>
H65Q/W130F/W156F	+ 0.0003
M69S/W130F/W156F	- 0.0001
D73S/W130F/W156F	+ 0.003
R79S/W130F/W156F	+ 0.0005
<b>W42F/W68F</b>	<b>QY 0.024</b>
Y153Q/W42F/W68F	+ 0.010

<sup>a</sup> Standard deviation of quantum yields for all proteins were less than  $\pm 3\%$  of their absolute quantum yields values; <sup>b</sup> + represents an increase in quantum yields of the mutants compared to their background; <sup>c</sup> - represents a decrease in quantum yields of the mutants compared to their background

Table 2-8: The effect of mutations on fluorescence intensity by affecting charge transfer states (in the single Trp to Phe substitution background)

<b>Protein</b>	<b>Quantum Yield (QY) <sup>a</sup></b>
<b>W42F</b>	<b>QY 0.029</b>
D64S/W42F	+ 0.0003 <sup>b</sup>
H65Q/W42F	- 0.001 <sup>c</sup>
M69S/W42F	+ 0.001
D73S/W42F	+ 0.001
R79S/W42F	- 0.001
<b>W130F</b>	<b>QY 0.041</b>
Y153Q/W130F	+ 0.005

<sup>a</sup> Standard deviation of quantum yields for all proteins were less than  $\pm 3\%$  of their absolute quantum yields values; <sup>b</sup> + represents an increase in quantum yields of the mutants compared to their background; <sup>c</sup> - represents a decrease in quantum yields of the mutants compared to their background

As explained above for H65Q, we were concerned that these increases were due to subtle conformational changes or partial unfolding because of the high numbers of mutations (Kosinski-Collins et al. 2004). To confirm this, the substitutions of D64S, H65Q, M69S, D73S, R79S and Y153Q were also constructed in the wild type and double Trp backgrounds (Table 2-7), which were more thermodynamically stable than the triple Trp mutants. The double Trp background was constructed by maintaining two Trps in each domain. Except for Y153Q, which showed a slight increase in fluorescence intensity, none of other substitutions displayed an increase in fluorescence intensity in the wild-type or double Trp backgrounds. There was no obvious difference in fluorescence intensities for the mutants in these more stable backgrounds (Table 2-7). The mutants D64S, H65Q, M69S, D73S and R79S displayed fluorescence intensity increases in the triple Trp background that were probably due to subtle conformation change or partial unfolding caused by the high number of substitutions.

Asp73 was predicted to be one of the strongest enhancers for the charge transfer process (See Appendix A). Asp64 may also stabilize the charge transfer complex, but less effectively than Asp73. The calculations predicted that the R79S mutant might cause an increase in fluorescence because Arg79 lies on the direction of electron transfer. The electron is transferred towards Arg79 and so the charge transfer state will be stabilized more than if a neutral residue were in this position. Because the distance from Arg79 to *Trp68* or *Trp156* is more than 10Å, without theoretical calculations, we did not test Arg79 in our initial survey of neighboring charged and polar amino acids. However, by the experimental measures, none of these substitutions showed significant effects on the fluorescence intensity. Possible reasons for the failure of these predictions are presented in the discussion part “*Charge transfer mechanism*”.

Arg152 and Asp155 were predicted to have little effect on the quantum yield of *Trp156* because they lie in a line perpendicular to the direction of electron transfer. Consistent with this prediction, the fluorescence intensity of the mutants R152S and D155S did not increase significantly.

As described above, we have observed FRET between the two Trps of each domain. The interaction between the Trps may obscure the effect of the substitutions of these potential charge transfer enhancers. In other words, even if the mutants in the wild type or double Trp background did destabilize the charge transfer complex and increase the fluorescence intensity of *Trp68* or *Trp156*, there may be more energy transfer from Trp42 or Trp130. If this were the case we would not see changes in fluorescence intensity.

To rule out this possibility the single Trp substitutions W42F and W130F were constructed to eliminate the interaction between Trp42 and *Trp68* in the N-terminal domain, and the interaction between Trp130 and *Trp156* in the C-terminal domain (Table 2-8). Trp42 and Trp130 are also sensitive to the electrostatic mutations, and therefore their fluorescence intensity may change and obscure the substitution effect. None of the substitutions caused an increase in fluorescence intensity in the W42F mutant background as compared to the background fluorescence intensity of W42F. Y153Q/W130F showed about 10% fluorescence intensity increase (quantum yield increases 0.005) compared to the W130F background.

## E. DISCUSSION

### 1. *Trp to Trp energy transfer*

We consider whether the observations attributed to FRET are physically reasonable. The distance between the indole rings of two Trps of the N-terminal domain is 12.2 Å and the distance between Trps of the C-terminal domain is 12.4 Å. These distances are within the range (4-16 Å) of typical Förster distances (the distance for which the probability of transfer is 50%) for energy transfer between Trps (Lakowicz 1999). In contrast, the distances between the Trps in different domains are more than 20 Å, so the possibility of the interdomain Trp energy transfer is very low. The experimental results are consistent with this. For significant transfer, the emission spectrum of the donor must overlap the absorption spectrum of the acceptor. Although we were not able to directly determine the extent of this overlap, the relative positions of the fluorescence spectra often qualitatively track the relative positions of absorption. The fluorescence spectra of single and double Trp mutants in Figs. 2 and 3 show that the maximum emission wavelengths of the donors, Trp42 and Trp130, are blue shifted about 10 nm compared to those *Trp68* and *Trp156* (Table 2-1). This implies that the emission of Trps 42 and 130 will overlap the absorption of *Trps 68* and *156*.

The remaining factor for efficient transfer is the orientation factor  $\kappa^2$  which is a function of the average relative orientation of the transition dipole vectors of the donor and acceptor during the excited state lifetime. Its value can range from 0 to 4. It is 2 when the vectors are parallel side by side, and 4 if parallel end-to-end, but goes through zero when parallel and tilted at 54 degrees to the line connecting donor and acceptor.  $\kappa^2$  is 2/3 when the chromophores are tumbling rapidly and randomly during the excited state lifetime. In the present protein environment,  $\kappa^2$  is expected to be approximately constant, but could vary because of the deformations of the protein structure. Tabulated experimental and computed transition dipole directions for the  ${}^1L_a \rightarrow$  Ground state transition for indole place the direction approximately between the line connecting atoms



CE3 and NE3 and the line connecting atoms CE3 and CD1 of the indole ring (Callis, 1997). Using the coordinates from 50 frames of a molecular dynamics simulation at 300 K gave  $\kappa^2 = 0.4 \pm 0.2$  and  $0.5 \pm 0.2$  for transfer from Trp42 and Trp130 respectively. In summary, all three critical factors are probably large enough to allow the extent of partial transfer observed.

Resonance energy transfer between aromatic amino acids often occurs in proteins due to the absorption and emission spectra overlap of phenylalanine, tyrosine and Trp (Lakowicz 1999). Applying Förster theory to the crystal structure of bovine  $\gamma$ B-crystallin, Borkman (1985) predicted that the efficiency of energy transfer from the protein's fifteen tyrosines to the four Trps would be approximately 83%. This prediction agreed well with the experimental value of 78% (Borkman et al. 1985). Although there are no previous reports of Trp-to-Trp energy transfer in the  $\beta$ - or  $\gamma$ -crystallins, homotransfer between Trps has been observed in other proteins. For example, in Barnase there is energy transfer from Trp71 to Trp94 and Trp94 is in turn quenched by His18 (Loewenthal et al. 1991; Willaert et al. 1992). According to the distance between the Trps in bovine  $\gamma$ B-crystallin ( $>12\text{\AA}$ ), Borkman et al. (1993) predicted that Trp-to-Trp energy transfer would not be possible in this protein. However, our experimental observations and theoretical considerations give a clear indication of partial transfer.

## *2. Charge transfer mechanism*

As in earlier papers (Callis and Liu 2004), the quantum yields were estimated here with electron transfer theory that has a universal electron transfer matrix element of  $V = 10 \text{ cm}^{-1}$  and a universal offset of  $D = -4000 \text{ cm}^{-1}$  from the computed energy gap. Thus, all quantum yields reflect only the adjusted average CT- $^1L_a$  energy gap and the standard deviation of this gap. The gap is modulated by the net electric potential difference between the initial electron distribution and that in the CT state. We are working on a more realistic model wherein the magnitude of  $V$  is computed.

It is interesting that the quantum yields for the pairs *Trps 68/156* and *Trps 42/130* are similar. While this might be expected given the similar homology in the two domains, especially regarding the positions of the Trps, inspection of Tables 4 and 5 shows that the individual terms contributing to computed energy gaps differ considerably between the homologous Trps, even though the net result is quite similar CT-<sup>1</sup>L<sub>a</sub> energy gaps and standard deviations. Table 2-5 also shows that the detailed backbone conformations differ considerably, as judged by the average gap in vacuum.

The method successfully captures the essence of the quantum yield behavior, predicting extremely low values for *Trp68* and *Trp156* and intermediate values for *Trp42* and *Trp130*. The highest fluorescence yields for single Trps in proteins are typically around 0.3, a value that varies only slightly with polarity of environment. The computations even correctly predict that *Trp130* is more fluorescent than *Trp42* and *Trp156* more than *Trp68*, although this is likely fortuitous given that all are a factor of 2-3 too low.

One of the important outcomes of this study is the testing of detailed predictions of the theoretical method by strategic mutations. Using a variant of the program that computes the average energy gap, contributions of individual residues and waters to the CT-<sup>1</sup>L<sub>a</sub> gap for each Trp were determined. (See Appendix A). Large contributions come from 4 sources: 1) charged residues that lie on the axis of electron transfer; 2) backbone atom contributions from nearby residues; 3) hydrogen bonding from very close waters; 4) dipole-dipole interactions from near waters; and 5) collective contributions from distant waters that are aligned by the charged groups of the protein. Contributions for the charged groups are predicted to be large at long range if lying on the electron transfer direction axis. For example, *Arg79* stabilizes the CT state for *Trp156* by 2000 cm<sup>-1</sup> even though 21 Å distant. On the basis of such calculations we anticipated that mutations of these charged residues to neutral residues would have an observable impact on the energy gap and thus measurably affect the quantum yield. However, as noted in the results section, replacement of the candidate charged residues with neutral residues failed to produce significant changes in quantum yield.

A more thorough consideration provides the likely reason for these negative results. First, every charged group has an orienting effect on the water, creating a collective dipole that opposes the direct effect of the charge on the CT state. Because charged groups are almost always on the surface, their effect on water is large. This is merely the microscopic manifestation of the large dielectric constant of water, which the simulations capture reasonably well. A more subtle effect comes from the fact that the more fluorescent Trps are also sensitive to electrostatic mutations. For example, Arg79 stabilizes the CT state of Trp130 by 1500 cm<sup>-1</sup>, i.e., almost as much as it stabilizes *Trp156*. Furthermore, because the quantum yield is a sigmoidal function of the energy gap, Trps such as 130 and 42 that fluoresce with about half the maximum possible efficiency are more sensitive to the electric field than those which are at the top or bottom (flatter regions) of the curve (Liu et al, 2005). Therefore changes in response to mutating away the charge of Arg79 are expected to be dominated by increased fluorescence from Trp130, if present. Another problem with mutating charges is that very often they are part of ion pairs. Removal of a charge may result in unpredictable repositioning of other charged groups, facilitated by the large, flexible nature of Lys, Arg, and Glu.

In water, cysteine is a powerful quencher of the indole ring by electron transfer and has been implicated as a quencher in some proteins. The ineffectiveness of Cys32 as a quencher of *Trp68* fluorescence, despite the S being only 4 Å from some ring atoms, is likely because the electrostatic factors are destabilizing. Electron transfer to Cys32 would be in the opposite direction from that to the amide (which is highly stabilized). Part of the reason for the amide CT stabilization is the high density of negative atoms in the vicinity of the Cys32 S.

### *3. The potential physiological role for lens UV absorption in protecting the retina*

Ultraviolet radiation is often classified into three bands based on their biological effects: UVA (400-320nm), UVB (320-290nm) and UVC (290-100nm). Under normal

conditions, the ozone layer filters out all UVC and 90% of UVB light and thus prevent them from reaching the earth's surface (McCarty et al. 2002). The cornea can absorb almost all the UV radiation of wavelength shorter than 295nm. However, significant radiation of wavelengths longer 300nm pass the cornea (Lerman 1980). The young crystallin lens absorbs the remaining UVB and UVA light of wavelength below 370nm. When the lens becomes more yellow with age, its UV absorption spectrum expands to include wavelengths up to 470nm (Oliva et al. 2005, Lerman 1987). It is a common clinical phenomenon that people who had cataract extraction surgery are sensitive to UV radiation (Lerman 1980, Berler et al. 1983; Pollack et al. 1997; Pollack et al. 1998). This sensitivity of the retina to UV radiation in the absence of the lens has been shown in animal models (Ham et al 1982; Noell et al. 1966). These observations indicate that one function of the lens is to protect the retina from UV light that transmitted by cornea. We suspect that one function of the highly conserved tryptophans in the crystallin proteins is to absorb UV reaching the lens, to protect the retina. The lens also contains low molecular weight molecules which may also act as UV filters protecting the retina, such as kynurenine and 3-hydroxykynurenine (Streete 2004).

#### *4. Does fluorescence quenching protect the crystallins from UV photodamage?*

Exposure to UV radiation not only causes damage to the retina photoreceptors (Massof, 1986) but also is an important risk factor for cataract formation (Colitz et al. 2005). Though only limited intensities of UV-B and UV-A light of wavelengths between 295nm and 400nm reach the lens, the cumulative exposure to ambient UV over decades may be significant in cataract formation (Hockwin 2000). UV-B at 300nm was most detrimental to the lens in the animal models (Merriam et al. 2000, and Hockwin 2000). Trp absorption at 300nm is the tail of the tryptophan UV absorption curve, but is still the most significant source of UV absorption at this wavelength in proteins (Lakowicz, 1999).

Trp radical formation and fluorescent material derived from Trps have been identified in lens exposed to UV light with wavelength longer than 295nm (Borkman et al. 1977; Lerman et al, 1978; Weiter et al. 1975). The excited singlet state Trps may then be photochemically degraded via photoionization reactions, which result in indole ring cleavage (Feitelson 1971; Bryant et al. 1975; Templer et al. 1976). Trp residues (as well as His, Met and Cys) were photochemically reactive in UV irradiated bovine  $\gamma$ B crystallin (Hott et al. 1992). Such UV induced Trp radical formation may play an important role in senile cataract formation (Borkman et al. 1977; Lerman et al. 1978; Weiter et al. 1975).

Tallmadge and Borkman (1990) studied Trps damage in bovine  $\gamma$ B crystallin irradiated in vitro at 295nm with 0.7mW/cm<sup>2</sup> output flux. Their results showed that the rates of photolysis of Trp42 and Trp131 were much higher than *Trp68* and *Trp157*. The structures of bovine  $\gamma$ B crystallin and HyD-Crys are highly homologous and their four Trps are conserved (Srikanthan et al. 2004; Bloemendal et al. 2004). We have shown that Trp42 and Trp130 are moderately fluorescent and *Trp68* and *Trp156* are extensively quenched in HyD-Crys. This suggests that quenching of *Trp68* and *Trp157* may protect Trps from photo-damage.

Pitts et al (1977) have established threshold levels of exposure throughout the near UV region (210-440nm) for cataract formation in rabbits. For instance, the threshold dose at 295nm was 0.75 J•cm<sup>-2</sup> and was 0.15 J•cm<sup>-2</sup> at 300nm. These results are on the same order as the maximum tolerable dose at 300nm (0.365 J•cm<sup>-2</sup>) measured in the rat (Soderberg et al. 2002). Borkman (1977) suggested a photon-to-Trp ratio of 20:1 to cause Trp destruction by estimates of the Trp photolysis yield in solution.

If the crystallins are absorbing incident UV radiation, fluorescence quenching of Trps may be a self-protective mechanism from damage induced by UV radiation. Photochemical reaction of Trp probably originates from excited singlet states and competes with fluorescence emission (Borkman et al. 1993). Quenching can shorten the lifetime of Trp excited singlet states, perhaps reducing the possibility that the electron

will go into a photochemical reaction. The highly quenched *Trp68* and *Trp156* may function as “energy sinks”. Our findings strongly suggest that energy from the ambient UV absorbed by these two Trps is almost completely dissipated through non-radiative quenching and therefore the chance of a photo-damage reaction may be reduced. It remains to be determined whether the quenching phenomenon in HyD-Crys is conserved though other crystallin proteins. If so, this would suggest that the backbone conformation of Trps in HyD-Crys may have evolved to provide efficient absorption of UV B radiation, while at the same time providing maximum protection from photodamage.

## F. CONCLUSION

*Trps 68* and *156* of HyD-Crys display abnormally low fluorescence intensity in the native state without the existence of the metal ligands or cofactors. An extensive investigation of mutated proteins combined with hybrid quantum mechanical-molecular mechanical (QM-MM) simulations strongly implicates efficient electron transfer from the excited indole ring to the backbone amide of these residues. Charged residues and nearby waters favorably stabilize these charge transfer events. Considerable resonance energy transfer from Trp42 to *Trp68* in the N-terminal domain and from Trp130 to *Trp156* in the C-terminal domain was observed and rationalized. The energy transfer to the weakly fluorescing Trps (*Trp68* and *Trp156*) serves to further reduce the overall quantum yield (and presumably excited state lifetime) of HyD-Crys. We speculate that this quenching may protect Trps in  $\gamma$ -crystallin from UV irradiation.

## **CHAPTER THREE:**

### **MECHANISM OF THE EFFICIENT TRYPTOPHAN FLUORESCENCE QUENCHING IN HUMAN $\gamma$ D CRYSTALLIN STUDIED BY TIME-RESOLVED FLUORESCENCE <sup>2</sup>**

---

<sup>2</sup> This work includes results of collaboration with Prof. Ludwig Brand and Dr. Dmitri Toptygin at Johns Hopkins University.  
Manuscript was accepted by Biochemistry.

## A. ABSTRACT

HyD-Crys has four highly conserved buried tryptophans (Trps), with two in each of the homologous  $\beta$ -sheet domains. In situ, these Trps will be absorbing UV radiation that reaches the lens. The dispersal of the excited state energy to avoid covalent damage is likely to be physiological relevant for the lens crystallins. Trp fluorescence is efficiently quenched in native HyD-Crys. Previous steady-state fluorescence measurements provide strong evidence for energy transfer from Trp42 to *Trp68* in the N-terminal domain and from Trp130 to *Trp156* in the C-terminal domain [Chen, J. et al. (2006) *Biochemistry* 45, 11552-63]. Hybrid quantum mechanical-molecular mechanical (QM-MM) simulations indicated that the fluorescence of *Trp68* and *Trp156* is quenched by fast electron transfer to the amide backbone. Here we report additional information obtained using time-resolved fluorescence spectroscopy. In the single-Trp containing proteins (Trp42-only, *Trp68-only*, Trp130-only, and *Trp156-only*), the highly quenched *Trp68* and *Trp156* have very short lifetimes,  $\tau \sim 0.1$  ns, whereas the moderately fluorescent Trp42 and Trp130 have longer lifetimes,  $\tau \sim 3$  ns. In the presence of the energy acceptor (*Trp68* or *Trp156*), the lifetime of the energy donor (Trp42 or Trp130) decreased from  $\sim 3$  ns to  $\sim 1$  ns. The intradomain energy transfer efficiency is 56% in the N-terminal domain and is 71% in the C-terminal domain. The experimental values of energy transfer efficiency are in good agreement with those calculated theoretically. The absence of a time-dependent red shift in the time-resolved emission spectra of Trp130 proves that its local environment is very rigid. Time-resolved fluorescence anisotropy measurements with the single-Trp containing proteins, Trp42-only and Trp130-only, indicate that the protein rotates as a rigid body and no segmental motion is detected. A combination of energy transfer with electron transfer results in short excited-state lifetimes of all Trps, which, together with the high rigidity of the protein matrix around Trps, could protect HyD-Crys from excited-state reactions causing permanent covalent damage.



## B. INTRODUCTION

Crystallins are the predominant structural proteins found in the vertebrate eye lens. The  $\alpha$ -,  $\beta$ - and  $\gamma$ -crystallins have a critical role in maintaining human eye lens transparency.  $\alpha$ -crystallins are major structural proteins but also function as molecular chaperones by forming large polydisperse multimers and interacting with non-native proteins to prevent them from aggregation (Augusteyn 2004; Reddy et al. 2006). The oligomeric  $\beta$ - and the monomeric  $\gamma$ -crystallins function solely as structural proteins. The  $\beta$ - and  $\gamma$ -crystallins both contain four homologous Greek key motifs organized into two domains. Most crystallin proteins are synthesized during embryonic development, with little protein turnover in adulthood (Oyster 1999), and therefore crystallins have to remain stable and soluble throughout life. Cataract, the most common cause of blindness worldwide, represents the aggregation of oxidatively damaged partially unfolded proteins. Mutations resulting in single amino acid substitutions of human  $\gamma$ D-crystallin (H $\gamma$ D-Crys) are associated with juvenile-onset cataracts (Graw 2004). Covalently damaged crystallins, including H $\gamma$ D-Crys, were found in inclusions separated from cataract lenses (Hanson 2000; Hanson 1998; Searle 2005). Oxidized tryptophan residues in H $\gamma$ D-Crys have been identified in aged cataractous human lens by mass spectrometry (Searle 2005).

H $\gamma$ D-Crys is the second most abundant  $\gamma$ -crystallin of the lens nucleus, the region formed earliest in eye development (Lampi 1997, Oyster 1999). H $\gamma$ D-Crys is a monomeric, 173-amino-acid protein. The crystal structure of H $\gamma$ D-Crys has been solved to 1.25Å resolution (Basak 2003). It is composed of  $\beta$ -sheets arranged in four Greek key motifs separated into two highly homologous domains (Figure 3-1). Each domain has two buried intrinsic Trps, Trp42 and *Trp68* in the N-terminal domain and Trp130 and *Trp156* in the C-terminal domain. These four Trps are conserved through all the vertebrate  $\beta$ - and  $\gamma$ -crystallins. To help the reader keep track of the special relationships among these four tryptophans, we will write the two efficiently quenched *Trp68* and *Trp156* in italics. The other two moderately fluorescent Trp42 and Trp130 will be in regular text.

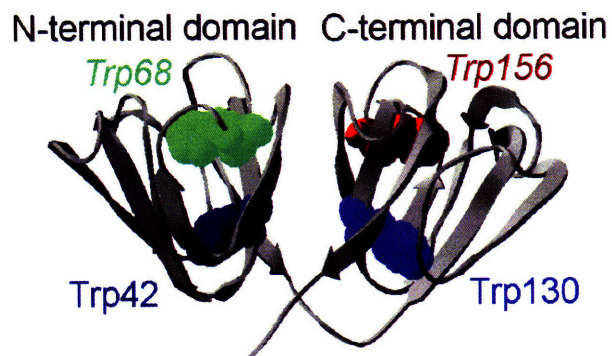


Figure 3-1. The crystal structure of wild-type HyD-Crys depicted in ribbon representation showing the four intrinsic tryptophans in spacefill, Trp42 and *Trp68* in the N-terminal domain and Trp130 and *Trp156* in the C-terminal domain (Protein Data Bank Code: 1HK0).

Ultraviolet (UV) radiation is one of the risk factors for the age-related cataracts (McCarty and Taylor 2002). Although only a small percent of the solar UV light can reach the eye, ocular lenses are continuously exposed to ambient UV radiation with wavelengths from 295nm to 400nm, which could cause cumulative photochemical damage (Lerman 1980). The UV radiation with the wavelength of 300nm is most detrimental to the eye lens in the animal model (Merriam 2000; Soderberg 2002). Inside proteins, only aromatic residues (e.g. Trp and Tyr) have weak absorption at 300nm, and Trp residue contributes the most to the absorbance at this wavelength (Lakowicz 1999). Photochemical reactions of Trps in crystallin proteins may play a key role in cataractogenesis (Kurzel 1973, Lerman 1980). The absorption of a photon by a Trp residue promotes Trp sidechain to an electronically excited state. At ambient temperature, excited Trp sidechain can take part in a photodamage reaction (Creed 1984), or it can emit a fluorescence photon, or it can transfer its excitation to another Trp, or it can lose its excitation due to a nonradiative quenching mechanism. There is a competition among these pathways of an excited state Trp residue. Both steady-state and time-resolved fluorescence measurements provide valuable information about fluorescence lifetimes, energy transfer, and quenching processes (Lakowicz 1999; Beechem and Brand 1985)

Steady-state fluorescence from the four Trps in HyD-Crys has been studied in great detail (Chen et al. 2006). In its native state HyD-Crys is less fluorescent than in its denatured state. In other words, the fluorescence of the native state HyD-Crys is quenched. Fluorescence quenching in the native state was also found in other  $\beta$ - and  $\gamma$ -crystallins (Bateman et al. 2003; Liang et al. 2004; Kim et al. 2002; Wenk et al. 2000; Das et al. 1998). The quantum yields of the individual Trps in HyD-Crys have been measured using single Trp containing proteins with the other three Trp residues replaced by Phe (Chen et al. 2006). The triple mutants, each containing three Trp to Phe substitutions and one native Trp, will be here referred to as Trp42-only, *Trp68-only*, Trp130-only and *Trp156-only*, respectively. It was found that Trp42-only and Trp130-only are moderately fluorescent, with quantum yields of 0.13 and 0.17, respectively. In contrast, *Trp68-only* and *Trp156-only* are extremely quenched, with the quantum yields of only about 0.01.

Hybrid quantum mechanical-molecular mechanics (QM-MM) simulations strongly indicate that the highly efficient quenching of *Trp68* and *Trp156* is due to fast electron transfer from the indole ring to the amide backbone (Chen et al. 2006). Nearby water molecules and surrounding polar residues stabilize the charge transfer state. The QM-MM method used to compute the electron transfer process was developed recently by Callis et al (Callis and Liu 2004; Callis and Vivian 2003; Kurz et al. 2005; Liu et al. 2005; Xu et al. 2006). The differences in the quantum yields between Trp42 and *Trp68* in the N-terminal domain, and between Trp130 and *Trp156* in the C-terminal domain, can be explained by the different rates of electron transfer from the indole ring to a local amide. A negative (positive) charge will decrease (increase) the quantum yield if it is closer to the indole ring than to the electron acceptor because these arrangements stabilize (destabilize) the charge transfer state (Callis and Liu 2004; Callis and Vivian 2003; Kurz et al. 2005; Liu et al. 2005; Xu et al. 2006). In the case of HyD-Crys, the electrostatic stabilization is much greater for *Trp68* (or *Trp156*) than for Trp42 (or Trp130). The theoretical predictions based on this effect are consistent with the quantum yields measured experimentally.

Steady-state fluorescence experiments provided evidence that Förster resonance energy transfer (FRET) also contributes to the quenching of Trp fluorescence in HyD-Crys (Chen et al. 2006). There is energy transfer from Trp42 to *Trp68* in the N-terminal domain and from Trp130 to *Trp156* in the C-terminal domain. If the energy acceptor (*Trp68* or *Trp156*) is substituted by Phe, the fluorescence intensity of the single Trp to Phe mutant (W68F or W156F) exceeds that of the wild-type HyD-Crys. In contrast, the substitution of the energy donor (Trp42 or Trp130) results in a decreased intensity of single mutant (W42F or W130F) compared to wild type. The comparison of steady-state fluorescence intensities of the triple Trp to Phe mutants (*Trp42-only*, *Trp68-only*, *Trp130-only*, and *Trp156-only*) and the double Trp to Phe mutants (*Trp42/Trp68* and *Trp130/Trp156*) further confirmed the presence of intradomain energy transfer (Chen et al. 2006).

Absorption of a UV photon by a Trp residue in crystallin promotes the sidechain of that Trp to an electronically excited state, in which it can remain for several nanoseconds. While the Trp sidechain is in the excited state, it can undergo an irreversible chemical reaction, resulting in covalent damage to the protein. It is thus important to be able to measure for how long each Trp residue remains in the excited state. Only a time-resolved fluorescence measurement can give a precise answer to this question. A few nanosecond time-resolved fluorescence studies have been reported for bovine crystallins. Borkman described time-resolved studies of bovine  $\alpha$ -crystallins and  $\gamma$ B-crystallin (Borkman et al. 1993a; Borkman 1993b), which contain two and four Trp residues, respectively. In those studies the time-resolved fluorescence was fit by a biexponential function, with a long lifetime of 2-3 ns and a short lifetime of 0.3-0.5ns. However, the authors did not address the question of the lifetimes of the individual Trp residues and whether they change in the presence of the other Trp residues or not. In the case of resonance energy transfer the lifetime of the donor is different in the absence and in the presence of the acceptor. In this chapter we describe a time-resolved fluorescence study of all triple and double Trp to Phe substitutions of HyD-Crys, which was designed to measure the donor lifetimes in the absence and in the presence of the acceptors.

Nanosecond and picosecond time-resolved fluorescence measurements have considerable advantages over the steady-state measurements. The rates of resonance energy transfer and other excited-state reactions can be measured directly in a time-resolved study. If the time resolution is combined with spectral resolution, then it becomes possible to tell the difference between a homogeneous ensemble of excited-state fluorophores in relaxing environments and a heterogeneous ensemble of excited-state fluorophores in static environments (Toptygin et al. 2001). This capability is very important in application to Trp fluorescence in proteins, because some proteins relax on the nanosecond time scales. For a protein with a single Trp and a single conformation it is possible to measure picosecond and nanosecond relaxation dynamics of the protein matrix (Toptygin et al. 2006). For a protein containing multiple Trps in different environments it is possible to separate the spectra corresponding to different lifetimes (Ross et al. 1981), which may provide a significant help in assigning multiple lifetimes to

multiple chromophores. In the present study we explore all of the capabilities of time-resolved fluorescence mentioned above.

A different kind of dynamic information can be obtained when the time resolution is combined with polarized fluorescence measurements (Beechem and Brand 1985). Time-resolved anisotropy measurements make it possible to tell the difference between the Brownian rotation of a globular protein as a whole and the segmental motion within the protein (Beechem and Brand, 1985). This provides a method of studying protein integrity and this method has been applied in this chapter.

## C. MATERIALS AND METHODS

### 1. Mutagenesis, Expression and Purification of Proteins

Double and triple tryptophan to phenylalanine substitutions were constructed by site directed mutagenesis (Konsinski-Collins et al. 2004). Primers (IDT-DNA) encoding the substitutions were used to amplify the gene for HyD-Crys with an N-terminal His<sub>6</sub> tag in a pQE.1 plasmid (Konsinski-Collins et al. 2004). The double mutation W68F/W130F, which was named as *Trp42/Trp156* in the text, was constructed by using the primer encoding the W130F substitution to amplify the W68F mutant plasmid. Other double mutants W68F/W156F, W42F/W130F, and W42F/W156F were created by an analogous procedure. All of the mutations were confirmed by DNA sequencing (Massachusetts General Hospital). The double mutants were named according to the remaining tryptophans present (*Trp42/Trp68*, *Trp130/Trp156*, *Trp42/Trp156*, *Trp68/Trp130*, *Trp42/Trp130*, and *Trp68/Trp156*). The triple tryptophan to phenylalanine substitutions were also named for the remaining native tryptophan (*Trp42-only*, *Trp68-only*, *Trp130-only*, and *Trp156-only*).

Wild-type and mutant HyD-Crys proteins were expressed and purified as described by Kosinski-Collins et al. (Kosinski-Collins et al. 2004). The proteins were expressed by *Escherichia coli* M15 [pREP4] cells. All of the mutant proteins expressed at levels similar to wild type and accumulated as native and soluble proteins. The proteins were purified by affinity chromatography using a Ni-NTA resin (Qiagen) as previously described (Konsinski-Collins et al. 2004). The purities of the proteins were confirmed by SDS-PAGE. Concentrations of purified proteins were calculated from absorbance data at 280nm using extinction coefficients computed by ProtParam tool (ExpASy) based on the amino acid composition (Gill and von Hippel 1989). The extinction coefficient was 23,970 cm<sup>-1</sup>M<sup>-1</sup> for triple tryptophan mutants, 29,660 cm<sup>-1</sup>M<sup>-1</sup> for double tryptophan mutants, and 41,040 cm<sup>-1</sup>M<sup>-1</sup> for wild-type HyD-Crys.

## *2. Time-Resolved Fluorescence Intensity and Anisotropy Measurements*

All fluorescence measurements were carried out in S buffer (10mM sodium phosphate buffer, 5mM DTT, and 1mM EDTA at pH7.0) at the temperature of 20°C. Different protein concentrations were used for HyD-Crys mutants with different numbers of Trp residues, so that the concentration of Trp residues was about 80μM in each protein sample.

Time-correlated single-photon counting (TCSPC) data were obtained using a home-built instrument described previously (see diagram 3-1) (Toptygin et al. 2006). Fluorescence was excited by a frequency-doubled output from a cavity-dumped dye laser. To minimize the excitation of tyrosine residues we tuned the exciting wavelength to 300nm. To minimize Trp photobleaching and subsequent contamination of the fluorescence signal by the emission from the photoproducts, the exciting power was attenuated to 50μW or less and the exciting beam was defocused so that the power density did not exceed 25μW/mm<sup>2</sup>. The exciting radiation was a train of vertically polarized 11ps wide pulses with a repetition rate of 4.1MHz. Photons were registered by two identical wings in T format. In each wing fluorescence emission passed through a polarizer and a monochromator, and was detected by a microchannel plate photomultiplier. In time-resolved anisotropy measurements the polarizers in two wings were set at 0° and 90° from the vertical.



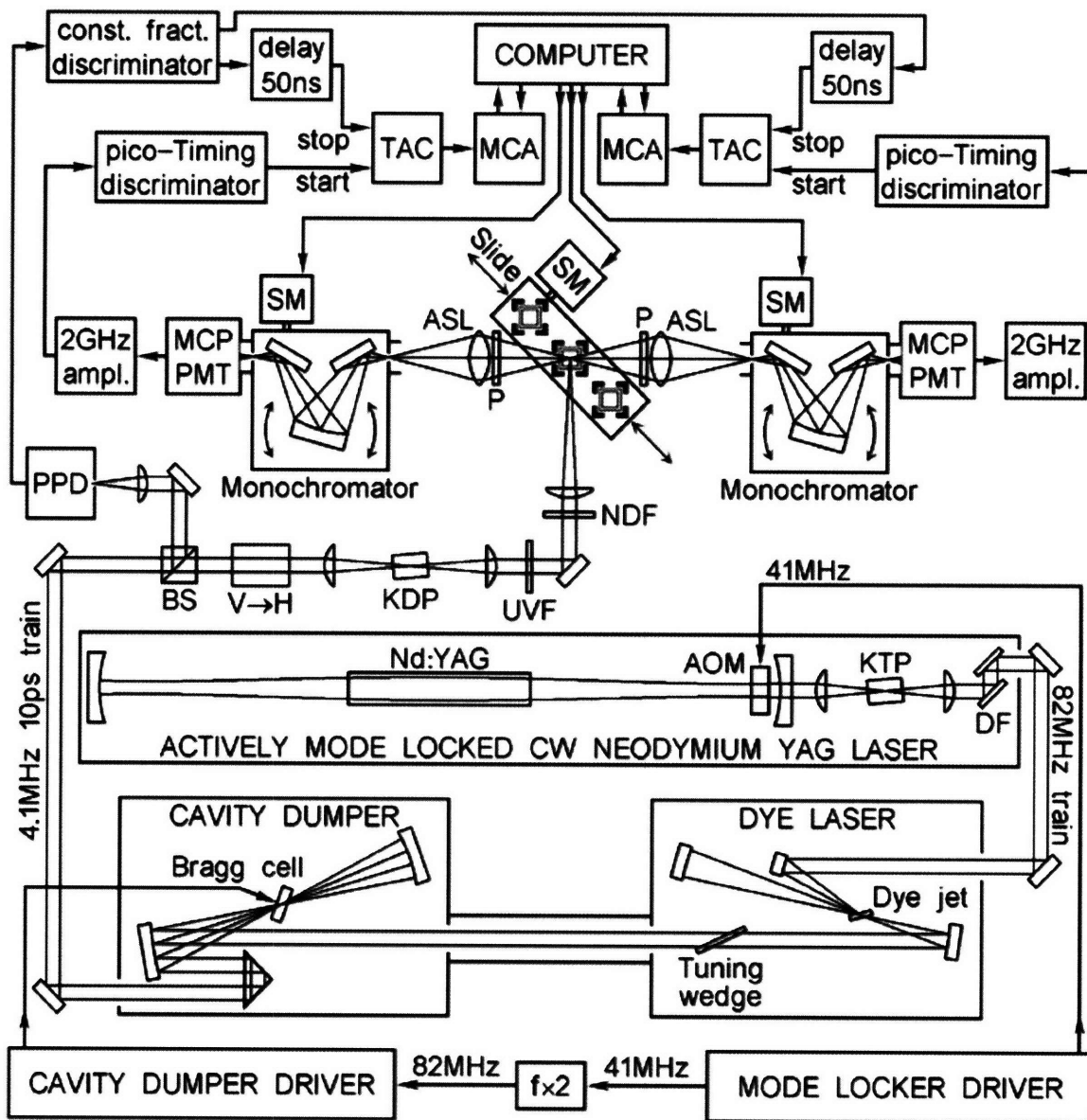


Diagram 3-1. Schematic diagram of the experimental setup for time-resolved fluorescence spectrophotometer (Courtesy of Toptygin et al. 2006).

The monochromators were tuned to 345nm, which excluded the highly polarized Raman scatter (peak near 333nm) from the 8nm bandwidth. In time-resolved intensity

measurements both polarizers were set at 55° from the vertical. The monochromators were scanned from 310nm to 440nm with 5nm steps. At each of the 27 emission wavelengths, fluorescence photons were counted for 300s by both wings simultaneously. To avoid pile up errors, photons in each wing were counted at a rate not exceeding 20kHz and stored in 2048 channels, with the timing calibration of 13.33ps/channel. Impulse response function (IRF) was recorded quasi-simultaneously (15s IRF recording after each 75s of fluorescence recording) using a ludox scatterer cell and had a full width of 65ps at half maximum. This represents the time resolution of the entire system.

### 3. *Steady-State Fluorescence and Absorption Measurements*

After each time-resolved intensity measurement, a steady-state fluorescence emission spectrum was taken with the same protein sample, using the same exciting wavelength and temperature, on an SLM-48000 fluorometer (SLM Instruments, Urbana, Illinois). The monochromator bandwidths were 2nm for the excitation and 4nm for the emission. The steady-state spectra were corrected for both the spectral variation of the emission channel sensitivity and the inner filter effect as described earlier (Toptygin et al. 2001). The corrected spectra were then used in renormalizing the pre-exponential amplitudes resulting from the global analysis of the time-resolved data (vide infra). An UV absorption spectrum of each protein sample was taken both before the beginning of the time-resolved and after the end of the steady-state fluorescence measurements. The two spectra were then compared, since a difference could indicate Trp photobleaching or protein aggregation. No significant changes in the absorption spectrum during the course of fluorescence measurements were found with any of the proteins studied in this work.

### 4. *Analysis of Time-resolved Intensity Data*

Each time-resolved fluorescence intensity curve was fitted by a numerical convolution of the quasi-simultaneously acquired IRF with the following model function:

$$F_m(t) = b_m + s_m \delta(t) + \theta(t) \sum_{n=1}^{N_{\text{exp}}} \alpha_{mn} \exp(-t / \tau_n) \quad (1)$$

The index  $m$  is relevant to the global analysis only, representing the serial number of the wavelength stop at which the emission was collected.  $\delta(t)$  and  $\theta(t)$  are Dirac delta and Heaviside step functions, respectively.  $N_{\text{exp}}$  denotes the total number of exponentials.  $b_m$ ,  $s_m$ ,  $\alpha_{mn}$ , and  $\tau_n$  are free fitting parameters.  $b_m$  is the photomultiplier background (dark counts).  $s_m$  is the intensity of scattered exciting radiation (including Raman).  $\alpha_{mn}$  is a pre-exponential amplitude and it is allowed to be positive or negative.  $\tau_n$  represents a time constant. A nonlinear weighted least-square algorithm was used to minimize  $\chi^2$ . The weights were calculated based on the Poissonian photon statistics. The quality of the fits was judged by the reduced  $\chi^2$  values, by plots of weighted residuals, and by the autocorrelation plots. The confidence intervals for the values of the fitting parameters were calculated using the diagonal elements of the inverted Hessian matrix, as described by Hamilton (Hamilton 1964).

### 5. Reversible Förster Resonance Energy Transfer Rates

If a protein contains two Trp residues, then the emission spectrum of each Trp residue will have at least some overlap with the absorption spectrum of the other Trp residue, therefore reversible energy transfer is possible. The rates of the forward ( $k_{12}$ ) and reverse ( $k_{21}$ ) energy transfer can be determined using the following equations (Porter 1972):

$$k_{12} = \frac{(\lambda_1 - k_1)(\lambda_2 - k_1)}{k_2 - k_1} \quad (2)$$

$$k_{21} = \frac{(\lambda_1 - k_2)(\lambda_2 - k_2)}{k_1 - k_2} \quad (3)$$

In these equations  $k_1$  represents the decay rate of Trp1 in the absence of Trp2,  $k_1=1/\tau_1$ , where  $\tau_1$  is the lifetime of Trp1 in the absence of Trp2. Likewise,  $k_2$  and  $\tau_2$  ( $k_2=1/\tau_2$ ) are the decay rate and the lifetime of Trp2 in the absence of Trp1, respectively. In the case where both Trps are present, two exponentials with the new time constants ( $\tau_1'$

and  $\tau_2'$ ) should be observed. The time constants  $\tau_1'$  and  $\tau_2'$  may not be attributable to individual Trp residues, since the decay of each Trp residue is described by the biexponential law. Parameters  $\lambda_1$  and  $\lambda_2$  in Equation 2 and 3 are defined as the inverses of the time constants  $\tau_1'$  and  $\tau_2'$ , i.e.,  $\lambda_1=1/\tau_1'$ ,  $\lambda_2=1/\tau_2'$ .

If the time-resolved fluorescence emission of Trp1 alone and/or Trp2 alone is not monoexponential, then the approach of Potter (1972) described above is not applicable. The equations to be used in this case of multiexponential fluorescence depend on the specific mechanism.

The approach we used in this work is based on the assumption that each Trp residue has only one conformation, consistent with the crystal structure of HyD-Crys. This means that for each Trps pair, there is definite value for donor-acceptor distance,  $\kappa^2$ , forward energy transfer rate  $k_{12}$ , and reverse rate  $k_{21}$ . Multiexponential fluorescence may have its origin in the time-variant rate of a nonradiative decay process, such as electron transfer from the excited-state Trp to the protein backbone (Chen et al. 2006). We also assumed that the amplitude-weighted mean lifetime of each Trp is wavelength invariant. This assumption was verified experimentally and only insignificant spectral variation of the mean lifetime was found. Under these assumptions the amplitude-weighted mean lifetimes of Trp1 and Trp2 can be substituted for  $\tau_1$  and  $\tau_2$ , which can be then used to calculate the values of  $k_1$  and  $k_2$  in Equations 2 and 3. Definition of  $\tau_1$  and  $\tau_2$  may still be ambiguous since it requires assignment of all the time constants to either Trp1 or Trp2. This assignment becomes possible in the case where one of the decay rates, for instance,  $k_2$ , is much greater than the other decay rate,  $k_1$ , and also much greater than both energy transfer rates,  $k_{12}$  and  $k_{21}$ . It is not difficult to show that in this case all the time constants resolved in the fluorescence of the double-Trp containing protein (Trp1/Trp2) will be either of the order of  $1/k_2$  (attributable to Trp2), or much longer than  $1/k_2$  (attributable to Trp1). We have to emphasize that this approach is applicable only in the cases where the mean lifetime of one Trp residue is at least an order of magnitude longer than the mean lifetime of the other Trp residue.

## 6. Calculation of the Förster Resonance Energy Transfer Efficiencies

The efficiency of Förster resonance energy transfer (FRET) was originally defined for the irreversible transfer. For the reversible energy transfer we use the following definitions of the energy transfer efficiency (Willaert 1992):

$$E_{12} = \frac{k_{12}}{k_1 + k_{12}} \quad (4)$$

$$E_{21} = \frac{k_{21}}{k_2 + k_{21}} \quad (5)$$

In this work the efficiency of energy transfer was measured experimentally and also calculated theoretically based on Förster equation (Forster 1959). The experimental values of the FRET efficiency were calculated from the experimental values of  $k_1$ ,  $k_2$ ,  $k_{12}$ , and  $k_{21}$  using Equations 4 and 5. The decay rate constant  $k_1$  or  $k_2$  was calculated as the inverse amplitude-weighted mean lifetime of the Trp1 or Trp2 in the absence of the other Trp residue. The experimental energy transfer rates  $k_{12}$  and  $k_{21}$  were obtained using Equations 3 and 4.

The theoretical values of energy transfer efficiency were calculated from the Förster radii  $R_0$  and the distances  $R$  between the centers of the donor and the acceptor (Forster 1959),

$$E_{theor} = \frac{R_0^6}{R_0^6 + R^6} \quad (6)$$

The values of  $R$  were determined from the crystal structure of HyD-Crys as described in the following section. The values of  $R_0$  were determined using the Förster equation (Forster 1959).

$$R_0^6 = \frac{9 \ln(10)}{128 \pi^5 n^4 N_A} \kappa^2 Q_D J \quad (7)$$

$N_A$  is Avogadro number.  $\kappa^2$  is the orientation factor determined from the crystal structure of HyD-Crys.  $Q_D$  is the quantum yield of the donor in the absence of the acceptor.  $J$  is the overlap integral.  $n$  is the refractive index of the medium. For  $n$  we used the value of 1.3567, which represents the refractive index of water at  $\lambda = 308.2\text{nm}$  and  $T=20^\circ\text{C}$  (Washburn 1926-1930).  $Q_D$  values have been reported previously (Chen et al. 2006). The values of the overlap integral were determined using the following equation.

$$J = \frac{\int c_1 \epsilon_A(\lambda) c_2^4 \lambda^4 F_D(\lambda) d\lambda}{\int F_D(\lambda) d\lambda} \quad (8)$$

Here  $c_1 = 1000\text{cm}^3/\text{liter}$  and  $c_2 = 10^{-7}\text{cm}/\text{nm}$  are unit conversion factors.  $\epsilon_A(\lambda)$  is the decadic molar extinction coefficient of the energy acceptor.  $F_D(\lambda)$  is the corrected emission spectrum of the donor. The integration was carried out over the spectral range from 286nm to 456nm, which completely included the emission spectrum of the donor.

The absorption spectra of the acceptors were measured using *Trp68-only* and *Trp156-only* for the energy transfer in the forward direction, and using *Trp42-only* and *Trp130-only* for the energy transfer in the reverse direction. The absorption values were converted to extinction coefficient values using the molar extinction coefficients of these mutants at 280nm, which were calculated as described in "mutagenesis, expression and purification of proteins". The extinction coefficient of fourteen tyrosine residues was subtracted from the extinction coefficient of each single-Trp HyD-Crys variant prior to the calculation of the overlap integral. The shape of the tyrosine absorption spectrum in a protein was modeled using the absorption spectrum of N-acetyl tyrosineamide in ethanol (the polarity of protein interior is closer to that of ethanol than to that of water). To make sure that the correct amount of tyrosine absorption is subtracted, we renormalized the experimental tyrosine extinction coefficient spectrum to the value of  $1280\text{M}^{-1}\text{cm}^{-1}$  at  $\lambda = 280\text{nm}$  that was also used in calculating the extinction coefficient of the protein (the extinction coefficient of Trp was assumed to be  $5690\text{M}^{-1}\text{cm}^{-1}$  at this wavelength) (Gill and von Hippel 1989). The contributions of cystines and phenylalanines was not subtracted from the protein absorption spectrum because all measurements were carried

out at reducing conditions, while cysteines and phenylalanines do not absorb appreciably at  $\lambda > 280\text{nm}$ .

The emission spectra of the donors were measured using Trp42-only and Trp130-only for the energy transfer in the forward direction, and using *Trp68-only* and *Trp156-only* for the energy transfer in the reverse direction. The conditions are described in the section “steady-state fluorescence and absorption measurements”. The use of the 300nm exciting wavelength prevented us from measuring the emission intensity at  $\lambda < 306\text{nm}$ . The Trp emission spectra were extended to  $\lambda < 306\text{nm}$  using the emission spectrum of 3-methylindole in cyclohexane-dioxane solvent mixture (83:17) (Chen et al. 2006). At  $\lambda > 306\text{nm}$  the emission spectrum of 3-methylindole matched the emission spectra of single-Trp containing proteins very well. The spectra were corrected for the spectral sensitivity variation of the instrument as described earlier (Toptygin et al. 2001) and used to calculate the overlap integral.

### 7. Determination of $R$ and $\kappa^2$ from Protein Crystal Structure

The values of  $R$  and  $\kappa^2$  were calculated from the crystal structure of HyD-Crys (PDB code: 1HK0) in two steps. First, the radius-vectors  $\vec{r}$  describing the coordinates of all fluorophore centers and the unit vectors  $\vec{u}$  describing the directions of all electronic transition were calculated by a computer program. The output of the program is included in the table B1 in Appendix B. The program determines the directions of the transition moments  ${}^1L_a$  and  ${}^1L_b$  for Trp relative to the indole nuclear frame using the information from Callis (Callis 1991). For the center of a Trp fluorophore the program takes the point at the middle of the bond connecting atoms CD2 and CE2.

Second, for selected Trp pairs and only for the electronic transitions involving the excited state  ${}^1L_a$ , we calculated the following vectors and scalars:

$$\vec{R} = \vec{r}_D - \vec{r}_A \quad (9)$$

$$R = \sqrt{(\vec{R} \cdot \vec{R})} \quad (10)$$

$$\kappa^2 = [(\vec{u}_D \cdot \vec{u}_A) - 3R^{-2}(\vec{R} \cdot \vec{u}_D)(\vec{R} \cdot \vec{u}_A)]^2 \quad (11)$$

Here  $\vec{r}_D$  and  $\vec{r}_A$  are the radius-vectors describing the absolute coordinates of the centers of the donor and the acceptor in the PDB file.  $\vec{R}$  is a vector connecting the center of the donor with the center of the acceptor.  $(\vec{a} \cdot \vec{b})$  denotes the scalar product of the vectors  $\vec{a}$  and  $\vec{b}$ .  $R$  is the distance between the centers of the donor and the acceptor.  $\vec{u}_D$  and  $\vec{u}_A$  are the unit vectors parallel to the directions of the  ${}^1L_a \leftrightarrow {}^1A$  transition dipole moments for the donor and the acceptor.  $\kappa^2$  is the orientation factor, which enters in the Förster equation. The values of  $R$  and  $\kappa^2$  are shown in the table B2 in Appendix B. The choice of exclusively  ${}^1L_a \leftrightarrow {}^1A$  transitions for Trp-Trp energy transfer calculations is dictated by the following two considerations. First, it is known that fluorescence emission from Trp residues in all proteins is entirely due to the  ${}^1L_a \rightarrow {}^1A$  transition (Callis 1997). Second, it is also known that the red tail ( $\lambda > 295\text{nm}$ ) in the absorption spectrum of Trp, which is responsible for the overlap between the absorption and emission spectra of Trp, is mainly due to the  ${}^1A \rightarrow {}^1L_a$  transition (Valeur and Weber 1977).

## D. RESULTS

### 1. Global Analysis of Time-Resolved Intensity Data

The results of the global analysis include the reduced  $\chi^2$ , a set of time constants  $\tau_i$ , and a set of pre-exponential amplitude spectra  $\alpha_i(\lambda)$  or  $\alpha_i(\nu)$ , where  $\lambda$  and  $\nu$  represent the emission wavelength and wavenumber, respectively. Figure 3-2 shows the pre-exponential amplitude spectra of Trp130-only HyD-Crys on a linear wavelength scale. Four exponential terms were required to obtain an adequate fit for this protein (reduced  $\chi^2 = 1.01$ ). Between four and six exponential terms were required for adequate global fits to



the data obtained with the other three single-Trp containing proteins, six double-Trp containing proteins, and wild-type HyD-Crys. Corresponding pre-exponential amplitude spectra are shown in Figures B1-B10 in Appendix B. 95% confidence intervals for the values of the pre-exponential factors  $\alpha_{mn}$  are depicted as error bars in these figures. For all but the fastest exponentials with  $\tau < 0.2\text{ns}$ , the 95% confidence intervals are so narrow that the gap between the upper and the lower error bar can be either barely visible or invisible.

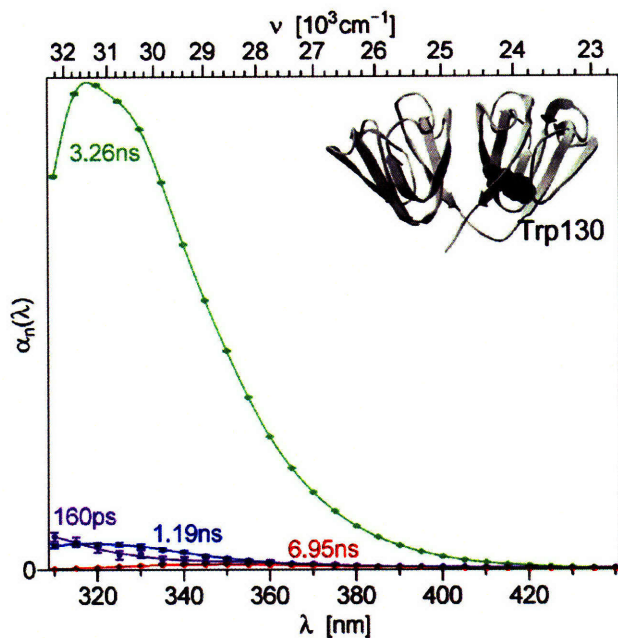


Figure 3-2. Pre-exponential amplitude spectra  $\alpha_i(\lambda)$  obtained by the global analysis of the fluorescence emission from Trp130-only HyD-Crys. Ribbon structure of wild-type HyD-Crys with Trp130 in spacefill is shown at the up-right corner. The values of the corresponding time constants  $\tau_i$  are shown near each spectrum using a matching color. The spectra have been renormalized using a corrected steady-state emission spectrum as described in Materials and Methods.

The origin of the multiple exponential terms can be in heterogeneity, or relaxation, or in a combination of the two. To distinguish between heterogeneity and relaxation we relied on the shape conservation criterion introduced and tested elsewhere (Toptygin et al. 2001). Figure 3-3 demonstrates the application of this heterogeneity criterion to the case of Trp130-only HyD-Crys. For homogeneous solutions of fluorophores in viscous solvents (Toptygin and Brand 2000) and for single-Trp containing proteins undergoing nanosecond scale relaxation in the excited state (Toptygin et al. 2001) the shape of the instantaneous emission spectrum should be time-invariant except for a parallel shift along the wavenumber axis. A variation in the shape of the instantaneous emission spectrum indicates the presence of heterogeneity, which is a result of emission from different fluorophores (e.g., Tyr and Trp) or from the same fluorophore in different environments (e.g., buried and solvent-exposed Trp residues). Although the instantaneous emission spectra in Figure 3-3 differ from one another very little, their shape is not conserved, which indicates the presence of heterogeneity.

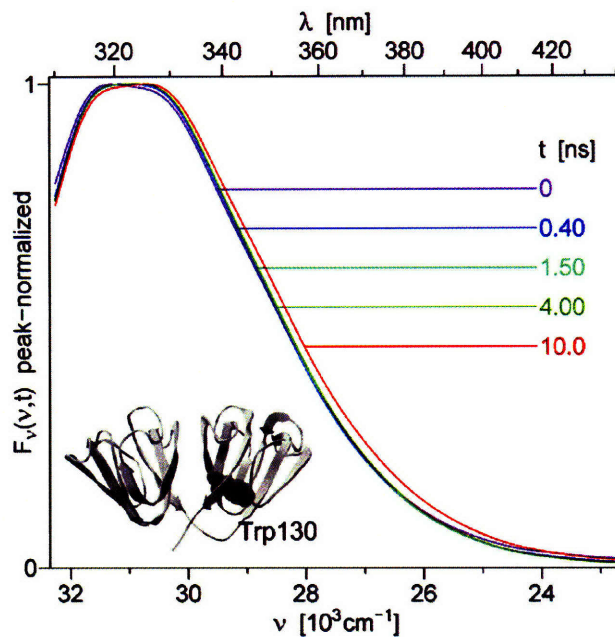


Figure 3-3. Instantaneous fluorescence emission spectra of Trp130-only at different times after excitation. These spectra were reconstructed from the pre-exponential amplitude spectra shown in Figure 3-2 and peak-normalized to facilitate shape comparison. Ribbon structure of wild-type H $\gamma$ D-Crys with Trp130 in spacefill is shown at the bottom. The spectra shown in the figure correspond to the following times after excitation: 0ns (purple), 0.40ns (blue), 1.50ns (dark-cyan), 4.00ns (yellow-green), and 10.0ns (red). The spectra are plotted on a linear wavenumber scale. A wavelength scale is shown at the top of the figure.

As an example of shape variation consider the instantaneous spectra at 0ns and 0.40ns after excitation. The 0.40ns spectrum (blue line) has a flat top, which is probably a result of a superposition of two unresolved peaks (unresolved vibrational structure). In the case of the 0ns spectrum (purple line) the peak on the left is slightly taller than the peak on the right. The purple curve and the blue curve cannot be superimposed by means of a parallel shift along the wavenumber axis, which reveals the contribution of heterogeneity (emission from multiple fluorophores). Since the instantaneous spectra at 0.40ns (blue line), 1.50ns (cyan line) and 4.00ns (green-yellow line) are practically identical, the contribution from the fluorophore that is responsible for the difference between the 0ns and 0.40ns spectra decays completely by  $t = 0.40\text{ns}$ . In Figure 3-2 we see only one exponential component with  $\tau$  shorter than 0.40ns, its spectrum is shown by the purple line. Based on the heterogeneity test we know that the fluorophore responsible for the 160ps component is not the same fluorophore that is dominant at 0.40ns, 1.50ns, and 4.00ns. Trp130 is most likely the dominant fluorophore in Trp130-only HyD-Crys, therefore the 160ps component is associated with a fluorophore other than Trp130. The peak of the spectrum associated with the 160ps exponential lies at the emission wavelength less than 310nm. Since the tyrosine emission peak is near 300nm and HyD-Crys contains 14 tyrosine residues, it is likely that tyrosine emission is the source of the 160ps component. The small amplitude of the 160ps component is a result of 300nm excitation, which is not optimum for exciting tyrosine residues. We have just one experiment in which we excited Trp130only HyD-Crys at 296nm (results not shown); in this case the relative contributions of the 160ps and 1.19ns components were found to be significantly greater, consistent with more efficient excitation of tyrosine at 296nm as compared to 300nm. This points to the fact that the 1.19ns component may also be due to tyrosine emission (at least in part).

A difference in shape is also observed between the instantaneous spectra at 4.00ns and 10.0ns. Neither the spectral variation between 0 and 0.40ns nor that between 4.00ns and 10.0ns can be attributed to protein and/or solvent relaxation around Trp130, since this mechanism cannot explain the variation in the spectral shape. The 10.0ns spectrum is wider than the 4.00ns spectrum, therefore the two spectra cannot be superimposed by

means of a parallel shift along the wavenumber axis. Since the wide spectrum is always more heterogeneous than the narrow one, this reveals the presence of heterogeneity in the 10ns spectrum. This heterogeneity can only be explained in terms of a long-lifetime fluorophore that outlives the main fluorophore in Trp130-only HyD-Crys and becomes a significant contributor at  $t = 10\text{ns}$ . Among the exponential components shown in Figure 3-2 there is only one component with a  $\tau$  longer than that of the dominant component. The spectrum associated with the  $\tau$  of 6.95ns has its maximum at 350nm and its shape closely resembles the spectra of solvent exposed Trp residues in proteins. It is possible that the 6.95ns component results from a small fraction of HyD-Crys in the unfolded state or from another trace contaminant protein.

The dominant component with  $\tau = 3.26\text{ns}$  clearly represents the emission of the main fluorophore in Trp130-only HyD-Crys, which is Trp130. The fractional mean amplitude  $\alpha\%$  of the 3.26ns component in the spectral range from 320nm to 340nm equals 91% (see Table 3-1).

Table 3-1: Lifetimes ( $\tau_i$ ), fractional amplitudes ( $\alpha_i$  %), and fractional intensity contributions ( $f_i$  %) for the single- and double-Trp containing proteins with both Trp residues in the same domain and the wild-type HyD-Crys.<sup>a</sup>

protein		$\tau_1$ ns	$\tau_2$ ns	$\tau_3$ ns	$\tau_4$ ns	$\chi^2$
		( $\alpha_1$ %, $f_1$ %)	( $\alpha_2$ %, $f_2$ %)	( $\alpha_3$ %, $f_3$ %)	( $\alpha_4$ %, $f_4$ %)	
Trps in the N-terminal domain	Trp42-only	— <sup>b</sup>	—	1.72	<b>2.85</b> <sup>c</sup>	1.00
				(25%, 18%)	(68%, 80%)	
	<i>Trp68</i> -only	<b>0.061</b>	<b>0.14</b>	—	—	1.02
		(68%, 31%)	(30%, 33%)			
	Trp42/ <i>Trp68</i>	<b>0.084</b>	—	0.48	<b>1.31</b>	1.06
		(51%, 7%)		(10%, 7%)	(37%, 75%)	
Trps in the C-terminal domain	Trp130-only	—	—	—	<b>3.26</b>	1.01
					(91%, 96%)	
	<i>Trp156</i> -only	<b>0.050</b>	<b>0.12</b>	0.27	—	1.01
		(36%, 13%)	(54%, 46%)	(9%, 17%)		
	Trp130/ <i>Trp156</i>	<b>0.080</b>	0.23	—	<b>0.94</b>	1.03
		(58%, 14%)	(17%, 11%)		(24%, 66%)	
wild type		<b>0.065</b>	0.16	0.82	1.41	1.01
		(44%, 6%)	(23%, 8%)	(17%, 32%)	(15%, 47%)	

<sup>a</sup> The lifetimes were obtained by the global analysis of the time-resolved fluorescence data from all 27 emission wavelengths. The amplitudes  $\alpha_i(\lambda)$  and intensity contributions  $f_i(\lambda) = \alpha_i(\lambda)\tau_i$  were integrated over the emission wavelength range from 320nm to 340nm and then renormalized to a unit sum. The fractional amplitudes ( $\alpha_i$ %) and fractional intensity contributions ( $f_i$ %) were shown in parentheses following the corresponding lifetime. <sup>b</sup> Some minor components with  $\alpha\% < 3\%$  or  $f\% < 2\%$  were not listed above in order to simplify the table. <sup>c</sup> The dominant lifetimes with  $\alpha\% > 30\%$  and/or  $f\% > 60\%$  were shown in boldface.

## 2. Lifetimes of Trp Residues in Single-Trp Containing Proteins and Double-Trp Containing Proteins with Both Trp Residues in the Same Domain

The amplitude spectra shown in Figure 3-2 and in Appendix B (Figure B1-B10) contain no negative amplitudes, and therefore there is no direct evidence of an excited state reaction or dielectric relaxation (Toptygin et al. 2001). In the absence of dielectric relaxation and excited state reactions the time constants  $\tau_i$  represent the lifetimes of excited state fluorophores. Using the information contained in the shapes of the pre-exponential amplitude spectra and time-resolved emission spectra we were able to assign each lifetime to a Trp residue in the native state HyD-Crys (peak near 320nm), to tyrosine residues (peak < 310nm), or to a trace contaminant (peak near 350nm). The lifetimes attributable to Trp residues in HyD-Crys are shown in Table 3-1. The table also gives the values of fractional mean amplitudes ( $\alpha_i$ ) averaged over the spectral range from 320nm to 340nm and the values of fractional mean steady state intensity contributions ( $f_i = \alpha_i\tau_i$ ) averaged over the same spectral range. The spectral range from 320nm to 340nm was chosen to minimize the contributions from tyrosine residues ( $\lambda < 320\text{nm}$ ) and solvent exposed Trp residues in trace contaminant proteins ( $\lambda > 340\text{nm}$ ). To emphasize the dominant components, in Tables 3-1 and 3-2 we highlighted the lifetimes with the fractional amplitudes greater than 30% and/or with the fractional intensity contributions greater than 60%.

In single-Trp containing proteins the highly quenched *Trp68* and *Trp156* (Chen et al. 2006) showed two or three short lifetimes between 0.05 and 0.27ns. In contrast, the moderately fluorescent *Trp42* and *Trp130* had much longer lifetimes. A single lifetime of 3.26ns can be attributed to *Trp130*, while two lifetimes of 1.72ns and 2.85ns can be attributed to *Trp42*, with the 2.85ns lifetime being dominant.

In the double-Trp containing proteins, with both Trp residues either in the N-terminal domain (*Trp42/Trp68*) or in the C-terminal domain (*Trp130/Trp156*), we observed one or two short lifetimes ( $\tau < 0.3\text{ns}$ ) attributable to the highly quenched *Trp68* or *Trp156*, and one or two longer lifetimes ( $\tau > 0.3\text{ns}$ ) attributable to the moderately fluorescent *Trp42* or *Trp130*. The lifetimes attributable to *Trp42* and *Trp130* became significantly shorter in the presence of *Trp68* and *Trp156*, respectively. The shortening



of the Trp42 and Trp130 lifetimes can be either due to the intradomain Förster resonance energy transfer from Trp42 to *Trp68* and from Trp130 to *Trp156* or due to some other mechanism, such as a change in the Trp environment resulting from a different structure of the mutated protein, however, in a previous study the structure of HyD-Crys was found to be unaffected by the Trp to Phe mutations (Kosinski-Collins et al. 2004).

The rationale of attributing all the lifetimes shorter than 0.3ns to *Trp68* or *Trp156* and all the lifetimes longer than 0.3ns to Trp42 or Trp130 was based not only on the values of the corresponding lifetimes in the single-Trp containing proteins, but also on the shapes of the corresponding pre-exponential amplitude spectra (Figure B1-B10 in Appendix B). For example, the shape of the spectrum corresponding to  $\tau = 1.31$ ns component in the double-Trp containing protein, Trp42/*Trp68*, (Figure 3-4) closely resembles the shape of the spectrum corresponding to  $\tau = 2.85$ ns component in Trp42-only protein (Figure 3-5), while the shape of the spectrum corresponding to  $\tau = 0.48$ ns component in Trp42/*Trp68* protein (Figure 3-4) closely resembles the shape of the spectrum corresponding to  $\tau = 1.72$ ns component in Trp42-only protein (Figure 3-5). The peaks of all the spectra corresponding to  $\tau < 0.3$ ns (*Trp68* and *Trp156*) were shifted slightly to the red relative to those corresponding to  $\tau > 0.3$ ns (Trp42 and Trp 130). The red shift probably has its origin in the environment of *Trp68* and *Trp156* being more polar than that of Trp42 and Trp130, which is consistent with crystal structure of HyD-Crys and the results of QM-MM calculations (Chen et al. 2006).

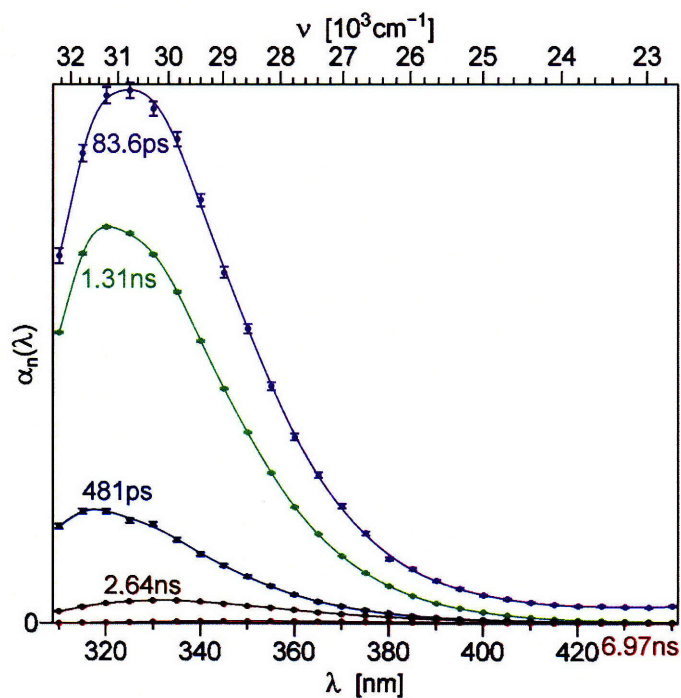


Figure 3-4. Pre-exponential amplitude spectra  $\alpha_i(\lambda)$  obtained by the global analysis of the fluorescence emission from Trp42/Trp68 H $\gamma$ D-Crys. The values of the corresponding time constants  $\tau_i$  are shown near each spectrum using a matching color.

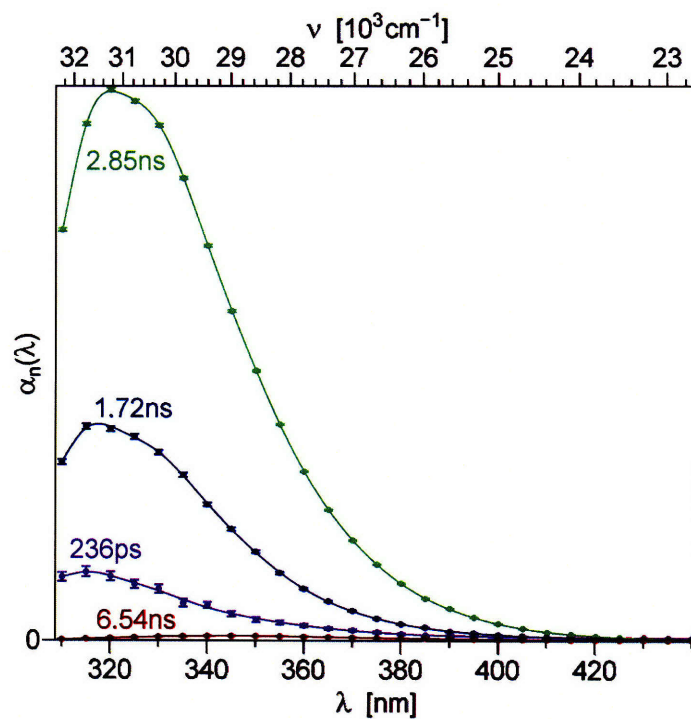


Figure 3-5. Pre-exponential amplitude spectra  $\alpha_i(\lambda)$  obtained by the global analysis of the fluorescence emission from Trp42-only H $\gamma$ D-Crys. The values of the corresponding time constants  $\tau_i$  are shown near each spectrum using a matching color.

Due to the fundamental limit on the number of exponential terms that can be resolved from experimental data, the total number of the resolved lifetimes in the double-Trp containing protein (e.g. Trp42/Trp130) may differ from the sum of the numbers of lifetimes in the corresponding two single-Trp containing proteins (e.g. Trp42-only and Trp130-only). Thus, it is not feasible to trace how much each of the individual lifetimes is changed by the presence of the second Trp residue in the same domain. The values of the amplitude weighted mean lifetimes should be compared in the case where the number of lifetimes attributed to the same Trp is different between the single-Trp and double-Trp containing protein. The mean lifetime of Trp42 alone equaled 2.55ns. In the presence of *Trp68* (the acceptor) the mean lifetime of Trp42 (the donor) decreased to 1.13ns, which was a 56% decrease. The mean lifetime of *Trp68* alone equaled 0.086ns and it became 0.084ns in the presence of Trp42. Since the difference between 0.086ns and 0.084ns was less than their estimated standard deviation ( $\pm 0.01$ ns), we cannot accurately quantify the effect of Trp42 on the lifetime of *Trp68*.

A similar pattern was observed in the C-terminal domain. Here the lifetime of Trp130 alone (energy donor) was 3.26ns and it decreased to 0.94ns in the presence of *Trp156* (energy acceptor), which was a 71% decrease. The mean lifetime of Trp 156 alone equaled 0.106ns, and it became 0.113ns in the presence of Trp130. Because the difference was less than the estimated standard deviation ( $\pm 0.01$ ns), it was not a significant change.

Since the single-Trp containing proteins have a total of eight lifetimes attributable to Trp residues (Table 3-1), one would expect to see eight lifetimes in the wild-type HyD-Crys, which has all four Trp residues. However, due to the limited number of exponential terms that can be resolved from experimental data, we see only four lifetimes attributable to Trp residues in the wild-type protein (Table 3-1). The dominant lifetime equaled 0.065ns, which was associated with the fractional amplitude of 44%. The 0.065ns and 0.16ns lifetimes represent unresolved fluorescence signals from both *Trp68* and *Trp156*. The 0.82ns and 1.41ns lifetimes represent unresolved fluorescence signals from both Trp42 and Trp130.

Figures 3-6 and 3-7 show deconvoluted fluorescence intensity on a logarithmic scale, as a function of time. These semi-log plots are for illustrative purposes only and were not used to judge the quality of fits to experimental data by model functions, since it is virtually impossible to see minute systematic deviations on a semi-log plot (Gafni and Brand 1976). In Figure 3-6 the time-resolved emission from Trp42-only protein is almost a straight line except at  $t < 0.5\text{ns}$ , suggesting that between 0.5ns and 8ns the time-resolved fluorescence appears to be monoexponential. The steep slope and significant curvature of the line of *Trp68-only* protein (dotted line) reveal exceptionally fast and non-monoexponential decay of *Trp68*. The time-resolved intensity of the double-Trp containing protein, *Trp42/Trp68*, exhibits two main phases. The steep slope at  $t < 0.2\text{ns}$  can be attributed to the fast decay of *Trp68*. At  $t > 0.2\text{ns}$  we observed a decrease in the slope, however, at  $t > 0.5\text{ns}$  the slope of the broken line (*Trp42/Trp68*) is still considerably steeper than that of the solid line (*Trp42-only*). This indicates that the decay rate of *Trp42* is increased by the energy transfer from *Trp42* to *Trp68*. If there were no interaction between these two Trps, one would expect the solid line (*Trp42-only*) and the broken line (*Trp42/Trp68*) to be parallel at  $t > 0.5\text{ns}$ . This was indeed found in the cases where little or no energy transfer was expected (Figures 3-8 and 3-9 described below.)

The time-resolved emission from the Trps in the C-terminal domain (Figure 3-7) shows very similar trends as those of the Trps in the N-terminal domain. The difference between the slopes of the broken line (*Trp130/Trp156*) and solid line (*Trp130-only*) in Figure 3-7 is greater than the difference between the slopes of the broken line (*Trp42/Trp68*) and solid line (*Trp42-only*) in Figure 3-6. The slope of a decay curve on a semi-log plot represents the decay rate, which equals  $k_r+k_{nr}$  in the absence of the acceptor and  $k_r+k_{nr}+k_{ET}$  in the presence of the acceptor. Here  $k_r$  is the radiative decay rate,  $k_{nr}$  is the nonradiative decay rate, and  $k_{ET}$  is the energy transfer rate. Thus, the difference between the slope of the broken line (*Trp42/Trp68* or *Trp130/Trp156*) and the slope of the solid line (*Trp42-only* or *Trp130-only*) equals to the energy transfer rate ( $k_{ET}$ ). This suggests that the rate of energy transfer between *Trp130* and *Trp156* in the C-terminal domain is greater than that the rate of energy transfer between *Trp42* and *Trp68* in the N-terminal domain. The donor-acceptor pair with the greater energy transfer rate also has greater energy transfer efficiency.

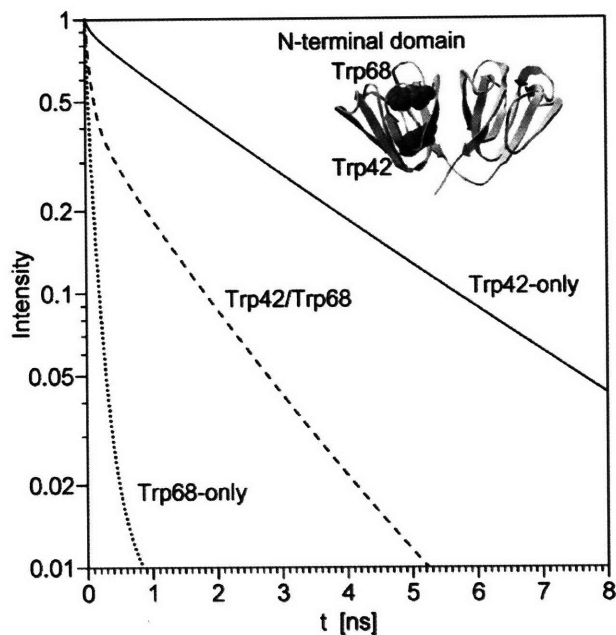


Figure 3-6. Deconvoluted fluorescence intensity in the emission wavelength range from 320nm to 340nm as a function of time after  $\delta$ -excitation for Trps in the N-terminal domain of HyD-Crys. Ribbon structure of wild-type HyD-Crys with Trp42 and Trp68 in spacefill is shown at the up-right corner. The solid line represents the emission of Trp42-only. The dotted line represents the emission of *Trp68-only*. The broken line represents the emission of *Trp42/Trp68* protein, containing both Trps.

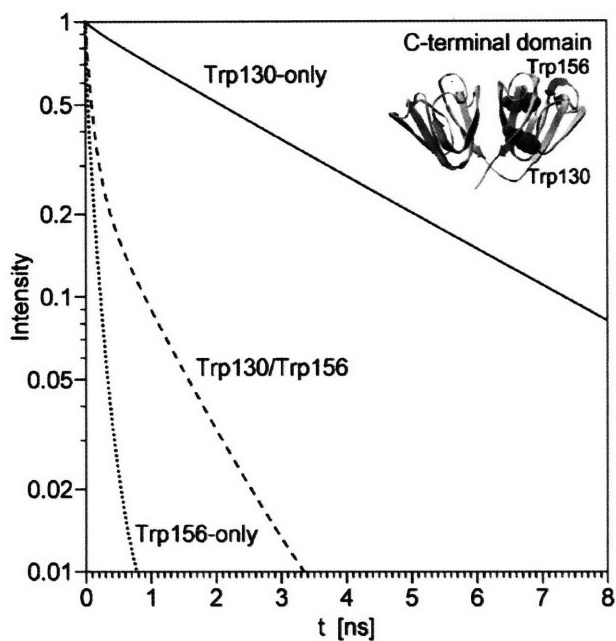


Figure 3-7. Deconvoluted fluorescence intensity in the emission wavelength range from 320nm to 340nm as a function of time after  $\delta$ -excitation for Trps in the C-terminal domain of H $\gamma$ D-Crys. Ribbon structure of wild-type H $\gamma$ D-Crys with Trp130 and Trp156 in spacefill is shown at the up-right corner. The solid line represents the emission of Trp130-only. The dotted line represents the emission of *Trp156-only*. The broken line represents the emission of Trp130/*Trp156* protein, containing both Trps.

### 3. Lifetimes for Double-Trp Containing proteins with the Two Trps in the Different Domains

Time- and spectrally-resolved fluorescence data were also obtained for four double-Trp containing proteins with the two Trps in the different domains. These mutants can be used as controls to further confirm the energy transfer observed in the mutants with both Trps in the same domain. Since for any combination of one Trp in the N- and one in the C-terminal domain the distance between the centers of the two Trps is greater than 18Å, little or no energy transfer is expected. The mutants *Trp42/Trp156* and *Trp68/Trp130* contain one moderately fluorescent Trp (*Trp42* or *Trp130*) and one highly quenched Trp (*Trp68* or *Trp156*). *Trp42/Trp130* mutant contains two moderately fluorescent Trps, whereas *Trp68/Trp156* mutant contains two highly quenched Trps. The lifetimes, fractional amplitudes, and fractional intensity contributions for the four mutants with the Trps in the different domains are shown in Table 3-2. The lifetimes of *Trp42/Trp156* protein can be simply assigned to *Trp42* and *Trp156* based on the lifetimes of *Trp42* alone and *Trp156* alone. The 2.83ns lifetime can be attributed to *Trp42*, since it is very close to the dominant lifetime of *Trp42* alone (2.85ns, see Table 3-1). The 0.085ns lifetime has very high amplitude ( $\alpha\% = 85\%$ ) and can be attributed to *Trp156*. Similarly, the 3.15ns lifetime of *Trp68/Trp130* protein can be attributed to *Trp130* that has a 3.26ns lifetime in the absence of *Trp68*, and the 0.065ns component can be attributed to *Trp68*.

*Trp42/Trp130* contains two moderately fluorescent Trp residues. The 3.12ns lifetime represents the unresolved mixture of the 2.85ns lifetime from *Trp42* alone and the 3.26ns lifetime from *Trp130* alone. The 1.77ns lifetime can be assigned to *Trp42* that exhibits a 1.72ns lifetime when it is alone (see *Trp42-only* in Table 3-1), while *Trp130-only* protein does not contain a close lifetime. *Trp68/Trp156* contains two highly quenched Trp residues. It exhibits two lifetimes (0.058ns and 0.13ns) that represent an unresolved mixture of two lifetimes from *Trp68-only* (0.061ns and 0.14ns) and two lifetimes from *Trp156-only* (0.050ns and 0.12ns).



Table 3-2. Decay constants of the double-Trp containing proteins with two Trps in the different domains. <sup>a</sup>

protein	$\tau_1$ ns ( $\alpha_1\%$ , $f_1\%$ )	$\tau_2$ ns ( $\alpha_2\%$ , $f_2\%$ )	$\tau_3$ ns ( $\alpha_3\%$ , $f_3\%$ )	$\chi^2$
Trp42/Trp156	<b>0.085</b> <sup>b</sup> (57%, 6%)	1.75 (9%, 20%)	<b>2.83</b> (19%, 67%)	1.03
Trp68/Trp130	<b>0.065</b> (52%, 3%)	— <sup>c</sup>	<b>3.15</b> (29%, 89%)	1.04
Trp42/Trp130	—	1.77 (22%, 14%)	<b>3.12</b> (73%, 84%)	1.03
Trp68/Trp156	<b>0.058</b> (52%, 24%)	<b>0.13</b> (43%, 46%)	0.32 (4%, 11%)	1.03

<sup>a</sup> The lifetimes were obtained by the global analysis of the time-resolved fluorescence data from all 27 emission wavelengths. The amplitudes  $\alpha_i(\lambda)$  and intensity contributions  $f_i(\lambda)=\alpha_i(\lambda)\tau_i$  were integrated over the emission wavelength range from 320nm to 340nm and then renormalized to a unit sum. The fractional amplitudes ( $\alpha_i\%$ ) and fractional intensity contributions ( $f_i\%$ ) were shown in parentheses following the corresponding lifetime. <sup>b</sup> The dominant lifetimes with  $\alpha\% > 30\%$  or  $f\% > 60\%$  were shown in boldface. <sup>c</sup> Some minor components with  $\alpha\% < 3\%$  or  $f\% < 5\%$  were not listed above in order to simplify the table.

Figures 3-8 and 3-9 show the time-resolved fluorescence intensity for some double-Trp containing proteins with the Trp residues in the different domains. The time-resolved emission from Trp42/*Trp156* protein, consists of a fast phase ( $t < 0.5\text{ns}$ ) and a slow phase ( $t > 0.5\text{ns}$ ) (Figure 3-8). The slope of the slow phase of Trp42/*Trp156* is nearly identical to that of Trp42-only protein (the solid line). Two straight lines with identical slopes on the semi-log scale correspond to two exponentials with equal lifetimes. This suggests that the lifetime of Trp42 is the same in the presence and in the absence of *Trp156*, therefore there is little or no energy transfer between Trp42 and *Trp156*. Similarly, from the data shown in Figure 3-9 it follows that there is little or no energy transfer between *Trp68* and Trp130 in the double-Trp containing protein, *Trp68/Trp130*.

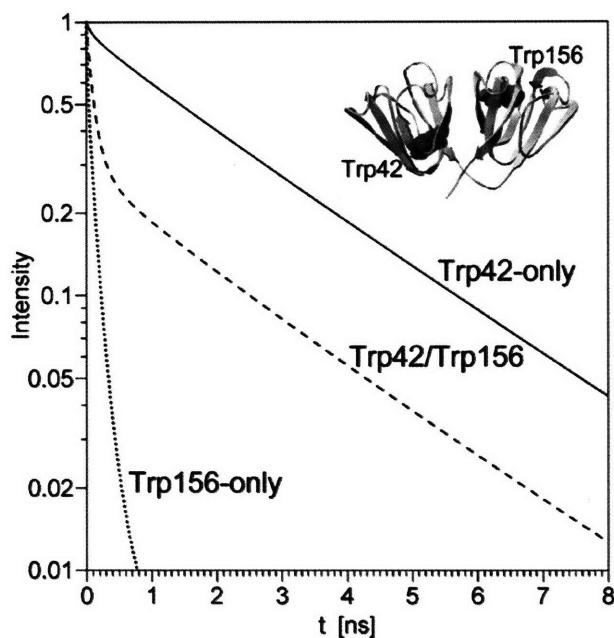


Figure 3-8. Deconvoluted fluorescence intensity in the emission wavelength range from 320nm to 340nm as a function of time after  $\delta$ -excitation for Trps in the different domains of HyD-Crys. Ribbon structure of wild-type HyD-Crys with Trp42 and Trp156 in spacefill is shown at the up-right corner. The solid line represents the emission of Trp42-only HyD-Crys (Trp in the N-terminal domain). The dotted line represents the emission of *Trp156-only* HyD-Crys (Trp in the C-terminal domain), and the broken line represents the emission of Trp42/*Trp156* protein containing both Trps.

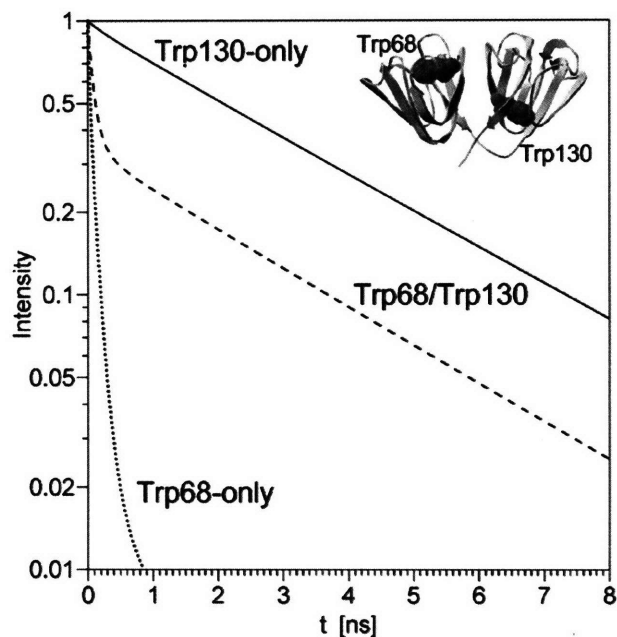
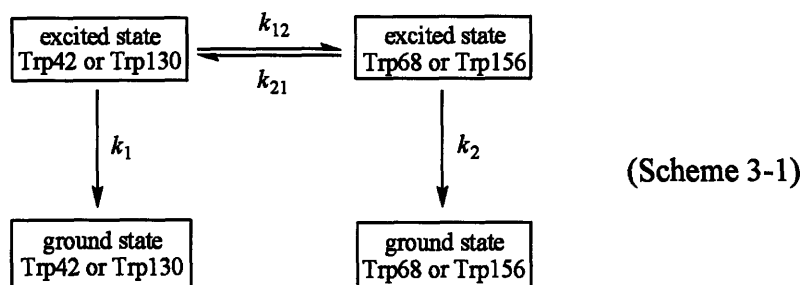


Figure 3-9. Deconvoluted fluorescence intensity in the emission wavelength range from 320nm to 340nm as a function of time after  $\delta$ -excitation for Trps in the different domains of H $\gamma$ D-Crys. Ribbon structure of wild-type H $\gamma$ D-Crys with Trp68 and Trp130 in spacefill is shown at the up-right corner. The solid line represents the emission of Trp130-only H $\gamma$ D-Crys (Trp in the C-terminal domain). The dotted line represents the emission of *Trp68-only* H $\gamma$ D-Crys (Trp in the N-terminal domain), and the broken line represents the emission of *Trp68/Trp130* protein containing both Trps.

#### 4. Reversible Förster Resonance Energy Transfer Rates



Reversible Förster resonance energy transfer between two Trps is illustrated in scheme 1. The rates of the forward ( $k_{12}$ ) and reverse ( $k_{21}$ ) energy transfer have been calculated for two pairs of Trps, for Trp42 and *Trp68* in the N-terminal domain as well as for Trp130 and *Trp156* in the C-terminal domain. We use index 1 for the moderately fluorescent Trps (Trp42 and Trp130) and 2 for the highly quenched Trps (*Trp68* and *Trp156*), and therefore  $k_{12}$  always describes energy transfer from a moderately fluorescent Trp to a highly quenched Trp, while  $k_{21}$  always describes energy transfer from a highly quenched Trp to a moderately fluorescent Trp. From Equation (3) it follows that  $k_{21}$  is directly proportional to  $(\lambda_2 - k_2)$ , where  $k_2$  is the inverse mean lifetime of the highly quenched Trp in the absence of the moderately fluorescent Trp, and  $\lambda_2$  is the inverse mean lifetime of the highly quenched Trp in the presence of the moderately fluorescent Trp. The technical details of calculating the mean lifetime for each Trp are described in Supporting Information. From experimental data we obtained the following values and standard deviations: for Trp42/*Trp68*  $k_2 = 11.6 \pm 1.3 \text{ ns}^{-1}$  and  $\lambda_2 = 12.0 \pm 1.4 \text{ ns}^{-1}$ , for Trp130/*Trp156*  $k_2 = 9.4 \pm 0.9 \text{ ns}^{-1}$  and  $\lambda_2 = 8.9 \pm 0.8 \text{ ns}^{-1}$ . Within experimental errors the values of  $\lambda_2$  and  $k_2$  are equal, therefore the differences  $(\lambda_2 - k_2)$  do not significantly differ from zero, and so do the rates  $k_{21}$ . The  $k_{21}$  values calculated using Equation (3) are  $0.4 \pm 1.9 \text{ ns}^{-1}$  for Trp42/*Trp68* and  $-0.5 \pm 1.1 \text{ ns}^{-1}$  for Trp130/*Trp156*. The negative  $k_{21}$  value makes no physical sense, however, since the absolute values of  $k_{21}$  are less than the

standard deviations in both cases, we conclude that the reverse energy transfer rate is small and cannot be accurately calculated from our experimental data.

If  $k_{21}=0$  and  $\lambda_2=k_2$  within experimental errors, then the term  $(\lambda_2-k_1)$  in the numerator of the fraction on the right hand side of Equation (2) cancels out with the term  $(k_2-k_1)$  in the denominator and the equation can be reduced to the following

$$k_{12} = \lambda_1 - k_1 \quad (12)$$

Using the reduced equation we obtained the following forward transfer rates:  $0.51 \pm 0.09$  ns<sup>-1</sup> for Trp42/Trp68 and  $0.70 \pm 0.09$  ns<sup>-1</sup> for Trp130/Trp156.

### 5. Förster Resonance Energy Transfer Efficiencies

The theoretical value of Förster resonance energy transfer efficiency ( $E_{\text{theor}}$ ) was determined by the distance between energy donor and acceptor ( $R$ ), the value of the spectral overlap integral ( $J$ ), the value of the orientation factor ( $\kappa^2$ ), and several other parameters. In this work the values of  $R$  and  $\kappa^2$  for all possible combinations of the donor Trps and acceptor Trps were calculated from the published crystal structure of HyD-Crys (Basak et al. 2003). Two  $\kappa^2$  values were in good agreement with those computed using a molecular dynamics simulation (Chen et al. 2006), while the remaining  $\kappa^2$  values and  $R$  values have not been previously reported. Experimental energy transfer efficiencies were calculated from the energy transfer rates  $k_{12}$  and  $k_{21}$  using Equations (4 and 5). Table 3-3 shows theoretical and experimental values of the forward and reverse energy transfer efficiencies for the two Trps in the N-terminal domain and the two Trps in the C-terminal domain.

The experimental value of the forward energy transfer efficiency in the C-terminal domain was about 71%, which was higher than that in the N-terminal domain (56%). The theoretical efficiencies for the forward energy transfer were fairly close to

the experimental values. The difference between the two domains in the forward energy transfer efficiency is due to the greater value of the overlap integral ( $J$ ) and the higher donor quantum yield ( $Q_D$ ) in the C-terminal domain than in the N-terminal domain. Theoretical energy transfer efficiencies for the reverse transfer, from quenched *Trp68* or *Trp156* to moderately fluorescent Trp42 or Trp130, do not exceed 5%. This results from the low quantum yields of *Trp68* and *Trp156*, which play the roles of the donors in the case of reverse energy transfer. Experimental values of the reverse energy transfer efficiency equal zero within experimental uncertainties.

Table 3-3. Calculated overlap integrals ( $J$ ), orientation factors ( $\kappa^2$ ), donor quantum yields ( $Q_D$ ), Förster radii ( $R_0$ ), center-to-center distances ( $R$ ), forward energy transfer rate ( $k_{12}$ ) or reverse energy transfer rate ( $k_{21}$ ), and the energy transfer efficiencies ( $E$ ) for the two Trps in each domain of HyD-Crys.

	Trp pairs			
	N-terminal domain		C-terminal domain	
	Trp42→Trp68	Trp68→Trp42	Trp130→Trp156	Trp156→Trp130
$J$ ( $\times 10^{-13}$ cm <sup>6</sup> •mol <sup>-1</sup> )	1.4 ± 0.3	0.87 ± 0.4	1.7 ± 0.4	1.1 ± 0.3
$\kappa^2$	0.56	0.56	0.57	0.57
<sup>a</sup> $Q_D$	0.13 ± 0.01	0.0076 ± 0.0008	0.17 ± 0.02	0.0099 ± 0.001
<sup>b</sup> $R_0$ (Å)	11.8 ± 0.5	6.8 ± 0.6	12.8 ± 0.6	7.4 ± 0.4
distance (Å)	12.2	12.2	12.4	12.4
$k_{12}$ or $k_{21}$ (ns <sup>-1</sup> )	0.51 ± 0.09	~ 0 <sup>c</sup>	0.70 ± 0.09	~ 0
<sup>d</sup> $E_{\text{theor}}$ (%)	44 ± 6	3 ± 1	55 ± 7	4 ± 1
<sup>e</sup> $E_{\text{exper}}$ (%)	56 ± 2	~ 0 <sup>c</sup>	71 ± 2	~ 0

<sup>a</sup>  $Q_D$  is the quantum yield determined by steady-state fluorescence using L-Trp (18). <sup>b</sup>  $R_0$  was calculated using the Förster equation from the values of  $J$ ,  $\kappa^2$ ,  $Q_D$ , and other parameters. <sup>c</sup> The experimental values of the reverse energy transfer rate ( $k_{21}$ ) and the reverse energy transfer efficiency ( $E_{\text{exper}}$ ) equal zero within experimental uncertainties. <sup>d</sup>  $E_{\text{theor}}$  is the theoretical energy transfer efficiency calculated from the values of  $R$  and  $R_0$ . <sup>e</sup>  $E_{\text{exper}}$  is the experimental value of energy transfer efficiency calculated using Equation (4 and 5).

The FRET efficiencies for two swapped Trp pairs are shown in Table 3-4. Both experimental and theoretical efficiency values are very close to zero when the donor and acceptor are in the different domains (Trp42→Trp156 and Trp130→Trp68). This results from large distances ( $R$ ) between Trp residues in the different domains.



Table 3-4. Calculated overlap integrals ( $J$ ), orientation factors ( $\kappa^2$ ), donor quantum yields ( $Q_D$ ), Förster radii ( $R_0$ ), center-to-center distances ( $R$ ), and the energy transfer efficiencies ( $E$ ) for two Trp pairs with the Trps in the different domains of HyD-Crys.

	crossed Trp pairs			
	Trp42→Trp156	Trp156→Trp42	Trp130→Trp68	Trp68→Trp130
$J(\times 10^{-13} \text{ cm}^6 \cdot \text{mol}^{-1})$	$1.3 \pm 0.4$	$1.0 \pm 0.4$	$1.8 \pm 0.3$	$1.0 \pm 0.3$
$\kappa^2$	0.05	0.05	0.03	0.03
<sup>a</sup> $Q_D$	$0.13 \pm 0.01$	$0.0099 \pm 0.001$	$0.17 \pm 0.02$	$0.0076 \pm 0.0008$
<sup>b</sup> $R_0$ (Å)	$7.9 \pm 0.4$	$4.9 \pm 0.3$	$7.8 \pm 0.3$	$4.2 \pm 0.2$
distance (Å)	22.3	22.3	21.8	21.8
<sup>c</sup> $E_{\text{theor}}$ (%)	$0.2 \pm 0.07$	$0.01 \pm 0.005$	$0.2 \pm 0.04$	$0.005 \pm 0.002$
<sup>d</sup> $E_{\text{exper}}$ (%)	$3 \pm 2$	— <sup>e</sup>	$3 \pm 2$	—

<sup>a</sup>  $Q_D$  is the quantum yield determined by steady-state fluorescence using L-Trp (18). <sup>b</sup>  $R_0$  was calculated using the Förster equation from the values of  $J$ ,  $\kappa^2$ ,  $Q_D$ , and other parameters. <sup>c</sup>  $E_{\text{theor}}$  is the theoretical energy transfer efficiency calculated from the values of  $R$  and  $R_0$ . <sup>d</sup>  $E_{\text{exper}}$  is the experimental value of energy transfer efficiency calculated using Equation (4 and 5). <sup>e</sup> — represents the fact that the experimental values of reverse energy transfer efficiency could not be determined.

## 6. Time-Resolved Emission Spectra of Trp130-only HyD-Crys

Time-resolved emission spectra (TRES) of Trp130-only HyD-Crys are shown in Figure 3-3. The difference between the spectra at 0ns and 0.40ns after excitation can be attributed to the short-lived contribution from tyrosine residues (see above). Likewise, the difference between the spectra at 4.00ns and 10.0ns is likely due to the solvent exposed Trp in a trace contaminant protein. The instantaneous spectra at 0.40ns, 1.50ns, and 4.00ns are almost identical, which shows that the time-dependent red shift is not observed with Trp130 in HyD-Crys during the time window between 0.40ns and 4.00ns. Nanosecond time-dependent red shifts are observed only if the protein has soft normal vibration modes that are coupled to the Trp static dipole moment change via the motion of charged groups or water molecules relative to the Trp sidechain. At least two possible explanations of the absence of the time-dependent red shift in Trp fluorescence in a protein can be considered. First, it is possible that the protein matrix around each Trp is so rigid that the polar groups within 5Å and charged groups within 10Å distance from the Trp cannot move. The second possibility is that there are no charged groups and no water molecules in close proximity to the Trp sidechain. In the case of HyD-Crys, Trp130 sidechain has no direct contact with water molecules. On the other hand, according to the crystal structure (Basak et al. 2003), the charged residues His87, Asp107, and Arg168 are close to Trp130 (Figure 3-10). The  $\delta$ -nitrogen of His87 is 4.1Å away from the indole nitrogen of Trp130. One of the carboxyl oxygen atoms of Asp107 is 4.9Å away from the indole carbon 5 of Trp130. The  $\delta$ -nitrogen of Arg168 is 5.4Å away from the indole carbon 6 of Trp130. If the sidechains of His87, Asp107, and Arg168 could move relative to the Trp130 sidechain on the nanosecond time scale, then the time-dependent red shift would have been observed. Since the shift is not observed, this suggests that the protein matrix around Trps of HyD-Crys is exceptionally rigid.

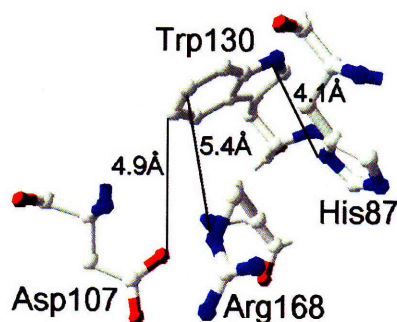


Figure 3-10: Crystal structure of charged residues close by Trp130 (PDB code 1HK0).

### 7. Time-Resolved Fluorescence Anisotropy

For Trp42 in the N-terminal domain and Trp130 in the C-terminal domain we measured the vertical and horizontal polarization components of the time-resolved fluorescence at only one emission wavelength (340nm). The two polarization components were fitted simultaneously by the model described in Materials and Methods. For both Trp42-only and Trp130-only adequate fits were achieved with monoexponential  $r(t)$ . The values of the parameters involved in  $r(t)$  and the reduced global  $\chi^2$  are shown in Table 3-5. The time-resolved anisotropy (TRA) of Trp130-only protein is shown in Figure 3-11 and 3-12. The TRA of Trp42-only protein is shown in Figure 3-12 and 3-13. The emission of Trp130 and Trp42 dominated over the emission from tyrosines and the trace contaminant. In the cases of *Trp68-only* and *Trp156-only* proteins Trp fluorescence emission intensity was dominant only during the first 0.5ns, and after that the signal from the trace contaminant became dominant. This means that in the TRA of *Trp68-only* or *Trp156-only* protein only the first 0.5ns are relevant to  $H\gamma D$ -Crys rotational dynamics.

Since the 0.5ns time window would be too short to study the rotational dynamics of a protein with ~21kD molecular weight, we did not measure the TRA of *Trp68-only* and *Trp156-only* proteins.

Table 3-5. Parameters for the time-resolved anisotropy of Trp42 in the N-terminal domain (N-td) and Trp130 in the C-terminal domain (C-td).<sup>a</sup>

domains	proteins	$\beta$	$\phi$	No. of exponentials	$\chi^2$
N-td	Trp42-only	0.245	11.1ns	single	1.01
C-td	Trp130-only	0.248	11.6 ns	single	1.05

<sup>a</sup>  $\beta$  and  $\phi$  represent the amplitude and correlation time, respectively.

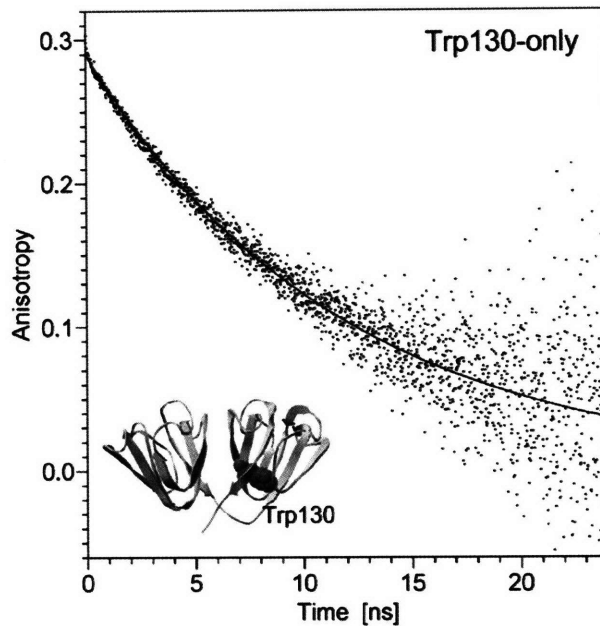


Figure 3-11: Time-resolved anisotropy of Trp130-only HyD-Crys. The solid line represents the  $r(t)$  function with the best fit parameters. Ribbon structure of wild-type HyD-Crys with Trp130 in spacefill is shown at the bottom. The dots represent the anisotropy values calculated from the vertical and horizontal polarization photon counts on a channel-by-channel basis. Since the data shown by the dots have not been deconvoluted from the IRF, they may differ significantly from the  $\delta$ -excitation  $r(t)$  model, however, it is difficult to see the difference because the width of the IRF (65ps) is comparable to the width of the solid line. The dots are shown for illustrative purposes only. The data represented by the dots are not raw experimental data and were not fitted by any model. Instead, we fitted the raw vertical and horizontal polarization data as described in Materials and Methods.

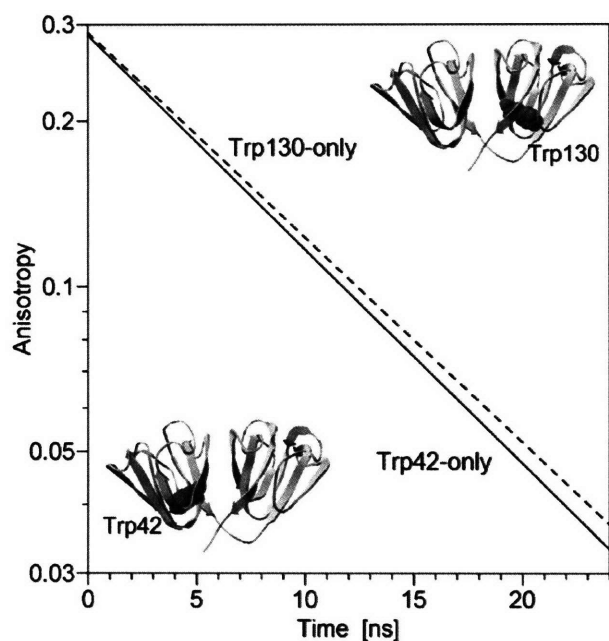


Figure 3-12: Semi-log plots of the best fit of time-resolved anisotropy models for Trp42-only and Trp130-only HyD-Crys. Ribbon structure of wild-type HyD-Crys with Trp130 in spacefill is shown at the up-right corner and the one with Trp42 in spacefill is shown at the bottom. The solid line represents the time-resolved anisotropy of Trp42 in the N-terminal domain and the broken line represents the time-resolved anisotropy of Trp130 in the C-terminal domain

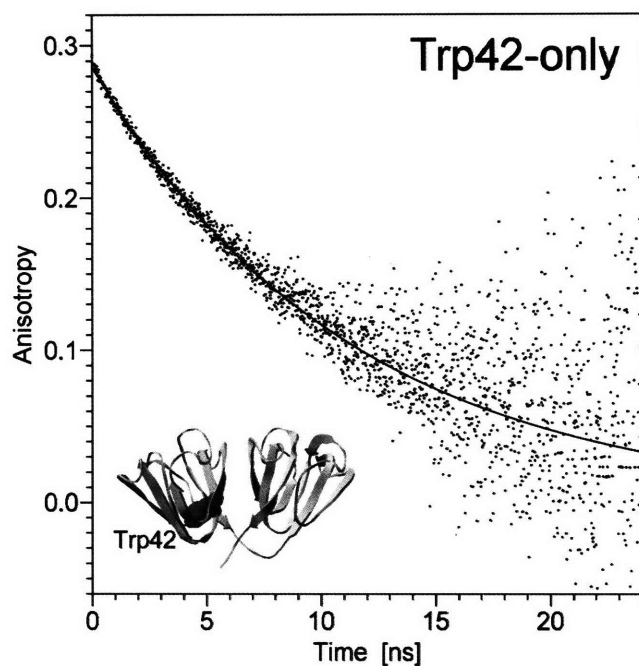


Figure 3-13. Time-resolved anisotropy of Trp42-only HyD-Crys. The solid line represents the  $r(t)$  function with the best-fit parameters. The dots represent the anisotropy values calculated from the vertical and horizontal polarization photon counts on a channel-by-channel basis

Multiexponential  $r(t)$  has been observed in many proteins (Beechem and Brand 1985). In proteins containing a single Trp residue multiexponential  $r(t)$  usually is interpreted in terms of segmental motion, such as the twisting of a small flexible tail in the F3W mutant of IIA<sup>Glc</sup> protein (Toptygin et al. 2001). In the case of HyD-Crys we observed monoexponential  $r(t)$ . Almost identical  $r(t)$  was observed with Trp42-only and Trp130-only protein (Figure 3-12). On the semi-log plot, the monoexponential  $r(t)$  shows up as straight line with slope inversely proportional to the rotational correlation time ( $\phi$ ). The values of the correlation time ( $\phi$ ) are nearly the same for Trp42-only and Trp130-only (Figure 3-12 and Table 3-5). The mass  $m$  of a spherical rotating object can be calculated from its rotational correlation time  $\phi$ , specific gravity  $\rho$ , solvent viscosity  $\eta$ , Boltzmann constant  $k_B$ , and absolute temperature  $T$ , using the Stokes equation (Lakowicz 1999),

$$m = \frac{k_B T \rho \phi}{\eta} \quad (13)$$

Based on the rotational correlation times from Table 3-5, Equation (13) gives the molecular mass of  $22.7 \pm 0.5$  kD. Since the actual molecular mass of both Trp42-only and Trp130-only HyD-Crys is 21.7 kD, it is most likely that in addition to the protein the rotating object also contains about  $1.0 \pm 0.5$  kD of water. The fact that  $r(t)$  is monoexponential implies that the sidechains of Trp42 nor Trp130 cannot rotate about the  $\chi_1$  and  $\chi_2$  angles and there is no segmental motion. In other words, HyD-Crys is a rigid protein with tight sidechain packing.

## E. DISCUSSION

The most striking feature of Trps in HyD-Crys is their short lifetimes in the native state. In the wild-type HyD-Crys, the lifetimes of two moderately fluorescent Trps (Trp42 and Trp130) were shortened resulted from the intradomain energy transfer from Trp42 to



*Trp68* in the N-terminal domain and from *Trp130* to *Trp156* in the C-terminal domain. The lifetimes of *Trp68* and *Trp156* are only  $\sim 0.1$  ns, which is due to the extremely fast electron transfer rates stabilized by the electrostatic environments of these two Trps. Photons in the portion of the ambient near-UV light are highly energetic and can transmit through cornea and be absorbed by the lens. The major chromophores inside the lens absorbing near UV light (300-400 nm) are tryptophan residues in crystallin proteins and some small molecules, such as kynurenine and 3-hydroxykynurine glucoside (Streete 2004; Hood 1999). Once the energy is absorbed by the electron in these molecules' atoms, the energy must be dissipated in some way, such as by breaking chemical bonds or by reradiating photons at another frequency. Covalent damage of Trp residues can lead to the indole ring cleavage, which might originate from Trp photoionization state with formation of a short lived Trp cation radical (Bent 1975, Bryant 1975). This may cause partial unfolding of protein and then result in protein aggregation. Non-radiative pathway (quenching) of Trps in HyD-Crys provides a deactivation channel to dissipate the energy absorbed from the ambient light. Quenching competes with the formation of Trp photoionization state and fluorescent state, and thus it can minimize the chance of photochemical reaction of Trps.

### 1. Time Constants $\tau_n$ of Multiple Trp Containing Proteins

Multiexponential time-resolved fluorescence emission has been often observed even for the single-Trp containing proteins (Beechem and Brand 1985). If the proteins contain more than one Trp, then each time constant cannot be simply assigned to individual Trp without enough experimental evidence. The study of a series Trp mutant of HyD-Crys demonstrated that the multiple exponential terms in proteins containing multiple Trps can be accurately assigned to each Trp in some cases, if the time-resolved emission of single-Trp proteins has been studied and the time constants corresponding to different Trps differ by an order of magnitude or more. For example, in the double-Trp mutant, *Trp68/Trp130*, the two exponential terms with the time constants of 65 ps and

169ps could be attributed to *Trp68*, and the two exponential terms with the time constants of 1.45ns and 3.15ns could be attributed to *Trp130*.

In the presence of intra-domain energy transfer between two Trps (*Trp42/Trp68* and *Trp130/Trp156*), which have been discussed in previous section, the mean lifetime of donor (*Trp42* or *Trp130*) was shortened, but all the time constants  $\tau_n$  attributable to the donor were still considerably longer than those attributable to the acceptor. Thus, it was possible to separate the donor exponentials from the acceptor exponentials. If no interaction occurred between two Trps, there were two possible circumstances. First, if the shortest  $\tau_n$  for one Trp (e.g. *Trp42* or *Trp130*) was at least three times longer than the longest  $\tau_n$  for the other Trp (e.g. *Trp156* or *Trp68*), then the instrument would be able to resolve the signals from these two Trps (e.g. *Trp42/Trp156* or *Trp68/Trp130*). Second, if the time constants of two Trps were very close, e.g. *Trp42/Trp130* or *Trp68/Trp156*, then the instrument could not resolve the exponential terms associated with the individual Trps. In the latter case the number of the resolved exponential terms for the double mutants was the same as the number of the exponential terms for either single-Trp containing protein. For example, six exponential terms were necessary to fit the time-resolved emission from *Trp68-only* and *Trp156-only*, and also six exponential terms were sufficient to fit the time-resolved emission of *Trp68/Trp156*. In this case the time constants  $\tau_n$  could not be called lifetimes or attributed to either Trp residue, whereas the sum of all exponential terms gave an excellent global fit to the time-resolved emission of the double-Trp protein in every part of the emission spectrum.

## 2. Multi-exponential Fluorescence of Trps and Charge Transfer Mechanism

The short mean lifetimes for *Trp68* and *Trp156* are consistent with their very low quantum yields computed by QM-MM methods developed by Callis et al (Callis and Liu 2004; Callis and Vivian 2003; Kurz et al. 2005; Liu et al. 2005; Xu et al. 2006; Chen et al. 2006). Compared to moderately fluorescent *Trp42* and *Trp130*, the extreme quenching of *Trp68* and *Trp156* arises essentially from their smaller CT-<sup>1</sup>L<sub>a</sub> energy gap and the larger fluctuations (Chen et al. 2006). When the energy gap is small and fluctuations are

large, the probability that the fluorescing and CT states will have the same energy is high. The quenching will occur under this circumstance because electron transfer (the quenching process) is only possible when the fluorescing and CT states have the same energy (Callis and Liu 2004). The energy of the CT state depends on the local electric field, and so is the electron transfer rate. In addition, the transfer rate depends on the distance between the Trp side chain and the protein backbone. Random Brownian motions of protein and solvent atoms are responsible for both the CT state energy fluctuations and Trp backbone distance fluctuations. Molecular dynamics (MD) simulations reveal that there are fluctuations lasting  $\sim 0.02$  ns that conceivably could attribute to the two exponential terms (0.061 ns and 0.144 ns) of *Trp68* and three exponential terms (0.050 ns, 0.116 ns, and 0.272 ns) of *Trp156*.

The highest fluorescence quantum yields for single Trps in proteins are normally close to 0.3 (Callis and Liu 2004), a value that varies only slightly depending on the polarity of the environment. The quantum yield (0.13) of Trp42 suggested there is moderate electron transfer quenching but the electron transfer rate is much less than *Trp68* or *Trp156* due to the difference in their electrostatic environments. The more fluorescent Trp42 has two exponential terms, 2.85 ns and 1.72 ns, with amplitude of 68% and 25%, respectively. The 1.72 ns exponential could possibly be attributable to the fluctuation of CT- $^1L_a$  energy gap of Trp42.

### 3. *Time-resolved fluorescence anisotropy*

Time-resolved anisotropy of the fluorescence emission from a probe attached to a protein molecule can provide information about the size of the macromolecule, about its flexibility, and whether the sidechain packaging in the environment of the fluorescent probe is tight or loose. During the analysis of the time-resolved anisotropy data we approximate the time-resolved anisotropy by a linear combination of exponential terms as described in Eq. (2). The resulting exponential terms  $\beta_n \exp(-t/\phi_n)$  are then sorted in accordance with the values of the rotational correlation times  $\phi_n$ . The rotation of the protein as a whole should result in the rotational correlation time (Lakowicz 1999)

$$\phi_0 = \frac{\eta V_1}{k_B T} \quad (15)$$

where  $\eta$  is the solvent viscosity,  $V_1$  is the volume of one protein molecule, including the volume of water trapped in internal cavities or tightly bound to protein surface,  $k_B$  is the Boltzmann constant, and  $T$  is the absolute temperature. If the protein molecule is not spherical (i.e., rod-like or disk-like), then instead of one rotational correlation time  $\phi_0$  we expect up to three rotational correlation times  $\phi_1$ ,  $\phi_2$ ,  $\phi_3$ . The longest and the shortest of these three  $\phi_n$  differ by less than 50%, therefore in practice the three exponential terms resulting from the non-spherical shape of a protein molecule cannot be resolved from the experimental data. In contrast to that, segmental motions of protein domains or secondary structure elements result in rotational correlation times  $\phi_n$  that are much shorter than  $\phi_0$  given by Eq. (15). For example, if the mass of the whole protein is  $N$  times greater than the mass of the rotating segment, then the rotational correlation time for the segment can be roughly estimated as  $\phi_0/N$ . For  $N > 3$  it should be easy to separate the exponential term corresponding to segmental motion from the one describing the rotation of the protein as a whole. Furthermore, if the sidechain packing in the environment of the fluorescent probe is not tight, then the rotation of the fluorescent probe about a flexible linker arm should be observed. In our experiments the moderately-fluorescent Trp residues in Trp42-only and Trp130-only were used as the fluorescent probes. The rotation of the Trp sidechain about the  $C_\alpha$ - $C_\beta$  bond and  $C_\beta$ - $C_\gamma$  bond can result in exponential terms with  $\phi_n \sim 100$ ps (Toptygin et al. 2007). In the case of Trp42-only and Trp130-only HyD-Crys we did not observe exponential terms with  $\phi_n \sim 100$ ps, which is indicative of very tight sidechain packing in the vicinity of the Trp residues. The observed time-resolved anisotropy was monoexponential, therefore no segmental motion of any kind was detected in HyD-Crys. This shows that HyD-Crys is a rigid molecule, containing no loose segments or secondary structure elements that could move significantly relative to the rest of the molecule.

#### *4. Ocular Lens Protects Retina from Near-UV Radiation*

In the intact eyes, very little UV radiation can reach the retina due to the cornea and lens absorption. Since cornea can only block the UV light with wavelength below 295nm, lens is the major filter for near-UV light (300-400nm). Trps in crystallin proteins and some other tryptophan derivatives inside the lens (e.g. kynurenine and 3-hydroxykynurenine), can both absorb UV and therefore prevent UV light from reaching the retina. Even though the Trp absorbance from 300nm to 320nm is only the tail of its UV absorption spectrum (Lakowicz 1999), considering the high protein concentration inside the lens, these portions are very important to shield off the retina from UV light. Near-UV light can damage the retina photoreceptor in a lensless eye in the animal models (Li et al., 1990; Ham 1982). Surgical removal of a cataract results in the loss of the natural lens filter and it might cause irreversible visual loss in the long run. Without appropriate implant of intraocular lens during cataract surgery, the retina can be damaged by ultraviolet energy from solar radiation (Werner 1989). For some patients with cataract surgery, the retina became more vulnerable to near-UV exposure (Berler 1983), and there is an increased risk of age-related macular degeneration (Pollack 1996, Liu 1989), which has been implicated as a consequence of photooxidative retina light damage (Zigman 1993).

#### *5. Properties of Trp in $\gamma$ -crystallin may be important to protect themselves from UV-induced photo reactions*

Excessive UV-B exposure not only can cause retina damage, but also is one of the risk factors for the cataract formation (Robman and Taylor 2005). World Health Organization estimated that UV radiation is directly responsible for 5% cataract-related disease. (WHO 2006). Cataracts formation was observed in certain animal model exposed to the near UV light (300-400nm). These changes seem to be associated with chemical alterations in the Trp residues of crystallin proteins or free Trp in the lens (Zigman 1977). Even though cornea can absorb almost all the light of wavelength shorter than 295nm, there is about 2-4mW/cm<sup>2</sup> sunlight in the range of 300-400nm could reach

the human lens (Zigman 1977). The young crystallin lenses transmit about 75 percent UV (300nm to 400nm), while the corresponding UV transmission dropped dramatically to 20 percent in the yellowish aged lenses due to the accumulations of small UV filters, such as 3-hydroxykynurenine glucoside (Lerman 1976; Van Heyningen 1973). Because crystallin proteins are under the stress of UV radiation throughout life, Trp residues in crystallins could be the potential major photoreaction target. The unique properties of Trps in H $\gamma$ D-Crys, including their highly hydrophobic environments, efficient quenching of the fluorescence intensity (short lifetimes), and no segmental motion around Trps, might have been evolved in crystallin fold to protect Trp residues from photo-induced reactions.

The Trps in H $\gamma$ D-Crys are highly buried inside the hydrophobic core of  $\beta$ -sheet fold. Solvent exposed Trps are more susceptible to photooxidation than buried Trp in proteins (Pigault 1984; Pigault 1988). Trp residues in a hydrophobic environment were photolyzed at a slower rate than those were solvent exposed (Jori 1971). Similar trends have also been observed for bovine crystallins. Bovine  $\alpha$ B-crystallin contains two Trps, Trp9 and Trp60. The photolysis rate of Trp9 is more rapid than Trp60 under UV radiation at 308nm (Borkman 1993). This was explained by more solvent exposure area of Trp9 than Trp60.

The short lifetimes of Trp in H $\gamma$ D-Crys might also minimize the chance of photochemical reaction of Trps. Tallmadge et al. irradiated bovine  $\gamma$ B-crystallin at 295nm with 0.7mW/cm<sup>2</sup> output. The photoreaction rates of moderately fluorescent Trp42 and Trp130 are much faster than quenched *Trp68* and *Trp156*. The photodamage rate of Trp42 is particularly fast among the four Trps. Based on the results of time-resolved fluorescence measurements of H $\gamma$ D-Crys, the lifetime of Trp42 is more than 10 times longer than *Trp68* and *Trp156*. It is likely that Trp42 has a higher chance to get into the photooxidation pathway than the quenched *Trp68* and *Trp156*.

Another property of Trps in H $\gamma$ D-Crys is that there is no segmental motion around Trp42 and Trp130, which indicated the exceptional rigidity of H $\gamma$ D-Crys. Even though crystallin proteins are in a reduced environment in the lens fibril cells due to high concentrations of ascorbic acid and glutathione, low level of oxygen is indeed present in the center of the lens (McNulty et al. 2004; Barbazetto et al. 2004). The diffusion rate of

oxygen presumably would be low in the rigid protein matrix, so the oxidative species have less chance to access Trp residues to cause oxidation.

## F. CONCLUSION

The excited-state lifetimes of the four Trp residues in HyD-Crys were measured individually in the absence and in the presence of other Trp residues. The mean lifetimes of *Trp68-only* and *Trp156-only* are always very short ( $\sim 0.1$  ns), indicating that these residues are highly quenched. We have previously shown that electron transfer to the protein backbone is the dominant quenching mechanism for *Trp68* and *Trp156* (Chen 2006). In contrast, the lifetimes of *Trp42-only* and *Trp130-only* are  $\sim 3$  ns, which shows that *Trp42* and *Trp130* are moderately fluorescent in the absence of the resonance energy transfer. The lifetime of *Trp42* (or *Trp130*) decreases to  $\sim 1$  ns in the presence of *Trp68* (or *Trp156*). This confirms the presence of the intradomain resonance energy transfer, from *Trp42* to *Trp68* in the N-terminal domain and from *Trp130* to *Trp156* in the C-terminal domain. The experimental value of energy transfer efficiency is 56% in the N-terminal domain and 71% in the C-terminal domain, which is very close to those values calculated theoretically using Förster equation and the crystal structure of the protein. No experimental evidence of interdomain energy transfer was found. Time-resolved fluorescence anisotropy data indicate that there is no segmental motion of Trp sidechains or larger protein segments, which leads us to the conclusion that the protein matrix of HyD-Crys is exceptionally rigid. We speculate that the shortening of Trp lifetimes in the wild type HyD-Crys and the rigidity of protein might have evolved as properties of  $\gamma$ -crystallin fold to protect Trps from photodegradation reactions induced by ambient UV light.

## **CHAPTER FOUR:**

### **THE $\gamma$ CRYSTALLIN FOLD PROTECTS CONSERVED TRYPTOPHAN RESIDUES FROM UV RADIATION DAMAGE BY FAST ELECTRON TRANSFER<sup>3</sup>**

---

<sup>3</sup> This work includes results of collaboration with Prof. Callis P. R. at Montana State University.



## A. ABSTRACT

Crystallins, the major protein class of the eye lens of many species, are important for maintaining the transparency and providing a proper refractive index gradient in the lens. This function is achieved through a composite of proteins, primarily consisting of the two-domain structural proteins,  $\beta$ - and  $\gamma$ -crystallins. We report here experiments and computational studies on the quenching of the tryptophan (Trp) fluorescence in the human  $\gamma$ S-crystallin (H $\gamma$ S-Crys). We identified that the fluorescence of H $\gamma$ S-Crys is quenched in its native state by fast electron transfer and intradomain Förster resonance energy transfer. The QM-MM calculations carried out by Prof. Callis P.R. showed that there is striking conservation of inferred electrostatically enabled excited state quenching by electron transfer to the backbone amide of  $\beta$ -,  $\gamma$ -crystallins despite the absence of precise sequence homology. Tallmadge and Borkman [Tallmadge and Borkman *Photochem Photobiol.* 1990] have reported that conserved quenched Trps in bovine  $\gamma$ B-crystallin were protected from photolysis relative to the more fluorescent Trps. All of above strongly suggests that the quenching is an evolved property of the protein fold that allows it to absorb ultraviolet light while suffering minimal photodamage.

## B. INTRODUCTION

Crystallins, the major proteins of the eye lens, are important to maintain the transparency and provide a proper refractive index gradient in the lens. The lens grows by adding layers of cells at the periphery, accumulating the oldest proteins in the nucleus and the more recently synthesized proteins in the cortex. Terminally differentiated fiber cells in the lens are enucleated and lose all other organelles, and therefore there is little protein turnover during aging.

The oligomeric  $\beta$ - and the monomeric  $\gamma$ -crystallins are major lens structural proteins, both containing four Greek key motifs organized into two domains.  $\beta$ B1,  $\beta$ B2,  $\beta$ B3,  $\beta$ A1/A3,  $\beta$ A2, and  $\beta$ A4;  $\gamma$ A,  $\gamma$ B,  $\gamma$ C,  $\gamma$ D,  $\gamma$ E,  $\gamma$ F and  $\gamma$ S are the  $\beta\gamma$ -crystallins expressed in the mammalian lens (Bloemendal et al. 2004). The  $\gamma$ -crystallin superfamily can be divided into two branches. One with multiple members in mammals organized in a six-gene cluster ( $\gamma$ A-F). The other one  $\gamma$ S is the only member.  $\gamma$ S-crystallin represents an early branch of the  $\gamma$ -crystallin family which has been conserved and highly expressed throughout the vertebrates (Wistow et al. 2005). The most abundant  $\gamma$ -crystallins in young human lens are  $\gamma$ C-,  $\gamma$ D-, and  $\gamma$ S-crystallin (Lampi et al. 1997). The proteins in the lens nucleus, including human  $\gamma$ C-, and  $\gamma$ D-crystallin are synthesized first and there is almost no protein turnover once they are formed. Cortex is the outside layer of the nucleus. H $\gamma$ S-Crys is especially abundant in the cortex, where protein synthesis continues in adulthood.

Cataract, the leading cause of the blindness worldwide, has been considered as a protein folding and deposition disease (Bloemendal et al. 2004). G18V mutation of H $\gamma$ S-Crys gene causes congenital cortical cataract in humans (Sun et al. 2005). UVB (290-320nm) radiation is one of the risk factors associated with cataract formation (Robman et al. 2005; McCarty et al. 2002). WHO estimates that one-fifth of world blindness from cataract may be due to the UV radiation exposure. Tryptophan (Trp) residue is the predominant chromophore inside proteins absorbing UVB radiation. Trp photodamage has long been believed to be responsible for the excessive UVB radiation induced cataract formation (Kurzel et al. 1977).

$\gamma$ S-crystallin is a two-domain monomeric protein, with two buried Trps in each domain. Thus far only the C-terminal domains of human (Fig. 4-1A) and bovine  $\gamma$ S-

crystallin have been solved by x-ray crystallography (Purkiss et al. 2002; Basak et al. 1998). Despite extensive efforts, both full-length and the N-terminal domain of  $\gamma$ S-crystallins have not been crystallized, which may be due to the intra- or interdomain flexibility (Wu et al. 2005). The solution structure of murine  $\gamma$ S-crystallin has been determined by NMR spectroscopy (Fig. 4-1B) (Wu et al. 2005). Compared to other  $\gamma$ -crystallins,  $\gamma$ S-crystallin has a four amino acid residue long N-terminal extension and lacks the two amino acid residue long C-terminal arm. The linker region of  $\gamma$ S-crystallin is one residue longer than that of  $\gamma$ B-crystallin, and two residues longer than that of the other  $\gamma$ -crystallins (Bloemendal et al. 2004). The NMR structure of murine  $\gamma$ S-crystallin showed that its two domains have highly homologous structures, similar as other  $\gamma$ -crystallin (Wu et al. 2005). Wenk et al. (2000) suggested that the domain interface may not be important for the stability of H $\gamma$ S-Crys.

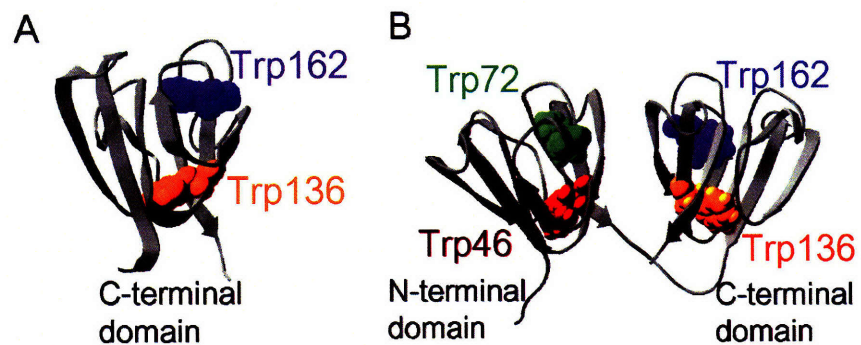


Figure 4-1. (A) The crystal structure of the C-terminal domain of HyS-Crys is shown as a ribbon diagram with Trp136 and Trp162 in space-fill (PDB code 1HA4). (B) The NMR structure of murine  $\gamma$ S-crystallin is depicted in ribbon representation showing the four Trps in space-fill, Trp46 and Trp72 in the N-terminal domain and Trp136 and Trp162 in the C-terminal domain (PDB code 1ZWO).

We report here experiments and computational studies on the quenching of the tryptophan fluorescence in the human  $\gamma$ D and  $\gamma$ -S eye lens crystallins that suggest that the quenching may be an evolved property of the protein fold that allows it to absorb ultraviolet light with minimal damage from associated photochemical covalent ring scission reactions. Recently developed theoretical methods (Callis and Liu 2004; Callis and Vivian 2003; Kurz et al. 2005; Liu et al. 2005; Xu et al. 2006; Callis et al. 2007) provide an understanding of Trp quenching via local electrostatic promotion of electron transfer from the excited Trp. Our crystallin experiments reveal how the structural features ensure rapid loss of excitation energy, thereby reducing photodamage risk. In addition, conserved Trps occupy positions that appear to be important to the vital structural stability of the crystallins. This is important because cataract has recently been proposed as a protein folding and deposition disease (Bloemendal et al. 2004).

The fluorescence intensity, lifetimes, and wavelength of tryptophan within proteins are highly sensitive to protein environment, and have long been exploited to follow a plethora of protein transformations that affect the local Trp environment. (Chen and Barkley 1998; Loewenthal et al. 1991; Beechem and Brand 1985; Eftink 1991). The 30-fold range of fluorescence quantum yields and lifetimes has recently been quantitatively explained in terms of electrostatically tuned electron transfer (Callis and Liu 2004). In general, the quenching of tryptophan fluorescence and associated electronic interactions have been viewed as an adventitious aspect of protein structure, not reflective of any fundamental biological properties.

For the  $\beta\gamma$ -crystallins, however, this is probably not the case, as revealed in our previous detailed investigation into the tryptophan fluorescence quenching mechanism in human  $\gamma$ D-crystallin (Chen et al. 2006). The homologous pair *Trp68* and *Trp156* is highly quenched in contrast to the homologous Trp42 and Trp130, which are moderately fluorescent. Furthermore, the fluorescence emission spectra of single and double Trp to Phe mutants indicate that there is energy transfer from Trp42 to *Trp68* in the N-terminal domain and from Trp130 to *Trp156* in the C-terminal domain. Hybrid quantum mechanical-molecular mechanical (QM-MM) simulations carried out by Prof. Callis P.R. indicated that electron transfer rates to the amide backbone of *Trp68* and *Trp156* are

extremely fast relative to those for Trp42 and Trp130. The charge transfer events of *Trp68* and *Trp156* are promoted by the net favorable location of several charged residues and nearby waters that electrostatically lower the energy of the resultant charge transfer state.

In this Chapter, we report a similar study on the quantum yields of four Trps in HyS-Crys, which shows essentially parallel behavior to HyD-Crys. We also report a tabulation of crystallographic structures showing remarkable structural (but not sequence) homology leading to conserved fluorescence properties of the conserved Trps of many other  $\beta\gamma$ -crystallins. Based on these results, we proposed that the crystallin backbone fold, sidechain packing, and waters around the quenched Trps have evolved to ensure dissipation the excited state energy of the Trps. This would allow the crystallins to absorb UV, thus protect the retina, but minimize damage to their own Trps.

## C. MATERIALS AND METHODS

### 1. *Mutagenesis, Expression, and Purification of Recombinant HyS-Crys*

The wild-type human  $\gamma$ S-crystallin gene was subcloned into the pQE-1 vector (Qiagen) as described before (Mills et al. 2007). Single, double, and triple Trp to Phe substitutions were constructed using site-directed mutagenesis. Mutant primers (IDT-DNA) were used to amplify a pQE.1 plasmid encoding HyS-Crys gene with an N-terminal 6-His tag. The single, double, and triple Trp to Phe substitutions (*Trp46-only*, *Trp72-only*, *Trp136-only*, and *Trp162-only*) were constructed as similar procedure described by Kosinski-Collins et al. (Kosinski-Collins et al. 2004). All of the mutations were confirmed by DNA sequencing (Massachusetts General Hospital).

The wild-type and mutant HyS-Crys proteins were expressed by *Escherichia coli* M15 [pREP4] cells. All of the mutants accumulated as native-like soluble proteins. The proteins were purified to over 98% homogeneity by affinity chromatography with a Ni-NTA resin as previously described (Kosinski-Collins et al. 2004).

## 2. Fluorescence Spectroscopy and Quantum Yield Determinations

The emission spectra of native and denatured proteins and the quantum yields of different proteins were measured using a Hitachi F-4500 fluorescence spectrophotometer as described previously (Chen et al. 2006). The spectra of native proteins were recorded in S buffer (10 mM sodium phosphate, 5 mM DTT, 1 mM EDTA at pH 7.0), and the denatured proteins were in S buffer plus 5.5 M guanidine hydrochloride (GuHCl). The band-pass was 10 nm for both excitation and emission. Trp fluorescence emission spectra of all the proteins were measured in the range of 310-420 nm with an excitation wavelength of 300 nm. The protein concentrations were 2.75  $\mu$ M except for the quantum yields measurements.

Quantum yields of the four Trps in HyS-Crys were measured using the triple-mutant proteins Trp46-only, *Trp72-only*, Trp136-only, and *Trp162-only*. Excitation wavelength of 300 nm was used in order to minimize tyrosine fluorescence. Because there were large portions of the blue edge of the emission spectra that could not be observed using a 300 nm excitation wavelength, the unobserved areas of the protein spectra were estimated by matching the longer wavelength areas of protein spectra with spectra of 3-methylindole (3MI) in different solvent systems (see Appendix C). The solvent system used to match 3MI spectra with the spectra of wild-type HyS-Crys, *Trp72-only*, and *Trp162-only* was cyclohexane-dioxane (66:34), and the spectra of 3MI in dioxane were used to match the spectra of Trp46-only. The spectra of 3MI in cyclohexane-dioxane (93:7) were used to match the spectra of Trp136-only.

## 3. QM-MM Simulations (carried out by Prof. Patrik Callis at Montana State University)

The hybrid QM-MM method used in this work has been described in recent publications (Callis and Liu 2004; Callis and Vivian 2003; Kurz et al. 2005; Liu et al. 2005; Xu et al. 2006) for applications to Trp fluorescence quenching in proteins. The method grew from an earlier QM-MM procedure used to predict the fluorescence wavelengths of Trp in proteins (Vivan and Callis 2001). Briefly, the QM method is Zerner's INDO/S-CIS method (Ridley and Zerner 1973), modified to include the local

electric fields and potentials at the atoms. The MM part is Charmm (version 31a) (MacKerell et al. 1998). Hydrogens were added to the crystal structure (PDB code 1HA4 and 1ZWM) and the entire protein solvated within a 30 or 35 Å radius sphere of TIP3 explicit water. The waters were held within the chosen radius with a quartic potential. The quantum mechanical part includes the selected Trp and the amide of the preceding residue, capped with hydrogens, i.e., N-formyltryptophanamide. The electric potential for each QM atom is determined by a simple Coulomb's Law sum over all non-QM atoms in the protein and solvent with dielectric constant = 1, and is added to the diagonal elements of the QM Fock Hamiltonian in the atomic orbital basis.

## D. RESULTS

### 1. *Fluorescence emission spectra and quantum yields*

Figs. 4-2 and 4-3 show the fluorescence emission spectra of native and denatured wild-type HyS-Crys and the different Trp to Phe mutants. All the spectra were taken under the same instrument settings, and therefore the areas under the spectra are in proportion to the quantum yields of the proteins. The fluorescence spectra of native and denatured double and triple Trp mutants, containing Trps only in the N-terminal domain (Trps 46 and/or *Trp72*), are shown in Fig. 4-2A. The spectra of Trps in the C-terminal domain are shown in Fig. 4-2B (Trps136 and/or *162*). Fig. 4-3A displays comparison of the native and denatured wild type and single mutants of the weakly fluorescent Trps (W72F and W162F). Fig. 4-3B shows the single substitutions of the moderately fluorescent Trp (W46F) and the strongly fluorescent Trp (W136F).

The fluorescence from *Trps 72* and *162* is weaker than that of Trps 46 and 136 (Fig. 4-2). The difference is more significant for the Trps in the C-terminal domain than the ones in the N-terminal domain. The areas under the curves of the unfolded proteins are approximately in proportion to the number of Trps contained in the proteins. It suggests that the environments of the four Trps are approximately identical in the denatured state. Quantitative determination of the quantum yields for wild type and the



triple mutants are summarized in Table 4-1. The average quantum yield for the triple Trp mutants is 0.090, about two times higher than that of the wild type.

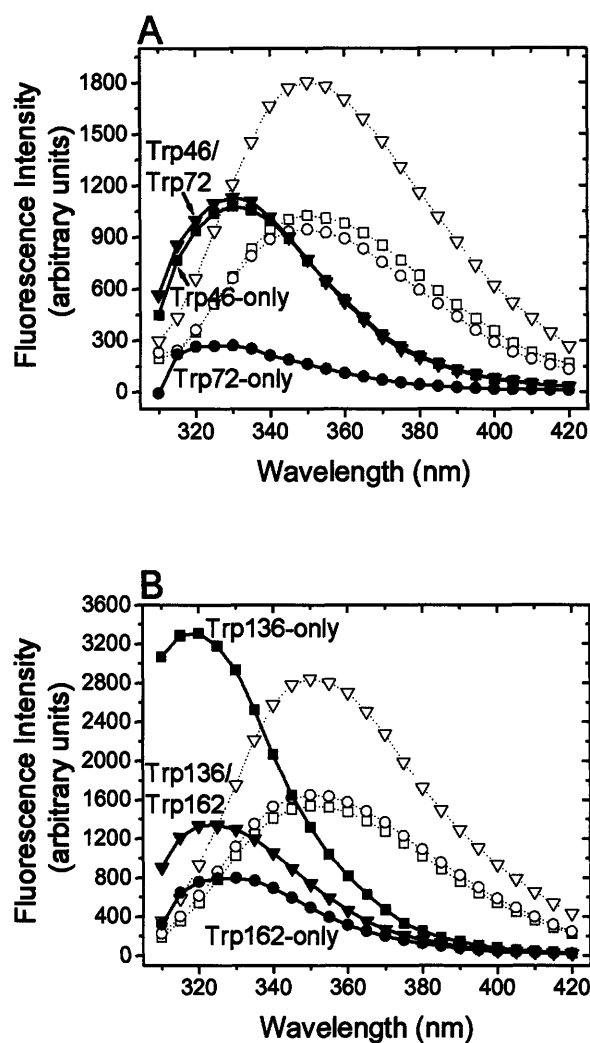


Figure 4-2. (A) Fluorescence emission spectra of native Trp46-only (■), *Trp72-only* (●), and Trp46/*Trp72* (▼) and denatured Trp46-only (□), *Trp72-only* (○), and Trp46/*Trp72* (∇). (B) Fluorescence emission spectra of native Trp136-only (■), *Trp162-only* (●), and Trp136/*Trp162* (▼) and denatured Trp136-only (□), *Trp162-only* (○), and Trp136/*Trp162* (∇). The solid lines represent the emission spectra of native proteins, and the dotted lines represent the unfolded proteins. Native proteins were incubated in S buffer, and unfolded proteins were incubated in S buffer plus 5.5 M GuHCl for 6 h at 37 °C. Excitation wavelength was at 300nm and the protein concentration was 2.75 μM. The buffer signal was subtracted from all spectra.

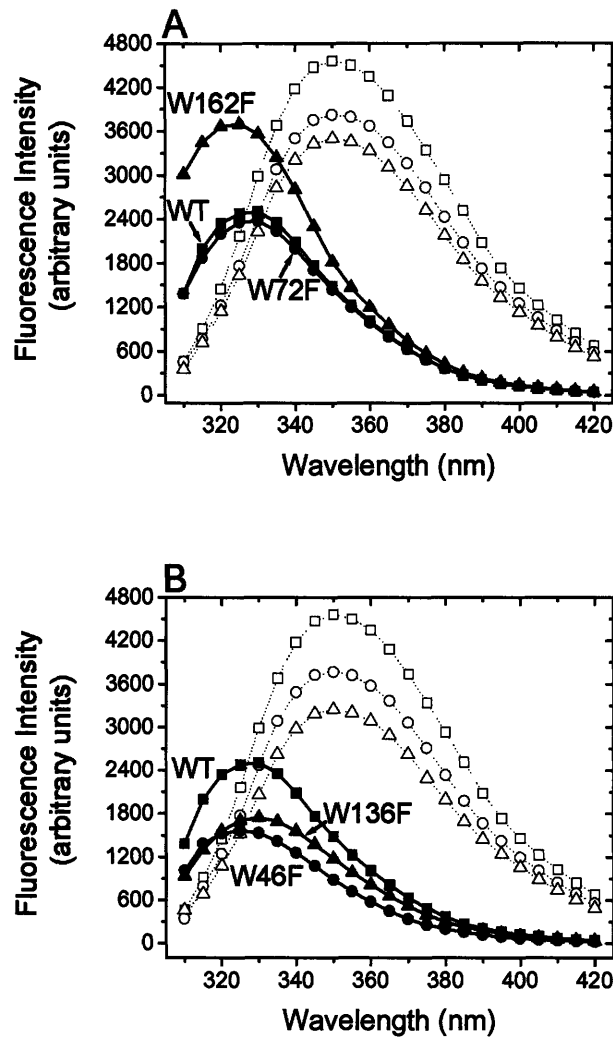


Figure 4-3. (A) Fluorescence emission spectra of native wild type (WT) (■), W72F (●), and W162F (▼) and denatured wild type (□), W72F (○), and W162F (▽). (B) Fluorescence emission spectra of native wild type (■), W46F (●), and W136F (▼) and denatured wild type (□), W46F (○), and W136F (▽). The solid lines represent the emission spectra of native proteins, and the dotted lines represent the unfolded proteins. Native proteins were incubated in S buffer, and unfolded proteins were incubated in S buffer plus 5.5 M GuHCl for 6 h at 37 °C. Excitation wavelength was at 300nm and the protein concentration was 2.75  $\mu$ M. The buffer signal was subtracted from all spectra.

Table 4-1: Maximum Fluorescence Emission Wavelengths and Quantum Yields of Wild Type and Triple Trp Mutants of HyS-Crys

HyS-Crys Proteins or Samples	Maximum Em Wavelength	Slope	QY	3MI Solvent system
L-Trp		2.24661E7	0.14	
Trp46-only	331nm	1.05812E7	0.066	100% Dioxane
Trp72-only	328nm	2.04575E6	0.013	Cyclohexane: Dioxane (66:34)
Trp46/Trp72	331nm	3.17049E6	0.020	100% Dioxane
Trp136-only	318nm	3.96132E7	0.25	Cyclohexane: Dioxane (93:7)
Trp162-only	328nm	4.8128E6	0.030	Cyclohexane: Dioxane (66:34)
Trp136/Trp162	324nm	5.5210E6	0.034	Cyclohexane: Dioxane (75:25)
Wild type	328nm	7.21332E6	0.045	Cyclohexane: Dioxane (66:34)

Fig. 4-4 displays 150 ps QM-MM trajectories that show INDO/S-computed transition energies for the fluorescing state (red) and the CT state (black) for Trps 42 and 68 of HyD-Crys. The relative gap between the states is the main determinant of electron transfer-based fluorescence quenching, and is seen to be considerably larger for Trp 42 than for *Trp* 68. These trajectories are representative of Trps 130 and 156 of HyD-Crys as well as Trps 136 and 162 of HyS-Crys. Electronic coupling of the fluorescing state to the CT state is similar in all cases.

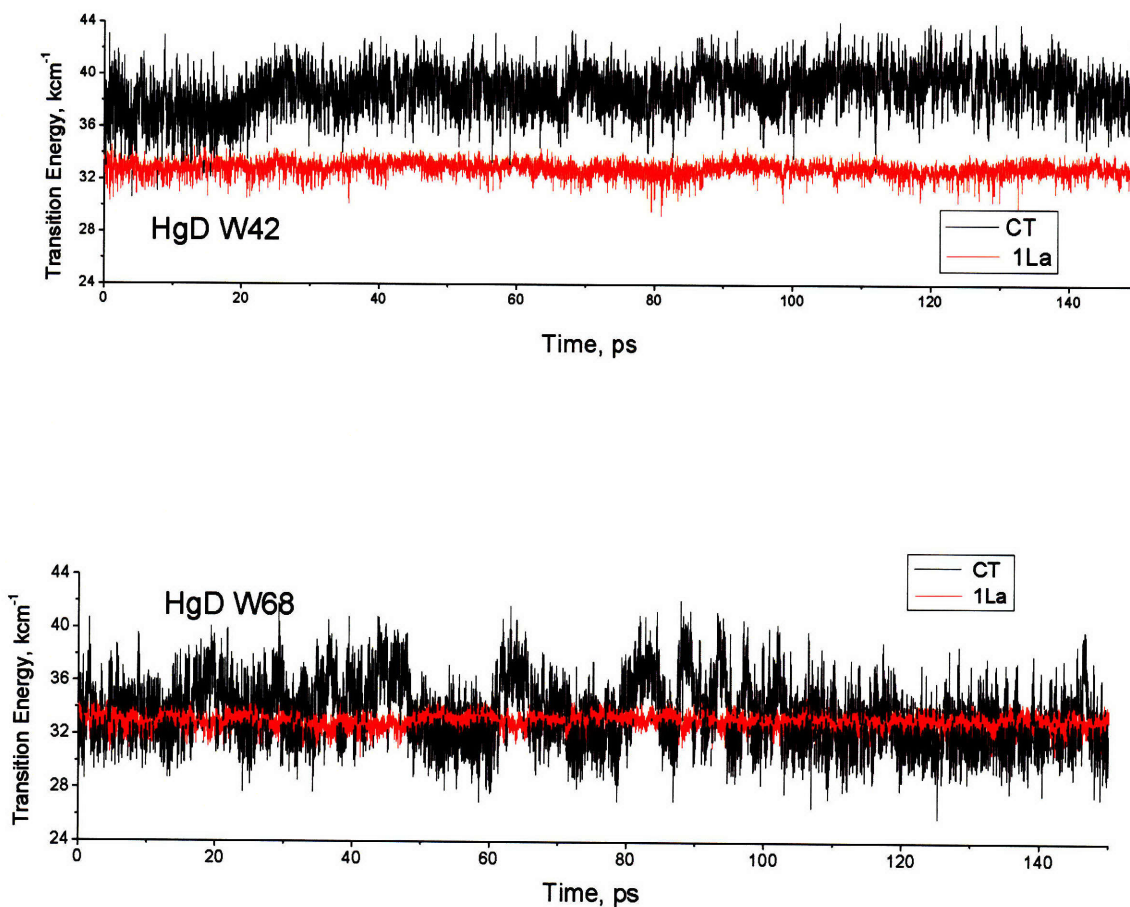


Figure 4-4. 150 ps QM-MM trajectories showing transition energies for the fluorescing state (red) and the CT state (black) for Trps 42 and 68 of human  $\gamma$ D-crystallin. The relative gap between the states is the main determinant of electron transfer based fluorescence quenching. The energy scale is in  $\text{kcm}^{-1}$ . ( $8 \text{ kcm}^{-1} = 1 \text{ eV} = 96.5 \text{ kJ/mol}$ . Fluctuations on the gap are on the order of 1 eV.

(Prof. Patrik Callis carried out QM-MM calculations and generated Figure 4-4.)

Table 4-2 and Figs. 4-5, 4-6, and 4-7 compare calculated ET rates and fluorescence quantum yields for H $\gamma$ D-Crys and  $\gamma$ S-crystallins Trps using two different procedures recently published, Procedure I (Callis and Liu 2004) and Procedure II (Callis et al. 2007). Common to both procedures is the same QM-MM trajectory of  $^1L_a$  and CT transition energies, with the all-important energy gap between the fluorescing and CT states being  $\sim 5000\text{ cm}^{-1}$  (0.6 eV) greater for the non-fluorescent Trps than for the fluorescent Trps. Both procedures are seen to predict the correct order of magnitude for the quantum yields. The low electron affinity of amides means that a CT state involving electron transfer from the excited Trp ring to an amide is energetically accessible only if the protein/solvent environment lowers the relative energy by making the electric potential at the amide carbonyl carbon effectively the same as on the ring, i.e., bringing the  $^1L_a$  and CT states into resonance so that energy is conserved during the electron transfer. Figs. 4-8 and 4-9 show that the lower CT energy for *Trps 68* and *156* comes from net average stabilization from both protein and water compared to *Trps 42* and *130*. The same pattern is found for the corresponding Trps of H $\gamma$ S-Crys and M $\gamma$ S-Crys (see Fig. C1 in Appendix C).

Table 4-2. Comparison of predicted and experimental quantum yields.

Residue	CT- <sup>1</sup> L <sub>a</sub> gap kilo•cm <sup>-1 a</sup>	Std. Dev. kilo•cm <sup>-1 a</sup>	ET rate Constant 10 <sup>9</sup> s <sup>-1 a</sup>	Predicted Quantum Yield <sup>a</sup>	Exp QY
HyDTrp42	5.2	1.7	0.86	0.040	0.13
HyDTrp68	0.34	2.5	11.8	0.003	0.008
HyDTrp130	6.0	1.6	0.33	0.087	0.17
HyDTrp156	1.0	2.6	10.4	0.004	0.01
HySTrp136	7.93	1.85	5.3	0.218	0.25
HySTrp162	0.42	2.64	1116	0.004	0.03
MySTrp46	4.13	2.65	326	0.014	0.066
MySTrp72	2.71	2.76	594	0.007	0.013
MySTrp136	8.18	1.94	10.6	0.193	0.25
MySTrp162	4.78	2.62	249	0.020	0.03

<sup>a</sup> Calculations were carried out by Prof. Callis P.R.

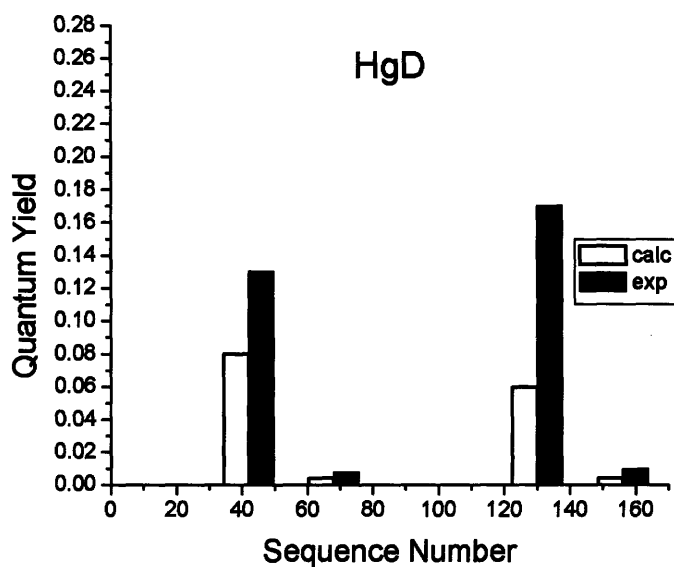


Figure 4-5. Comparison of experimental and calculated fluorescence quantum yields for Trps 42, 68, 130, and 156 of H $\gamma$ D-Crys . Unfilled bars = calculated; filled bars = experiment. (Prof. Patrik Callis carried out QM-MM calculations and generated Figure 4-5.)

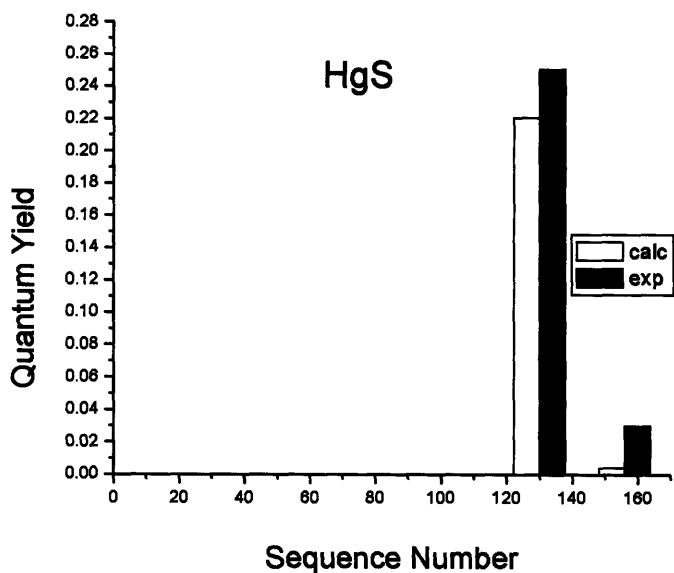


Figure 4-6. Comparison of experimental and calculated fluorescence quantum yields for Trps 136, and 162 of H $\gamma$ S-Crys (C-terminal) . Unfilled bars = calculated; filled bars = experiment. (Prof. Patrik Callis carried out QM-MM calculations and generated Figure 4-6.)



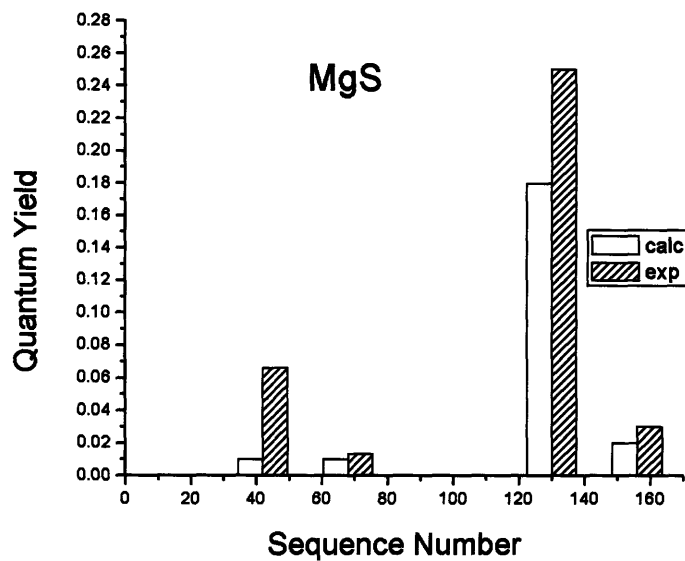


Figure 4-7. Comparison of experimental and calculated fluorescence quantum yields for Trps 46, 72, 136, and 162 of MyS-Crys. Unfilled bars = calculated; filled bars = experiment. (Experimental values are those from HyS.)

(Prof. Patrik Callis carried out QM-MM calculations and generated Figure 4-7.)

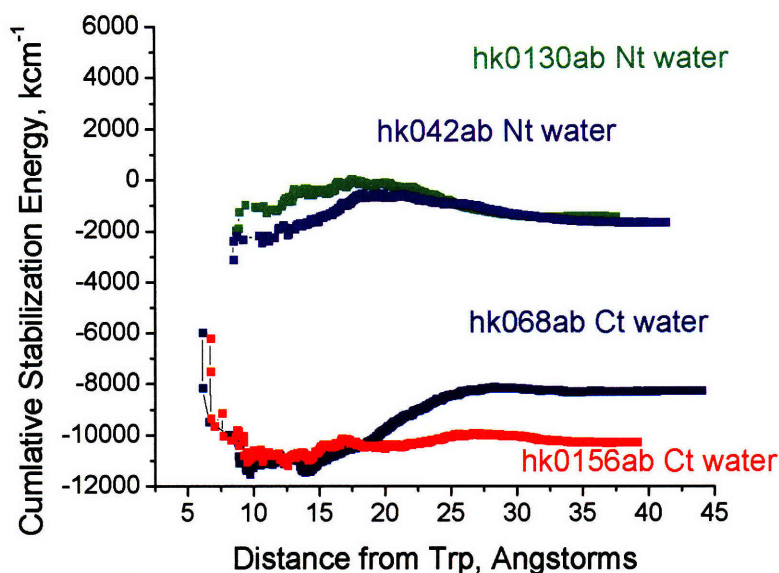


Figure 4-8. Computed electrostatic stabilization of the charge transfer state due to protein and water for Trps 42, 68, 130, and 156 of H<sub>7</sub>D-Crys. The first point is net stabilization from protein. All other points at each distance are the cumulative stabilization from protein + all waters closer to the Trp than that distance. (Prof. Patrik Callis generated Figure 4-8.)

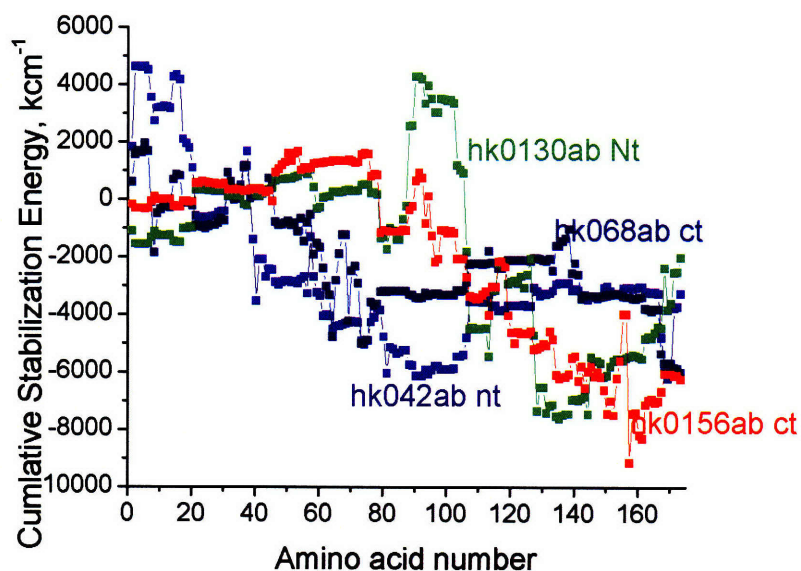


Figure 4-9. Computed electrostatic stabilization of the charge transfer state due to protein for Trps 42, 68, 130, and 156 of H<sub>7</sub>D-Crys. Points are the cumulative stabilization from all residues up to and including that residue. (Prof. Patrik Callis carried out QM-MM calculations and generated Figure 4-9.)

Examination of the electrostatic contributions from nearby waters show that the non-fluorescent *Trps 68* and *156* of H $\gamma$ D-Crys and their counterparts in H $\gamma$ S-Crys have two tightly bound waters that contribute strongly to stabilizing the CT state. These two waters are prominent in the crystal structures of 10  $\gamma$ - and  $\beta$ -crystallins from a variety of species (Basak et al. 2003; Purkiss et al. 2002; Van Montfort et al. 2003; Basak et al. 1998; Kumaraswamy et al. 1996; Chirgadze et al. 1996; Norledge et al. 1997; Shimeld et al. 2005). One is usually an H-bond donor to the O of the Trp amide, and stabilizes because the protons are near the amide C atom. The other is usually an H-bond acceptor from the HE1 on the N of the indole ring. This stabilizes because of the proximity of the negative water O atom near the ring, which is positive in the CT state.

The quenched *Trp162* of H $\gamma$ S-Crys, as with *Trps 68* and *156* of H $\gamma$ D-Crys, has two water molecules close by with formation of hydrogen bonds to stabilize the electron transfer (Fig. 4-10). One water molecule is an H-bond donor to the Trp backbone carbonyl O of the acceptor amide. This H-bond places the positive charge of the H near the backbone C atom to stabilize the charge transfer state. The second water molecule accepts an H-bond from the Trp indole NH, and the proximity of the negative charge of the water O to the indole ring stabilizes the charge transfer from the ring to the C of the Trp amide. Together, the two waters stabilize the CT state by  $\sim 0.5$  eV on average. These water hydrogen bonds to the Trp are transiently broken multiple times during the 150 ps trajectories, but never for more than about 100 fs (Fig. C2 in Appendix C). When the Wat132 H-bond is broken, it is H-bonded to the backbone O of Phe56 or the sidechain HE of Gln142 and trapped nearby. A similar behavior is found with Wat137 which is kept nearby by and H-bond donated to the backbone O of Ser72. This pattern is widely repeated. For *Trp156*, Wat263 is trapped near the carbonyl by HN of Leu144 and O of Gln54, and Wat270 is held by Asn160. For *Trp157* of H $\gamma$ S-Crys, Arg142 hold a water near the carbonyl and ser161 holds a water near the HN of the ring.

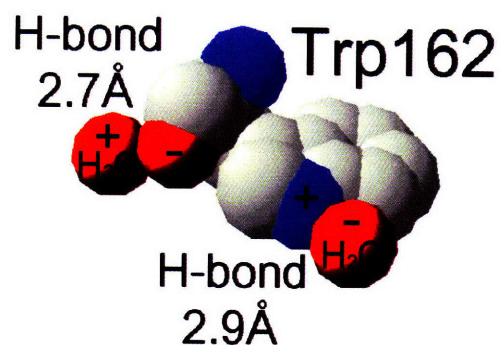


Figure 4-10. The two crystallographic water molecules are stabilizing the electron transfer from the indole ring to the amide backbone of Trp162 in the HyS-Crys (PDB code 1HA4).

## 2. Förster resonance energy transfer

The fluorescence emission spectra of single, double, and triple Trp mutants (Fig. 4-2 and 4-3) strongly suggest that there is intradomain Förster resonance energy transfer in the both C-terminal domain and N-terminal domains. In the C-terminal domain, highly fluorescent Trp136 acts as energy donor and weakly fluorescent *Trp162* functions as the energy acceptor. In Fig. 4-3A, when *Trp162* was substituted with Phe, the integrated fluorescence intensity of W162F was 34% higher than wild type. In contrast, as shown in

Fig. 4-3B, the integrated fluorescence intensity of W136F decreased 25% compared to wild type. The spectra provide convincing evidence that Trp136 is the energy donor. The maximal emission wavelength for Trp136 is blue shifted about 10 nm compared to *Trp162*, consistent with a less polar environment for Trp136. A large portion of the excitation energy from Trp136 is not emitted due to the energy transfer to the weakly emitting *Trp162*. As shown in Fig. 4-3B, because of the positive contribution of Trp136 to the overall fluorescence intensity of wild-type HyS-Crys, a decrease in fluorescence intensity was observed for its Phe substitution (W136F).

The results of the fluorescence emission spectra of double Trp mutants (*Trp136/Trp162*) further confirmed resonance energy transfer in the C-terminal domain. Fluorescence intensity of the double mutant *Trp136/Trp162* was not equal to the simple addition of *Trp136-only* and *Trp162-only* fluorescence but was 1.6 times higher than the intensity of *Trp162-only* and 51% lower than the intensity of *Trp136-only* (Fig. 4-2A).

The resonance energy transfer was observed not only in the C-terminal domain, but also in the N-terminal domain. Moderately fluorescent Trp46 functions as the energy donor and weakly fluorescent *Trp72* is the energy acceptor. Because of the energy transfer from Trp46 to *Trp72* in the N-terminal domain, the intensity of the double Trp mutant, *Trp46/Trp72*, is essentially equal to that of *Trp46-only* (Fig. 4-2A), whereas it would be equal to the addition of the intensity of both *Trp46-only* and *Trp72-only* if there is no energy transfer. The energy donor, Trp46, makes positive contribution to the overall fluorescence intensity of wild-type HyS-Crys, and therefore substitution of Trp46 (W46F) caused decreases in fluorescence intensities compared to wild type (Fig. 4-3B). In Fig. 4-3A, when the energy acceptor *Trp72* was substituted with Phe, the fluorescence intensity of W72F was approximately equal to that of wild type. Because the intensity of the donor Trp46 is somewhat low, even though the Förster energy transfer is efficient in the N-terminal domain, the intensity of W72F was not higher than that of wild type. In summary, because there is little uncertainty in the absolute value of the fluorescence intensity, and because of the somewhat low quantum yield of Trp46, the differences between various Trp spectra in the N-terminal domain were not comparable to those in the C-terminal domain, but the energy transfers are quite efficient in both domains.

There is no significant interdomain energy transfer from the highly fluorescent Trp136 in the C-terminal domain to the weakly fluorescent *Trp72* in the N-terminal domain based on the spectra of the double Trp mutant Trp136/*Trp162* in Fig. 4-2B and the single Trp mutant W46F (containing Trps 136, 162, and 72) in Fig. 4-3B. In the case of the interdomain energy transfer from Trp136 to *Trp72*, the fluorescence intensity of the double Trp mutant Trp136/*Trp162* (containing Trp136 and 162 but not potential energy acceptor *Trp72*) should be higher than the single Trp mutant W46F (containing Trps 136 and 162, and potential energy acceptor *Trp72*). Because of the similar fluorescence intensities of both Trp136/*Trp162* and W46F, there is probably no interdomain energy transfer from Trp136 to *Trp72*. Similarly, the comparison of the double Trp mutant Trp46/*Trp72* (containing Trps 46 and 72 but not potential energy acceptor *Trp162*) in Fig. 4-2A and single Trp mutant W136F (containing Trps 46 and 72, and potential energy acceptor *Trp 162*) in Fig. 4-3B suggests that there is little or no energy transfer from moderately fluorescent Trp46 in the N-terminal domain to the weakly fluorescent *Trp162* in the C-terminal domain.

## E. DISCUSSION

### 1. Conservation of fluorescence quenching by charge transfer in $\beta$ -, $\gamma$ -crystallins

Based on the available fluorescence data, the quenching of fluorescence intensity of native state  $\gamma$ -crystallins is conserved (Liang et al. 2004; Chen et al. 2006; Kosinski-Collins et al. 2004; Flaugh et al. 2005; Flaugh et al. 2006; Mills et al. 2007; Wenk et al. 2000; Bateman et al. 2003), which is correlated with the conservation of the nearby water molecules and dihedral angles of Trps (Table 4-3). The highly quenched Trps (Trps 68/156 in HyD-Crys and Trps 72/162 in HyS-Crys) are buried in the hydrophobic core--yet forming H-bonds with two water molecules nearby to stabilize the electron transfer. Thus far the crystal structures of nine different  $\gamma$ -crystallins have been resolved (Bloemendal et al. 2004). It is striking that in these  $\gamma$ -crystallins all of Trps at homologous position (as Trps 72/162 in HyS-Crys) have similar dihedral angles and two water molecules within 3.1 Å (Table 4-3). The two water molecules stabilize the charge transfer events by forming H-bonds with the Trp indole ring and backbone, respectively (see Fig. 4-11). Unlike  $\gamma$ -crystallin,  $\beta$ -crystallins contain not only buried Trps but also solvent exposed Trps. In human  $\beta$ B1-crystallin, buried Trp218 also displays similar dihedral angles and H-bond formations with two water molecules. Fluorescence quenching phenomena of native state crystallins have been confirmed for human  $\gamma$ C-,  $\gamma$ D-, and  $\gamma$ S-Crys, and human  $\beta$ A1-,  $\beta$ A3-,  $\beta$ A4-, and  $\beta$ B1-crystallin. To our knowledge, there is no reported comparison for the fluorescence intensity of native and denatured bovine and rat  $\gamma$ -crystallins.

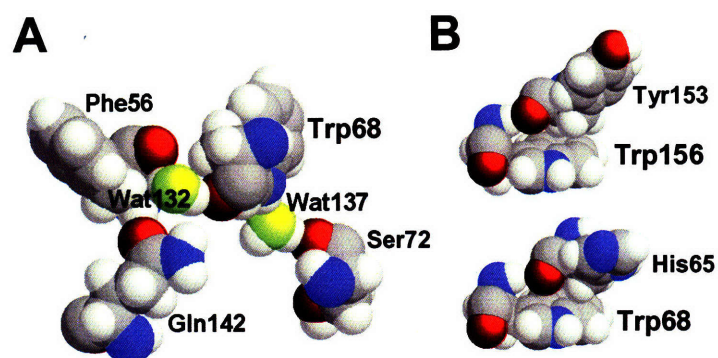


Figure 4-11. The two crystallographic water molecules (yellow oxygens) that most stabilize the electron transfer from the indole ring to the amide backbone of Trp68 in the HyD-Crys (PDB code 1HK0). These sites do not appear to be accessible, but Wat132 is trapped by an additional H-bond to Gln142 and/or Phe56, and Wat 137 is usually also hbonded to Ser72.



Table 4-3 Summary of fluorescence quenching phenomena and conformation of Trps at homologous position (*Trp 68* and *156*) in crystallins.

Crystallin <sup>a</sup>	Quenching of Trps <sup>b</sup>	PDB Code	Dihedral Angles and Distance between Trp and Its Close by Waters
Human $\gamma$ C-crystallin	Yes	— <sup>c</sup>	— <sup>c</sup>
Human $\gamma$ D-crystallin	Yes	1HK0	<p><b>Trp68</b> <math>\omega = 167.7^\circ</math>, <math>\psi = -108.66^\circ</math>, <math>\phi = 18.77^\circ</math>, <math>\chi_1 = 60.5</math>, <math>\chi_2 = 79.1</math>  H<sub>2</sub>O137 (2.9Å from NE1), H<sub>2</sub>O132 (2.8Å from O=C)  His65 O is ~3.5Å from CG</p> <p><b>Trp157<sup>d</sup></b> <math>\omega = 171.83^\circ</math>, <math>\psi = -101.27^\circ</math>, <math>\phi = 12.10^\circ</math>, <math>\chi_1 = 58.4</math>, <math>\chi_2 = 86.3</math>  H<sub>2</sub>O270 (2.9Å from NE1), H<sub>2</sub>O263 (2.7Å from O=C)  Tyr154 O is ~3.5Å from CG</p>
Human $\gamma$ S-crystallin	Yes	1HA4 <sup>e</sup> (C-td)	<p>Chain A<sup>f</sup>:  <b>Trp157</b> <math>\omega = 176.55^\circ</math>, <math>\psi = -111.57^\circ</math>, <math>\phi = 23.87^\circ</math>, <math>\chi_1 = 61.0</math>, <math>\chi_2 = 74.4</math>  H<sub>2</sub>O37 (2.9Å from NE1) in chain Z<sup>g</sup>, H<sub>2</sub>O36 (2.7Å from O=C) in chain Z  Pro154 O is ~3.5Å from CG</p> <p>Chain B:  <b>Trp157</b> <math>\omega = 176.10^\circ</math>, <math>\psi = -115.94^\circ</math>, <math>\phi = 22.01^\circ</math>, <math>\chi_1 = 56.7</math>, <math>\chi_2 = 72.0</math>  H<sub>2</sub>O47 (3.0Å from NE1) in chain Y, H<sub>2</sub>O42 (3.1Å from O=C) in chain Y  Pro154 O is ~3.5Å from CG</p>
Human $\beta$ A1-crystallin	Yes	—	—
Human $\beta$ A3-crystallin	Yes	—	—
Human $\beta$ A4-crystallin	Yes	—	—
Human $\beta$ B1-crystallin	Yes predicted	1OKI	<p>Chain A:  <b>Trp218</b> <math>\omega = 170.49^\circ</math>, <math>\psi = -103.52^\circ</math>, <math>\phi = 13.71^\circ</math>, <math>\chi_1 = 60.4</math>, <math>\chi_2 = 81.9</math>  H<sub>2</sub>O190 (3.1Å from NE1) in chain Z, H<sub>2</sub>O172 (2.9Å from O=C) in chain Z  Trp215 O is ~3.5Å from CG</p> <p><b>Trp126</b> <math>\omega = 170.08^\circ</math>, <math>\psi = -100.10^\circ</math>, <math>\phi = -22.53^\circ</math>, <math>\chi_1 = 67.7</math>, <math>\chi_2 = 65.8</math>  H<sub>2</sub>O110 (2.8Å from NE1) in chain Z  Trp123 O is ~3.5Å from CG</p> <p>Chain B:  <b>Trp218</b> <math>\omega = 170.68^\circ</math>, <math>\psi = -107.81^\circ</math>, <math>\phi = 14.19^\circ</math>, <math>\chi_1 = 61.4</math>, <math>\chi_2 = 80.1</math>  H<sub>2</sub>O202 (3.1Å from NE1) in chain Y, H<sub>2</sub>O183 (2.8Å from O=C) in chain Y  Trp215 O is ~3.5Å from CG</p> <p><b>Trp126</b> <math>\omega = 171.50^\circ</math>, <math>\psi = -100.11^\circ</math>, <math>\phi = -23.52^\circ</math>, <math>\chi_1 = 69.1</math>, <math>\chi_2 = 64.7</math>  H<sub>2</sub>O114 (2.8Å from NE1) in chain Y  Trp123 O is ~3.5Å from CG</p>

			Note here that Trp123 and Trp215 play a similar role as His65 and Tyr153 do in 1HK0; they would be highly quenched by Forster transfer
Human $\beta$ B2-crystallin	No predicted	1YTQ	N.A.
Rat $\beta$ B2-crystallin	No	1E7N <sup>g</sup> (N-td)	N.A.
Crystallin <sup>h</sup>	Quenching of Trps <sup>b</sup>	PDB	Dihedral Angles and Distance between Trp and Its Close by Waters
Bovine $\gamma$ S-crystallin	Not reported	1A7H <sup>c</sup> (C-td)	Chain A: <i>Trp157</i> $\omega = 175.50^\circ$ , $\psi = -109.30^\circ$ , $\phi = 17.31^\circ$ , $\chi_1 = 59.5$ , $\chi_2 = 77.5$ H <sub>2</sub> O202 (2.9Å from NE1) in chain A, H <sub>2</sub> O203 (2.8Å from O=C) in chain A Pro154 O is 3.5Å from CD1  Chain B: <i>Trp157</i> $\omega = 176.13^\circ$ , $\psi = -112.31^\circ$ , $\phi = 17.20^\circ$ , $\chi_1 = 59.5$ , $\chi_2 = 78.8$ H <sub>2</sub> O213 (3.0Å from NE1) in chain B gln143 NE1 is close to O Pro154 O is 3.5Å from CD1
Bovine $\gamma$ B-crystallin	Not reported predicted	1AMM	<i>Trp68</i> $\omega = 173.90^\circ$ , $\psi = -112.42^\circ$ , $\phi = 15.92^\circ$ , $\chi_1 = 59.4$ , $\chi_2 = 83.4$ H <sub>2</sub> O229 (2.9Å from NE1), H <sub>2</sub> O237 (2.8Å from O=C) Tyr65 O is 3.5Å from CG  <i>Trp157</i> $\omega = 175.83^\circ$ , $\psi = -101.18^\circ$ , $\phi = 8.82^\circ$ , $\chi_1 = 57.9$ , $\chi_2 = 87.8$ H <sub>2</sub> O210 (2.9Å from NE1), H <sub>2</sub> O226 (2.8Å from O=C) Tyr154 O is 3.5Å from CG
Bovine $\gamma$ D-crystallin	Not reported	1ELP	Chain A: <i>Trp68</i> $\omega = 178.53^\circ$ , $\psi = -102.96^\circ$ , $\phi = 9.71^\circ$ , $\chi_1 = 64.1$ , $\chi_2 = 75.4$ H <sub>2</sub> O312 (2.8Å from NE1) in chain B, H <sub>2</sub> O137 (2.8Å from O=C) in chain A Tyr65 O is 3.5Å from CG  <i>Trp157</i> $\omega = 179.02^\circ$ , $\psi = -99.78^\circ$ , $\phi = 8.18^\circ$ , $\chi_1 = 53.1$ , $\chi_2 = 86.6$ H <sub>2</sub> O206 (3.1Å from NE1) in chain A, H <sub>2</sub> O66 (2.6Å from O=C) in chain A Tyr154 O is 3.5Å from CG  Chain B: <i>Trp68</i> $\omega = 178.76^\circ$ , $\psi = -102.79^\circ$ , $\phi = 18.18^\circ$ , $\chi_1 = 60.0$ , $\chi_2 = 73.7$ H <sub>2</sub> O23 (3.0Å from NE1) in chain B, H <sub>2</sub> O12 (2.8Å from O=C) in chain B Tyr65 O is 3.5Å from CG  <i>Trp157</i> $\omega = 178.97^\circ$ , $\psi = -107.69^\circ$ , $\phi = 5.53^\circ$ , $\chi_1 = 43.3$ , $\chi_2 = 90.9$ H <sub>2</sub> O268 (2.9Å from NE1) in chain B, H <sub>2</sub> O10 (2.6Å from O=C) in chain B Tyr154 O is 3.5Å from CG
Bovine $\gamma$ E-crystallin	Not reported	1M8U	<i>Trp68</i> $\omega = 177.72^\circ$ , $\psi = -100.08^\circ$ , $\phi = 13.57^\circ$ , $\chi_1 = 62.4$ , $\chi_2 = 75.1$ H <sub>2</sub> O6 (2.9Å from NE1), H <sub>2</sub> O2 (2.8Å from O=C) Tyr65 O is 3.5Å from CG  <i>Trp157</i> $\omega = 178.33^\circ$ , $\psi = -103.62^\circ$ , $\phi = 16.98^\circ$ , $\chi_1 = 61.2$ , $\chi_2 = 79.3$ H <sub>2</sub> O7 (3.0Å from NE1), H <sub>2</sub> O50 (3.0Å from O=C) Tyr154 O is 3.5Å from CG
Bovine $\gamma$ F-	Not	1A45	<i>Trp68</i> $\omega = 178.74^\circ$ , $\psi = -127.74^\circ$ , $\phi = 16.11^\circ$ , $\chi_1 = 65.8$ , $\chi_2 = 75.5$

crystallin	reported		H <sub>2</sub> O1200 (2.9Å from NE1), H <sub>2</sub> O1265 (2.5Å from O=C) Tyr65 O is 4.0Å from CG  <i>Trp157</i> $\omega = 178.18^\circ$ , $\psi = -98.03^\circ$ , $\phi = 12.56^\circ$ , $\chi_1 = 64.1$ , $\chi_2 = 73.7$ H <sub>2</sub> O1201 (2.8Å from NE1), H <sub>2</sub> O1209 (2.6Å from O=C) Tyr154 O is 3.3Å from CG
Murine $\gamma$ S-crystallin	Not reported	1ZWM (NMR structure) <sup>i</sup>	<i>Trp72</i> $\omega = 179.89^\circ$ , $\psi = -107.70^\circ$ , $\phi = 9.85^\circ$ , $\chi_1 = 148.3$ , $\chi_2 = 62.4$  <i>Trp162</i> $\omega = 178.68^\circ$ , $\psi = -97.65^\circ$ , $\phi = 11.04^\circ$ , $\chi_1 = -54.3$ , $\chi_2 = -43.0$ Pro159 O is 3.7Å from CG
Rat $\gamma$ E-crystallin	Not reported	1A5D	Chain A: <i>Trp68</i> $\omega = 176.00^\circ$ , $\psi = -113.21^\circ$ , $\phi = 17.53^\circ$ , $\chi_1 = 64.7$ , $\chi_2 = 76.3$ H <sub>2</sub> O218 (3.3Å from NE1), H <sub>2</sub> O286 (2.8Å from O=C) Tyr65 O is 3.3Å from CG  <i>Trp157</i> $\omega = 179.52^\circ$ , $\psi = -107.75^\circ$ , $\phi = 21.00^\circ$ , $\chi_1 = 59.0$ , $\chi_2 = 78.0$ H <sub>2</sub> O220 (3.0Å from NE1), H <sub>2</sub> O246 (3.1Å from O=C) Tyr154 O is 3.6Å from CG  Chain B: <i>Trp68</i> $\omega = 177.66^\circ$ , $\psi = -110.62^\circ$ , $\phi = 15.07^\circ$ , $\chi_1 = 63.4$ , $\chi_2 = 81.8$ H <sub>2</sub> O317 (3.2Å from NE1) Tyr65 O is 3.5Å from CG  <i>Trp157</i> $\omega = 178.64^\circ$ , $\psi = -97.26^\circ$ , $\phi = 11.74^\circ$ , $\chi_1 = 58.3$ , $\chi_2 = 87.2$ H <sub>2</sub> O318 (2.7Å from NE1), H <sub>2</sub> O307 (2.7Å from O=C) Tyr154 O is 3.7Å from CG
Ciona $\beta$ $\gamma$ -crystallin	Not reported	2BV2	Chain A: <i>Trp70</i> $\omega = 168.47^\circ$ , $\psi = -105.76^\circ$ , $\phi = 5.63^\circ$ , $\chi_1 = 67.9$ , $\chi_2 = 82.0$ H <sub>2</sub> O50 (3.1Å from NE1) in chain Z, H <sub>2</sub> O37 (3.1Å from O=C) in chain Z, H <sub>2</sub> O45 (2.6Å from O=C) in chain Z Pro67 O is 3.5Å from CG  Chain B: <i>Trp70</i> $\omega = 173.60^\circ$ , $\psi = -108.29^\circ$ , $\phi = 9.21^\circ$ , $\chi_1 = 66.3$ , $\chi_2 = 87.2$ H <sub>2</sub> O (3.0Å from NE1) in chain Y Pro67 O is 3.6Å from CG

<sup>a</sup> Crystallins with reported fluorescence emission spectra of native and denature state proteins are listed here. <sup>b</sup> Quenching of Trp fluorescence emission refers to the lower fluorescence intensity in the native state protein respected to the denatured state protein. <sup>c</sup> — The crystal structure is unknown. <sup>d</sup> The amino acid sequence number is consistent with the protein data base. <sup>e</sup> Structure of the C-terminal domain. <sup>f</sup> Chain identifier from the PDB file. <sup>g</sup> Structure of the N-terminal domain. <sup>h</sup> Crystallins with known crystal structure but without reported fluorescence data are listed. <sup>i</sup> The coordinates of murine  $\gamma$ S-crystallin (PDB code: 1ZWM) contain 20 models. Only the dihedral angles of model 1 were listed in the table, and those from other models were summarized in the Table 1S in Supporting Information.

A second strikingly conserved structural feature is the presence of an aromatic residue or proline occurring at sequence number  $n-3$ , where  $n$  is the position of a conserved weakly fluorescent Trp. This may be relevant to increasing the quenching of these Trps because the backbone carbonyl from the  $n-3$  residue is always pressed into the face of the Trp ring, with the N-3 O atom always close to 3.5 Å from the CG of the Trp, as shown in Fig. 4-11. A preliminary simulation shows that ~50% of the time, the lowest CT state has the electron transferred to the N-3 amide instead of the Trp amide. In Table 4-3 it is seen that for  $\gamma$ B-,  $\gamma$ D-,  $\gamma$ E- and  $\gamma$ F-crystallines, the N-3 residue is Tyr, with the exception of *Trp68* of H $\gamma$ D-Crys, for which it is His. For the  $\gamma$ S-crystallins, it is Pro, and for the  $\beta$ -crystallins it is Trp. Forster transfer is expected to be rapid and complete to the nearby low-fluorescent Trp so that the additional Trps in the  $\beta$ -crystallins should not fluoresce well. The sequence alignment of the residues described above is shown in Fig. 4-12.

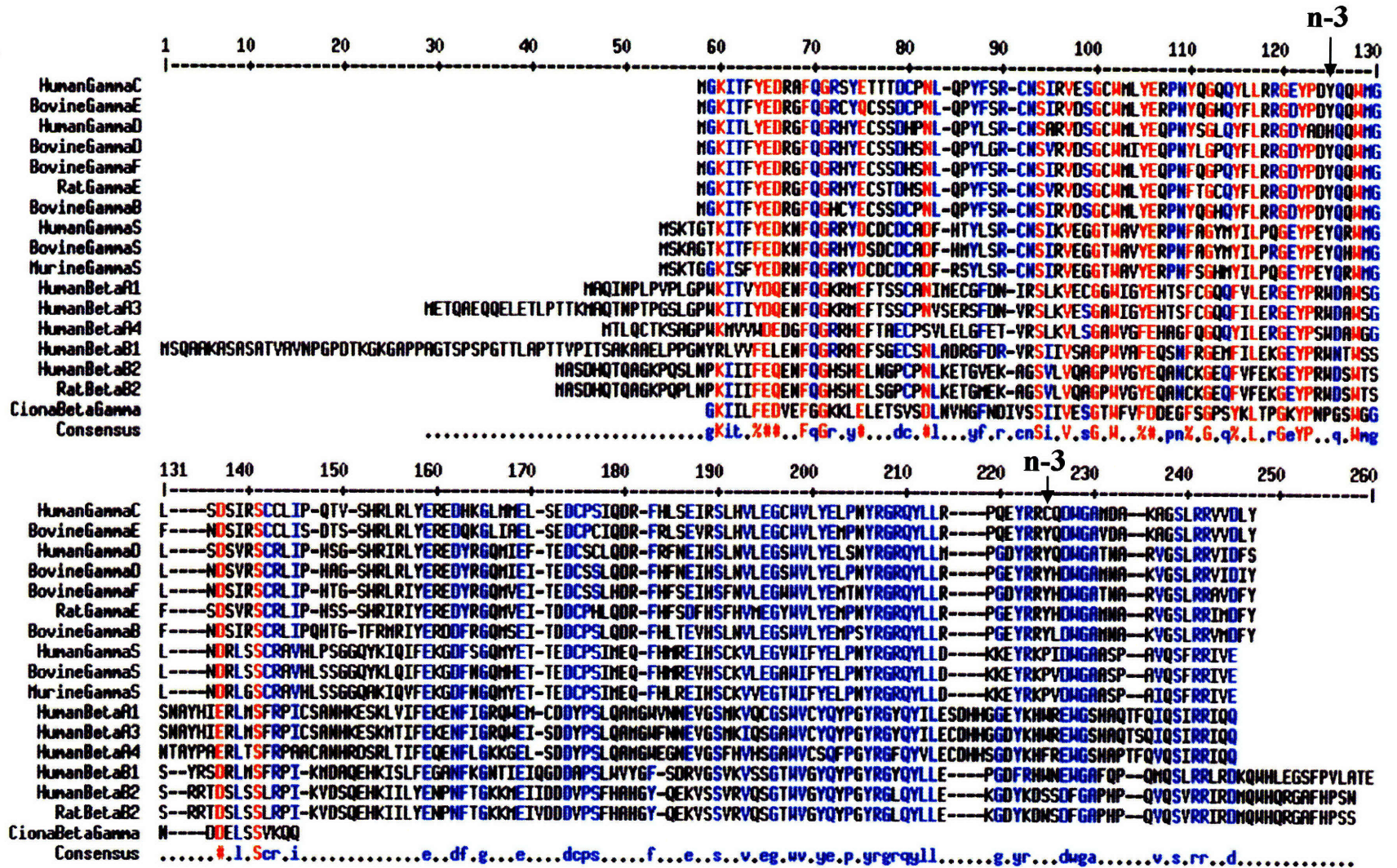


Figure 4-12. Amino acid sequence alignment of  $\gamma$ - and  $\beta$ -crystallin with known crystal structure or NMR structure. An aromatic residue or proline occurring at sequence number n-3, where n is the position of a conserved weakly fluorescent Trp.

## 2. Have crystallin folds evolved to protect Trps from UV irradiation damage by photoinduced electron transfer?

Tallmadge and Borkman (1990) irradiated bovine  $\gamma$ B-crystallin in vitro by using UV light at 295nm with 0.7mW/cm<sup>2</sup> output. Photolysis rate of Trps 42 or Trp131 were much faster than *Trps 68* or *157*. Because bovine  $\gamma$ B-crystallin is homologous protein of HyD-Crys and we have shown that for HyD-Crys Trp42 and Trp130 are moderately fluorescent and *Trps 68* or *156* are highly quenched, these results strongly indicate that quenching may protect *Trp68* or *156* from photodamage. The main function of the lens is to transmit and focus light on the retina without distortion. A further function of the human lens is to filter light between 295-400nm from reaching the retina. Therefore, the lens is continually under photooxidative stress. The solar UV light absorbed by the lens can be potentially harmful to this tissue. These deleterious effects may occur at ambient radiation over an extended period or at high doses over a short period of time. There is a significant correlation between UV radiation and the prevalence of senile cataract (Hollows and Moran 1981; Taylor 1980).

Once Trp reaches an excited state either by direct absorption of photons or by the energy transfer from Tyr (Borkman and Phillips 1985), the energy is dissipated through the various routes, such as fluorescence quenching (probably electron transfer to the backbone amide), photoionization, and direct conversion to vibrational energy. These processes compete with each other. Kurzel proposed that photoionization from the excited singlet state of Trp was the photoreactive state causing lens proteins damage (Kurzel et al. 1973). Photoionization is the primary process resulting in the decomposition of Trp. The population of singlet excited state therefore enhances the possibility of Trp photoionization reaction. The quenching of Trp fluorescence can pull the singlet excited state back to the ground state, and therefore decrease the chance of Trp photoionization reaction. The final product of the photoinduced decomposition involves the cleavage of the C(2-3) bond of the indole ring to form N-formylkynurenine (NFK). NFK was the final product of Trp photodestruction. The covalent damaged Trp inside the hydrophobic core of  $\gamma$ -crystallin can induce partial unfolding of proteins and further cause protein aggregation.



Excessive exposure to ultraviolet B radiation is directly related with high risk of cortical cataract (Robman and Taylor 2005) but has little effects on rates of nuclear cataract. The anterior cortical surface likely receives the most radiant energy, which can partially explain the findings of higher cortical cataract risk under UV-B exposure. The quenching of H $\gamma$ S-Crys is not as efficient as H $\gamma$ D-Crys. Presumably  $\gamma$ S-crystallin might be more susceptible to photodamage than  $\gamma$ D-crystallin. Because  $\gamma$ S-crystallin is abundant in the cortex region and  $\gamma$ D-crystallin mainly locates in the nuclear region, the less resistance of  $\gamma$ S-crystallin to UV radiation might contribute to the prevalence of UV induced cortical cataract. The sunlight radiance in the near-UV range (300-400nm) reaching the human lens would be approximately 3-4mW $\cdot$ cm<sup>-2</sup> (Zigman 1979). Since cornea absorbed most of the UV light with wavelength shorter than 295nm, the adult human lens absorbs nearly all light from 295-400nm. The UV action spectrum on the lens has a maximum at 300nm. Bachem et al. pointed out that wavelengths up to 313nm may be effective in causing lens damage (Bachem 1956). Majority of the radiation on proteins is absorbed by Trp residues, which is probably the key species for long-term, low-level radiation damage to the lens.

The efficient quenching mechanisms of  $\gamma$ -crystallins we reported here and previously (Chen et al. 2006) may provide a pathway to dissipate the energy absorbed from solar UV light and therefore protect Trp residues from photodamage. Similar protective function has also been proposed for other fluorophores in the eye system. Dillon et al. observed a very short fluorescence lifetime (<10ps) for 3-hydroxyl kynurenine in the lens and suggested that this fast fluorescence decay may provide a harmless deactivation path for the ambient UV radiation. Some NAD(P)H dependent metabolic enzymes and cellular retinol-binding protein, were recruited into cornea or vertebrate lenses to function as structure proteins. NAD(P)H and didehydroretinol were also proposed to protect other proteins against UV-induced damage by the competitive absorption of UVB (Estey et al. 2007). The conservation of quenching of Trp fluorescence in  $\gamma$ -crystallins may have been evolved to be a property of crystallin fold. The four conserved buried tryptophans have probably been a feature of the crystallin sequence since the evolution of the lens in early vertebrate. Selection for protection again

UV damage may have been more intense at an earlier time or may continue to the present.

## **F. CONCLUSION**

The conservation of inferred electrostatically enabled photoinduced excited state quenching in the absence of precise sequence homology, coupled with observation of Tallmadge and Borkman that the conserved Trps in bovine  $\gamma$ B-crystallin were protected from photochemistry relative to the more fluorescent Trps, strongly suggests that the quenching is an evolved property.



**CHAPTER FIVE:**

**CONCLUDING DISCUSSIONS**

## A. CONSERVATION OF FLUORESCENCE QUENCHING OF TRYPTOPHANS IN VERTEBRATE $\beta\gamma$ -CRYSTALLINS

In general, the quenching of tryptophan fluorescence and associated electronic interactions have been viewed as an adventitious aspect of protein structure, not reflective of any fundamental biological properties. For the  $\beta\gamma$ -crystallins, however, this is probably not the case, as revealed in detailed investigation into the Trp fluorescence quenching mechanism in HyD-Crys (Chapter 2 and 3) and HyS-Crys (Chapter 4).

The fluorescence emission spectrum and x-ray crystal structure is not available for all of the known vertebrate  $\beta\gamma$ -crystallins. However, based on the available fluorescence data, the quenching of fluorescence intensity of native state protein is highly conserved for human  $\gamma$ C-,  $\gamma$ D-, and  $\gamma$ S-crystallin, and human  $\beta$ A1-,  $\beta$ A3-,  $\beta$ A4-, and  $\beta$ B1-crystallin (Liang et al. 2004; Chen 2006; Kosinski-Collins 2004; Flaugh 2005; Mills 2007; Wenk 2000; Bateman 2003). The quenching of fluorescence intensity in bovine and rat  $\gamma$ -crystallins is also predicted by theoretical calculations (Chapter 4).

Conservation of fluorescence quenching of Trps in vertebrate  $\beta\gamma$ -crystallin can shed light on the evolution of the vertebrate lens. Vertebrates have evolved sophisticated eyes with lens for their vision systems. Based on an embryological aspect the lens is quite different from the rest of the components of the eye. The eye is primarily of neural origin while the lens develops from a non-neural ectodermal placode (Lovicu and Robinson 2004). Many researchers have speculated how the lens has evolved but the origin of the lens is still controversial. Sea squirt *Ciona intestinalis* belong to invertebrate urochordates, and is one of the closest relatives of the vertebrates (Shimeld et al. 2005). *Ciona intestinalis* only has basic light detecting organs without a differentiated lens or retina. Interestingly, an expressed  $\beta\gamma$ -crystallin gene has been identified in the sea squirt *Ciona intestinalis* and the protein has been purified and crystallized (Shimeld et al. 2005). The crystal structure of *Ciona*  $\beta\gamma$ -crystallin suggests that its two Trps (Trp44 and Trp70) have similar conformations as the Trps in HyD-Crys. Upon theoretical calculations

(personal communication with Prof. Callis P.R.), the computed quantum yield is 0.14 for Trp44 and is 0.007 for Trp70. The predicted fluorescence pattern of Trps in *Ciona*  $\beta\gamma$ -crystallin is strikingly similar as the conserved Trps in vertebrate  $\beta\gamma$ -crystallin. Shimeld et al. (2005) proposed that the evolution of the vertebrates lens is via the co-option and combination of ancient gene regulatory networks (Shimeld et al. 2005). Further investigation on the conservation of fluorescence quenching of Trp in *Ciona*  $\beta\gamma$ -crystallin and other vertebrate  $\beta\gamma$ -crystallin will provide important information on the evolution of the vertebrate lens.

## **B. CRYSTALLINS AND UV RADIATION**

Ocular tissues are directly exposed to ambient sunlight, including potentially damaging UV. Almost all  $\beta$ -,  $\gamma$ -crystallins of vertebrate lenses contain four conserved Trp residues, which apparently play a crucial role in protecting the retina from UVB (290-320 nm) photodamage. Because the terminally differentiated fiber cells in the lens are enucleated and lose all other organelles, there is little protein turnover during aging, thereby shifting the risk of UVB photodamage to the Trps of the long-lived crystallins. UVB-induced Trp photodamage has long been believed to be responsible for cataract formation, the leading cause of the blindness worldwide. (Kurzel et al. 1973; Robman et al. 2005; McCarty et al. 2002). Indeed, the World Health Organization (WHO) estimates that one-fifth of world blindness from cataract may be due to the UV radiation exposure (WHO 2006). Under the stress of accumulative ambient UV exposure, the human eye lens has developed several strategies to minimize the potential photodamage.

## 1. *UV filters*

UV filters are a group of small molecules biosynthesized from tryptophan that absorb the UV. Van Heyningen (1971) identified the major UV filter is a primate lens-specific compound, 3-hydroxykynurenine glucoside (3OHKG). These tryptophan-derived UV filters have broad absorption spectra, and thus little light with wavelength less than 400nm can transmit through to the retina (Ellozy et al. 1994). However, UV filters are unstable due to their kynurenine side chain (Taylor et al. 2002). *In vitro* experiments showed that their deaminated products are reactive and can bind to crystallins. The binding can change the spectroscopic properties of crystallins. This process is proposed to be associated with age related nuclear cataract formation (Truscott and Augusteyn 1977). Kynurenine is also one of the final photolysis products of tryptophan residues in proteins. Some fraction of these molecules in the lens may be the product of UV damage (Lerman 1980).

## 2. *Fluorescence Quenching of Trps in $\beta\gamma$ -crystallins may protect themselves from UV induced photodamage*

The quenching (short lifetimes) of Trp in HyD-Crys might minimize the chance of photochemical reaction of Trps. Tallmadge and Borkman (1990) irradiated bovine  $\gamma$ B-crystallin at 295nm with 0.7mW/cm<sup>2</sup> output. The photoreaction rates of moderately fluorescent Trp42 and Trp130 are much faster than quenched *Trp68* and *Trp156*. The photodamage rate of Trp42 was particularly fast among the four Trps. Based on the results of fluorescence measurements of HyD-Crys, the lifetime of Trp42 is more than 10 times longer than *Trp68* and *Trp156*. It is likely that Trp42 has a higher chance to get into the photooxidation pathway than the quenched *Trp68* and *Trp156*. Non-radiative pathway (quenching) of Trps in HyD-Crys provides a deactivation channel to dissipate the energy absorbed from the ambient light. Quenching competes with the formation of Trp photoionization state and fluorescent state, and thus it can minimize the chance of photochemical reaction of Trps.

### 3. Interaction with $\alpha$ -crystallin

UV radiation can lead to covalent cross-linking and aggregation formation of  $\gamma$ -crystallin (Hott and Borkman 1992; Hott and Borkman 1993). Molecular chaperone  $\alpha$ -crystallin inhibits UV radiation induced aggregation of  $\beta$ - and  $\gamma$ -crystallin (Hott and Borkman 1992). Each  $\gamma$ -crystallin monomer requires one to four  $\alpha$ -crystallin subunits for protection (Borkman et al. 1996). The mechanism by which  $\alpha$ -crystallin protects proteins from aggregation is not well understood. *In vitro* biochemical analysis has shown that  $\alpha$ -crystallin can recognize and bind partially folded or unfolded proteins to prevent thermal aggregation of substrate proteins, including  $\beta$ - and  $\gamma$ -crystallin (Horwitz 1992; Horwitz 1993; Sathish et al. 2004). The same may be true for prevention of UV induced aggregation by  $\alpha$ -crystallin.

### C. CONCLUDING REMARKS

Understanding the quenching mechanism of Trp is an important topic in the field of biophysical chemistry. The knowledge on the conserved conformation of quenched Trps in  $\beta$ - and  $\gamma$ -crystallins may be useful for protein design. In the ophthalmology community, UV-B radiation has long been recognized as an important risk factor for mature-onset cataract development. However, how the UV radiation causes the opacity of the lens still need further investigation. Our final goal is to develop new strategies or treatment to prevent UV induced cataract formation.

## CHAPTER SIX: REFERENCES

- Alpert, B., D. M. Jameson, and G. Weber. 1980. Tryptophan emission from human hemoglobin and its isolated subunits. *Photochem Photobiol* 31:1-4.
- Alpert, B., and R. Lopez-Delgado. 1976. Fluorescence lifetimes of haem proteins excited into the tryptophan absorption band with synchrotron radiation. *Nature* 1976:445-446.
- Augusteyn, R. C. 2004. alpha-crystallin: a review of its structure and function. *Clin Exp Optom* 87:356-366.
- Ayala, M. N., R. Michael, and P. G. Soderberg. 2000. Influence of exposure time for UV radiation-induced cataract. *Invest Ophthalmol Vis Sci* 41:3539-3543.
- Bachem, A. 1956. Ophthalmic ultraviolet action spectra. *Am J Ophthalmol* 41:969-975.
- Bagby, S., S. Go, S. Inouye, M. Ikura, and A. Chakrabartty. 1998. Equilibrium folding intermediates of a Greek key beta-barrel protein. *J Mol Biol* 276:669-681.
- Basak, A., O. Bateman, C. Slingsby, A. Pande, N. Asherie, O. Ogun, G. B. Benedek, and J. Pande. 2003. High-resolution X-ray crystal structures of human gammaD crystallin (1.25 Å) and the R58H mutant (1.15 Å) associated with aculeiform cataract. *J Mol Biol* 328:1137-1147.
- Basak, A. K., R. C. Kroone, N. H. Lubsen, C. E. Naylor, R. Jaenicke, and C. Slingsby. 1998. The C-terminal domains of gammaS-crystallin pair about a distorted twofold axis. *Protein Eng* 11:337-344.
- Bateman, O. A., R. Sarra, S. T. van Genesen, G. Kappe, N. H. Lubsen, and C. Slingsby. 2003. The stability of human acidic beta-crystallin oligomers and hetero-oligomers. *Exp Eye Res* 77:409-422.
- Bax, B., R. Lapatto, V. Nalini, H. Driessen, P. F. Lindley, D. Mahadevan, T. L. Blundell, and C. Slingsby. 1990. X-ray analysis of beta B2-crystallin and evolution of oligomeric lens proteins. *Nature* 347:776-780.
- Beechem, J. M., and L. Brand. 1985. Time-resolved fluorescence of proteins. *Annu Rev Biochem* 54:43-71.
- Bent, D. V., and E. Hayon. 1975. Excited state chemistry of aromatic amino acids and related peptides. III. Tryptophan. *J Am Chem Soc* 97:2612-2619.
- Berler, D. K., and R. Peyser. 1983. Light intensity and visual acuity following cataract surgery. *Ophthalmology* 90:933-936.
- Bloemendal, H., W. de Jong, R. Jaenicke, N. H. Lubsen, C. Slingsby, and A. Tardieu. 2004. Ageing and vision: structure, stability and function of lens crystallins. *Prog Biophys Mol Biol* 86:407-485.
- Bloemendal, H., and W. W. de Jong. 1991. Lens proteins and their genes. *Prog Nucleic Acid Res Mol Biol* 41:259-281.
- Blundell, T., P. Lindley, L. Miller, D. Moss, C. Slingsby, I. Tickle, B. Turnell, and G. Wistow. 1981. The molecular structure and stability of the eye lens: x-ray analysis of gamma-crystallin II. *Nature* 289:771-777.
- Borkman, R. F. 1977. Ultraviolet action spectrum for tryptophan destruction in aqueous solution. *Photochem Photobiol* 26:163-166.
- Borkman, R. F. 1984. Cataracts and photochemical damage in the lens. *Ciba Found Symp* 106:88-109.

- Borkman <sup>a</sup>, R. F., A. Douhal, and K. Yoshihara. 1993. Picosecond fluorescence decay in photolyzed lens protein alpha-crystallin. *Biochemistry* **32**:4787-4792.
- Borkman <sup>b</sup>, R. F., A. Douhal, and K. Yoshihara. 1993. Picosecond fluorescence decay of lens protein gamma-II crystallin. *Biophys Chem* **47**:203-211.
- Borkman, R. F., G. Knight, and B. Obi. 1996. The molecular chaperone alpha-crystallin inhibits UV-induced protein aggregation. *Exp Eye Res* **62**:141-148.
- Borkman, R. F., and S. R. Phillips. 1985. Tyrosine-to-tryptophan energy transfer and the structure of calf gamma-II crystallin. *Exp Eye Res* **40**:819-826.
- Boyle, D. L., L. Takemoto, J. P. Brady, and E. F. Wawrousek. 2003. Morphological characterization of the Alpha A- and Alpha B-crystallin double knockout mouse lens. *BMC Ophthalmol* **3**:3.
- Brady, J. P., D. Garland, Y. Douglas-Tabor, W. G. Robison, Jr., A. Groome, and E. F. Wawrousek. 1997. Targeted disruption of the mouse alpha A-crystallin gene induces cataract and cytoplasmic inclusion bodies containing the small heat shock protein alpha B-crystallin. *Proc Natl Acad Sci U S A* **94**:884-889.
- Brady, J. P., D. L. Garland, D. E. Green, E. R. Tamm, F. J. Giblin, and E. F. Wawrousek. 2001. AlphaB-crystallin in lens development and muscle integrity: a gene knockout approach. *Invest Ophthalmol Vis Sci* **42**:2924-2934.
- Brakenhoff, R. H., H. J. Aarts, F. H. Reek, N. H. Lubsen, and J. G. Schoenmakers. 1990. Human gamma-crystallin genes. A gene family on its way to extinction. *J Mol Biol* **216**:519-532.
- Bryant, F. D., R. Santus, and L. I. Grossweiner. 1975. Laser Flash-Photolysis of Aqueous Tryptophan. *Journal of Physical Chemistry* **79**:2711-2716.
- Burley, S. K., and G. A. Petsko. 1985. Aromatic-aromatic interaction: a mechanism of protein structure stabilization. *Science* **229**:23-28.
- Callis, P., and T. Liu. 2004. Quantitative predictions of fluorescence quantum yields for tryptophan in proteins. *J. Phys. Chem. B* **108**:4248-4259.
- Callis, P., and J. Vivian. 2003. Understanding the variable fluorescence quantum yield of tryptophan in proteins using QM-MM simulations. Quenching by charge transfer to the peptide backbone. *Chem. Phys. Lett.* **369**:409-414.
- Callis, P. R. 1991. Molecular-Orbital Theory of the 1Lb and 1La States of Indole. *Journal of Chemical Physics* **95**:4230-4240.
- Callis, P. R. 1997. 1La and 1Lb transitions of tryptophan: applications of theory and experimental observations to fluorescence of proteins. *Methods Enzymol* **278**:113-150.
- Callis, P. R., A. Petrenko, P. L. Muino, and J. R. Tusell. 2007. Ab initio prediction of tryptophan fluorescence quenching by protein electric field enabled electron transfer. *J Phys Chem B* **111**:10335-10339.
- Chang, M. C., J. W. Petrich, D. B. McDonald, and G. R. Fleming. 1983. Nonexponential fluorescence decay of tryptophan, tryptophylglycine, and glycytryptophan. *J. Am. Chem. Soc.* **105**:3819 - 3824.
- Chen, J., S. L. Flaugh, P. R. Callis, and J. King. 2006. Mechanism of the highly efficient quenching of tryptophan fluorescence in human gammaD-crystallin. *Biochemistry* **45**:11552-11563.
- Chen, R. 1967. Fluorescence quantum yields of tryptophan and tyrosine. *Anal. Lett.* **1**:35-42.

- Chen, R. F., J. R. Knutson, H. Ziffer, and D. Porter. 1991. Fluorescence of tryptophan dipeptides: correlations with the rotamer model. *Biochemistry* **30**:5184-5195.
- Chen, Y., and M. D. Barkley. 1998. Toward understanding tryptophan fluorescence in proteins. *Biochemistry* **37**:9976-9982.
- Chen, Y., B. Liu, H.-T. Yu, and M. D. Barkley. 1996. The Peptide Bond Quenches Indole Fluorescence. *J. Am. Chem. Soc* **118**:9271 - 9278.
- Chirgadze, Y. N., H. P. Driessen, G. Wright, C. Slingsby, R. E. Hay, and P. F. Lindley. 1996. Structure of bovine eye lens gammaD (gammaIIIb)-crystallin at 1.95 Å. *Acta Crystallogr D Biol Crystallogr* **52**:712-721.
- Colitz, C. M., J. A. Bomser, and D. F. Kusewitt. 2005. The endogenous and exogenous mechanisms for protection from ultraviolet irradiation in the lens. *Int Ophthalmol Clin* **45**:141-155.
- Colucci, W. J., L. Tilstra, M. C. Sattler, F. R. Fronczek, and M. D. Barkley. 1990. Conformational studies of a constrained tryptophan derivative: implications for the fluorescence quenching mechanism. *J. Am. Chem. Soc.* **112**:9182 - 9190.
- Cowgill, R. W. 1963. Fluorescence and the structure of proteins. I. Effects of substituents on the fluorescence of indole and phenol compounds. *Arch Biochem Biophys* **100**:36-44.
- Craescu, C. T., N. Rouviere, A. Popescu, E. Cerpolini, M. C. Lebeau, E. E. Baulieu, and J. Mispelter. 1996. Three-dimensional structure of the immunophilin-like domain of FKBP59 in solution. *Biochemistry* **35**:11045-11052.
- Creed, D. 1984. The photophysics and photochemistry of the near-UV absorbing amino acids-I. Tryptophan and its simple derivatives. *Photochemistry and Photobiology* **39**:537-562.
- Das, B. K., and J. J. Liang. 1998. Thermodynamic and kinetic characterization of calf lens gammaF-crystallin. *Int J Biol Macromol* **23**:191-197.
- Dillon, J., and S. J. Atherton. 1990. Time resolved spectroscopic studies on the intact human lens. *Photochem Photobiol* **51**:465-468.
- Dillon, J., R. H. Wang, and S. J. Atherton. 1990. Photochemical and photophysical studies on human lens constituents. *Photochem Photobiol* **52**:849-854.
- Eftink, M. R. 1991. Fluorescence techniques for studying protein structure. *Methods Biochem Anal* **35**:127-205.
- Ellozy, A. R., R. H. Wang, and J. Dillon. 1994. Model studies on the photochemical production of lenticular fluorophores. *Photochem Photobiol* **59**:479-484.
- Estey, T., J. Piatigorsky, N. Lassen, and V. Vasiliou. 2007. ALDH3A1: a corneal crystallin with diverse functions. *Exp Eye Res* **84**:3-12.
- Evans, P., K. Wyatt, G. J. Wistow, O. A. Bateman, B. A. Wallace, and C. Slingsby. 2004. The P23T cataract mutation causes loss of solubility of folded gammaD-crystallin. *J Mol Biol* **343**:435-444.
- Feitelson, J. 1971. The formation of hydrated electrons from the excited state of indole derivatives. *Photochemistry and Photobiology*. **13**:87-96.
- Flaugh, S. L., M. S. Kosinski-Collins, and J. King. 2005. Interdomain side-chain interactions in human gammaD crystallin influencing folding and stability. *Protein Sci* **14**:2030-2043.
- Forster, T. 1959. Transfer mechanisms of electronic excitation. *Discussions of the Faraday Society* **27**:7-17.



- Forsyth, W. E. 1969. Smithsonian Physical Tables. in *Smithsonian Miscellaneous Collections*. Smithsonian Institution Press, Washington D.C. .
- Fu, L., and J. J. Liang. 2002. Conformational change and destabilization of cataract gammaC-crystallin T5P mutant. *FEBS Lett* **513**:213-216.
- Gafni, A., and L. Brand. 1976. Fluorescence Decay Studies of Reduced Nicotinamide Adenine-Dinucleotide in Solution and Bound to Liver Alcohol-Dehydrogenase. *Biochemistry* **15**:3165-3171.
- Gill, S. C., and P. H. von Hippel. 1989. Calculation of protein extinction coefficients from amino acid sequence data. *Anal Biochem* **182**:319-326.
- Grinvald, A., and I. Z. Steinberg. 1974. Fast relaxation processes inn a protein revealed by the decay kinetics of tryptophan fluorecence. *Biochemistry* **13**:5170-5178.
- Gupta, R., and O. P. Srivastava. 2004. Deamidation affects structural and functional properties of human alphaA-crystallin and its oligomerization with alphaB-crystallin. *J Biol Chem* **279**:44258-44269.
- Hains, P. G., and R. J. Truscott. 2007. Post-translational modifications in the nuclear region of young, aged, and cataract human lenses. *J Proteome Res* **6**:3935-3943.
- Haley, D. A., M. P. Bova, Q. L. Huang, H. S. McHaourab, and P. L. Stewart. 2000. Small heat-shock protein structures reveal a continuum from symmetric to variable assemblies. *J Mol Biol* **298**:261-272.
- Ham, W. T., Jr., H. A. Mueller, J. J. Ruffolo, Jr., D. Guerry, 3rd, and R. K. Guerry. 1982. Action spectrum for retinal injury from near-ultraviolet radiation in the aphakic monkey. *Am J Ophthalmol* **93**:299-306.
- Hamill, S. J., E. Cota, C. Chothia, and J. Clarke. 2000. Conservation of folding and stability within a protein family: the tyrosine corner as an evolutionary cul-de-sac. *J Mol Biol* **295**:641-649.
- Hamilton, W. C. 1964. *Statistics in physical science. Estimation, hypothesis testing, and least squares*. Ronald Press, New York.
- Hammond, C. J., D. D. Duncan, H. Snieder, M. de Lange, S. K. West, T. D. Spector, and C. E. Gilbert. 2001. The heritability of age-related cortical cataract: the twin eye study. *Invest Ophthalmol Vis Sci* **42**:601-605.
- Hammond, C. J., H. Snieder, T. D. Spector, and C. E. Gilbert. 2000. Genetic and environmental factors in age-related nuclear cataracts in monozygotic and dizygotic twins. *N Engl J Med* **342**:1786-1790.
- Hanson, S. R., A. Hasan, D. L. Smith, and J. B. Smith. 2000. The major in vivo modifications of the human water-insoluble lens crystallins are disulfide bonds, deamidation, methionine oxidation and backbone cleavage. *Exp Eye Res* **71**:195-207.
- Hanson, S. R., D. L. Smith, and J. B. Smith. 1998. Deamidation and disulfide bonding in human lens gamma-crystallins. *Exp Eye Res* **67**:301-312.
- Harding, J. J. 2002. Viewing molecular mechanisms of ageing through a lens. *Ageing Res Rev* **1**:465-479.
- Harley, M. J., D. Toptygin, T. Troxler, and J. F. Schildbach. 2002. R150A mutant of F TraI relaxase domain: reduced affinity and specificity for single-stranded DNA and altered fluorescence anisotropy of a bound labeled oligonucleotide. *Biochemistry* **41**:6460-6468.

- Harris, D. L., and B. S. Hudson. 1990. Photophysics of tryptophan in bacteriophage T4 lysozymes. *Biochemistry* **29**:5276-5285.
- Harris, D. L., and B. S. Hudson. 1991. Fluorescence and molecular dynamics study of the internal motion of the buried tryptophan in bacteriophage T4 lysozyme: Effects of temperature and alteration of nonbonded networks. *Chem. Phys.* **158**:353-382.
- Hemmingsen, J. M., K. M. Gernert, J. S. Richardson, and D. C. Richardson. 1994. The tyrosine corner: a feature of most Greek key beta-barrel proteins. *Protein Sci* **3**:1927-1937.
- Hennecke, J., A. Sillen, M. Huber-Wunderlich, Y. Engelborghs, and R. Glockshuber. 1997. Quenching of tryptophan fluorescence by the active-site disulfide bridge in the DsbA protein from *Escherichia coli*. *Biochemistry* **36**:6391-6400.
- Heon, E., M. Priston, D. F. Schorderet, G. D. Billingsley, P. O. Girard, N. Lubsen, and F. L. Munier. 1999. The gamma-crystallins and human cataracts: a puzzle made clearer. *Am J Hum Genet* **65**:1261-1267.
- Herman, B., M. Parry-Hill, I. Johnson, and M. Davidson. 2006. Fluorescence Microscopy Interactive Java Tutorials, Photobleaching. in *Optical Microscopy*.
- Heyningen, R. V. 1973. The glucoside of 3-OH-kynurenine and other fluorescent compounds in human lens. Pages 151-168 in K. Elliot and D. W. Fitzsimmons, editors. *Ciba Foundation Symposium*. Elsevier, Amsterdam.
- Hibbard, L. B., N. J. Kirk, and R. F. Borkman. 1985. The effect of pH on the aerobic and anaerobic photolysis of tryptophan and some tryptophan-containing dipeptides. *Photochem Photobiol* **42**:99-106.
- Hochstrasser, R. M., and D. K. Negus. 1984. Picosecond fluorescence decay of tryptophans in myoglobin. *Proc Natl Acad Sci U S A* **81**:4399-4403.
- Hollows, F., and D. Moran. 1981. Cataract--the ultraviolet risk factor. *Lancet* **2**:1249-1250.
- Hood, B. D., B. Garner, and R. J. Truscott. 1999. Human lens coloration and aging. Evidence for crystallin modification by the major ultraviolet filter, 3-hydroxy-kynurenine O-beta-D-glucoside. *J Biol Chem* **274**:32547-32550.
- Horwitz, J. 1992. Alpha-crystallin can function as a molecular chaperone. *Proc Natl Acad Sci U S A* **89**:10449-10453.
- Horwitz, J. 1993. Proctor Lecture. The function of alpha-crystallin. *Invest Ophthalmol Vis Sci* **34**:10-22.
- Horwitz, J. 2000. The function of alpha-crystallin in vision. *Semin Cell Dev Biol* **11**:53-60.
- Hott, J. L., and R. F. Borkman. 1992. Analysis of photo-oxidized amino acids in tryptic peptides of calf lens gamma-II crystallin. *Photochem Photobiol* **56**:257-263.
- Hott, J. L., and R. F. Borkman. 1993. Concentration dependence of transmission losses in UV-laser irradiated bovine alpha-, beta H-, beta L- and gamma-crystallin solutions. *Photochem Photobiol* **57**:312-317.
- Hyman, L. 1987. Epidemiology of eye disease in the elderly. *Eye* **1** ( Pt 2):330-341.
- Jori, G., and G. Galiazzo. 1971. Proflavine-sensitized selective photooxidation of the tryptophyl residues in papain. *Photochem Photobiol* **14**:607-619.
- Kamel, I. D., and J. A. Parker. 1973. Protection from ultraviolet exposure in aphakic erythroptosis. *Can J Ophthalmol* **8**:563-565.

- Kim, K. K., R. Kim, and S. H. Kim. 1998. Crystal structure of a small heat-shock protein. *Nature* **394**:595-599.
- Kim, Y. H., D. M. Kapfer, J. Boekhorst, N. H. Lubsen, H. P. Bachinger, T. R. Shearer, L. L. David, J. B. Feix, and K. J. Lampi. 2002. Deamidation, but not truncation, decreases the urea stability of a lens structural protein, betaB1-crystallin. *Biochemistry* **41**:14076-14084.
- Kinsey, V. E. 1948. Spectral transmission of the eye to ultraviolet radiations. *Arch Ophthalmol* **39**:508-513.
- Kmoch, S., J. Brynda, B. Asfaw, K. Bezouska, P. Novak, P. Rezacova, L. Ondrova, M. Filipec, J. Sedlacek, and M. Elleder. 2000. Link between a novel human gammaD-crystallin allele and a unique cataract phenotype explained by protein crystallography. *Hum Mol Genet* **9**:1779-1786.
- Knutson, J. R., J. M. Beechem, and L. Brand. 1983. Simultaneous Analysis of Multiple Fluorescence Decay Curves - a Global Approach. *Chemical Physics Letters* **102**:501-507.
- Kosinski-Collins, M. S., S. L. Flaugh, and J. King. 2004. Probing folding and fluorescence quenching in human gammaD crystallin Greek key domains using triple tryptophan mutant proteins. *Protein Sci* **13**:2223-2235.
- Kosinski-Collins, M. S., and J. King. 2003. In vitro unfolding, refolding, and polymerization of human gammaD crystallin, a protein involved in cataract formation. *Protein Sci* **12**:480-490.
- Kumaraswamy, V. S., P. F. Lindley, C. Slingsby, and I. D. Glover. 1996. An eye lens protein-water structure: 1.2 Å resolution structure of gammaB-crystallin at 150 K. *Acta Crystallogr D Biol Crystallogr* **52**:611-622.
- Kurz, L. C., B. Fite, J. Jean, J. Park, T. Erpelding, and P. Callis. 2005. Photophysics of tryptophan fluorescence: link with the catalytic strategy of the citrate synthase from *Thermoplasma acidophilum*. *Biochemistry* **44**:1394-1413.
- Kurzel, R. B., M. Wolbarsht, B. S. Yamanashi, G. W. Staton, and R. F. Borkman. 1973. Tryptophan excited states and cataracts in the human lens. *Nature* **241**:132-133.
- Kurzel, R. B., M. L. Wolbarsht, and B. S. Yamanashi. 1977. Ultraviolet Radiation Effects on the Human Eye. *Photochemical and Photobiological Reviews* **2**:133-167.
- Kuznetsova, I. M., and K. K. Turoverov. 1998. [What determines the characteristics of the intrinsic UV-fluorescence of proteins? Analysis of the properties of the microenvironment and features of the localization of their tryptophan residues]. *Tsitologiya* **40**:747-762.
- Lakowicz, J. 1999. *Principles of fluorescence spectroscopy*, 2nd edition. Kluwer Academic/Plenum, New York.
- Lampi, K. J., K. K. Amyx, P. Ahmann, and E. A. Steel. 2006. Deamidation in human lens betaB2-crystallin destabilizes the dimer. *Biochemistry* **45**:3146-3153.
- Lampi, K. J., Y. H. Kim, H. P. Bachinger, B. A. Boswell, R. A. Lindner, J. A. Carver, T. R. Shearer, L. L. David, and D. M. Kapfer. 2002. Decreased heat stability and increased chaperone requirement of modified human betaB1-crystallins. *Mol Vis* **8**:359-366.
- Lampi, K. J., Z. Ma, S. R. Hanson, M. Azuma, M. Shih, T. R. Shearer, D. L. Smith, J. B. Smith, and L. L. David. 1998. Age-related changes in human lens crystallins

- identified by two-dimensional electrophoresis and mass spectrometry. *Exp Eye Res* **67**:31-43.
- Lampi, K. J., Z. Ma, M. Shih, T. R. Shearer, J. B. Smith, D. L. Smith, and L. L. David. 1997. Sequence analysis of betaA3, betaB3, and betaA4 crystallins completes the identification of the major proteins in young human lens. *J Biol Chem* **272**:2268-2275.
- Lapatto, R., V. Nalini, B. Bax, H. Driessen, P. F. Lindley, T. L. Blundell, and C. Slingsby. 1991. High resolution structure of an oligomeric eye lens beta-crystallin. Loops, arches, linkers and interfaces in beta B2 dimer compared to a monomeric gamma-crystallin. *J Mol Biol* **222**:1067-1083.
- Lerman, S. 1980. *Radiant energy and the eye*. Chapter 3: Biological and chemical effects of ultraviolet radiation. Macmillan Publishing Co., Inc, New York.
- Lerman, S. 1987. Chemical and physical properties of the normal and aging lens: spectroscopic (UV, fluorescence, phosphorescence, and NMR) analyses. *Am J Optom Physiol Opt* **64**:11-22.
- Lerman, S., and R. Borkman. 1978. Ultraviolet radiation in the aging and cataractous lens. A survey. *Acta Ophthalmol (Copenh)* **56**:139-149.
- Lerman, S., J. F. Kuck, Jr., R. Borkman, and E. Saker. 1976. Acceleration of an aging parameter (fluorogen) in the ocular lens. *Ann Ophthalmol* **8**:558-561.
- Li, Z. L., M. O. Tso, L. M. Jampol, S. A. Miller, and M. Waxler. 1990. Retinal injury induced by near-ultraviolet radiation in aphakic and pseudophakic monkey eyes. A preliminary report. *Retina* **10**:301-314.
- Liang, J. J. 2004. Interactions and chaperone function of alphaA-crystallin with T5P gammaC-crystallin mutant. *Protein Sci* **13**:2476-2482.
- Liu, I. Y., L. White, and A. Z. LaCroix. 1989. The association of age-related macular degeneration and lens opacities in the aged. *Am J Public Health* **79**:765-769.
- Liu, T., P. R. Callis, B. H. Hesp, M. de Groot, W. J. Buma, and J. Broos. 2005. Ionization potentials of fluorindoles and the origin of nonexponential tryptophan fluorescence decay in proteins. *J Am Chem Soc* **127**: 4104-4113.
- Loewenthal, R., J. Sancho, and A. R. Fersht. 1991. Fluorescence spectrum of barnase: contributions of three tryptophan residues and a histidine-related pH dependence. *Biochemistry* **30**:6775-6779.
- Lovicu, F., and M. Robinson. 2004. *Development of the Ocular Lens*. Cambridge University Press, Cambridge, UK.
- Ma, Z., S. R. Hanson, K. J. Lampi, L. L. David, D. L. Smith, and J. B. Smith. 1998. Age-related changes in human lens crystallins identified by HPLC and mass spectrometry. *Exp Eye Res*. **67**:21-30.
- MacDonald, J. T., A. G. Purkiss, M. A. Smith, P. Evans, J. M. Goodfellow, and C. Slingsby. 2005. Unfolding crystallins: the destabilizing role of a beta-hairpin cysteine in betaB2-crystallin by simulation and experiment. *Protein Sci* **14**:1282-1292.
- Mackay, D. S., U. P. Andley, and A. Shiels. 2003. Cell death triggered by a novel mutation in the alphaA-crystallin gene underlies autosomal dominant cataract linked to chromosome 21q. *Eur J Hum Genet* **11**:784-793.

- Mackay, D. S., O. B. Boskovska, H. L. Knopf, K. J. Lampi, and A. Shiels. 2002. A nonsense mutation in CRYBB1 associated with autosomal dominant cataract linked to human chromosome 22q. *Am J Hum Genet* **71**:1216-1221.
- MacKerell, A. D., D. Bashford, M. Bellott, R. L. Dunbrack, J. D. Evanseck, M. J. Field, S. Fischer, J. Gao, H. Guo, S. Ha, D. Joseph-McCarthy, L. Kuchnir, K. Kuczera, F. T. K. Lau, C. Mattos, S. Michnick, T. Ngo, D. T. Nguyen, B. Prodhom, W. E. Reiher, B. Roux, M. Schlenkrich, J. C. Smith, R. Stote, J. Straub, M. Watanabe, J. Wiórkiewicz-Kuczera, D. Yin, and M. Karplus. 1998. All-Atom Empirical Potential for Molecular Modeling and Dynamics Studies of Proteins. *J. Phys. Chem. B* **102**:3586 - 3616.
- MacRae, T. H. 2000. Structure and function of small heat shock/alpha-crystallin proteins: established concepts and emerging ideas. *Cell Mol Life Sci* **57**:899-913.
- Mandal, K., S. K. Bose, B. Chakrabarti, and R. J. Siezen. 1985. Structure and stability of gamma-crystallins. I. Spectroscopic evaluation of secondary and tertiary structure in solution. *Biochim Biophys Acta* **832**:156-164.
- Massof, R., S. Sykes, L. Rapp, W. Robison, H. Zwick, and B. Hochheimer. 1986. Chapter 4: Optical radiation damage to the ocular photoreceptors. Pages 69-88 in M. Waxler and V. Hitchins, editors. *Optical radiation and visual health*. CRC Press, Inc., Boca Raton, Florida.
- McCarty, C. A., and H. R. Taylor. 2002. A review of the epidemiologic evidence linking ultraviolet radiation and cataracts. Pages 21-31 in O. Hockwin, M. Kojima, N. Takahashi, and D. H. Sliney, editors. *Progress in Lens and Cataract Research*. Karger, S. Inc., Basel.
- McNulty, R., H. Wang, R. T. Mathias, B. J. Ortwerth, R. J. Truscott, and S. Bassnett. 2004. Regulation of tissue oxygen levels in the mammalian lens. *J Physiol* **559**:883-898.
- Merriam, J. C., S. Lofgren, R. Michael, P. Soderberg, J. Dillon, L. Zheng, and M. Ayala. 2000. An action spectrum for UV-B radiation and the rat lens. *Invest Ophthalmol Vis Sci* **41**:2642-2647.
- Messina-Baas, O. M., L. M. Gonzalez-Huerta, and S. A. Cuevas-Covarrubias. 2006. Two affected siblings with nuclear cataract associated with a novel missense mutation in the CRYGD gene. *Mol Vis* **12**:995-1000.
- Mills, I. A., S. L. Flaugh, M. S. Kosinski-Collins, and J. A. King. 2007. Folding and stability of the isolated Greek key domains of the long-lived human lens proteins gammaD-crystallin and gammaS-crystallin. *Protein Sci* **16**:2427-2444.
- Nanda, V., and L. Brand. 2000. Aromatic interactions in homeodomains contribute to the low quantum yield of a conserved, buried tryptophan. *Proteins* **40**:112-125.
- Nandrot, E., C. Slingsby, A. Basak, M. Cherif-Chefchaoui, B. Benazzouz, Y. Hajaji, S. Boutayeb, O. Gribouval, L. Arbogast, A. Berraho, M. Abitbol, and L. Hilal. 2003. Gamma-D crystallin gene (CRYGD) mutation causes autosomal dominant congenital cerulean cataracts. *J Med Genet* **40**:262-267.
- Noell, W. K., V. S. Walker, B. S. Kang, and S. Berman. 1966. Retinal damage by light in rats. *Invest Ophthalmol* **5**:450-473.
- Norledge, B. V., S. Trinkl, R. Jaenicke, and C. Slingsby. 1997. The X-ray structure of a mutant eye lens beta B2-crystallin with truncated sequence extensions. *Protein Sci* **6**:1612-1620.

- Oliva, M. S., and H. Taylor. 2005. Ultraviolet radiation and the eye. *Int Ophthalmol Clin* **45**:1-17.
- Oyster, C. 1999. *The human eye: structure and function*. Chapter 12. The lens and the vitreous. Sinauer Associates, Inc., Sunderland, MA.
- Pan, C. P., P. R. Callis, and M. D. Barkley. 2006. Dependence of tryptophan emission wavelength on conformation in cyclic hexapeptides. *J Phys Chem B Condens Matter Mater Surf Interfaces Biophys* **110**:7009-7016.
- Pande, A., J. Pande, N. Asherie, A. Lomakin, O. Ogun, J. King, and G. B. Benedek. 2001. Crystal cataracts: human genetic cataract caused by protein crystallization. *Proc Natl Acad Sci U S A* **98**:6116-6120.
- Pande, A., J. Pande, N. Asherie, A. Lomakin, O. Ogun, J. A. King, N. H. Lubsen, D. Walton, and G. B. Benedek. 2000. Molecular basis of a progressive juvenile-onset hereditary cataract. *Proc Natl Acad Sci U S A* **97**:1993-1998.
- Piatigorsky, J., and G. J. Wistow. 1989. Enzyme/crystallins: gene sharing as an evolutionary strategy. *Cell* **57**:197-199.
- Pigault, C., and D. Gerard. 1984. Influence of the location of tryptophanyl residues in proteins on their photosensitivity. *Photochem Photobiol* **40**:291-297.
- Pitts, D. G., A. P. Cullen, P. D. Hacker, and W. H. Parr. 1977. Ocular ultraviolet effects from 295 nm to 400 nm in the rabbit eye. U.S. Department of Health, Education and Welfare, Washington, D. C.
- Pollack, A., A. Bukelman, M. Zalish, H. Leiba, and M. Oliver. 1998. The course of age-related macular degeneration following bilateral cataract surgery. *Ophthalmic Surg Lasers* **29**:286-294.
- Pollack, A., A. Marcovich, A. Bukelman, and M. Oliver. 1996. Age-related macular degeneration after extracapsular cataract extraction with intraocular lens implantation. *Ophthalmology* **103**:1546-1554.
- Porter, G. B. 1972. Reversible energy transfer. *Theoret. chim. Acta (Berl.)* **24**:265-270.
- Prendergast, F. G. 1991. Time-resolved fluorescence techniques: methods and applications in biology. *Curr. Opin. Struct. Biol.* **1**:1054-1059.
- Purkiss, A. G., O. A. Bateman, J. M. Goodfellow, N. H. Lubsen, and C. Slingsby. 2002. The X-ray crystal structure of human gamma S-crystallin C-terminal domain. *J Biol Chem* **277**:4199-4205.
- Rahmani, B., J. M. Tielsch, J. Katz, J. Gottsch, H. Quigley, J. Javitt, and A. Sommer. 1996. The cause-specific prevalence of visual impairment in an urban population. The Baltimore Eye Survey. *Ophthalmology* **103**:1721-1726.
- Raman, B., and C. M. Rao. 1994. Chaperone-like activity and quaternary structure of alpha-crystallin. *J Biol Chem* **269**:27264-27268.
- Rao, S. C., C. M. Rao, and D. Balasubramanian. 1990. The Conformational Status of a Protein Influences the Aerobic Photolysis of Its Tryptophan Residues - Melittin, Beta-Lactoglobulin and the Crystallins. *Photochemistry and Photobiology* **51**:357-362.
- Reddy, G. B., P. A. Kumar, and M. S. Kumar. 2006. Chaperone-like activity and hydrophobicity of alpha-crystallin. *IUBMB Life* **58**:632-641.
- Ridley, J., and M. Zerner. 1973. An intermediate neglect of differential overlap technique for spectroscopy: Pyrrole and the azines. *Theor. Chim. Acta (Berlin)* **32**:111 - 134.

- Robman, L., and H. Taylor. 2005. External factors in the development of cataract. *Eye* **19**:1074-1082.
- Ross, J. B. A., K. W. Rousslang, and L. Brand. 1981. Time-Resolved Fluorescence and Anisotropy Decay of the Tryptophan in Adrenocorticotropin-(1-24). *Biochemistry* **20**:4361-4369.
- Rouviere, N., M. Vincent, C. T. Craescu, and J. Gallay. 1997. Immunosuppressor binding to the immunophilin FKBP59 affects the local structural dynamics of a surface beta-strand: time-resolved fluorescence study. *Biochemistry* **36**:7339-7352.
- Rowe, N. G., P. G. Mitchell, R. G. Cumming, and J. J. Wans. 2000. Diabetes, fasting blood glucose and age-related cataract: the Blue Mountains Eye Study. *Ophthalmic Epidemiol* **7**:103-114.
- Santhiya, S. T., M. Shyam Manohar, D. Rawley, P. Vijayalakshmi, P. Namperumalsamy, P. M. Gopinath, J. Loster, and J. Graw. 2002. Novel mutations in the gamma-crystallin genes cause autosomal dominant congenital cataracts. *J Med Genet* **39**:352-358.
- Sathish, H. A., H. A. Koteiche, and H. S. McHaourab. 2004. Binding of destabilized betaB2-crystallin mutants to alpha-crystallin: the role of a folding intermediate. *J Biol Chem* **279**:16425-16432.
- Searle, B. C., S. Dasari, P. A. Wilmarth, M. Turner, A. P. Reddy, L. L. David, and S. R. Nagalla. 2005. Identification of protein modifications using MS/MS de novo sequencing and the OpenSea alignment algorithm. *J Proteome Res* **4**:546-554.
- Sellers, D., and C. A. Ghiron. 1973. Role of the tryptophan fluorescent state in the UV induced inactivation of beta-trypsin. *Photochem Photobiol* **18**:393-402.
- Shimeld, S. M., A. G. Purkiss, R. P. Dirks, O. A. Bateman, C. Slingsby, and N. H. Lubsen. 2005. Urochordate betagamma-crystallin and the evolutionary origin of the vertebrate eye lens. *Curr Biol* **15**:1684-1689.
- Sillen, A., J. Hennecke, D. Roethlisberger, R. Glockshuber, and Y. Engelborghs. 1999. Fluorescence quenching in the DsbA protein from Escherichia coli: complete picture of the excited-state energy pathway and evidence for the reshuffling dynamics of the microstates of tryptophan. *Proteins* **37**:253-263.
- Singh, K., B. Groth-Vasselli, T. F. Kumosinski, and P. N. Farnsworth. 1995. alpha-Crystallin quaternary structure: molecular basis for its chaperone activity. *FEBS Lett* **372**:283-287.
- Sliney, D. H. 1986. Physical factors in cataractogenesis: ambient ultraviolet radiation and temperature. *Invest Ophthalmol Vis Sci* **27**:781-790.
- Slingsby, C., and O. A. Bateman. 1990. Quaternary interactions in eye lens beta-crystallins: basic and acidic subunits of beta-crystallins favor heterologous association. *Biochemistry* **29**:6592-6599.
- Smirnov, A. V., D. S. English, R. L. Rich, J. Lane, L. Teyton, A. W. Schwabacher, S. Luo, R. W. Thornburg, and J. W. Petrich. 1997. Photophysics and Biological Applications of 7-Azaindole and Its Analogs. *J. Phys. Chem. B* **101**:2758-2769.
- Soderberg, P. G., S. Lofgren, M. Ayala, X. Dong, M. Kakar, and V. Mody. 2002. Toxicity of ultraviolet radiation exposure to the lens expressed by maximum tolerable dose. Pages 70-75 in O. Hockwin, M. Kojima, N. Takahashi, and D. H. Sliney, editors. *Progress in lens and cataract research*. Karger, S. Inc., Basel.

- Srikanthan, D., O. A. Bateman, A. G. Purkiss, and C. Slingsby. 2004. Sulfur in human crystallins. *Exp Eye Res* **79**:823-831.
- Stephan, D. A., E. Gillanders, D. Vanderveen, D. Freas-Lutz, G. Wistow, A. D. Baxevanis, C. M. Robbins, A. VanAuken, M. I. Quesenberry, J. Bailey-Wilson, S. H. Juo, J. M. Trent, L. Smith, and M. J. Brownstein. 1999. Progressive juvenile-onset punctate cataracts caused by mutation of the gammaD-crystallin gene. *Proc Natl Acad Sci U S A* **96**:1008-1012.
- Streete, I. M., J. F. Jamie, and R. J. Truscott. 2004. Lenticular levels of amino acids and free UV filters differ significantly between normals and cataract patients. *Invest Ophthalmol Vis Sci* **45**:4091-4098.
- Subramaniam, V., T. M. Jovin, and R. V. Rivera-Pomar. 2001. Aromatic amino acids are critical for stability of the bicoid homeodomain. *J Biol Chem* **276**:21506-21511.
- Sun, H., Z. Ma, Y. Li, B. Liu, Z. Li, X. Ding, Y. Gao, W. Ma, X. Tang, X. Li, and Y. Shen. 2005. Gamma-S crystallin gene (CRYGS) mutation causes dominant progressive cortical cataract in humans. *J Med Genet* **42**:706-710.
- Swamy, M. S., A. Abraham, and E. C. Abraham. 1992. Glycation of human lens proteins: preferential glycation of alpha A subunits. *Exp Eye Res* **54**:337-345.
- Tallmadge, D. H., and R. F. Borkman. 1990. The rates of photolysis of the four individual tryptophan residues in UV exposed calf gamma-II crystallin. *Photochem Photobiol* **51**:363-368.
- Tallmadge, D. H., J. S. Huebner, and R. F. Borkman. 1989. Acrylamide quenching of tryptophan photochemistry and photophysics. *Photochem Photobiol* **49**:381-386.
- Taylor, H. R. 1980. The prevalence of corneal disease and cataracts in Australian aborigines in Northwestern Australia. *Aust J Ophthalmol* **8**:289-301.
- Taylor, H. R., S. K. West, F. S. Rosenthal, B. Munoz, H. S. Newland, H. Abbey, and E. A. Emmett. 1988. Effect of ultraviolet radiation on cataract formation. *N Engl J Med* **319**:1429-1433.
- Taylor, L. M., J. Andrew Aquilina, J. F. Jamie, and R. J. Truscott. 2002. UV filter instability: consequences for the human lens. *Exp Eye Res* **75**:165-175.
- Templer, H., and P. J. Thistlethwaite. 1976. Flash photolysis of aqueous tryptophan, alanyl tryptophan and tryptophyl alanine. *Photochem Photobiol* **23**:79-83.
- Toptygin, D., and L. Brand. 2000. Spectrally- and time-resolved fluorescence emission of indole during solvent relaxation: a quantitative model. *Chemical Physics Letters* **322**:496-502.
- Toptygin, D., A. M. Gronenborn, and L. Brand. 2006. Nanosecond relaxation dynamics of protein GB1 identified by the time-dependent red shift in the fluorescence of tryptophan and 5-fluorotryptophan. *Journal of Physical Chemistry B* **110**:26292-26302.
- Toptygin, D., R. S. Savtchenko, N. D. Meadow, and L. Brand. 2001. Homogeneous spectrally- and time-resolved fluorescence emission from single-tryptophan mutants of IIA(Glc) protein. *Journal of Physical Chemistry B* **105**:2043-2055.
- Toptygin, D., X. Wen, D. Barrick, and L. Brand. 2007. Time-resolved fluorescence of individual Trp residues in ordered and disordered regions of the Drosophila Notch receptor. in Biophysical Society meeting, Long Beach, CA.
- Truscott, R. J., and R. C. Augusteyn. 1977. Changes in human lens proteins during nuclear cataract formation. *Exp Eye Res* **24**:159-170.



- Ueda, Y., M. K. Duncan, and L. L. David. 2002. Lens proteomics: the accumulation of crystallin modifications in the mouse lens with age. *Invest Ophthalmol Vis Sci* **43**:205-215.
- Valeur, B., and G. Weber. 1977. Resolution of the fluorescence excitation spectrum of indole into the 1La and 1Lb excitation bands. *Photochem Photobiol* **25**:441-444.
- van Boekel, M. A., D. M. van Aalten, G. J. Caspers, B. Roll, and W. W. de Jong. 2001. Evolution of the aldose reductase-related gecko eye lens protein rhoB-crystallin: a sheep in wolf's clothing. *J Mol Evol* **52**:239-248.
- Van Heyningen, R. 1973. The glucoside of 3-hydroxykynurenine and other fluorescent compounds in the human lens. In *The Human Lens in Relation to Cataract. Ciba Found Symp* **19**:151-171.
- van Montfort, R. L., E. Basha, K. L. Friedrich, C. Slingsby, and E. Vierling. 2001. Crystal structure and assembly of a eukaryotic small heat shock protein. *Nat Struct Biol* **8**:1025-1030.
- Van Montfort, R. L., O. A. Bateman, N. H. Lubsen, and C. Slingsby. 2003. Crystal structure of truncated human betaB1-crystallin. *Protein Sci* **12**:2606-2612.
- van Rheede, T., R. Amons, N. Stewart, and W. W. de Jong. 2003. Lactate dehydrogenase A as a highly abundant eye lens protein in platypus (*Ornithorhynchus anatinus*): epsilon (epsilon)-crystallin. *Mol Biol Evol* **20**:994-998.
- Vander, D. E. 1969. Fluorescence solvent shifts and singlet excited state pK's of indole derivatives. *Bull. Soc. Chim. Belges* **78**:69-75.
- Vivian, J. T., and P. R. Callis. 2001. Mechanisms of tryptophan fluorescence shifts in proteins. *Biophys J* **80**:2093-2109.
- Voorter, C. E., W. A. De Haard-Hoekman, M. M. Hermans, H. Bloemendal, and W. W. De Jong. 1990. Differential synthesis of crystallins in the developing rat eye lens. *Exp Eye Res* **50**:429-437.
- Wald, G. 1952. Alleged effects of the near ultraviolet on human vision. *J Opt Soc Am* **42**:171-177.
- Walker, M. L., and R. F. Borkman. 1989. Light scattering and photocrosslinking in the calf lens crystallins gamma-II, III and IV. *Exp Eye Res* **48**:375-383.
- Wang, K., M. E. Rodgers, D. Toptygin, V. A. Munsen, and L. Brand. 1998. Fluorescence study of the multiple binding equilibria of the galactose repressor. *Biochemistry* **37**:41-50.
- Washburn, E. W. 1926 - 1930. *International Critical Tables of Numerical Data, Physics, Chemistry and Technology*, New York, London.
- Weisenborn, P. C. M., H. Meder, M. R. Egmond, T. J. Visser, and A. Hoek. 1996. Photophysics of the single tryptophan residue in *Fusarium solani* Cutinase: Evidence for the occurrence of conformational substates with unusual fluorescence behaviour. *Biophys. Chem.* **58**:281-288.
- Weiter, J. J., and E. D. Finch. 1975. Paramagnetic species in cataractous human lenses. *Nature* **254**:536-537.
- Wenk, M., R. Herbst, D. Hoeger, M. Kretschmar, N. H. Lubsen, and R. Jaenicke. 2000. Gamma S-crystallin of bovine and human eye lens: solution structure, stability and folding of the intact two-domain protein and its separate domains. *Biophys Chem* **86**:95-108.

- Werner, J. S., and L. Spillmann. 1989. UV-absorbing intraocular lenses: safety, efficacy, and consequences for the cataract patient. *Graefes Arch Clin Exp Ophthalmol* **27**:248-256.
- Werten, P. J., B. Roll, D. M. van Aalten, and W. W. de Jong. 2000. Gecko iota-crystallin: how cellular retinol-binding protein became an eye lens ultraviolet filter. *Proc Natl Acad Sci U S A* **97**:3282-3287.
- West, S. K., D. D. Duncan, B. Munoz, G. S. Rubin, L. P. Fried, K. Bandeen-Roche, and O. D. Schein. 1998. Sunlight exposure and risk of lens opacities in a population-based study: the Salisbury Eye Evaluation project. *Jama* **280**:714-718.
- WHO. 2006. Global disease burden from solar ultraviolet radiation. in. WHO, WHO sites, Media centre, Fact sheets
- Willaert, K., R. Loewenthal, J. Sancho, M. Froeyen, A. Fersht, and Y. Engelborghs. 1992. Determination of the excited-state lifetimes of the tryptophan residues in barnase, via multifrequency phase fluorometry of tryptophan mutants. *Biochemistry* **31**:711-716.
- Wistow, G. 1990. Evolution of a protein superfamily: relationships between vertebrate lens crystallins and microorganism dormancy proteins. *J Mol Evol* **30**:140-145.
- Wistow, G., S. L. Bernstein, M. K. Wyatt, A. Behal, J. W. Touchman, G. Bouffard, D. Smith, and K. Peterson. 2002. Expressed sequence tag analysis of adult human lens for the NEIBank Project: over 2000 non-redundant transcripts, novel genes and splice variants. *Mol Vis* **8**:171-184.
- Wistow, G., C. Jaworski, and P. V. Rao. 1995. A non-lens member of the beta gamma-crystallin superfamily in a vertebrate, the amphibian *Cynops*. *Exp Eye Res* **61**:637-639.
- Wistow, G., B. Turnell, L. Summers, C. Slingsby, D. Moss, L. Miller, P. Lindley, and T. Blundell. 1983. X-ray analysis of the eye lens protein gamma-II crystallin at 1.9 Å resolution. *J Mol Biol* **170**:175-202.
- Wistow, G., K. Wyatt, L. David, C. Gao, O. Bateman, S. Bernstein, S. Tomarev, L. Segovia, C. Slingsby, and T. Vihtelic. 2005. gammaN-crystallin and the evolution of the betagamma-crystallin superfamily in vertebrates. *Febs J* **272**:2276-2291.
- Wistow, G. J., J. W. Mulders, and W. W. de Jong. 1987. The enzyme lactate dehydrogenase as a structural protein in avian and crocodilian lenses. *Nature* **326**:622-624.
- Wu, Z., F. Delaglio, K. Wyatt, G. Wistow, and A. Bax. 2005. Solution structure of (gamma)S-crystallin by molecular fragment replacement NMR. *Protein Sci* **14**:3101-3114.
- Xu, J., D. Toptygin, K. J. Graver, R. A. Albertini, R. S. Savtchenko, N. D. Meadow, S. Roseman, P. R. Callis, L. Brand, and J. R. Knutson. 2006. Ultrafast Fluorescence Dynamics of Tryptophan in the Proteins Monellin and IIA(Glc). *J Am Chem Soc* **128**:1214-1221.
- Yuan, T., A. M. Weljie, and H. J. Vogel. 1998. Tryptophan fluorescence quenching by methionine and selenomethionine residues of calmodulin: orientation of peptide and protein binding. *Biochemistry* **37**:3187-3195.
- Zheng, Y., F. Mamdani, D. Toptygin, L. Brand, J. T. Stivers, and P. A. Cole. 2005. Fluorescence analysis of a dynamic loop in the PCAF/GCN5 histone acetyltransferase. *Biochemistry* **44**:10501-10509.

- Zigman, S. 1977. Near UV light and cataracts. *Photochem Photobiol* **26**:437-441.
- Zigman, S. 1993. Ocular light damage. *Photochem Photobiol* **57**:1060-1068.
- Zigman, S., M. Datiles, and E. Torczynski. 1979. Sunlight and human cataracts. *Invest Ophthalmol Vis Sci* **18**:462-467.
- Zigman, S., J. Schultz, and T. Yulo. 1973. Possible roles of near UV light in the cataractous process. *Exp Eye Res* **15**:201-208.
- Zigman, S., and T. Vaughan. 1974. Near-ultraviolet light effects on the lenses and retinas of mice. *Invest Ophthalmol* **13**:462-465.

## **CHAPTER SEVEN**

## **APPENDICES**

**APPENDIX A. SUPPORTING INFORMATION FOR CHAPTER TWO:  
MECHANISM OF THE HIGHLY EFFICIENT QUENCHING OF TRYPTOPHAN  
FLUORESCENCE IN HUMAN  $\gamma$ D CRYSTALLIN**

Tables A1-A8 list the all residues that contribute average stabilizing or destabilizing values exceeding 500  $\text{cm}^{-1}$  for the 4 tryptophans in Human  $\gamma$ D-Crystallin ( $1000 \text{ cm}^{-1} = 2.86 \text{ kcal/mol}$ . An energy change of this amount would change an equilibrium constant or rate constant by a factor of 100 at room temperature). The tables also include the average distance of the residues from the Trp in question, and the standard deviation of the contribution for the 5000 snapshots analyzed during a 50 ps molecular dynamics trajectory using Charmm 26b.

Segments: 1HK0 = protein. WAT1 = crystallographic water. SOLV = added water.

**Table A1.** Residues that *stabilize* Trp68.

		Distance	Shift, $\text{cm}^{-1}$	Std Dev	Segment
69	MET	6.19	-3399	369	1HK0
303	TIP3	6.2	-2738	826	WAT1
73	ASP	10.89	-2000	168	1HK0
8	ASP	13.71	-1964	124	1HK0
7	GLU	14.12	-1893	104	1HK0
139	ARG	15.36	-1545	122	1HK0
64	ASP	8.09	-1453	347	1HK0
167	ARG	14.54	-1419	148	1HK0
308	TIP3	6.62	-1226	482	WAT1
17	GLU	17.92	-967	47	1HK0
55	TYR	7.02	-930	271	1HK0
58	ARG	10.63	-923	215	1HK0
38	ASP	16.24	-897	117	1HK0
61	ASP	11.54	-856	149	1HK0
46	GLU	12.01	-780	149	1HK0
1738	TIP3	7.24	-759	389	SOLV
62	TYR	6.91	-682	156	1HK0
72	SER	10.47	-662	115	1HK0
21	ASP	18.27	-642	53	1HK0
300	TIP3	6.53	-532	448	WAT1
141	ARG	15.15	-528	129	1HK0

**Table A2.** Residues that *destabilize* Trp68.

		Distance	Shift, cm <sup>-1</sup>	Std Dev	Segment
54	GLN	12.08	548	73	1HK0
44	LEU	7.96	551	97	1HK0
1	GLY	17.59	628	60	1HK0
107	ASP	19.94	641	61	1HK0
67	GLN	5.84	666	165	1HK0
66	GLN	7.8	786	389	1HK0
142	GLN	10.85	894	300	1HK0
134	GLU	17.1	960	106	1HK0
2	LYS	17.76	992	84	1HK0
14	ARG	19.03	1026	48	1HK0
36	ARG	13.31	1202	109	1HK0
76	ARG	14.5	1303	133	1HK0
9	ARG	12.02	1520	194	1HK0
70	GLY	5.89	1533	348	1HK0
31	ARG	14.55	1741	99	1HK0
65	HSD	6.74	1747	601	1HK0

**Table A3.** Residues that *stabilize* Trp42.

		Distance	Shift, cm <sup>-1</sup>	Std Dev	Segment
174	TIP3	5.83	-2716	1190	WAT1
58	ARG	11.02	-2309	255	1HK0
21	ASP	8.58	-2186	362	1HK0
17	GLU	12.04	-1986	106	1HK0
167	ARG	14.97	-1797	194	1HK0
40	GLY	7.78	-1611	222	1HK0
38	ASP	10.54	-1425	247	1HK0
168	ARG	17.19	-1101	63	1HK0
7	GLU	17.86	-964	44	1HK0
59	ARG	11.58	-897	231	1HK0
8	ASP	19.63	-804	46	1HK0
73	ASP	18.19	-632	59	1HK0
43	MET	6.61	-610	116	1HK0
39	SER	9.62	-603	230	1HK0
81	ILE	6.85	-562	444	1HK0
61	ASP	13.97	-536	158	1HK0
56	PHE	9.25	-534	98	1HK0
88	ARG	23.54	-509	32	1HK0

**Table A4.** Residues that *destabilize* Trp42.

		Distance	Shift, cm <sup>-1</sup>	Std Dev	Segment
36	ARG	13.59	566	123	1HK0
106	GLU	22.94	612	46	1HK0
127	GLU	20.24	653	46	1HK0
31	ARG	19.8	675	47	1HK0
76	ARG	16.15	725	55	1HK0
173	SER	16.04	927	124	1HK0
317	TIP3	8.11	995	727	WAT1
14	ARG	19.57	1046	59	1HK0
82	PRO	9.89	1052	146	1HK0
107	ASP	20.02	1206	84	1HK0
41	CYS	4.78	1399	398	1HK0
57	LEU	7.29	2083	267	1HK0
171	ASP	11.48	2276	254	1HK0
2	LYS	10.12	2658	269	1HK0



**Table A5.** Residues that *stabilize* Trp156.

		Distance	Shift, cm <sup>-1</sup>	Std Dev	Segment
157	GLY	3.43	-5142	471	1HK0
79	ARG	15.21	-1998	244	1HK0
430	TIP3	6.71	-1854	1318	WAT1
119	GLU	12.67	-1688	168	1HK0
93	GLU	15.23	-1573	91	1HK0
95	GLU	11.69	-1381	191	1HK0
441	TIP3	6.69	-1287	584	WAT1
134	GLU	11.79	-1223	192	1HK0
96	ASP	12.85	-901	100	1HK0
1404	TIP3	7.65	-877	927	SOLV
103	GLU	18.15	-871	43	1HK0
141	ARG	12.16	-854	357	1HK0
113	ASP	21.7	-822	41	1HK0
150	TYR	6.84	-812	195	1HK0
434	TIP3	9.22	-785	1252	WAT1
160	ASN	10.3	-785	174	1HK0
76	ARG	21.85	-766	59	1HK0
143	TYR	7.31	-761	264	1HK0
107	ASP	18.6	-667	69	1HK0
54	GLN	11.18	-662	436	1HK0
106	GLU	21.03	-649	43	1HK0
127	GLU	18.11	-603	54	1HK0
120	ILE	9.83	-590	169	1HK0
420	TIP3	8.82	-531	250	WAT1

**Table A6.** Residues that *destabilize* Trp156.

		Distance	Shift, cm <sup>-1</sup>	Std Dev	Segment
1547	TIP3	7.54	502	625	SOLV
142	GLN	12.31	511	69	1HK0
139	ARG	18.87	564	75	1HK0
144	LEU	10.49	566	192	1HK0
154	GLN	7.69	608	334	1HK0
168	ARG	18.41	611	64	1HK0
21	ASP	20.79	646	85	1HK0
88	ARG	18.78	731	45	1HK0
116	ARG	21.85	877	36	1HK0
90	ARG	15.66	880	51	1HK0
94	ARG	16.35	951	69	1HK0
114	ARG	20.73	974	51	1HK0
46	GLU	17.24	985	151	1HK0
98	ARG	16.17	1004	89	1HK0
162	ARG	13.06	1173	138	1HK0
153	TYR	7.2	1288	497	1HK0
155	ASP	4.65	1584	502	1HK0
158	ALA	6.21	1711	271	1HK0

**Table A7.** Residues that *stabilize* Trp130.

		Distance	Shift, cm <sup>-1</sup>	Std Dev	Segment
106	GLU	10.21	-2740	246	1HK0
107	ASP	8.65	-2682	382	1HK0
127	GLU	9.56	-2661	380	1HK0
128	GLY	6.91	-2624	369	1HK0
103	GLU	11.88	-2170	144	1HK0
79	ARG	15.59	-1520	161	1HK0
169	VAL	7.18	-1466	356	1HK0
1	GLY	19.6	-1067	165	1HK0
113	ASP	18.34	-979	64	1HK0
131	VAL	5.88	-894	133	1HK0
93	GLU	19.1	-851	37	1HK0
59	ARG	18.49	-756	71	1HK0
144	LEU	9.06	-615	71	1HK0
58	ARG	15.01	-615	105	1HK0
119	GLU	19.3	-595	44	1HK0

**Table A8.** Residues that *destabilize* Trp130.

		Distance	Shift, cm <sup>-1</sup>	Std Dev	Segment
173	SER	18.8	509	92	1HK0
126	LEU	10.88	562	72	1HK0
94	ARG	22.01	635	29	1HK0
403	TIP3	8.87	636	547	WAT1
162	ARG	18.03	697	54	1HK0
86	SER	10.75	704	95	1HK0
82	PRO	12.21	727	144	1HK0
129	SER	4.73	825	504	1HK0
116	ARG	21.09	940	53	1HK0
171	ASP	13.96	1076	102	1HK0
21	ASP	19.96	1308	109	1HK0
90	ARG	12.42	1703	151	1HK0
145	LEU	7.26	1975	359	1HK0
168	ARG	7.15	2104	611	1HK0
114	ARG	14.96	2283	186	1HK0
88	ARG	10.23	2774	308	1HK0

Figures A1-A10 show how to match 3MI spectra with the spectra of triple Trps mutants (W42-only, W68-only, W130-only and W156-only) for the extrapolation of the quantum yields of four Trps in HyD-Crys on the blue side.

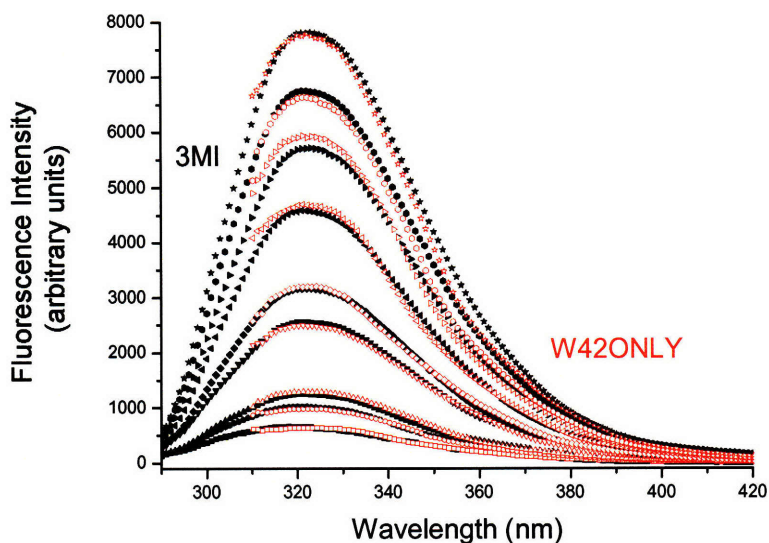


Figure A1. Matching of native W42-only fluorescence emission spectra (open symbols, red) with spectra of 3MI in Cyclohexane: Dioxane (83:17) (closed symbols, black). Fluorescence emission spectra of 3MI were measured in the range of 290 to 420nm using an excitation wavelength of 280nm. Spectra of W42-only were recorded from 310 to 420nm with an excitation wavelength of 300nm. The buffer or solvent signal was subtracted from all spectra.

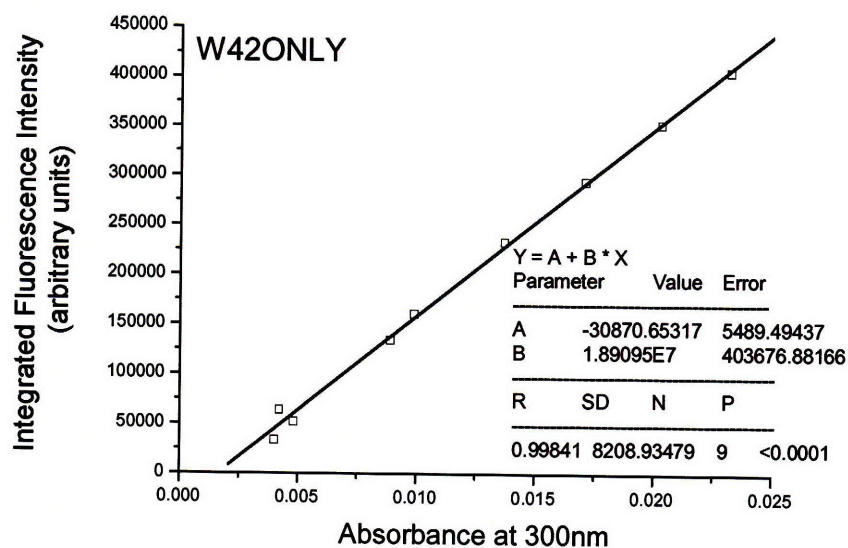


Figure A2. The linear curve of integrated fluorescence intensity (from 297nm to 420nm) calculated from overlapped spectra of 3MI versus the corresponding absorbance of W42-only at 300nm.

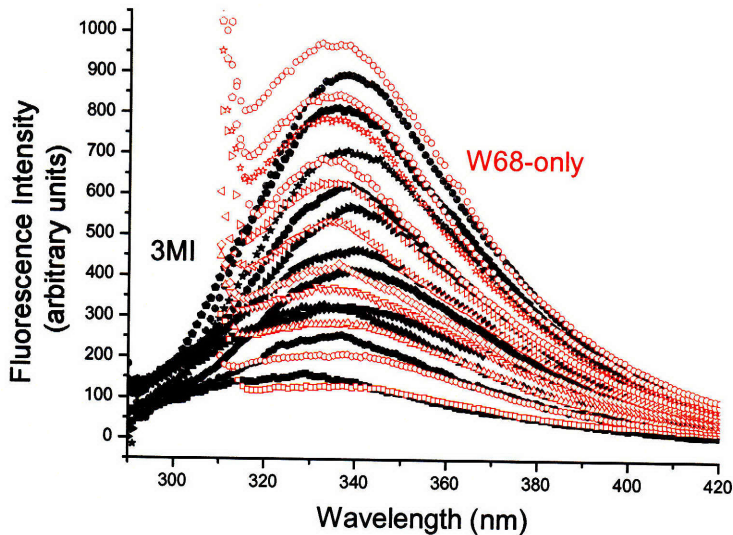


Figure A3. Matching of native W68-only fluorescence emission spectra (open symbols, red) with spectra of 3MI in Methanol: Dioxane (25:75) (closed symbols, black). Fluorescence emission spectra of 3MI were measured in the range of 290 to 420nm using an excitation wavelength of 280nm. Spectra of W68-only were recorded from 310 to 420nm with an excitation wavelength of 300nm. The buffer or solvent signal was subtracted from all spectra.

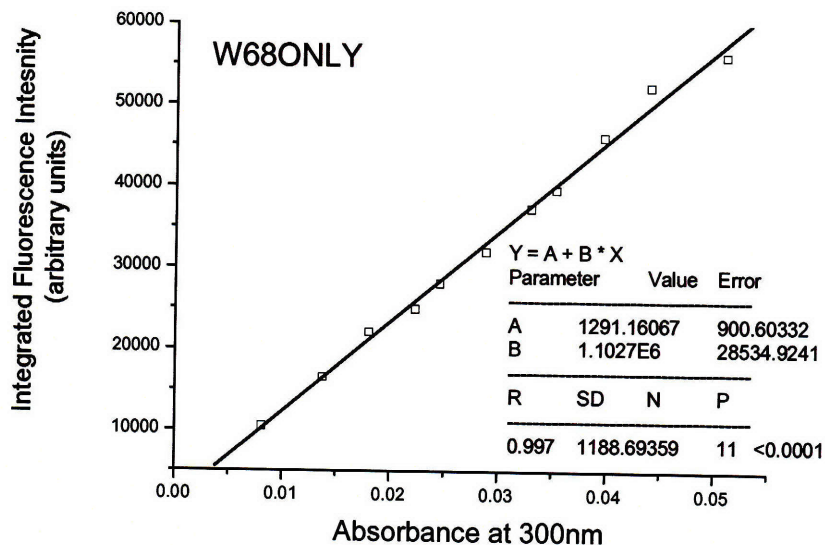


Figure A4. The linear curve of integrated fluorescence intensity (from 297nm to 420nm) calculated from overlapped spectra of 3MI versus the corresponding absorbance of W68-only at 300nm.

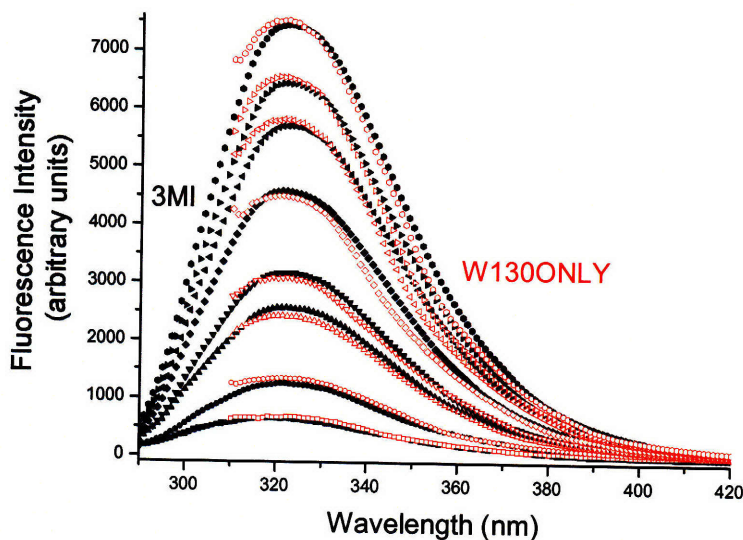


Figure A5. Matching of native W130-only fluorescence emission spectra (open symbols, red) with spectra of 3MI in Cyclohexane: Dioxane (83:17) (closed symbols, black). Fluorescence emission spectra of 3MI were measured in the range of 290 to 420nm using an excitation wavelength of 280nm. Spectra of W130-only were recorded from 310 to 420nm with an excitation wavelength of 300nm. The buffer or solvent signal was subtracted from all spectra.



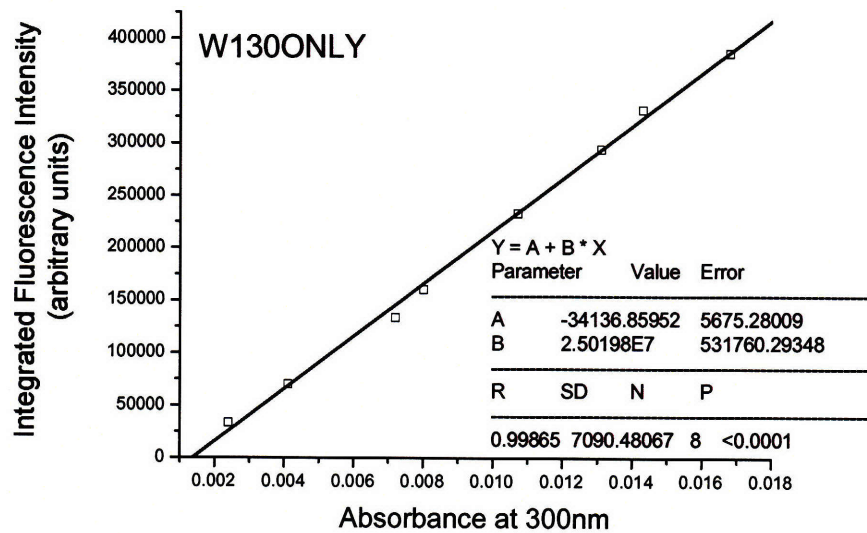


Figure A6. The linear curve of integrated fluorescence intensity (from 297nm to 420nm) calculated from overlapped spectra of 3MI versus the corresponding absorbance of W130-only at 300nm.

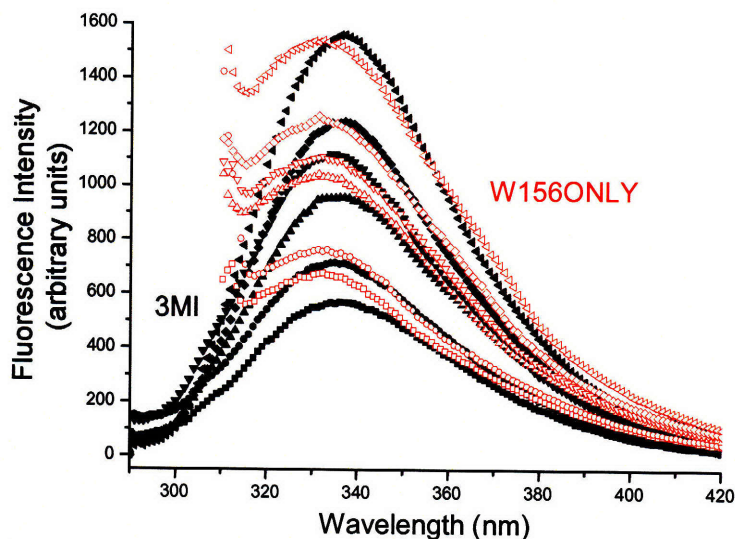


Figure A7. Matching of native W156-only fluorescence emission spectra (open symbols, red) with spectra of 3MI in Methanol: Dioxane (10:90) (closed symbols, black). Fluorescence emission spectra of 3MI were measured in the range of 290 to 420nm using an excitation wavelength of 280nm. Spectra of W156-only were recorded from 310 to



420nm with an excitation wavelength of 300nm. The buffer or solvent signal was subtracted from all spectra.

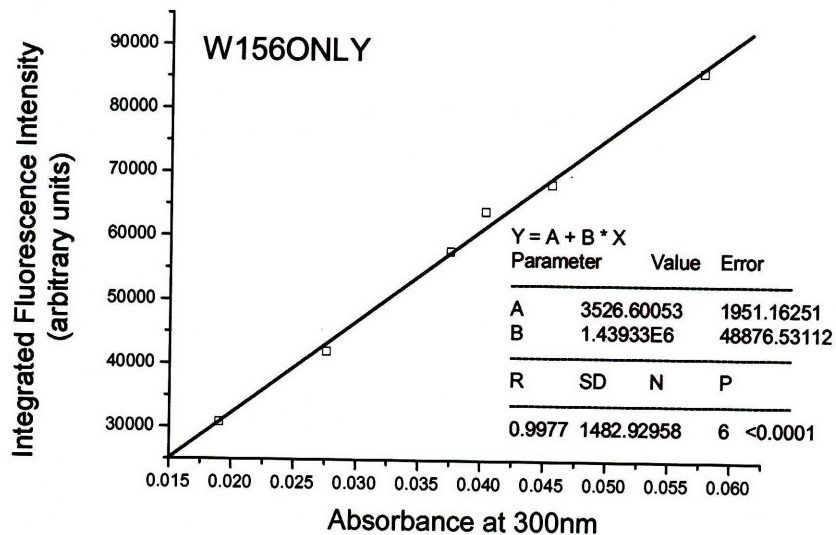


Figure A8. The linear curve of integrated fluorescence intensity (from 297nm to 420nm) calculated from overlapped spectra of 3MI versus the corresponding absorbance of W156-only at 300nm.

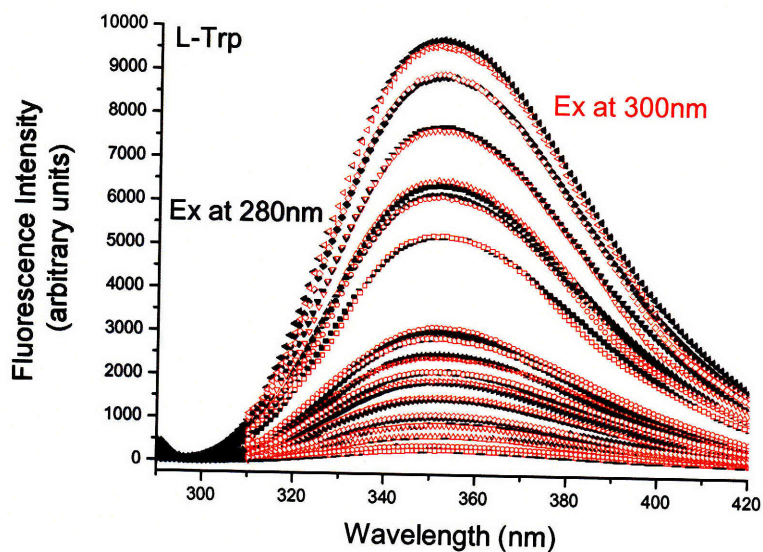


Figure A9. Matching of fluorescence emission spectra of L-Trp with excitation (Ex)<sup>1</sup> wavelength at 300nm (open symbols, red) with spectra of L-Trp (Ex at 280nm) (closed symbols, black). Fluorescence emission spectra of L-Trp were measured in the range of

290 to 420nm using an excitation wavelength of 280nm and in the range of 310 to 420nm with an excitation wavelength of 300nm, respectively. The buffer signal was subtracted from all spectra.

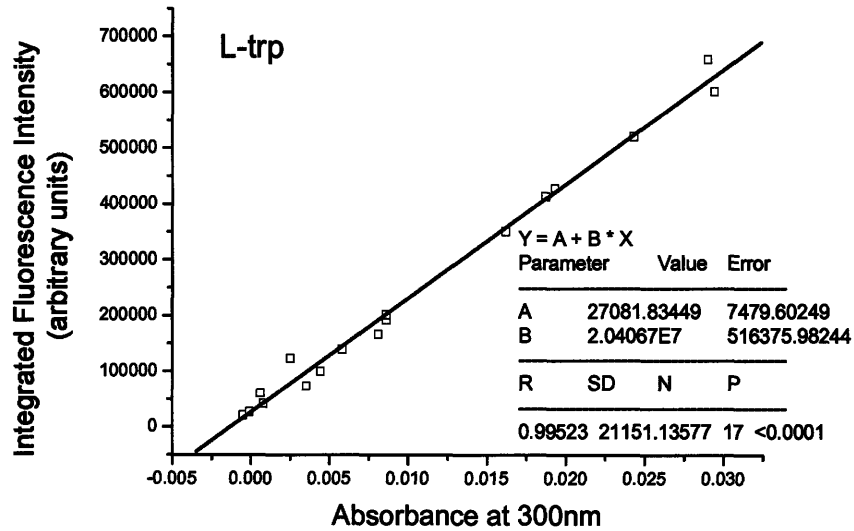


Figure A10. The standard curve of L-Trp. After matching the emission spectra of L-Trp (Ex at 280nm) with the spectra of L-Trp (Ex at 300nm), the integrated fluorescence intensity of L-Trp (from 297nm to 420nm, Ex at 280nm) and the absorbance of corresponding L-Trp (Ex at 300nm) at 300nm were used to calculate the slope of the standard curve.

The slopes of the linear curves, Figures A2, A4, A6, A8 and A10, were used to calculate the quantum yields of four Trps in HyD-Crys according to equation (1) in the Materials and Methods in chapter two. According to the similar method, the quantum yield of wild-type HyD-Crys was calculated by matching the spectra of protein with the spectra of 3MI in Cyclohexane: Dioxane (70:30).

**APPENDIX B. SUPPORTING INFORMATION FOR CHAPTER THREE:  
MECHANISM OF THE EFFICIENT TRYPTOPHAN FLUORESCENCE  
QUENCHING IN HUMAN  $\gamma$ D CRYSTALLIN STUDIED BY TIME-RESOLVED  
FLUORESCENCE**

Contents

- Figure B1. Pre-exponential amplitude spectra  $\alpha_i(\lambda)$  of Trp42-only  
Figure B2. Pre-exponential amplitude spectra  $\alpha_i(\lambda)$  of *Trp68-only*  
Figure B3. Pre-exponential amplitude spectra  $\alpha_i(\lambda)$  of Trp42/*Trp68*  
Figure B4. Pre-exponential amplitude spectra  $\alpha_i(\lambda)$  of *Trp156-only*  
Figure B5. Pre-exponential amplitude spectra  $\alpha_i(\lambda)$  of Trp130/*Trp156*  
Figure B6. Pre-exponential amplitude spectra  $\alpha_i(\lambda)$  of wild type  
Figure B7. Pre-exponential amplitude spectra  $\alpha_i(\lambda)$  of Trp42/*Trp156*  
Figure B8. Pre-exponential amplitude spectra  $\alpha_i(\lambda)$  of *Trp68/Trp130*  
Figure B9. Pre-exponential amplitude spectra  $\alpha_i(\lambda)$  of Trp42/*Trp130*  
Figure B10. Pre-exponential amplitude spectra  $\alpha_i(\lambda)$  of *Trp68/Trp156*  
Figure B11. Time-resolved anisotropy of Trp42-only  
Table B1. Coordinates of the centers and the directions of transition dipole moments  
for all Trps  
Table B2. Values of  $R$  and  $\kappa^2$  for Trps pair calculated from the crystal structure of  
HyD-Crys  
Calculation of mean lifetimes of Trps in HyD-Crys

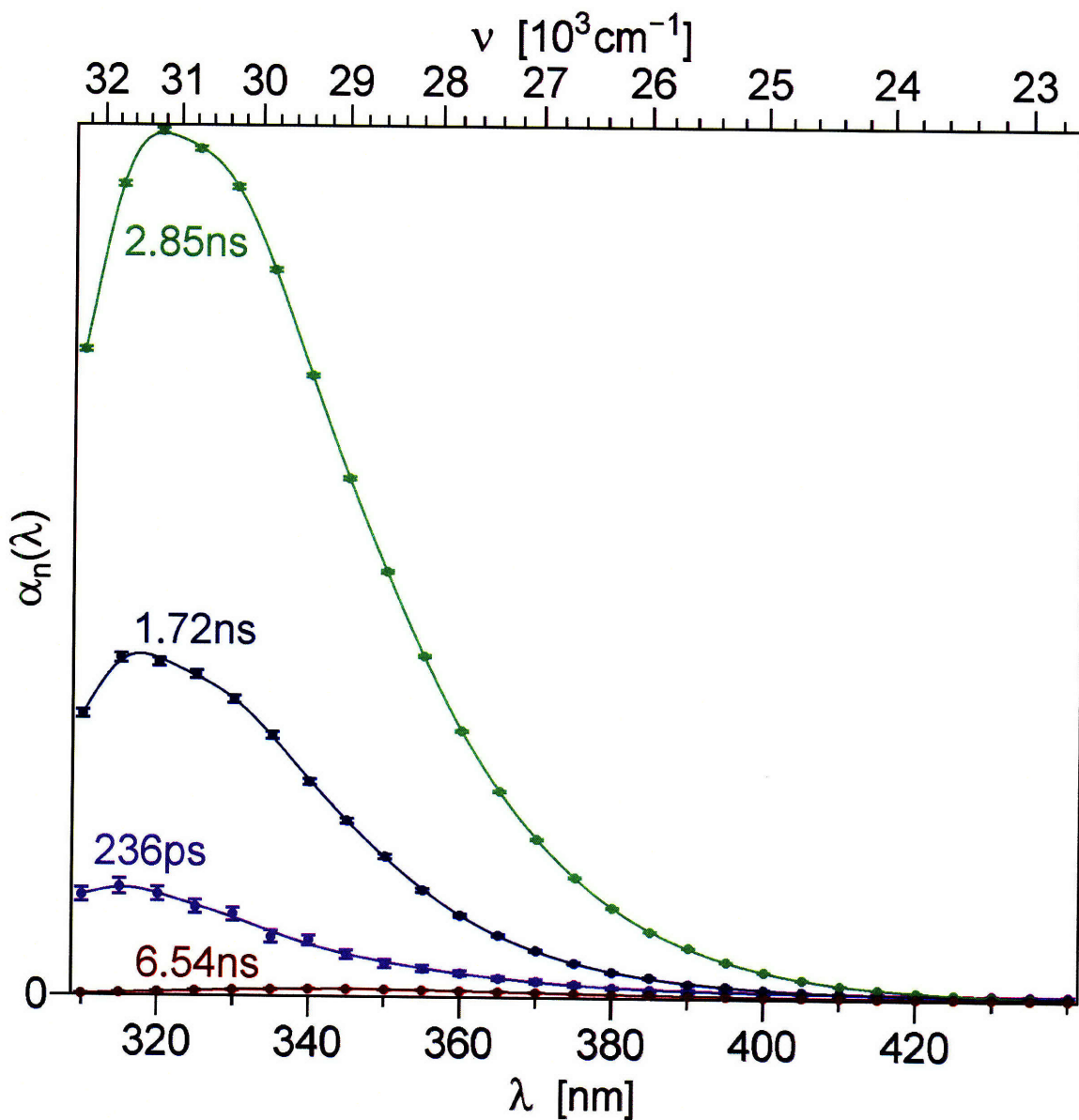


Figure B1. Pre-exponential amplitude spectra  $\alpha_i(\lambda)$  obtained by the global analysis of the fluorescence emission from Trp42-only H $\gamma$ D-Crys. The values of the corresponding time constants  $\tau_i$  are shown near each spectrum using a matching color.

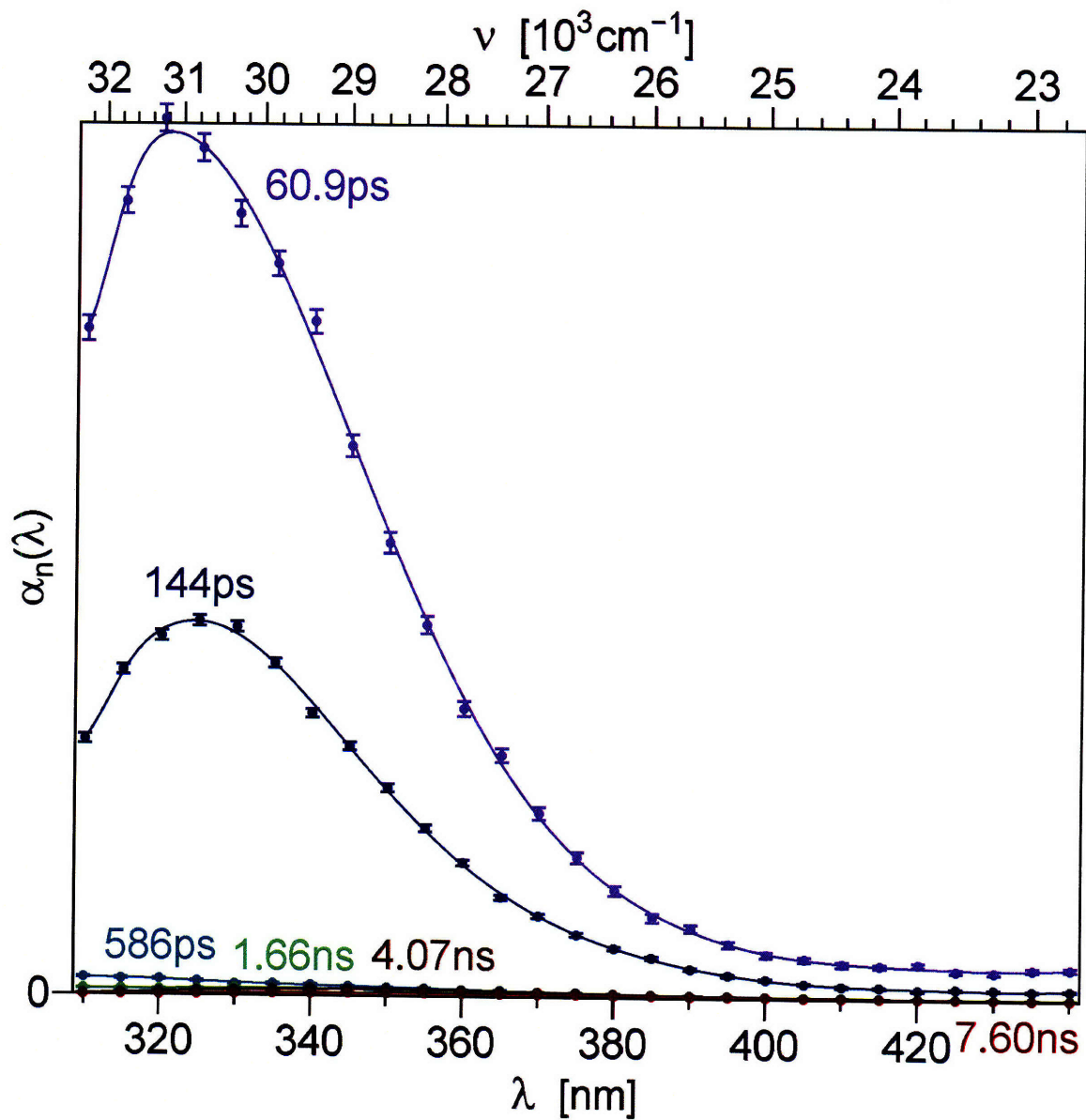


Figure B2. Pre-exponential amplitude spectra  $\alpha_i(\lambda)$  obtained by the global analysis of the fluorescence emission from *Trp68-only* H $\gamma$ D-Crys. The values of the corresponding time constants  $\tau_i$  are shown near each spectrum using a matching color.

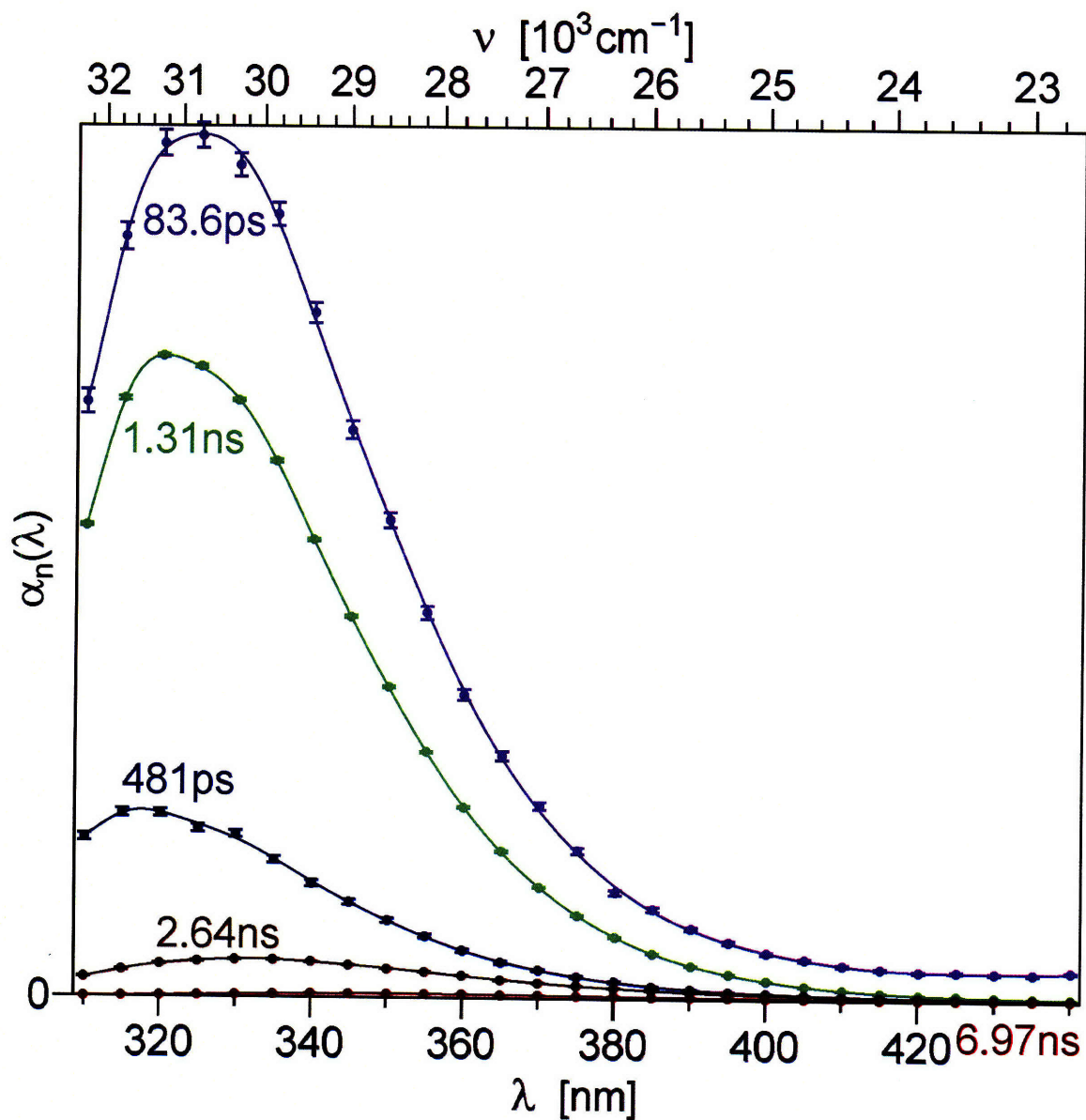


Figure B3. Pre-exponential amplitude spectra  $\alpha_i(\lambda)$  obtained by the global analysis of the fluorescence emission from Trp42/Trp68 H $\gamma$ D-Crys. The values of the corresponding time constants  $\tau_i$  are shown near each spectrum using a matching color.

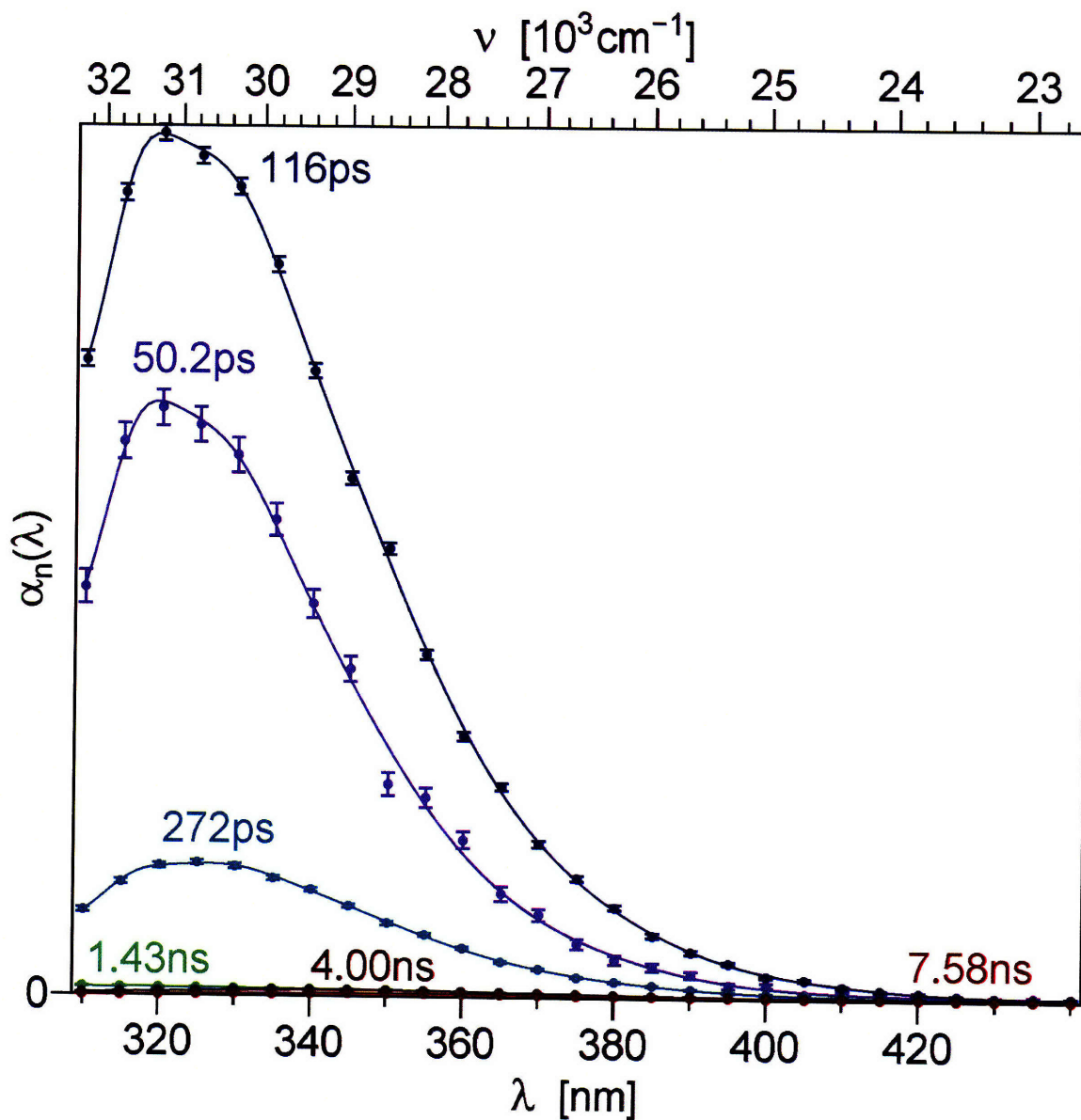


Figure B4. Pre-exponential amplitude spectra  $\alpha_i(\lambda)$  obtained by the global analysis of the fluorescence emission from *Trp156-only* H $\gamma$ D-Crys. The values of the corresponding time constants  $\tau_i$  are shown near each spectrum using a matching color.



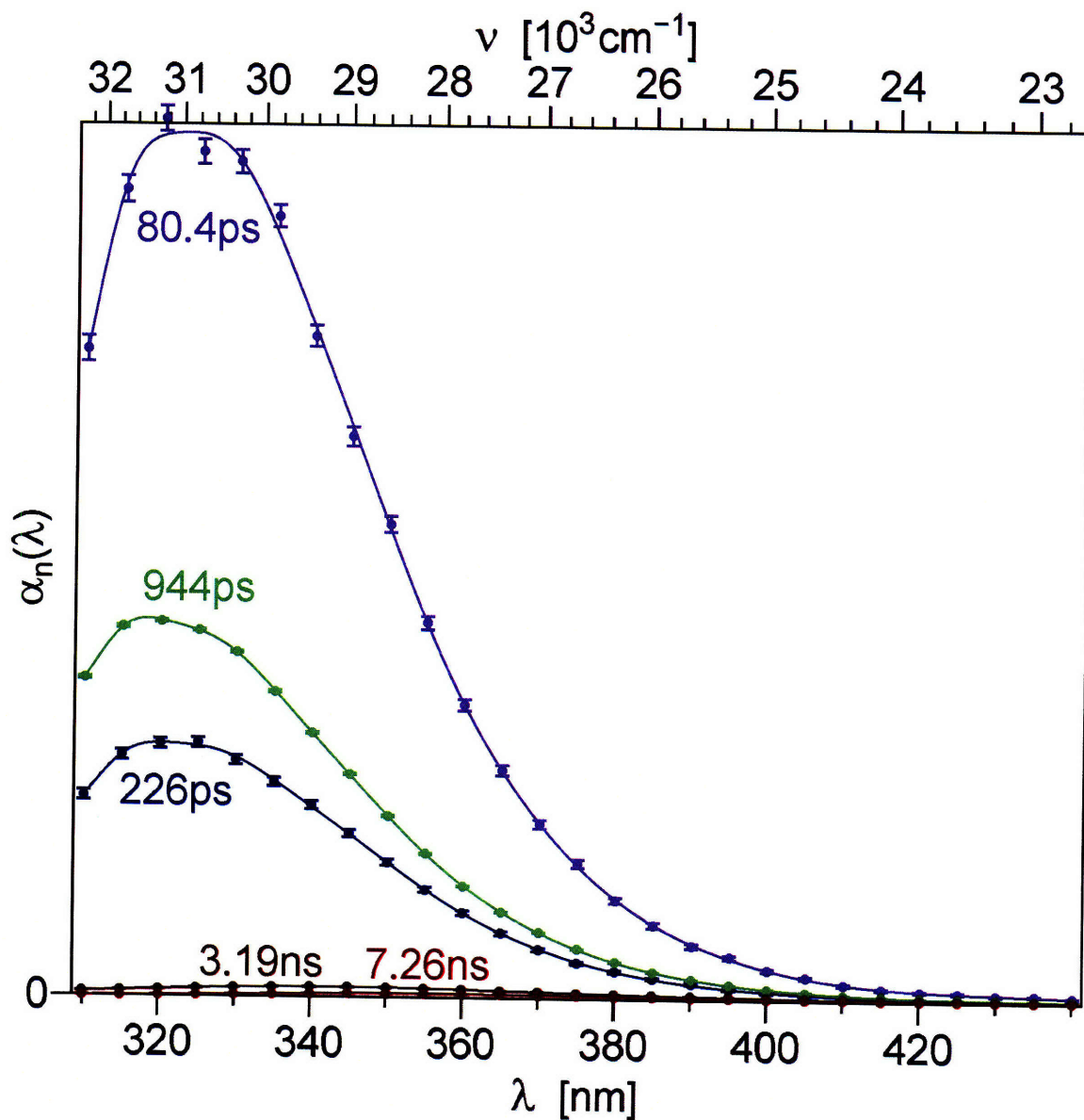


Figure B5. Pre-exponential amplitude spectra  $\alpha_i(\lambda)$  obtained by the global analysis of the fluorescence emission from Trp130/Trp156 HyD-Crys. The values of the corresponding time constants  $\tau_i$  are shown near each spectrum using a matching color.



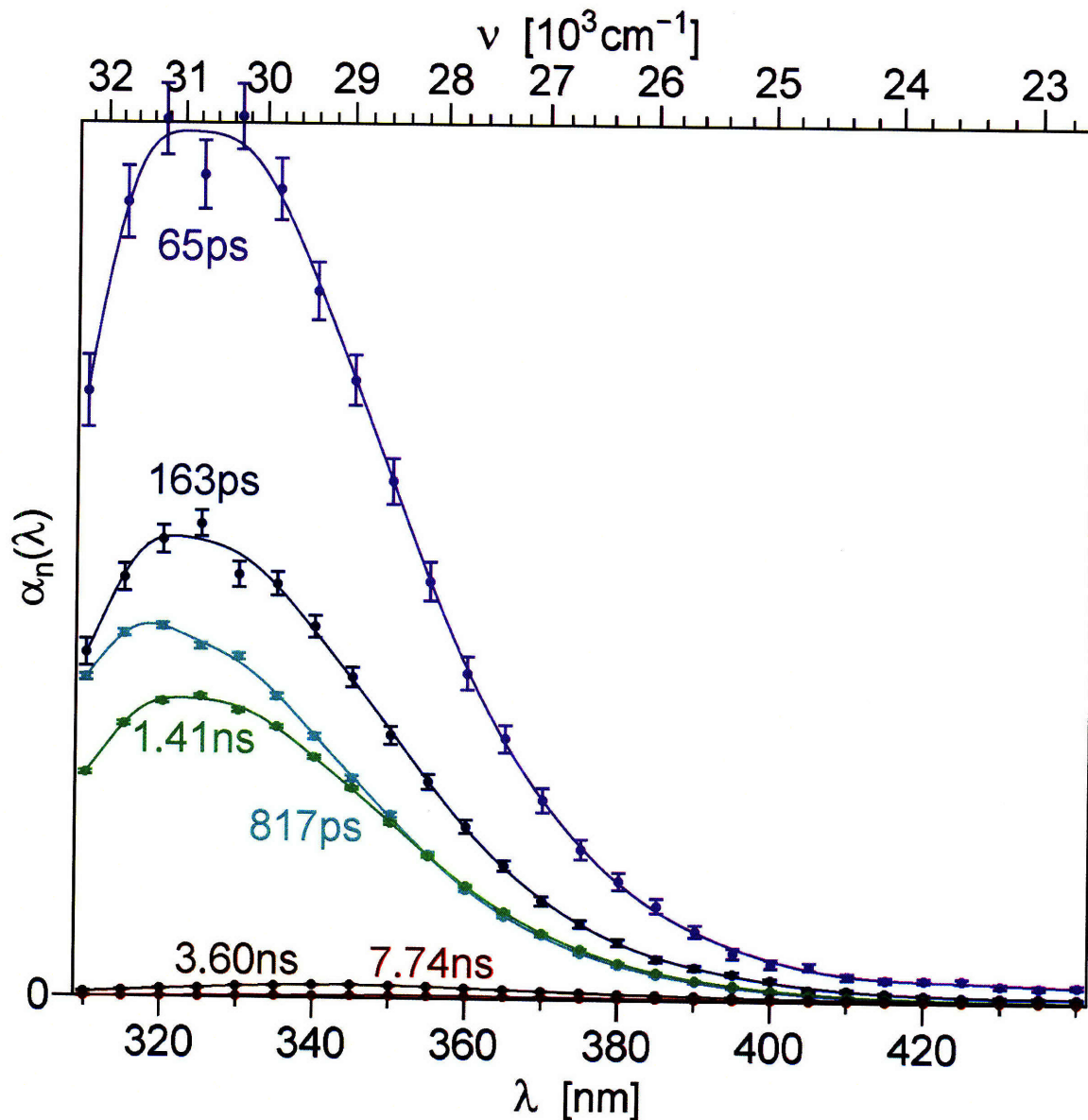


Figure B6. Pre-exponential amplitude spectra  $\alpha_i(\lambda)$  obtained by the global analysis of the fluorescence emission from wild-type HyD-Crys. The values of the corresponding time constants  $\tau_i$  are shown near each spectrum using a matching color.

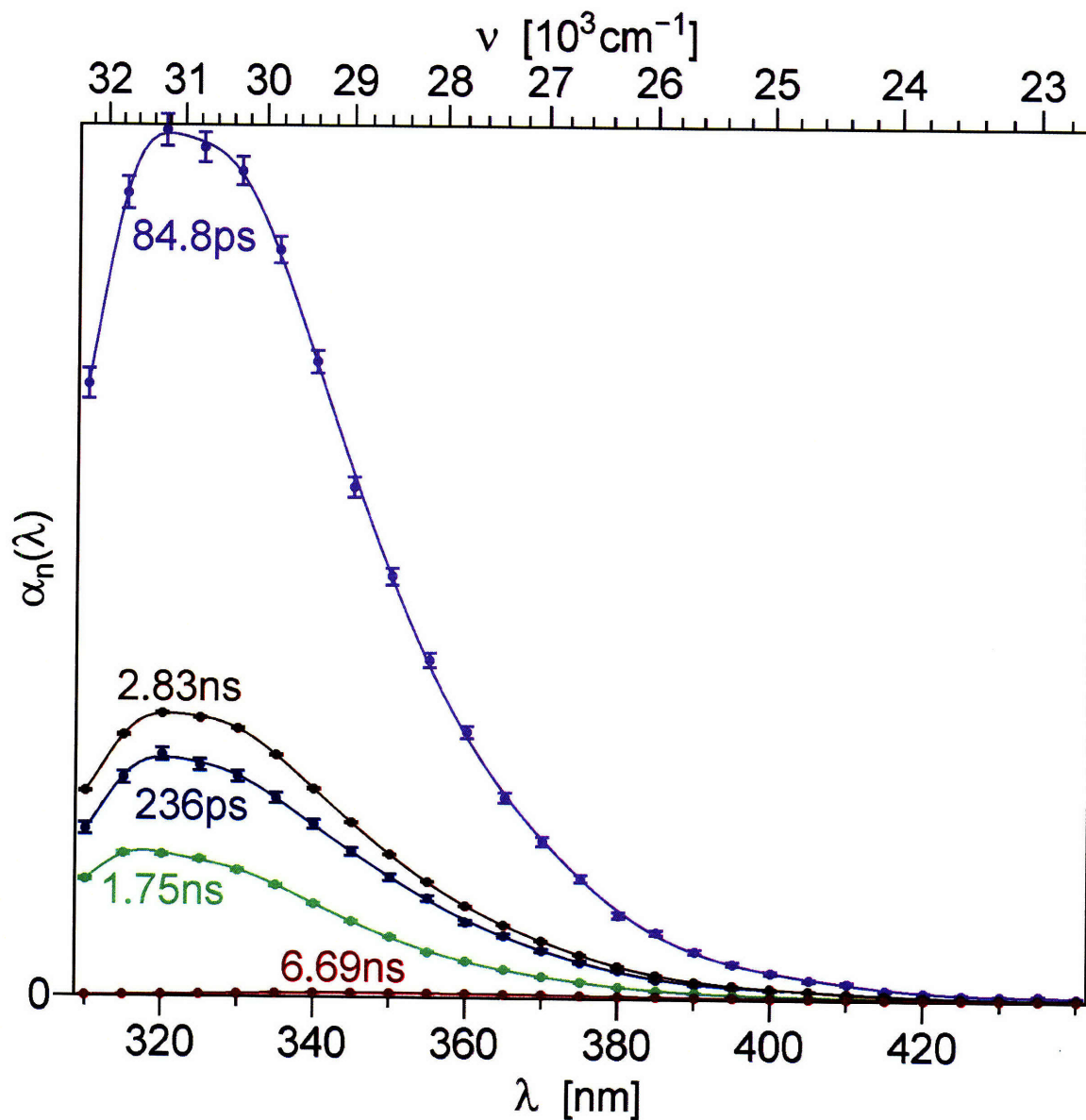


Figure B7. Pre-exponential amplitude spectra  $\alpha_i(\lambda)$  obtained by the global analysis of the fluorescence emission from Trp42/Trp156 H $\gamma$ D-Crys. The values of the corresponding time constants  $\tau_i$  are shown near each spectrum using a matching color.

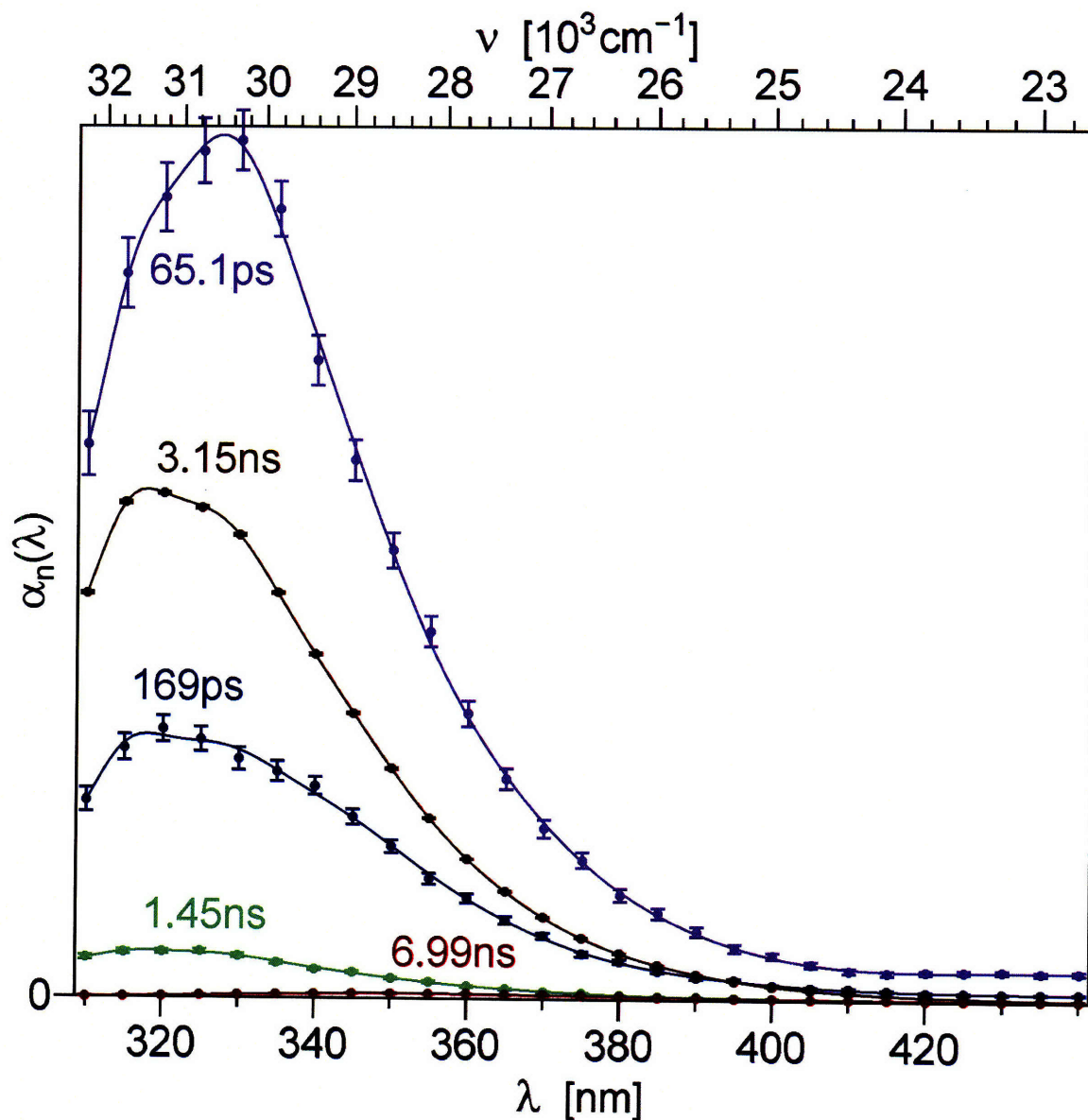


Figure B8. Pre-exponential amplitude spectra  $\alpha_i(\lambda)$  obtained by the global analysis of the fluorescence emission from *Trp68/Trp130* H $\gamma$ D-Crys. The values of the corresponding time constants  $\tau_i$  are shown near each spectrum using a matching color.

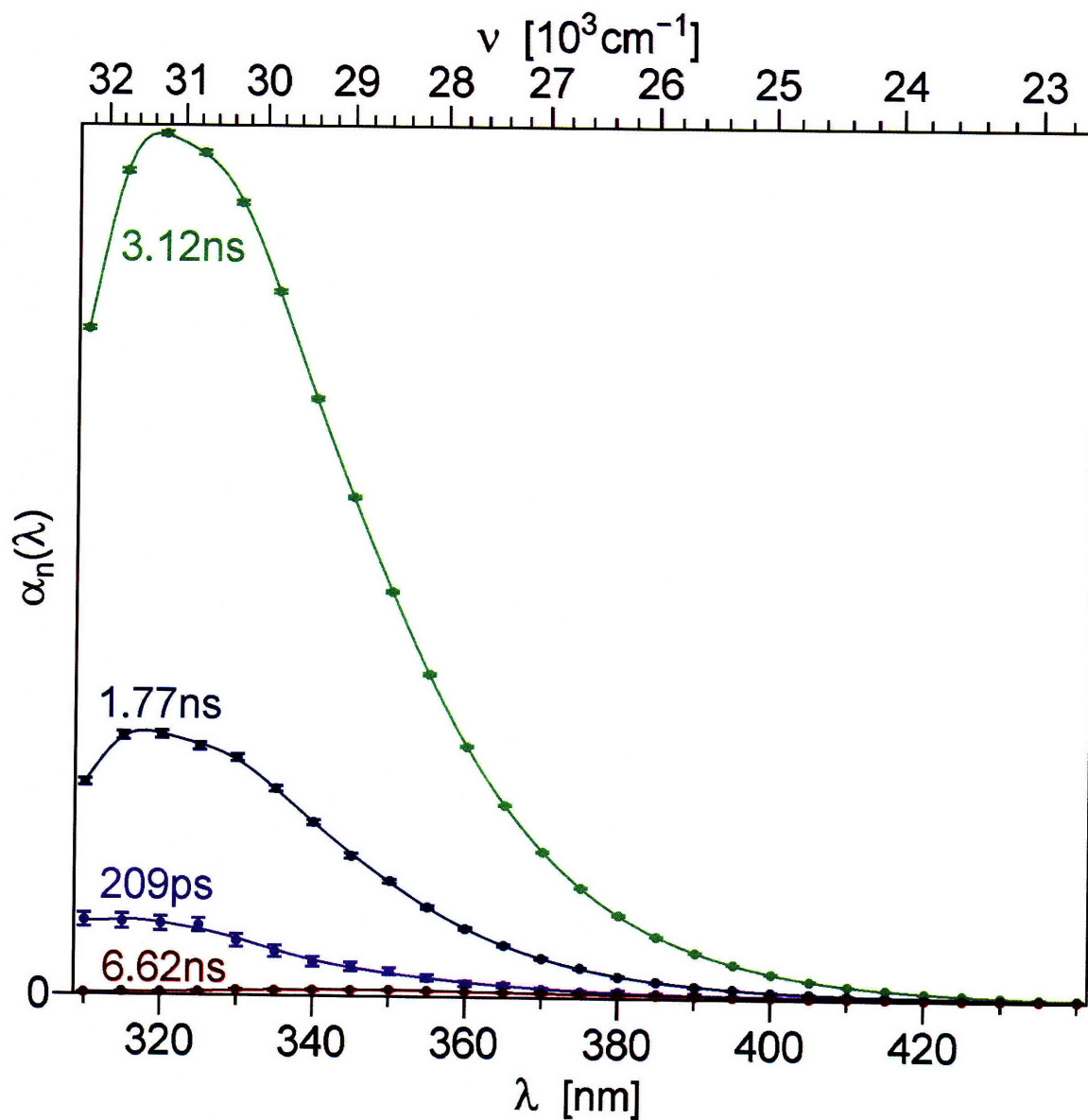


Figure B9. Pre-exponential amplitude spectra  $\alpha_i(\lambda)$  obtained by the global analysis of the fluorescence emission from Trp42/Trp130 H $\gamma$ D-Crys. The values of the corresponding time constants  $\tau_i$  are shown near each spectrum using a matching color.

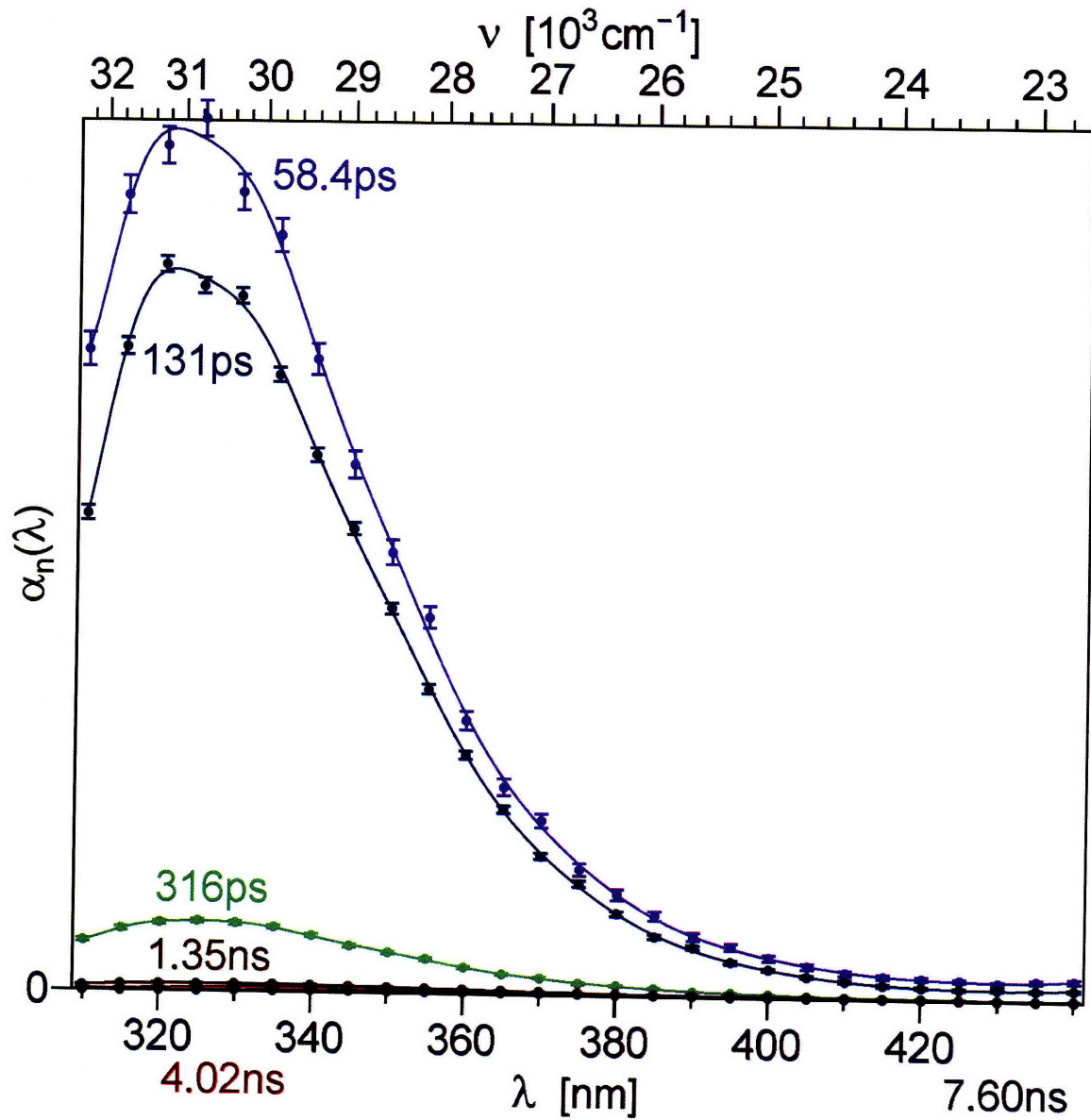


Figure B10. Pre-exponential amplitude spectra  $\alpha_i(\lambda)$  obtained by the global analysis of the fluorescence emission from *Trp68/Trp156* H $\gamma$ D-Crys. The values of the corresponding time constants  $\tau_i$  are shown near each spectrum using a matching color.

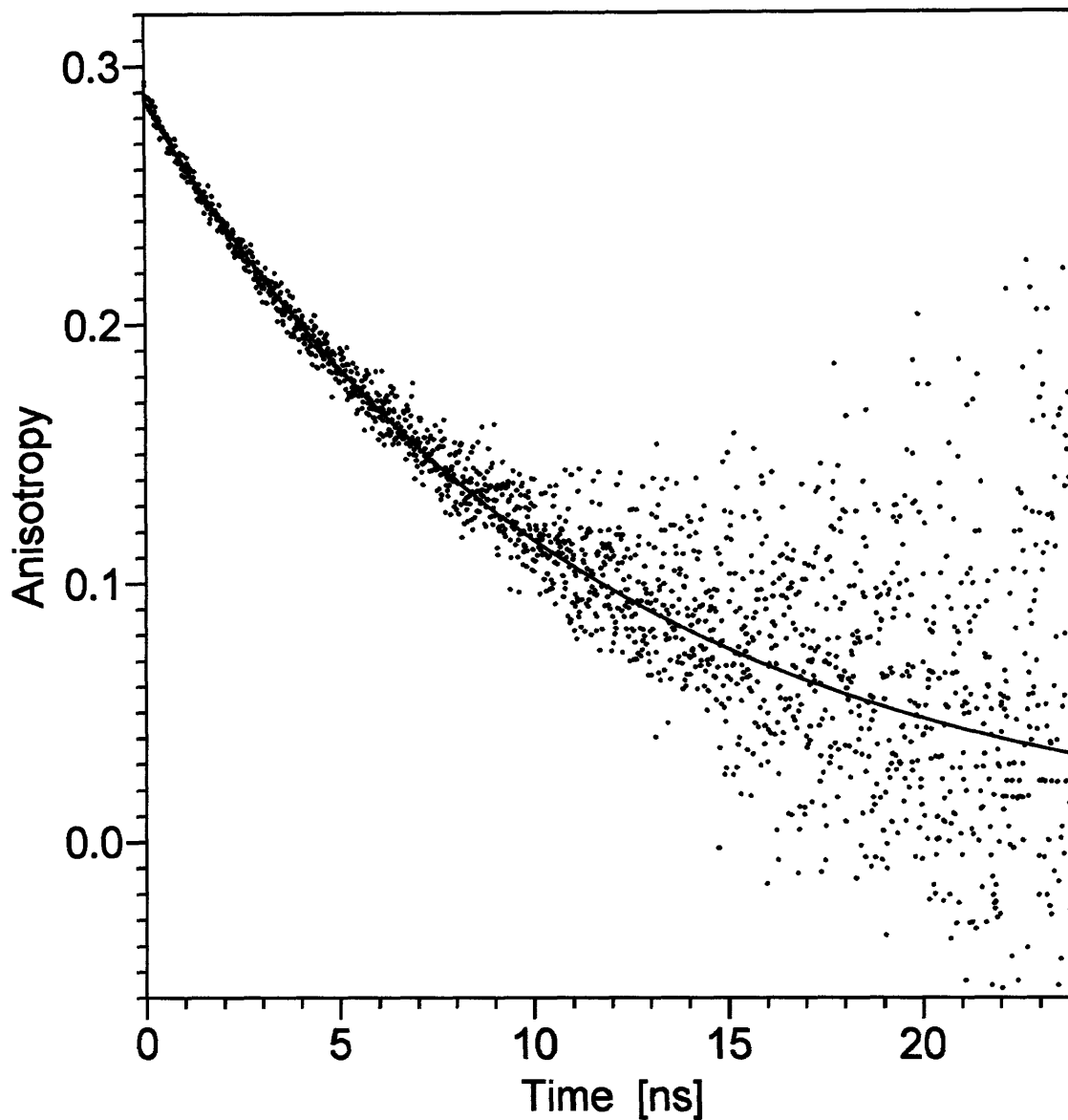


Figure B11. Time-resolved anisotropy of Trp42-only HyD-Crys. The solid line represents the  $r(t)$  function with the best-fit parameters. The dots represent the anisotropy values calculated from the vertical and horizontal polarization photon counts on a channel-by-channel basis.

Table B1. Coordinates of the centers and directions of  $^1L_a$  and  $^1L_b$  transition moments for all Trps in HyD-Crys, determined by the program pdb2opt from the crystal structure of HyD-Crys (PDB code: 1HK0). Only the part of the program output relevant to Trps is shown here; the information relevant to Tyrs and Phes has been omitted. The lines starting with GROUP include the name of a residue containing an aromatic fluorescent group, protein chain ID, and the residue sequence number. The lines starting with CENTER contain the x, y, and z coordinates of the aromatic group center. The lines starting with DIRECTION contain the name of an electronic transition and the x, y, and z components of a unit vector parallel to the transition dipole moment.

```

GROUP          TRP X  42
CENTER                1.236  -5.866   8.514
DIRECTION TRANSITION 1LA  -0.7990 -0.2478  0.5479
DIRECTION TRANSITION 1LB   0.0288  0.8363  0.5475

GROUP          TRP X  68
CENTER                -1.543   6.011   7.634
DIRECTION TRANSITION 1LA   0.8843  0.4670  0.0028
DIRECTION TRANSITION 1LB   0.0799 -0.0079  0.9968

GROUP          TRP X 131
CENTER                8.666  -1.661  25.291
DIRECTION TRANSITION 1LA   0.5034 -0.8211 -0.2689
DIRECTION TRANSITION 1LB   0.1042  0.2904 -0.9512

GROUP          TRP X 157
CENTER                16.917   5.555  19.557
DIRECTION TRANSITION 1LA  -0.5985  0.6979 -0.3933
DIRECTION TRANSITION 1LB  -0.3003 -0.5830 -0.7549

```

Table B2. Values of  $R$  and  $\kappa^2$  for Trp pairs, calculated from the data in Table 1S using Eqs (15-17).

Residue Transition $\leftrightarrow$ Residue Transition	$R$	$\kappa$	$\kappa^2$
TRP X 42 $^1L_a \leftrightarrow$ TRP X 68 $^1L_a$	12.229	-0.7461	0.5567
TRP X 42 $^1L_a \leftrightarrow$ TRP X 131 $^1L_a$	18.824	-0.2669	0.0713
TRP X 42 $^1L_a \leftrightarrow$ TRP X 157 $^1L_a$	22.322	-0.2329	0.0543
TRP X 68 $^1L_a \leftrightarrow$ TRP X 131 $^1L_a$	21.791	-0.1713	0.0293
TRP X 68 $^1L_a \leftrightarrow$ TRP X 157 $^1L_a$	21.980	1.4051	1.9744
TRP X 131 $^1L_a \leftrightarrow$ TRP X 157 $^1L_a$	12.370	-0.7580	0.5746

$R$  represents the distance between the centers of the donor and acceptor.  $\kappa^2$  represents the orientation factor.

## Calculation of mean lifetimes of Trps in HyD-Crys.

The mean lifetimes were calculated using the following equation:

$$\bar{\tau} = \frac{\sum_i \alpha_i \cdot \tau_i}{\sum_i \alpha_i}$$

Here  $\bar{\tau}$  represents the amplitude-weighted mean lifetime,  $\alpha_i$  represents pre-exponential factor, and  $\tau_i$  represents lifetime

- 1) Trp42 alone: average lifetime =  $\frac{0.678 * 2.85 + 0.250 * 1.72}{0.678 + 0.250} = 2.55(ns)$
- 2) The average lifetime of Trp42 in the presence of Trp68  
=  $\frac{0.098 * 0.48 + 0.365 * 1.31}{0.098 + 0.365} = 1.13(ns)$
- 3) The average lifetime of Trp42 in the presence of Trp156  
=  $\frac{0.089 * 1.75 + 0.186 * 2.83}{0.089 + 0.186} = 2.48(ns)$
- 4) Trp130 alone: average lifetime is 3.26ns
- 5) The average lifetime of Trp130 in the presence of Trp156 is 0.94ns
- 6) The average lifetime of Trp130 in the presence of Trp68 is 3.15ns



**APPENDIX C. SUPPORTING INFORMATION FOR CHAPTER FOUR: THE  $\gamma$   
CRYSTALLIN FOLD PROTECTS CONSERVED TRYPTOPHAN RESIDUES  
FROM UV RADIATION DAMAGE BY FAST ELECTRON TRANSFER**

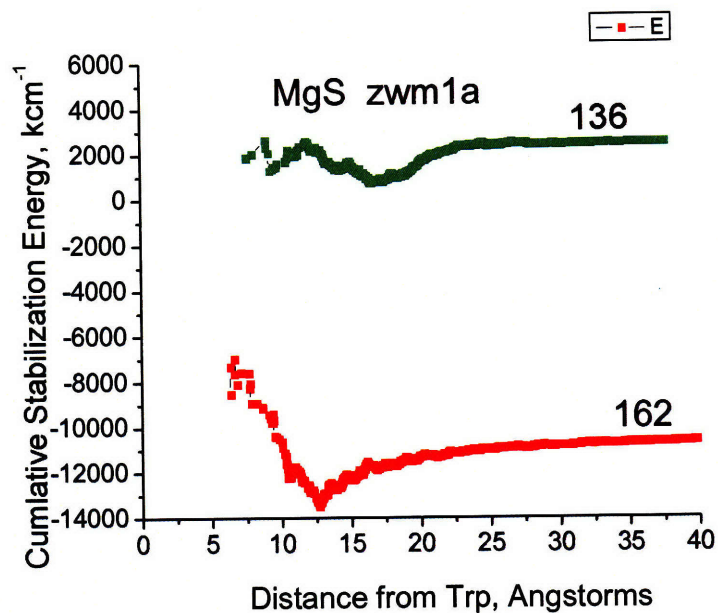
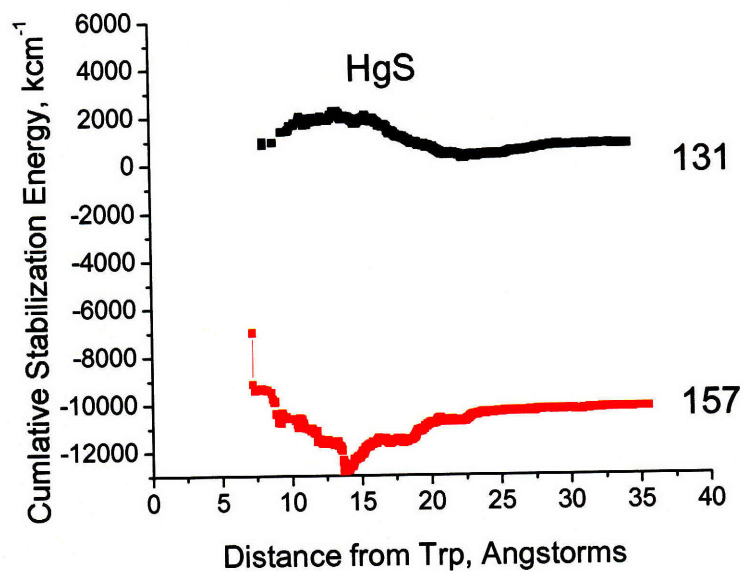


Figure C1. Computed electrostatic stabilization of the charge transfer state due to protein for Trps of H $\gamma$ S-Crys and Trps in murine  $\gamma$ S-crystallin. Points are the cumulative stabilization from all residues up to and including that residue.

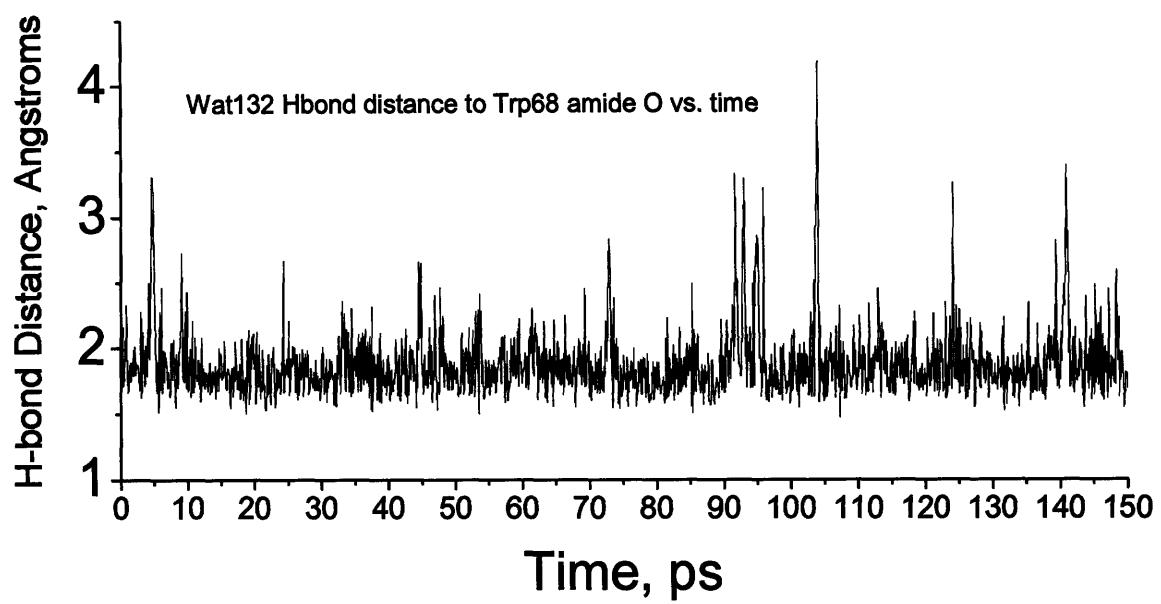


Figure C2. Water 132 hydrogen bond distance to Trp68 amide O versus time.

Table C1. Summary of dihedral angles of *Trp72* and *Trp162* of murine  $\gamma$ S-crystallin based on its NMR structure (PDB code: 1ZWM).

Crystallin	Quenching of Trps <sup>b</sup>	PDB	Dihedral Angles
Murine $\gamma$ S-crystallin	Not reported	1ZWM (NMR structure)	Model 2: <b>Trp72</b> $\omega = -179.94^\circ$ , $\psi = -108.27^\circ$ , $\phi = 10.39^\circ$ , $\chi_1 = 148.1$ , $\chi_2 = 62.5$ <b>Trp162</b> $\omega = 178.48^\circ$ , $\psi = -101.74^\circ$ , $\phi = 16.39^\circ$ , $\chi_1 = 44.7$ , $\chi_2 = 50.1$
			Model 3: <b>Trp72</b> $\omega = 179.86^\circ$ , $\psi = -107.68^\circ$ , $\phi = 9.90^\circ$ , $\chi_1 = 148.5$ , $\chi_2 = 61.9$ <b>Trp162</b> $\omega = 178.71^\circ$ , $\psi = -97.89^\circ$ , $\phi = 11.34^\circ$ , $\chi_1 = -55.5$ , $\chi_2 = -44.1$
			Model 4: <b>Trp72</b> $\omega = 179.92^\circ$ , $\psi = -107.98^\circ$ , $\phi = 10.14^\circ$ , $\chi_1 = 148.6$ , $\chi_2 = 62.7$ <b>Trp162</b> $\omega = 178.33^\circ$ , $\psi = -103.00^\circ$ , $\phi = 14.16^\circ$ , $\chi_1 = 57.2$ , $\chi_2 = 60.9$
			Model 5: <b>Trp72</b> $\omega = 179.93^\circ$ , $\psi = -108.04^\circ$ , $\phi = 10.60^\circ$ , $\chi_1 = 147.3$ , $\chi_2 = 63.4$ <b>Trp162</b> $\omega = 178.88^\circ$ , $\psi = -96.2^\circ$ , $\phi = 10.71^\circ$ , $\chi_1 = -77.8$ , $\chi_2 = 24.2$
			Model 6: <b>Trp72</b> $\omega = 179.86^\circ$ , $\psi = -108.21^\circ$ , $\phi = 10.59^\circ$ , $\chi_1 = 147.7$ , $\chi_2 = 63.5$ <b>Trp162</b> $\omega = 178.66^\circ$ , $\psi = -98.22^\circ$ , $\phi = 11.40^\circ$ , $\chi_1 = -62.4$ , $\chi_2 = -48.5$
			Model 7: <b>Trp72</b> $\omega = -179.88^\circ$ , $\psi = -108.09^\circ$ , $\phi = 11.74^\circ$ , $\chi_1 = 147.8$ , $\chi_2 = 63.8$ <b>Trp162</b> $\omega = 178.60^\circ$ , $\psi = -97.93^\circ$ , $\phi = 11.29^\circ$ , $\chi_1 = -54.8$ , $\chi_2 = -39.4$
			Model 8: <b>Trp72</b> $\omega = 178.09^\circ$ , $\psi = -110.42^\circ$ , $\phi = 16.30^\circ$ , $\chi_1 = 64.5$ , $\chi_2 = 63.1$ <b>Trp162</b> $\omega = 178.56^\circ$ , $\psi = -97.42^\circ$ , $\phi = 11.16^\circ$ , $\chi_1 = -54.9$ , $\chi_2 = -42.5$
			Model 9: <b>Trp72</b> $\omega = 179.88^\circ$ , $\psi = -108.22^\circ$ , $\phi = 6.77^\circ$ , $\chi_1 = 151.3$ , $\chi_2 = 59.4$ <b>Trp162</b> $\omega = 178.53^\circ$ , $\psi = -98.06^\circ$ , $\phi = 11.06^\circ$ , $\chi_1 = -52.2$ , $\chi_2 = -38.1$
			Model 10: <b>Trp72</b> $\omega = 179.96^\circ$ , $\psi = -108.38^\circ$ , $\phi = 11.06^\circ$ , $\chi_1 = 148.0$ , $\chi_2 = 63.4$ <b>Trp162</b> $\omega = 178.66^\circ$ , $\psi = -97.65^\circ$ , $\phi = 11.68^\circ$ , $\chi_1 = -55.2$ , $\chi_2 = -45.5$
			Model 11: <b>Trp72</b> $\omega = 179.82^\circ$ , $\psi = -107.80^\circ$ , $\phi = 10.29^\circ$ , $\chi_1 = 147.8$ , $\chi_2 = 62.3$ <b>Trp162</b> $\omega = 179.69^\circ$ , $\psi = -100.31^\circ$ , $\phi = 10.68^\circ$ , $\chi_1 = 171.7$ , $\chi_2 = 38.0$
			Model 12: <b>Trp72</b> $\omega = 179.91^\circ$ , $\psi = -108.07^\circ$ , $\phi = 10.42^\circ$ , $\chi_1 = 147.3$ , $\chi_2 = 63.1$ <b>Trp162</b> $\omega = 179.85^\circ$ , $\psi = -99.66^\circ$ , $\phi = 9.53^\circ$ , $\chi_1 = 178.8$ , $\chi_2 = 17.5$
			Model 13: <b>Trp72</b> $\omega = 179.98^\circ$ , $\psi = -108.30^\circ$ , $\phi = 11.09^\circ$ , $\chi_1 = 147.1$ , $\chi_2 = 62.8$ <b>Trp162</b> $\omega = 178.70^\circ$ , $\psi = -98.11^\circ$ , $\phi = 10.96^\circ$ , $\chi_1 = -56.9$ , $\chi_2 = -45.2$
			Model 14: <b>Trp72</b> $\omega = -179.78^\circ$ , $\psi = -108.01^\circ$ , $\phi = 9.84^\circ$ , $\chi_1 = 148.9$ , $\chi_2 = 62.7$ <b>Trp162</b> $\omega = 179.68^\circ$ , $\psi = -100.18^\circ$ , $\phi = 9.03^\circ$ , $\chi_1 = 178.0$ , $\chi_2 = 17.6$
			Model 15: <b>Trp72</b> $\omega = -179.79^\circ$ , $\psi = -108.37^\circ$ , $\phi = 9.08^\circ$ , $\chi_1 = 148.6$ , $\chi_2 = 61.8$ <b>Trp162</b> $\omega = 178.69^\circ$ , $\psi = -97.55^\circ$ , $\phi = 11.85^\circ$ , $\chi_1 = -60.5$ , $\chi_2 = -47.6$
			Model 16: <b>Trp72</b> $\omega = -179.99^\circ$ , $\psi = -107.95^\circ$ , $\phi = 10.95^\circ$ , $\chi_1 = 148.6$ , $\chi_2 = 63.4$ <b>Trp162</b> $\omega = 178.93^\circ$ , $\psi = -98.60^\circ$ , $\phi = 11.75^\circ$ , $\chi_1 = -72.0$ , $\chi_2 = -53.6$
			Model 17: <b>Trp72</b> $\omega = 179.92^\circ$ , $\psi = -107.90^\circ$ , $\phi = 9.80^\circ$ , $\chi_1 = 148.5$ , $\chi_2 = 62.1$ <b>Trp162</b> $\omega = 178.80^\circ$ , $\psi = -98.13^\circ$ , $\phi = 11.71^\circ$ , $\chi_1 = -54.0$ , $\chi_2 = -44.9$
			Model 18:

			<b>Trp72</b> $\omega = 179.88^\circ, \psi = -107.96^\circ, \phi = 9.93^\circ, \chi_1 = 147.6, \chi_2 = 62.9$ <b>Trp162</b> $\omega = 178.75^\circ, \psi = -95.79^\circ, \phi = 10.74^\circ, \chi_1 = -76.7, \chi_2 = 24.0$
			Model 19: <b>Trp72</b> $\omega = 179.96^\circ, \psi = -107.92^\circ, \phi = 9.90^\circ, \chi_1 = 148.0, \chi_2 = 63.0$ <b>Trp162</b> $\omega = 178.87^\circ, \psi = -97.80^\circ, \phi = 11.43^\circ, \chi_1 = -56.0, \chi_2 = -45.2$
			Model 20: <b>Trp72</b> $\omega = -179.93^\circ, \psi = -107.84^\circ, \phi = 11.06^\circ, \chi_1 = 147.0, \chi_2 = 63.8$ <b>Trp162</b> $\omega = 178.58^\circ, \psi = -97.68^\circ, \phi = 11.01^\circ, \chi_1 = -58.2, \chi_2 = -44.5$

Figures C1-C14 show how to match 3MI spectra with the spectra of Trp mutants (Trp46-only, Trp72-only, Trp46/Trp72, Trp136-only, Trp162-only, and Trp136/Trp162) and wild type for the extrapolation of the quantum yields of Trps in HyS-Crys on the blue side.

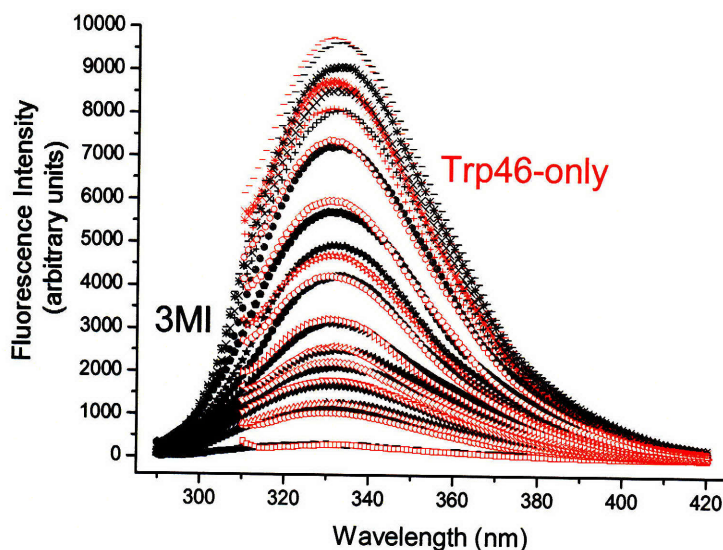


Figure C1. Matching of native Trp46-only fluorescence emission spectra (open symbols, red) with spectra of 3MI in Dioxane (closed symbols, black). Fluorescence emission spectra of 3MI were measured in the range of 290 to 420nm using an excitation wavelength of 280nm. Spectra of Trp46-only were recorded from 310 to 420nm with an excitation wavelength of 300nm. The buffer or solvent signal was subtracted from all spectra.

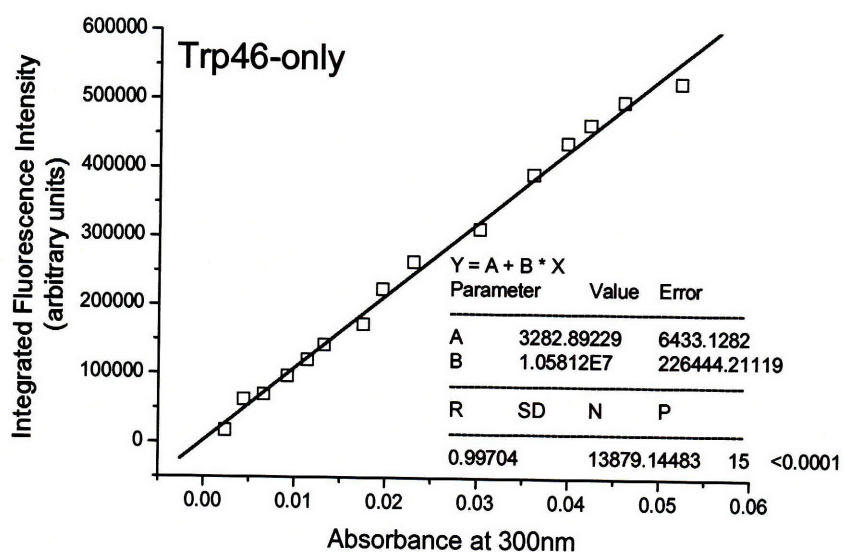


Figure C2. The linear curve of integrated fluorescence intensity (from 297nm to 420nm) calculated from overlapped spectra of 3MI versus the corresponding absorbance of Trp46-only at 300nm.

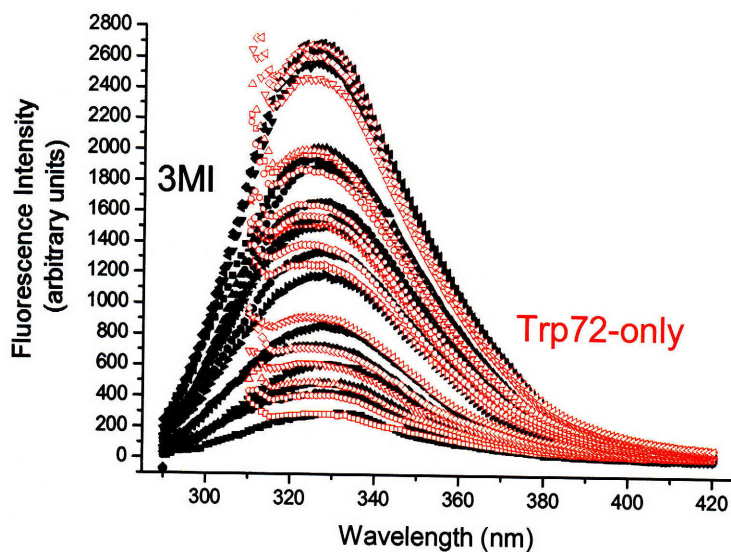


Figure C3. Matching of native Trp72-only fluorescence emission spectra (open symbols, red) with spectra of 3MI in Cyclohexane: Dioxane (66:34) (closed symbols, black). Fluorescence emission spectra of 3MI were measured in the range of 290 to 420nm using an excitation wavelength of 280nm. Spectra of Trp72-only were recorded from 310 to 420nm with an excitation wavelength of 300nm. The buffer or solvent signal was subtracted from all spectra.



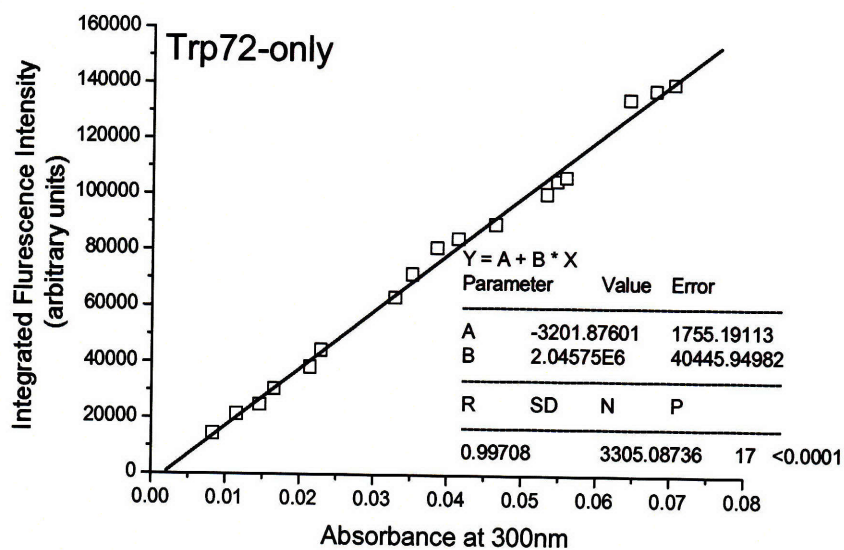


Figure C4. The linear curve of integrated fluorescence intensity (from 297nm to 420nm) calculated from overlapped spectra of 3MI versus the corresponding absorbance of Trp72-only at 300nm.

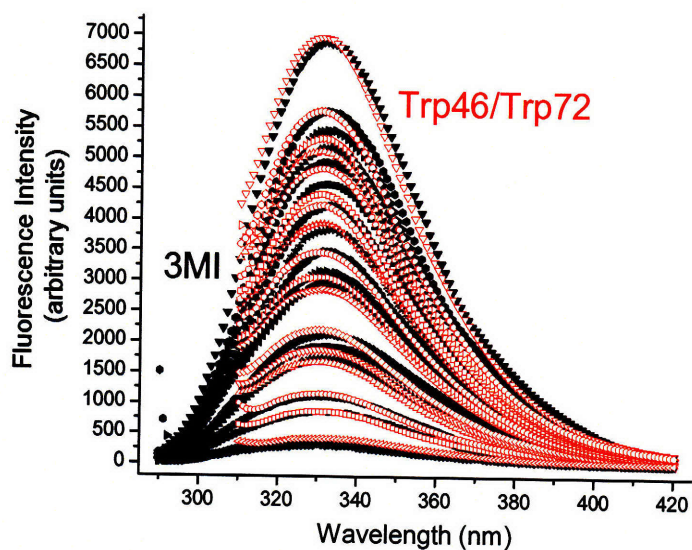


Figure C5. Matching of native Trp46/Trp72 fluorescence emission spectra (open symbols, red) with spectra of 3MI in Dioxane (closed symbols, black). Fluorescence emission spectra of 3MI were measured in the range of 290 to 420nm using an excitation wavelength of 280nm. Spectra of Trp46/72 were recorded from 310 to 420nm with an excitation wavelength of 300nm. The buffer or solvent signal was subtracted from all spectra.

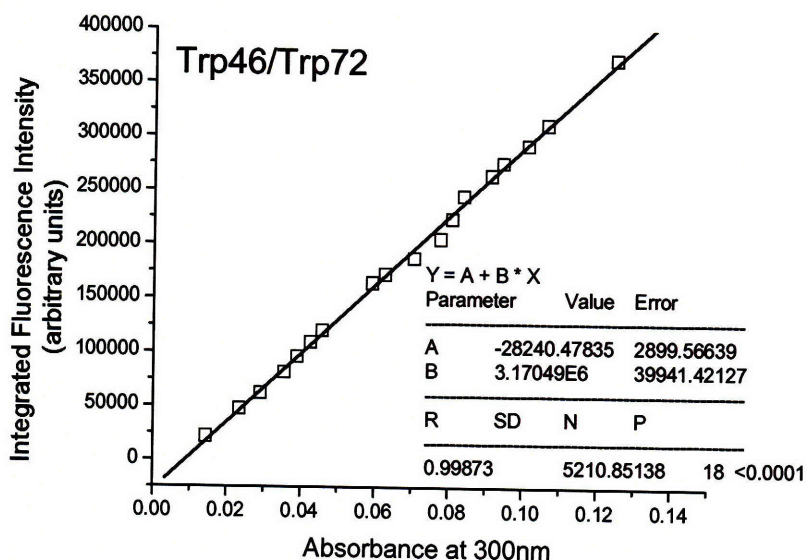


Figure C6. The linear curve of integrated fluorescence intensity (from 297nm to 420nm) calculated from overlapped spectra of 3MI versus the corresponding absorbance of Trp46/72 at 300nm.

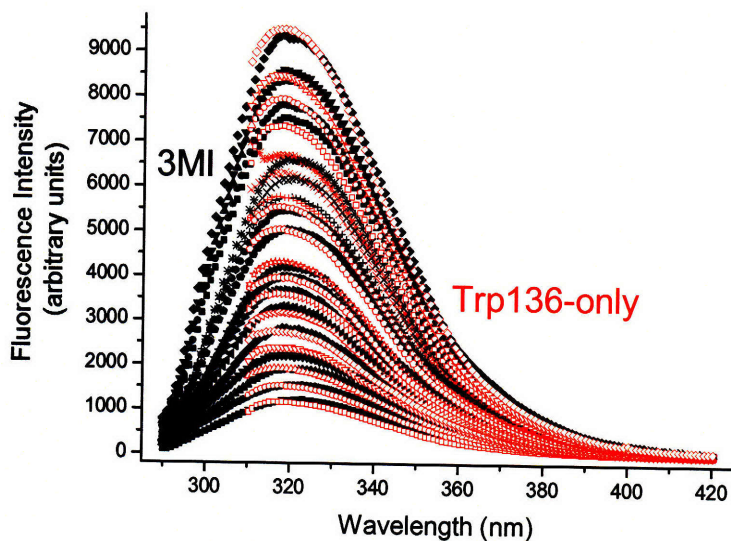


Figure C7. Matching of native Trp136-only fluorescence emission spectra (open symbols, red) with spectra of 3MI in Cyclohexane: Dioxane (93:7) (closed symbols, black). Fluorescence emission spectra of 3MI were measured in the range of 290 to 420nm using an excitation wavelength of 280nm. Spectra of Trp136-only were recorded from 310 to 420nm with an excitation wavelength of 300nm. The buffer or solvent signal was subtracted from all spectra.



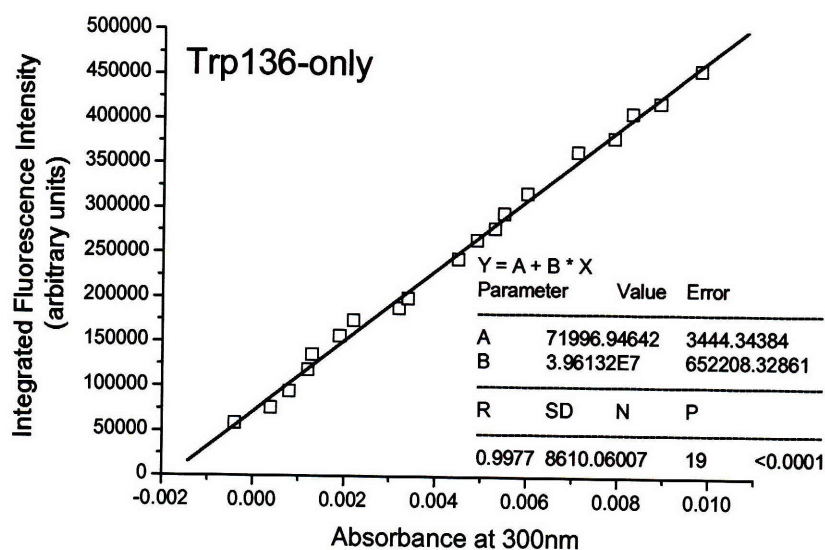


Figure C8. The linear curve of integrated fluorescence intensity (from 297nm to 420nm) calculated from overlapped spectra of 3MI versus the corresponding absorbance of Trp136-only at 300nm.

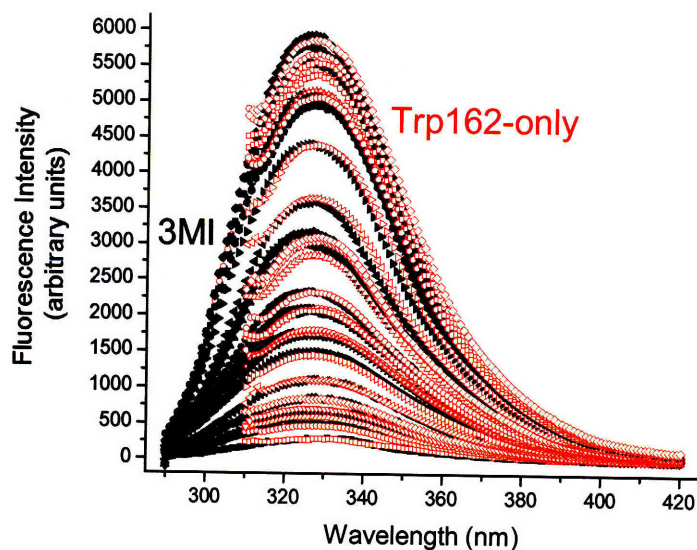


Figure C9. Matching of native Trp162-only fluorescence emission spectra (open symbols, red) with spectra of 3MI in Cyclohexane: Dioxane (66:34) (closed symbols, black). Fluorescence emission spectra of 3MI were measured in the range of 290 to 420nm using an excitation wavelength of 280nm. Spectra of Trp162-only were recorded from 310 to 420nm with an excitation wavelength of 300nm. The buffer or solvent signal was subtracted from all spectra.

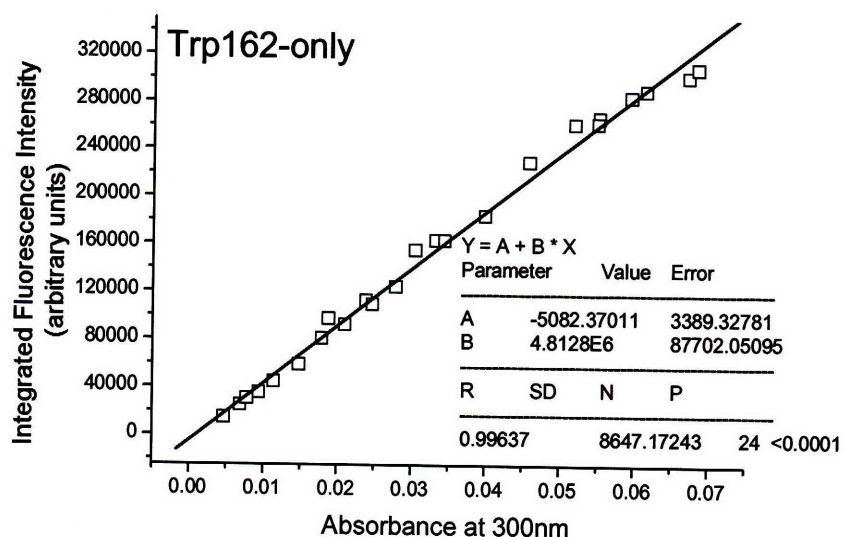


Figure C10. The linear curve of integrated fluorescence intensity (from 297nm to 420nm) calculated from overlapped spectra of 3MI versus the corresponding absorbance of Trp162-only at 300nm.

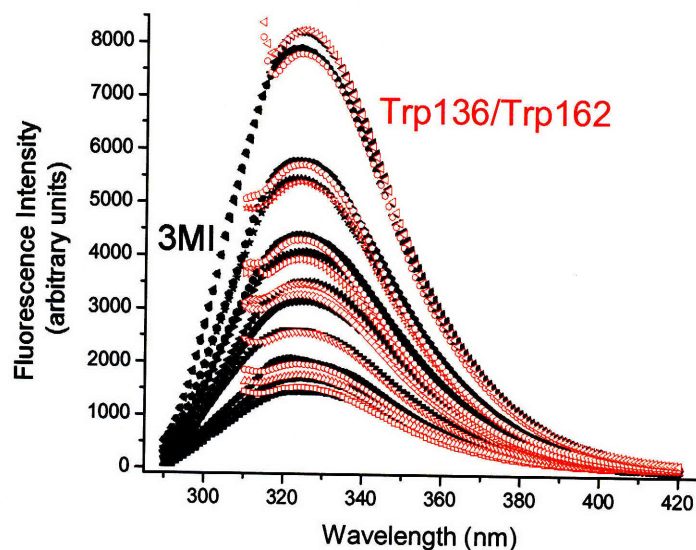


Figure C11. Matching of native Trp136/Trp162 fluorescence emission spectra (open symbols, red) with spectra of 3MI in Cyclohexane: Dioxane (75:25) (closed symbols, black). Fluorescence emission spectra of 3MI were measured in the range of 290 to 420nm using an excitation wavelength of 280nm. Spectra of Trp136/Trp162 were

recorded from 310 to 420nm with an excitation wavelength of 300nm. The buffer or solvent signal was subtracted from all spectra.

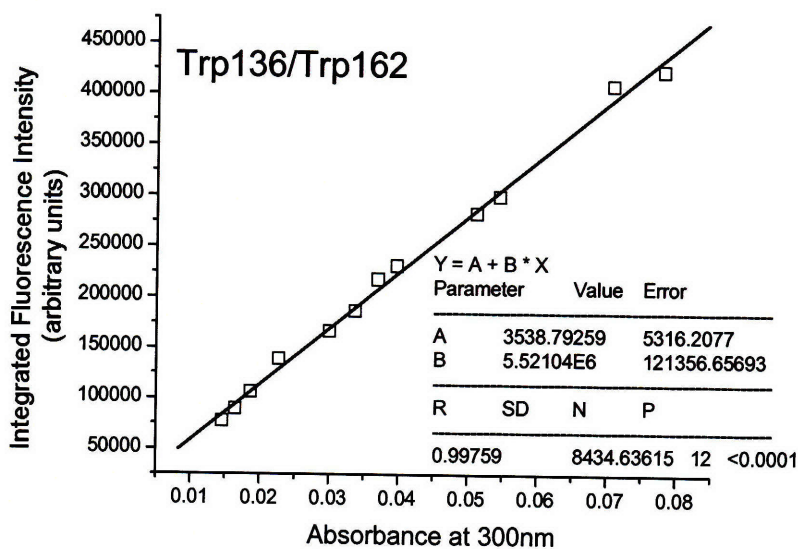


Figure C12. The linear curve of integrated fluorescence intensity (from 297nm to 420nm) calculated from overlapped spectra of 3MI versus the corresponding absorbance of Trp136/Trp162 at 300nm.

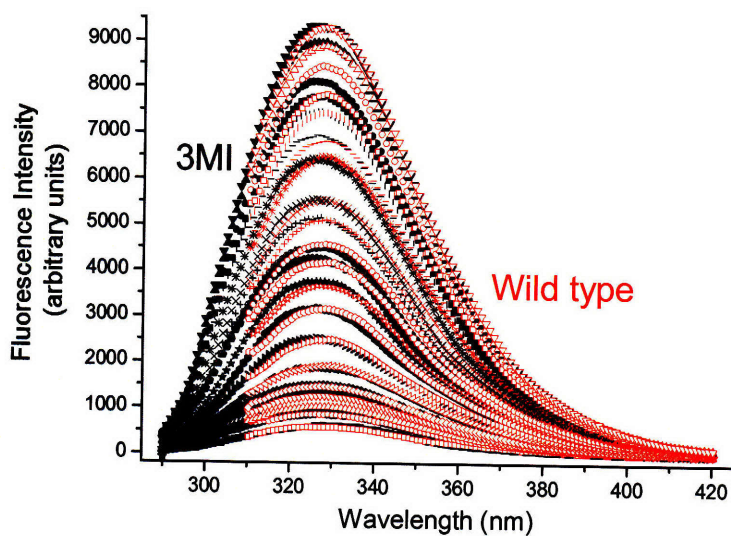


Figure C13. Matching of native fluorescence emission spectra of wild type (open symbols, red) with spectra of 3MI in Cyclohexane: Dioxane (66:34) (closed symbols, black). Fluorescence emission spectra of 3MI were measured in the range of 290 to 420nm using an excitation wavelength of 280nm. Spectra of wild type were recorded from 310 to 420nm with an excitation wavelength of 300nm. The buffer or solvent signal was subtracted from all spectra.



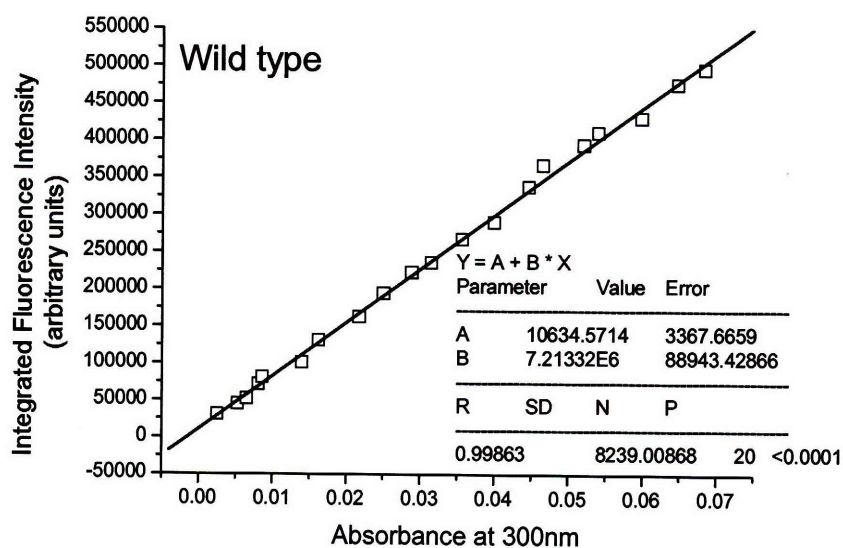


Figure C14. The linear curve of integrated fluorescence intensity (from 297nm to 420nm) calculated from overlapped spectra of 3MI versus the corresponding absorbance of wild type at 300nm.

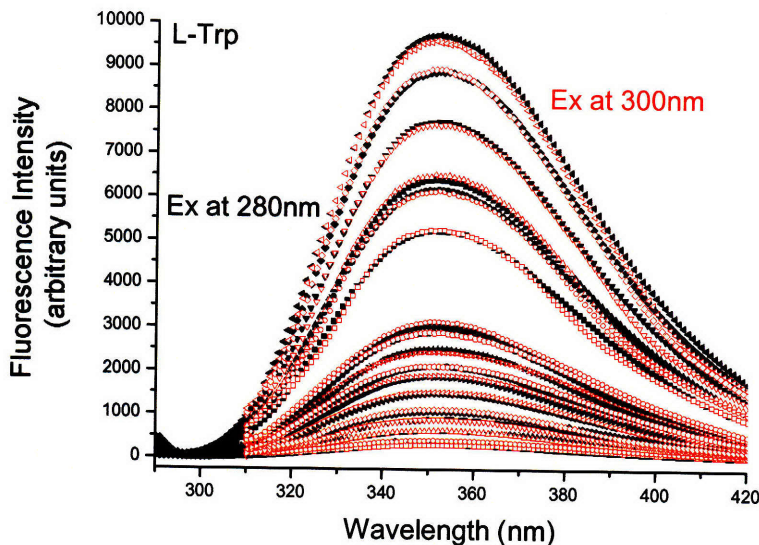


Figure C15. Matching of fluorescence emission spectra of L-Trp with excitation (Ex)<sup>1</sup> wavelength at 300nm (open symbols, red) with spectra of L-Trp (Ex at 280nm) (closed symbols, black). Fluorescence emission spectra of L-Trp were measured in the range of 290 to 420nm using an excitation wavelength of 280nm and in the range of 310 to 420nm with an excitation wavelength of 300nm, respectively. The buffer signal was subtracted from all spectra.

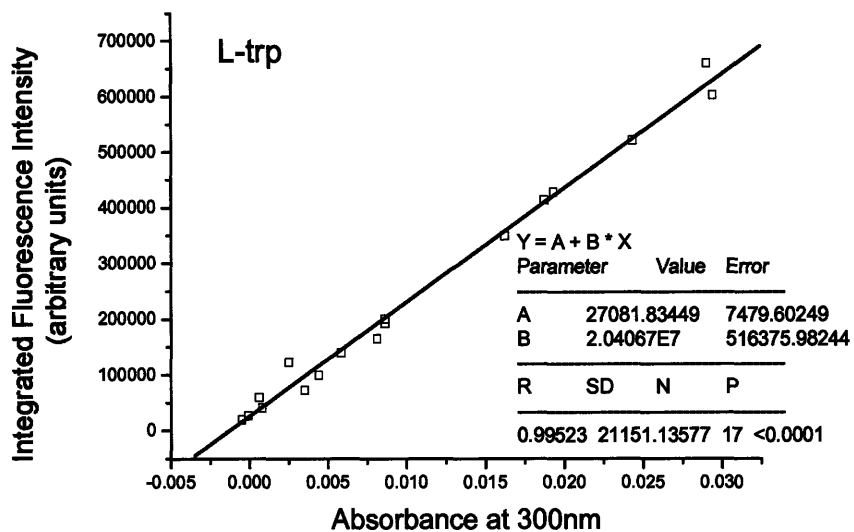


Figure C16. The standard curve of L-Trp. After matching the emission spectra of L-Trp (Ex at 280nm) with the spectra of L-Trp (Ex at 300nm), the integrated fluorescence intensity of L-Trp (from 297nm to 420nm, Ex at 280nm) and the absorbance of corresponding L-Trp (Ex at 300nm) at 300nm were used to calculate the slope of the standard curve.

The slopes of the linear curves, Figures C2, C4, C6, C8, C10, C12, and C14 were used to calculate the quantum yields of Trp mutants and the wild type of H $\gamma$ S-Crys according to equation (1) in the Materials and Methods in Chapter two.

## Curriculum Vitae

Jiejin Chen

### Education

---

2003-degree expected on Sep. 2008	Massachusetts Institute of Technology Candidate for Ph.D. degree in Chemistry, Division of Biochemistry	Cambridge, MA
2000-2003	Peking University Health Science Center Master of Chemical Biology	Beijing, P.R.China
1996-2000	Peking University Health Science Center Bachelor of Pharmaceutical Science	Beijing, P.R.China

### Publications

---

1. **Jiejin Chen**, Shannon L. Flaugh, Patrik R. Callis, Jonathan King. Mechanism of the highly efficient quenching of tryptophan fluorescence in human  $\gamma$ D-crystallin, *Biochemistry* 2006, Vol 45 (38) 11551-11563.
2. **Jiejin Chen**, Dmitri Toptygin, Ludwig Brand, Jonathan King. The efficient fluorescence quenching mechanism of human  $\gamma$ D-crystallin studied by time-resolved fluorescence spectroscopy (accepted by *Biochemistry*).
3. **Jiejin Chen**, Patrik R. Callis, Jonathan King. How the  $\gamma$ -crystallin fold has evolved to protect the tryptophan residues from UV radiation: Mechanism of fast electron transfer (manuscript in preparation).

### Research Experience

---

<u>Massachusetts Institute of Technology</u> Research Assistant	Cambridge, MA 2003-degree expected on Sep. 2008
<u>Johns Hopkins University</u> Visiting Student	Baltimore, MD Feb.-May 2007
<u>Amgen Inc.</u> Temporary Visiting Student	Thousand Oaks, CA Aug.-Oct. 2006
<u>Peking University Health Science Center</u> Research Assistant	Beijing, P.R. China 2000-2003